PIPELINE FLOW OF COARSE PARTICLES IN FLUIDS WITH YIELD STRESSES

A Thesis Submitted to the College of

Graduate Studies and Research

in Partial Fulfilment of the Requirements

for the Degree of Doctor of Philosophy

in the Department of Chemical Engineering

University of Saskatchewan

Saskatoon

by

Kelly Blue Hill

June 1996

© Copyright Kelly Blue Hill, 1996.

The University of Saskatchewan claims copyright in conjunction with the author. Use shall not be made of the material contained herein without proper acknowledgement.

National Library of Canada
Acquisitions and Bibliographic Services
395 Wellington Street
Ottawa ON K1A 0N4
Canada

Bibliothèque nationale du Canada
Acquisitions et services bibliographiques
395, rue Wellington
Ottawa ON K1A 0N4
Canada

Your file Votre référence

Our file Notre référence

The author has granted a non-exclusive licence allowing the National Library of Canada to reproduce, loan, distribute or sell copies of this thesis in microform, paper or electronic formats.

L'auteur a accordé une licence non exclusive permettant à la Bibliothèque nationale du Canada de reproduire, prêter, distribuer ou vendre des copies de cette thèse sous la forme de microfiche/film, de reproduction sur papier ou sur format électronique.

The author retains ownership of the copyright in this thesis. Neither the thesis nor substantial extracts from it may be printed or otherwise reproduced without the author's permission.

L'auteur conserve la propriété du droit d'auteur qui protège cette thèse. Ni la thèse ni des extraits substantiels de celle-ci ne doivent être imprimés ou autrement reproduits sans son autorisation.

0-612-23990-X

Canada

UNIVERSITY OF SASKATCHEWAN

College of Graduate Studies and Research

SUMMARY OF DISSERTATION

Submitted in partial fulfilment

of the requirements for the

DEGREE OF DOCTOR OF PHILOSOPHY

by

Kelly Blue Hill

Department of Chemical Engineering
University of Saskatchewan

Fall 1996

Examining Committee:

Dr. S. Yannacopoulis	~~Dean/ Associate Dean~~/ Dean's Designate, Chair, College of Graduate Studies and Research
Dr. B. Milne	Chair of Advisory Committee, Department of Chemical Engineering
Dr. C.A. Shook	Supervisor, Department of Chemical Engineering
Dr. J.D. Bugg	Department of Mechanical Engineering
Dr. G.A. Hill	Department of Chemical Engineering
Dr. S. Rohani	Department of Chemical Engineering

External Examiner:

Dr. K.C. Wilson
Department of Civil Engineering
Queen's University
Kingston, Ontario
K7L 3N6

Pipeline Flow of Coarse Particles in Fluids with Yield Stresses

Horizontal pipe flow of coarse particle slurries with carrier fluids which exhibited a yield stress were examined. Experimental measurements were made to investigate the effect the fluid yield stress had on the transport of the coarse particles. These results were used to evaluate two numerical models intended to describe these flows.

Experimental tests used clay suspensions which were found to follow the Bingham fluid model. The suspensions had large yield stresses which were capable of supporting the particles when the fluid was stationary. The coarse particles were large in relation to the pipe size. Slurry flows were mostly laminar but turbulent flows were also observed.

The first numerical model considered the laminar flow of slurries by representing them as a continua with a viscosity which varied with position in the pipe. A finite element method was used to predict the velocity distribution in the pipe from a specified pressure gradient and coarse particle concentration profile. This velocity distribution was used to predict a concentration distribution based on a dispersive mechanism in laminar flow.

The second numerical model was mechanistically based and represented the slurries by two stratified layers with different coarse particle concentrations. This model was used in both laminar and turbulent flow. The effects of the fluid yield stress on model predictions were considered.

BIOGRAPHICAL

April, 1989 B.Sc., Chemical Engineering, University of Saskatchewan

In presenting this thesis in partial fulfilment of the requirements for a Postgraduate degree from the University of Saskatchewan, I agree that the Libraries of this University may make it freely available for inspection. I further agree that permission for copying of this thesis in any manner, in whole or in part, for scholarly purposes may be granted by the professor or professors who supervised my thesis work or, in their absence, by the Head of the Department or the Dean of the College in which my thesis work was done. It is understood that any copying or publication or use of this thesis or parts thereof for financial gain shall not be allowed without my written permission. It is also understood that due recognition shall be given to me and to the University of Saskatchewan in any scholarly use which may be made of any material in my thesis.

Requests for permission to copy or make use of material in this thesis in whole or part should be addressed to:

Head of the Department of Chemical Engineering

University of Saskatchewan

Saskatoon, Saskatchewan, S7N 5A4

ABSTRACT

Horizontal pipe flow of coarse particle slurries with carrier fluids which exhibited yield stresses were examined. Experimental measurements were made to investigate the effect the fluid yield stresses had on the transport of the coarse particles (1.7 mm and 4.4 mm) in a 52 mm diameter pipeloop. These results were used to evaluate two numerical models intended to describe these flows.

Experimental tests used clay suspensions which were found to follow the Bingham fluid model. The suspensions had large yield stresses (3 to 25 Pa) which were capable of supporting the particles when the fluid was stationary. These particles were relatively large in relation to the pipe size. Slurry flows were mostly laminar but turbulent flows were also observed.

The first numerical model considered the laminar flow of slurries by representing them as continua with a viscosity which varied with position in the pipe. A finite element method was used to predict the velocity distribution in the pipe from a specified pressure gradient and coarse particle concentration profile. This velocity distribution was then used to predict the concentration distribution based on a dispersive mechanism in laminar flow.

The second numerical model was also mechanistically based and represented the slurries as two stratified layers with different coarse particle concentrations. This model was used for both laminar and turbulent flow. The effects of the fluid yield stresses on model predictions were considered.

ACKNOWLEDGEMENTS

I wish to give my most sincere thanks to Dr. C.A. Shook for his encouragement and belief in my abilities. Under his tutelage, I learned much more than can be reflected by a single thesis.

I would also like to thank the members of my advisor committee for their support. They were Dr. B. Milne, Dr. S. Rohani and Dr. G.A. Hill of the Department of Chemical Engineering, Dr. J.D. Bugg of the Department of Mechanical Engineering and the external examiner, Dr. K.C. Wilson of the Department of Civil Engineering at Queen's University. I also wish to thank former committee members Dr. M.N. Esmail and Dr. W. DeCoursey.

Dr. R.G. Gillies of the Saskatchewan Research Council provided valuable advice during the analysis of the experimental results. Mr. P. Schergevitch assisted with the preparation of equipment drawings.

I would also like to acknowledge the financial support of the College of Graduate Studies and Research.

TABLE OF CONTENTS

ABSTRACT			iii
ACKNOWLEDGEMENTS			iv
TABLE OF CONTENTS			v
LIST OF TABLES			viii
LIST OF FIGURES			ix
LIST OF SYMBOLS			xiv
1	INTRODUCTION		1
	1.1	Present work	4
2	LITERATURE REVIEW		6
	2.1	Bingham fluid model	7
	2.2	Single particle behaviour in a fluid	12
	2.3	Multiparticle systems	18
	2.4	Pipe flow of coarse particle slurries	24
		2.4.1 Two-layer model	30
		2.4.2 Laminar flow of coarse particle slurries	33
		2.4.3 Alternative flow models	38
3	EXPERIMENTAL PROCEDURES AND CONDITIONS		41
	3.1	52 mm diameter pipeloop tests	41
	3.2	Magnetic particle velocity	45
	3.3	Velocity probe	47
	3.4	Gamma ray densitometer	48
	3.5	Magnetic flowmeter	52
	3.6	Concentric cylinder viscometer	52
	3.7	Test conditions	53
		3.7.1 Kaolin/Bentonite suspensions	53
		3.7.2 Solid material	54
		3.7.3 Test matrix	55
4	EXPERIMENTAL RESULTS AND DISCUSSION		58
	4.1	Concentration profiles for large spheres in water	58
		4.1.1 Particle size and in-situ concentration effects	61
	4.2	Water slurry pressure gradients in turbulent flow	63

4.2.1 Two-layer model predictions for water slurries 70
4.3 Magnetic particle velocities in water slurries 78
4.4 Flow of Kaolin/Bentonite suspensions 80
4.4.1 Couette flow of Kaolin/Bentonite suspensions 80
4.4.2 Pipe flow of Kaolin/Bentonite suspensions 84
4.5 Concentration profiles in Kaolin/Bentonite slurries 91
4.5.1 Concentration profiles for 1.7 mm sphere slurries 92
4.5.2 Concentration profiles for 4.4 mm spheres in low yield stress fluids 97
4.5.3 Concentration profiles for 4.4 mm spheres in high yield stress fluids 101
4.5.4 Concentration profiles for 4.1 mm gravel slurries 107
4.5.5 Comparison of concentration profiles in Kaolin/ Bentonite suspensions 111
4.6 Particle velocity profiles in Kaolin/Bentonite slurries 117
4.7 Kaolin/Bentonite slurry pressure gradients 120
4.7.1 Pressure gradients of 1.7 mm sphere slurries 120
4.7.2 Pressure gradients for 4.4 mm spheres in low yield stress fluids 125
4.7.3 Pressure gradients for 4.4 mm spheres in high yield stress fluids 127
4.7.4 Pressure gradients for 4.1 mm gravel slurries 129
4.7.5 Pressure gradient estimates in laminar flow 131
4.7.5.1 Flow in a partially blocked pipe 131
4.7.5.2 Contact load contributions to pressure gradients 134
4.7.5.3 Pseudohomogeneous pressure gradients 134
4.8 Magnetic particle velocities in Kaolin/Bentonite slurries 138
4.9 Particle velocities near the wall for Kaolin/Bentonite slurries 143

5 NUMERICAL SIMULATION OF SLURRY FLOW 151
5.1 Finite element model 151
5.1.1 Solution domain for laminar flow in a pipe 156
5.1.2 Local viscosity 156
5.1.3 Modification for non-Newtonian fluids 158
5.1.4 Concentration distribution prediction 160
5.2 Finite element simulations 165
5.2.1 Glycol slurry simulations 165
5.2.2 Oil slurry simulations 170
5.2.3 Kaolin/Bentonite slurry simulations 172
5.2.4 Summary 177
5.2.5 Sensitivity analysis of model 180
5.3 Two-layer model predictions 185

5.3.1 The distribution of solids 185
5.3.2 Fluid friction 189
5.3.3 Interfacial friction factor 192
5.4 Two-layer model simulations 196
5.4.1 Glycol and sand slurry predictions 199
5.4.2 Oil and sand slurry predictions 201
5.4.3 Kaolin/Bentonite slurry predictions 203
5.4.4 Oil sand overburden slurries 209
5.4.5 Summary 214

6 CONCLUSIONS AND RECOMMENDATIONS 216
6.1 Conclusions 216
6.2 Recommendation 218

REFERENCES 220

APPENDIX A : Two-layer model 224

APPENDIX B : Pipeline data acquisition program 229
B.1 Acquisition program FLUID.FOR 229
B.2 Assembly language macro ADINP.MAC 236

APPENDIX C : Finite element pipe flow program 237

APPENDIX D : Two layer model program 254

LIST OF TABLES

Table 3.1 : Particle size distribution of gravel following tests. 56
Table 3.2 : Test conditions for two inch diameter pipeloop. 57
Table 4.1 : Concentric cylinder viscometry results. 92
Table 4.2 : Slurry test conditions and required particle support yield stress. 93
Table 5.1 : Numerical simulation test cases. 166
Table 5.2 : Experimental test conditions simulated with two-layer model. 197
Table 5.3 : Two-layer model parameter specifications. 198

LIST OF FIGURES

Figure 2.1 : Pressure gradient of 0.18 mm sand in water flowing in a 53 mm diameter pipe (Shook et al., 1973). 28
Figure 2.2 : Pressure gradient of 0.18 mm sand in ethylene glycol flowing in a 53 mm diameter pipe (Shook et al., 1973). 29
Figure 2.3 : Conceptual representation of the two-layer model. 31
Figure 3.1 : 52 mm diameter test pipeloop. 42
Figure 3.2 : Magnetic particle detection and timing system. 46
Figure 3.3 : Conductivity L-probe and associated electronics. 49
Figure 3.4 : Gamma ray densitometer and associated electronics. 51
Figure 4.1 : Concentration profiles in a 53 mm pipe for 1.7 mm glass spheres in water. 59
Figure 4.2 : Concentration profiles in a 53 mm pipe for 4.4 mm glass spheres in water. 60
Figure 4.3 : Concentration profiles for spheres in water at an in-situ concentration of 0.15 and a bulk velocity of 1.75 m/s. 62
Figure 4.4 : Concentration profiles for spheres in water at an in-situ concentration of 0.25 and a bulk velocity of 1.75 m/s. 64
Figure 4.5 : Concentration profiles for 1.7 mm spheres in water at a bulk velocity of 1.75 m/s. 65
Figure 4.6 : Concentration profiles for 4.4 mm spheres in water at a bulk velocity of 1.75 m/s. 66
Figure 4.7 : Pressure gradients in a 53 mm pipe for 1.7 mm glass spheres in water. 68
Figure 4.8 : Pressure gradients in a 53 mm pipe for 4.4 mm glass spheres in water. 69
Figure 4.9 : Pressure gradients predicted by two-layer model for 1.7 mm spheres in water. 71
Figure 4.10 : Excess pressure gradients predicted by two-layer model for 1.7 mm spheres in water. 73
Figure 4.11 : Pressure gradients predicted by two-layer model for 4.4 mm spheres in water. 74
Figure 4.12 : Excess pressure gradients predicted by two-layer model for 4.4 mm spheres in water. 76
Figure 4.13 : Magnetic particle velocities in water and 1.7 mm sphere slurries. 79
Figure 4.14 : Magnetic particle velocities in water and glass sphere slurries with in-situ concentrations of 0.15. 81
Figure 4.15 : Magnetic particle velocities in water and glass sphere slurries with in-situ concentrations of 0.25. 82
Figure 4.16 : Use of the Bingham fluid model to characterize Kaolin/Bentonite suspensions. 83
Figure 4.17 : Comparison of Bingham model parameters for a Kaolin suspension. 86

Figure 4.18 : Comparison of Bingham model parameters for a Kaolin/Bentonite suspension with a low yield stress. 87
Figure 4.19 : Comparison of Bingham model parameters for a Kaolin/Bentonite suspension with a moderate yield stress. 89
Figure 4.20 : Comparison of Bingham model parameters for a Kaolin/Bentonite suspension with a high yield stress. 90
Figure 4.21 : Concentration profiles for 15% 1.7 mm spheres in a Kaolin/ Bentonite suspension. 95
Figure 4.22 : Concentration profiles for 25% 1.7 mm spheres in a Kaolin/ Bentonite suspension. 96
Figure 4.23 : Concentration profiles for 1.7 mm spheres in Kaolin/Bentonite suspensions at a bulk velocity of 0.8 m/s. 98
Figure 4.24 : Concentration profiles for 1.7 mm spheres in Kaolin/Bentonite suspensions at a bulk velocity of 1.6 m/s. 99
Figure 4.25 : Concentration profiles for 4.4 mm spheres in Kaolin/Bentonite suspensions with low yield stresses at a bulk velocity of 0.8 m/s. 100
Figure 4.26 : Concentration profiles for 4.4 mm spheres in Kaolin/Bentonite suspensions with low yield stresses at a bulk velocity of 1.6 m/s. 102
Figure 4.27 : Concentration profiles for 15% 4.4 mm spheres in a Kaolin/ Bentonite suspension with a high yield stress. 104
Figure 4.28 : Concentration profiles for 15% 4.4 mm spheres in Kaolin/ Bentonite suspensions with high yield stresses at a bulk velocity of 0.8 m/s. 105
Figure 4.29 : Concentration profiles for 15% 4.4 mm spheres in Kaolin/ Bentonite suspensions with high yield stresses at a bulk velocity of 1.6 m/s. 106
Figure 4.30 : Concentration profiles for 15% 4.1 mm gravel in a Kaolin/ Bentonite suspension. 108
Figure 4.31 : Concentration profiles for 25% 4.1 mm gravel in a Kaolin/ Bentonite suspension. 109
Figure 4.32 : Concentration profiles for 4.1 mm gravel in Kaolin/Bentonite suspensions at a bulk velocity of 0.8 m/s. 110
Figure 4.33 : Concentration profiles for 4.1 mm gravel in Kaolin/Bentonite suspensions at a bulk velocity of 1.6 m/s. 112
Figure 4.34 : Concentration profiles for 15% coarse particles in Kaolin/ Bentonite suspensions at a bulk velocity of 0.8 m/s. 113
Figure 4.35 : Concentration profiles for 15% coarse particles in Kaolin/ Bentonite suspensions at a bulk velocity of 1.6 m/s. 114
Figure 4.36 : Concentration profiles for 25% coarse particles in Kaolin/ Bentonite suspensions at a bulk velocity of 0.8 m/s. 115
Figure 4.37 : Concentration profiles for 25% coarse particles in Kaolin/ Bentonite suspensions at a bulk velocity of 1.6 m/s. 116

Figure 4.38 : Particle velocity profiles for 1.7 mm spheres in Kaolin/Bentonite suspensions. 118
Figure 4.39 : Particle velocity profiles for 4.4 mm spheres in Kaolin/Bentonite suspensions with low yield stresses. 119
Figure 4.40 : Particle velocity profiles for 4.4 mm spheres in Kaolin/Bentonite suspensions with high yield stresses. 121
Figure 4.41 : Particle velocity profiles for 4.1 mm gravel in Kaolin/Bentonite suspensions. 122
Figure 4.42 : Pressure gradients for 1.7 mm spheres in Kaolin/Bentonite suspensions. 124
Figure 4.43 : Pressure gradients for 4.4 mm spheres in Kaolin/Bentonite suspensions with low yield stresses. 126
Figure 4.44 : Pressure gradients for 4.4 mm spheres in Kaolin/Bentonite suspensions with high yield stresses. 128
Figure 4.45 : Pressure gradients for 4.1 mm gravel in Kaolin/Bentonite suspensions. 130
Figure 4.46 : Pressure gradient estimates for 1.7 mm spheres in Kaolin/ Bentonite suspensions in laminar flow. 132
Figure 4.47 : Pressure gradient estimates for 25% 4.1 mm gravel in a Kaolin/ Bentonite suspension in laminar flow. 133
Figure 4.48 : Pseudohomogeneous pressure gradient estimates for 1.7 mm spheres in Kaolin/Bentonite suspensions in laminar flow. 137
Figure 4.49 : Magnetic particle velocities in Kaolin/Bentonite suspensions with 1.7 mm spheres. 140
Figure 4.50 : Magnetic particle velocities in low yield stress Kaolin/Bentonite suspensions with 4.4 mm spheres. 141
Figure 4.51 : Magnetic particle velocities in two significantly different Kaolin/ Bentonite suspensions with 15% 4.4 mm spheres. 142
Figure 4.52 : Magnetic particle velocities in Kaolin/Bentonite suspensions with 4.1 mm gravel. 144
Figure 4.53 : Particle velocities near the wall for 1.7 mm spheres in Kaolin/ Bentonite suspensions. 145
Figure 4.54 : Particle velocities near the wall for 4.4 mm spheres in Kaolin/ Bentonite suspensions with low yield stresses. 146
Figure 4.55 : Particle velocities near the wall for 4.4 mm spheres in Kaolin/ Bentonite suspensions with high yield stresses. 148
Figure 4.56 : Particle velocities near the wall for 4.1 mm gravel in Kaolin/ Bentonite suspensions. 149
Figure 4.57 : Particle velocities near the wall for 4 mm particles in Kaolin/ Bentonite suspensions. 150
Figure 5.1 : Finite element solution mesh. 157
Figure 5.2 : Predicted velocity and concentration profiles for 20% 0.43 mm sand in ethylene glycol at a bulk velocity of 0.93 m/s. 168

Figure 5.3 : Predicted velocity and concentration profiles for 20% 0.43 mm sand in ethylene glycol at a bulk velocity of 1.15 m/s. 169
Figure 5.4 : Predicted velocity and concentration profiles for 20% 0.43 mm sand in a 1440 mPa.s oil at a bulk velocity of 0.11 m/s. 171
Figure 5.5 : Predicted velocity and concentration profiles for 20% 0.43 mm sand in a 2380 mPa.s oil at a bulk velocity of 0.06 m/s. 173
Figure 5.6 : Predicted velocity and concentration profiles for 15% 1.7 mm spheres in a Kaolin/Bentonite suspension at a bulk velocity of 1.6 m/s. 175
Figure 5.7 : Predicted velocity and concentration profiles for 15% 4.4 mm spheres in a Kaolin/Bentonite suspension with a low yield stress at a bulk velocity of 0.8 m/s. 176
Figure 5.8 : Predicted velocity and concentration profiles for 15% 4.4 mm spheres in a Kaolin/Bentonite suspension with a 17 Pa yield stress at a bulk velocity of 1.6 m/s. 178
Figure 5.9 : Predicted velocity and concentration profiles for 15% 4.4 mm spheres in a Kaolin/Bentonite suspension with a 25 Pa yield stress at a bulk velocity of 1.6 m/s. 179
Figure 5.10 : The sensitivity of finite element velocity predictions to the specified concentration distribution with a low viscosity fluid. 181
Figure 5.11 : The sensitivity of Runge-Kutta concentration predictions to the specified velocity distribution with a low viscosity fluid. 183
Figure 5.12 : The sensitivity of finite element velocity predictions to the specified concentration distribution with a high viscosity fluid. 184
Figure 5.13 : The sensitivity of two-layer model predictions to the lower layer concentration. 188
Figure 5.14 : The effect of fluid model selection on pressure gradient predictions of the two-layer model. 190
Figure 5.15 : Magnetic particle velocities and layer velocity predictions for different interfacial friction formulations. 194
Figure 5.16 : Two-layer model pressure gradient predictions for an ethylene glycol and 20% 0.43 mm sand slurry. 200
Figure 5.17 : Two-layer model pressure gradient predictions for an oil and 20% 0.43mm sand slurry. 202
Figure 5.18 : Two-layer model pressure gradient predictions for 15% 1.7 mm spheres in a Kaolin/Bentonite suspension. 204
Figure 5.19 : Two-layer model pressure gradient predictions for 25% 1.7 mm spheres in a Kaolin/Bentonite suspension. 205
Figure 5.20 : Two-layer model pressure gradient predictions for 15% 4.4 mm spheres in a Kaolin/Bentonite suspension with a low yield stress. 207
Figure 5.21 : Two-layer model pressure gradient predictions for 15% 4.4 mm spheres in a Kaolin/Bentonite suspension with a high yield stress. 208
Figure 5.22 : Two-layer model pressure gradient predictions for 15% 4.1 mm gravel in a Kaolin/Bentonite suspension. 210

Figure 5.23 : Two-layer model pressure gradient predictions for 1.9 mm gravel and oil sand overburden in a 263 mm diameter pipe. 212
Figure 5.24 : Two-layer model pressure gradient predictions for 55 mm rock and oil sand overburden in a 263 mm diameter pipe. 213

LIST OF SYMBOLS

A	cross-sectional area
B	Bagnold number (Equation 2.25)
Bi	Bingham number ($\tau_y d/\mu_p V_-$)
C	bulk concentration (v/v)
c	local concentration (v/v)
C_c	contact load fraction (v/v)
C_D	particle drag coefficient
C_{DB}	particle drag coefficient in a Bingham fluid (Equation 2.17)
C'_{DB}	modified particle drag coefficient in a Bingham fluid (Equation 2.18)
C_{lim}	limiting concentration in lower layer (v/v)
C_{max}	maximum concentration (v/v)
C_r	in-situ concentration (v/v)
C_v	delivered concentration (v/v)
D	pipe diameter (m)
D_{eq}	hydraulic equivalent diameter (4A/S, m)
d	particle diameter (m)
f	Fanning fluid friction factor
g	acceleration due to gravity (m/s^2)
h	elevation change of pipe (Equations A.8 to A.10 , m)
Δh	change in bed height (Equation 2.28, m)
He	Hedstrom number ($D^2\tau_y\rho_f/\mu_p^2$)
I	weighted residual integral (Equation 5.2)
i	slurry headloss (m water/m)
i_w	water headloss (m water/ m)
K	constant
L	length of pipe (m)
L_{coil}	distance between magnetic pick-up coils (m)
L_e	entrance length (m)
L_{sp}	equivalent length of viscometer spindle (m)
N	beam intensity
N_0	unattenuated beam intensity
P	pressure (Pa)
ΔP	change in pressure (Pa)
Q	dynamic parameter (Equation 2.16)
R	pipe radius (m)
r	radial distance (m)
$R(x,y)$	residual equation (5.1)
R_{cup}	radius of viscometer cup (m)
R_{sp}	radius of viscometer spindle (m)
Re	pipe Reynolds number ($DV\rho_f/\mu$)

Re_p	particle Reynolds number ($dV_\infty\rho_f/\mu$)
Re_{pB}	particle Reynolds number in a Bingham fluid ($dV_\infty\rho_f/\mu_p$)
Re'_{pB}	modified particle Reynolds number in a Bingham fluid ($dV_{\infty B}\rho_f/\mu_p$)
Re_{*B}	shear velocity Reynolds number for a Bingham fluid ($Du_*\rho_f/\mu_p$)
S	perimeter length (m)
S_s	ratio of solid to fluid density (ρ_s/ρ_f)
t_{int}	interval time (s)
U_b	bulk velocity (m/s)
u_*	shear velocity (Equation 2.11, m/s)
V	velocity (m/s)
V_∞	particle settling velocity at infinite dilution (m/s)
$V_{\infty B}$	particle settling velocity at infinite dilution in a Bingham fluid (m/s)
w	local velocity in the axial direction (m/s)
x	fluid path length (Equation 3.1, m)
x_w	wall path length (Equation 3.1, m)
y	distance (m)
Y_G	yield-gravity number ($\tau_y/(\rho_s - \rho_f)gd$)
α	angle of internal friction
β	angle defining the position of the hypothetical interface
Δ	rate of deformation tensor
$\dot{\gamma}_{ij}$	shear rate at constant i in the direction j
η	effective viscosity of a non-Newtonian fluid
η_s	coefficient of sliding friction
θ	angle of outward normal to domain boundary
κ	absorption coefficient (Equation 3.1)
κ_w	absorption coefficient for the pipe wall (Equation 3.1)
λ	linear concentration (Equation 2.25)
μ	Newtonian viscosity (Pa.s)
μ_d	particle dispersive viscosity
μ_i	viscosity of element i (Pa.s)
μ_p	plastic viscosity (Pa.s)
μ_r	relative viscosity (μ_m/μ_f)
ξ	stress ratio (τ_y/τ_w)
ρ	density (kg/m^3)
T	torque (N.m)
τ	viscous stress tensor
τ_{ij}	shear stress at constant i in the direction j
τ_{sij}	interparticle stress (Pa)
τ_{sp}	shear stress on viscometer spindle (Pa)
τ_w	shear stress at the wall (Pa)
τ_y	fluid yield stress (Pa)

$\tau_{y\,min}$ minimum yield stress to support a particle (Equation 2.14, Pa)
Φ_i weighting function of element i
ϕ geometric shape function (Equation 2.35)
ϕ_i linear shape function of element i
ω angular velocity (s^{-1})

Superscript:
T vector transpose

Subscripts:
f fluid
m mixture
p particle
s solid
r,θ,z cylindrical coordinates
x,y,z Cartesian coordinates
1 upper layer
2 lower layer
12 hypothetical interface

1 INTRODUCTION

The use of slurry pipeline technology extends over a wide range of industrial applications. Besides its traditional uses, there is a continual expansion into new fields of application. While slurry flows have been investigated for many years, there are still many aspects of these flows which require further understanding before they can be exploited in industrial systems. This incomplete understanding is largely the result of the complex interactions between the flow constituents. Common applications of slurry pipeline technology include process tailings disposal, horizontal well clean-out, and both short and long distance transport of various materials such as coal and minerals. In the latter case, slurry pipelining of raw ore to a processing plant can extend the life of the plant even after local resources have been exhausted. As the scope of slurry application expands, further investigation is needed to ensure proper design and operation of these systems.

The design of a pipeline system requires a good understanding of the flow behaviour of the particular slurry being transported. Industrial pipeline systems can be very large so that overdesign is very costly while underdesign can be disastrous. In the case of a tailings pipeline, the proper selection of pump type and size, pipe size and operating velocity are critical to economical and reliable operation. The pump must be able to operate with the particular slurry and provide the required flowrate and discharge pressure. The pipe must be sized to match the flowrate and discharge pressure while producing a velocity above the

limiting value for formation of a stationary deposit.

Fine particle slurries can resemble homogeneous fluids so that pipeline design may not be overly difficult. Such mixtures are often treated as fluid continua so that the well-established design methods for liquids may be used. However when coarse particles are present, such an approach is not warranted. The coarse particles may have high settling velocities in the carrier fluid and therefore travel at a reduced velocity near the bottom of the pipe. Pipeline design for transport of these slurries must use appropriate methods to predict the deposit velocity and the pressure losses or energy consumptions.

Operation of slurry pipelines can be in either the laminar or turbulent flow regimes so an understanding of both situations is needed. The high velocities, low viscosities and large pipe diameters of many tailings disposal systems usually lead to turbulent flow. In pipelines where velocities are low, when the carrier fluid is viscous or when small pipe diameters are used, the flow can become laminar. With some slurries, changes of pipe size or velocity may result in the transition from one flow regime to another. For these slurries, a thorough understanding of the behaviour in both flow regimes is especially important for proper economic evaluation and selection of operating conditions.

The carrier fluid of a slurry may sometimes be intentionally altered to change the flow behaviour of the slurry. For example, a carrier fluid may be made more viscous in order to reduce particle settling rates with the intention of aiding the transport of the solid material. This change in fluid properties may lead to laminar flow. Laminar flows may have the additional benefits of lower fluid friction losses and pipe wear when compared to turbulent flow. However, laminar flow lacks the particle suspension capability which

turbulent flow provides and inhibits the formation of a stationary deposit.

Carrier fluids with non-Newtonian properties are of interest because they occur naturally in some industrial operations such as oil sand tailings disposal. Non-Newtonian fluids are also used in other areas such as well drilling. The effect of these carrier fluids on slurry flow needs to be addressed for system design and operation. These non-Newtonian fluids are typically of moderate viscosity so that either laminar or turbulent flow can occur depending on the application.

One type of non-Newtonian fluid which is of particular interest is that which exhibits a yield stress. Under static conditions, a fluid with a sufficient yield stress can support the immersed weight of particles so that their settling velocities are low or negligible. The well drilling industry relies on this phenomenon in the selection of a drilling mud. Besides lubricating the drill bit and carrying away cuttings, the drilling mud is able to support the cuttings so they do not settle in the vertical well bore at times when the mud flow is interrupted.

In laminar pipe flow of a fluid with a yield stress, a region of unsheared fluid exists near the longitudinal axis. It is often hoped that this unsheared region may provide some benefit to particle transport. However, at present the effect of solid particles on the behaviour of the fluid in this region and the interaction between the two phases is a source of speculation. Settling rates of particles are often used to help describe particle behaviour but their values in yield stress fluids under shear are unknown. This and other uncertainties make it unclear as to what the benefits of such a fluid would be in horizontal slurry flows which contain large particles.

Similar uncertainties exist when the slurry flow is turbulent. The effect of a yield stress on turbulent slurry behaviour is still somewhat unclear. In particular, it is unknown whether a yield stress, which is observed in laminar flow, still exists when the flow becomes turbulent.

1.1 Present work

The present work is an investigation of horizontal pipe flow of coarse particle slurries with carrier fluids which exhibit yield stresses. The intent of the work is to advance the present state of knowledge available for the design and operation of these pipelines. As such, particular attention is paid to aspects of concern for designers such as pressure losses and particle deposition. The work contains both experimental and numerical modelling components in order to address these issues and to explore their interrelationship.

The experimental work used slurries containing large (1.7 mm and 4.4 mm) glass spheres in water and in Kaolin\Bentonite clay suspensions flowing in a 52 mm diameter pipeloop. Tests were also performed with 4.1 mm gravel in the clay suspension carrier. The Kaolin\Bentonite suspensions exhibited substantial yield stresses and the flow was usually laminar. Various experimental measurements are made with each of the slurries. The experimental results are useful for evaluating predictive flow models which are intended to aid the pipeline designer.

Two flow models are considered for their usefulness in describing the behaviour of these slurries. The models are modified to account for the existence of a yield stress in the carrier fluid.

The first model considers a slurry to be a fluid continuum with a distributed

viscosity. It uses a finite element method to predict the velocity distribution in the laminar flow regime. With coarse particles present in the flow, the factors governing the concentration distribution are also examined with this model. The second model is a version of the two-layer model which has been applied previously to the laminar and turbulent flow regimes.

2 LITERATURE REVIEW

For the purpose of performing fluid flow calculations, the rheological behaviour of the fluid is expressed by a mathematical relationship which relates the applied shear stress to the shear rate. This can be stated, using general tensor notation, as

$$\tau = -\eta \Delta \tag{2.1}$$

where τ is the viscous stress tensor, η is the effective viscosity, and Δ is the rate of deformation tensor (Bird et al., 1960). For Newtonian fluids, η is merely the Newtonian viscosity. For non-Newtonian fluids, η is a function of the shear rate. The class of non-Newtonian fluids which is of particular interest here is those with yield stresses.

Yield stress fluids are characterized as deforming elastically at very low applied stresses. Once a critical minimum stress is applied, the fluid begins to flow. Fine-particle suspensions, high concentration slurries or emulsions and some polymer solutions display this behaviour. A number of continuum fluid models can be used to describe the shear stress - shear rate relationship of yield stress fluids. The most common of these are the two parameter Bingham plastic model and the three parameter Herschel-Bulkley model. The fluids used in the present investigation could be represented adequately by the Bingham fluid model.

2.1 Bingham fluid model

For a Bingham fluid, the effective viscosity in Equation 2.1 is expressed as (Bird et al., 1960):

$$\eta = \frac{\tau_y}{|\sqrt{\tfrac{1}{2}(\Delta:\Delta)}|} + \mu_p \qquad \textit{for } \tfrac{1}{2}(\tau:\tau) > \tau_y^2 \tag{2.2a}$$

$$\Delta = 0 \qquad \textit{for } \tfrac{1}{2}(\tau:\tau) < \tau_y^2 \tag{2.2b}$$

where τ_y is the yield stress and μ_p is the plastic viscosity. D.G. Thomas (1963) reported that for fine particle suspensions, these two model parameters varied with the volumetric concentration of the particles. He found that the yield stress varied with the solids concentration raised to the power 3 while the plastic viscosity increased exponentially with concentration.

It is apparent from Equation 2.2a that at high shear rates, the yield stress effect diminishes and the effective viscosity approaches the plastic viscosity. At low shear rates, the yield stress term, and therefore the effective viscosity, can become large. Equation 2.2b is the criterion defining the limit at which shear ceases and only elastic deformation occurs.

For pipe flow calculations the relationships describing the behaviour of a Bingham fluid in axial tube flow and in tangential flow in an annulus are needed. For these one dimensional shear conditions, Equations 2.1 and 2.2 reduce to:

$$\tau_{ij} = \tau_y - \mu_p \dot{\gamma}_{ij} \qquad \textit{where} \quad \tau_{ij} > \tau_y \tag{2.3a}$$

$$\dot{\gamma}_{ij} = 0 \qquad \textit{where} \quad \tau_{ij} < \tau_y \tag{2.3b}$$

where τ_{ij} is the shear stress and $\dot{\gamma}_{ij}$ is the shear rate at constant i in the direction j.

For tube flow, a force balance on concentric shells shows that the shear stress varies linearly with radial position from zero on the pipe axis to some finite value at the wall:

$$\tau_{rz} = r\frac{\tau_w}{R} \tag{2.4}$$

where τ_{rz} is the shear stress at distance r from the pipe centreline and R is the pipe radius. τ_w is the shear stress at the wall which is given by

$$\tau_w = \frac{D\Delta P}{4L} \tag{2.5}$$

where D is the pipe diameter, ΔP is the pressure drop over pipe length L. The quantity $\Delta P/L$ is the pressure gradient.

Integrating the shear rate of Equation 2.3 from the pipe centre to the pipe wall gives the velocity distribution. Integrating the velocity distribution gives the Buckingham equation which relates the bulk velocity, V, to the wall shear stress.

$$\frac{8V}{D} = \frac{\tau_w}{\mu_p}\left[1 - \frac{4\xi}{3} + \frac{\xi^4}{3}\right] \qquad \textit{where} \quad \xi = \frac{\tau_y}{\tau_w} \tag{2.6}$$

Equations 2.5 and 2.6 can be used to infer the Bingham model parameters from velocity and pressure gradient measurements. Alternatively they can be used to predict the velocity and pressure gradient relationship for a fluid whose model parameters have been inferred from independent viscometry measurements.

One of the most useful viscometers is the concentric cylinder or Couette viscometer. One version of this device has the inner spindle rotating and the outer cylinder, or cup, stationary. The fluid is restricted to tangential flow in the annular gap between the spindle and the cup. The shear stress in this device varies in accordance with the following relation:

$$\tau_{r\theta} = r^2 \frac{\tau_{sp}}{R_{sp}^2} \tag{2.7}$$

where $\tau_{r\theta}$ is the shear stress at constant r in the direction θ and τ_{sp} is the shear stress on the surface of the spindle whose radius is R_{sp}. The shear stress at the spindle is determined by a force balance to be

$$\tau_{sp} = \frac{T}{2\pi R_{sp}^2 L_{sp}} \tag{2.8}$$

where T is the measured torque on the spindle and L_{sp} is the spindle's equivalent length. For viscometers with a small gap between the spindle and the cup, the shear stress and shear rate are nearly constant. The shear rate is then given by

$$\dot{\gamma}_{r\theta} = \frac{\omega R_{sp}}{R_{cup} - R_{sp}} \tag{2.9}$$

where $\dot{\gamma}_{r\theta}$ is the shear rate at constant r in the direction θ, ω is the angular velocity in reciprocal seconds and R_{cup} is the radius of the stationary cup. Equations 2.8 and 2.9 can be used to infer the Bingham model parameters of Equation 2.3 directly. When the gap between the spindle and the cup is large, Equations 2.8 and 2.9 are not appropriate and a more rigorous approach must be used. In any case, the shear stress decreases in the gap between the spindle and the cup and a condition of incomplete shear can occur if the shear stress drops below the yield stress. This condition of incomplete shear must be considered before the viscometry results can be evaluated.

Thus far, only laminar flow of a Bingham fluid has been considered but turbulent flow is also of interest. The effect of a yield stress in turbulent flow has been the cause of considerable research. D.G. Thomas (1964) suggested that in turbulent flow of suspensions, significant deflocculation can occur as a result of the turbulent stresses. Deflocculation was believed to be highest near the pipe wall. Since the yield stress of a suspension is believed to be very dependent on the floc structure, deflocculation may lead to a reduction in yield stress.

Hanks (1978) proposed a model to predict the friction losses for yield power law fluids in pipe flow. The model predicts a smooth transition from laminar to turbulent flow and is able to predict the transition velocity between the flow regimes. The turbulent flow portion of the model uses a modified mixing length approach. The effect of the yield stress is expressed in terms of the dimensionless Hedstrom number, He, in the equations. The Hedstrom number arises naturally when the Buckingham equation (2.6) is made dimensionless and is defined as

$$He = \frac{D^2 \tau_y \rho_f}{\mu_p^2} \tag{2.10}$$

Wilson and Thomas (1985) suggested that non-Newtonian fluids which followed the Bingham or pseudoplastic fluid models, and later the yield-power law or Herschel-Bulkley model (Thomas and Wilson, 1987), cause a thickening of the viscous sublayer near the pipe wall. The increase in thickness of the sublayer is assumed to correspond to the increase in area under the rheogram relating shear stress to shear rate for the non-Newtonian fluid compared to that of a Newtonian fluid. The area under the rheogram of the non-Newtonian fluid is evaluated between a shear rate of zero and the shear rate which corresponds to the wall shear stress. This area is compared to the area for a Newtonian fluid with the same upper limit of shear stress and shear rate. Fluid behaviour in the thickened viscous sublayer is characterized by the effective viscosity of the non-Newtonian fluid evaluated at the wall shear stress. The effective viscosity of a Bingham fluid is given by Equation 2.2.

With a smooth pipe, the non-Newtonian fluid bulk velocity in the Wilson-Thomas model is given by

$$V = u_* \left[2.5 \ln Re_{*B} + 2.5 \ln \left(\frac{(1 - \xi)^2}{1 + \xi} \right) + \xi (14.1 + 1.25 \xi) \right] \tag{2.11}$$

$$\text{where} \qquad \xi = \frac{\tau_y}{\tau_w}, \quad u_* = \sqrt{\frac{\tau_w}{\rho_f}}, \quad Re_{*B} = \frac{D u_* \rho_f}{\mu_p} \tag{2.11a}$$

where u_* is the shear velocity. Wilson and Thomas compared their predictions to those of Hanks (1978) and also to other measurements and showed that their model gave better predictions.

Many investigators have conducted experiments with clay slurries. Xu et al. (1993) reported experimental measurements made with Kaolin suspensions in both laminar and turbulent flow. The Wilson and Thomas equation (2.11) was found to overpredict the observed pressure gradient somewhat in the turbulent region. It was inferred that a reduced plastic viscosity existed at the pipe wall and it was suggested that this reduction was the result of deflocculation as proposed by D.G. Thomas (1964). The intersection of the turbulent flow pressure gradient prediction with that of the Buckingham equation (2.6) for laminar flow was noted to agree well with the observed laminar to turbulent transition.

Xu et al. found that yield stress values inferred from laminar pipe flow tests and from concentric cylinder viscometry showed good agreement. However the plastic viscosities inferred from laminar pipe flows were found to be about 50% higher than the values inferred from concentric cylinder viscometry. In turbulent flow, the inferred plastic viscosities were lower than those inferred from viscometry.

2.2 Single particle behaviour in a fluid

Interactions between the fluid and solid components of a slurry can be exceedingly complex but some understanding of these interactions is needed if reliable slurry flow predictions are to be made. Particle settling velocities, which are an important aspect of the behaviour of coarse particle slurries, are difficult to predict except in the simplest cases. One

such case is the settling of a single spherical particle in a stagnant fluid. Provided the settling takes place far from system boundaries, the terminal falling velocity can be determined by equating drag and gravitational forces which gives

$$V_\infty = \sqrt{\frac{4gd(S_s - 1)}{3C_D}} \tag{2.12}$$

where V_∞ is the settling velocity at infinite dilution, g is the acceleration due to gravity, d is the particle diameter, S_s is the ratio of the solids density to the fluid density and C_D is the drag coefficient.

The drag coefficient for spheres is expressed as a function of the particle Reynolds number, Re_p, and can be given by the equations (Wallis, 1969)

$$C_D = \frac{24}{Re_p} \qquad for\ Re_p = \frac{dV_\infty \rho_f}{\mu} < 0.2 \tag{2.13a}$$

$$C_D = \frac{24}{Re_p}\left(1 + 0.15\,Re_p^{0.687}\right) \qquad for\ 0.2 < Re_p < 1000 \tag{2.13b}$$

$$C_D = 0.44 \qquad for\ 1000 < Re_p < 3 \times 10^5 \tag{2.13c}$$

Particle settling in a fluid with a yield stress is complicated by the fact that the bulk of the fluid is stagnant. It is even possible that a particle in the fluid may not settle,

depending on the value of the yield stress. The yield stress above which a particle may be supported is an important limit which needs to be determined. For a spherical particle, a force balance between its immersed weight and the vertical component of the shear stress on its surface can predict a value of the minimum yield stress required. The shear stress over the entire surface is taken to be the yield value. The minimum yield stress, $\tau_{y\,min}$, required to support the particle is then given by (Shook and Roco, 1991)

$$\tau_{y\,min} = \frac{(\rho_s - \rho_f) g d}{1.5 \pi} \tag{2.14}$$

Some workers (Beris et al., 1985 and Atapattu et al., 1988) prefer to report the balance of yield and gravitational forces in terms of the dimensionless yield-gravity group, Y_G, which is given by

$$Y_G = \frac{\tau_y}{(\rho_s - \rho_f) g d} \tag{2.15}$$

From Equation 2.14, the critical yield-gravity number would be 0.212. Ansley and Smith (1967) remarked that the shear stress around the sphere is not well understood and may not be uniformly the yield stress. They provided experimental evidence that particle support occurred at yield-gravity numbers in the range of 0.068 to 0.084. Beris et al. (1985) performed particle settling calculations using a finite element method and obtained a yield-gravity number of 0.143 at the point where a particle no longer settled in the fluid. Atapattu et al. (1988) commented on this large variation of the critical yield-gravity number in the

literature and suggested that it may be in part due to selection of yield stress values. They suggested that the yield stress obtained from fitting the Bingham model to flow data was not appropriate and that the true yield stress should be measured at very low shear rates.

When settling of a particle in a yield stress fluid does occur, and the yield stress is below the required minimum value, the drag coefficient is observed to be higher than for a comparable Newtonian fluid. Ansley and Smith (1967) investigated this phenomenon and proposed a fluid flow pattern around a settling sphere. The flow pattern took the shape of a toroid whose section was centred along the equator of the sphere. Outside this toroid, the fluid was assumed to be solid-like. Beris et al. (1985) in their finite element analysis used a free boundary approach which predicted a flow pattern around the sphere which was the same shape as that which Ansley and Smith had proposed.

Based on the flow pattern, Ansley and Smith suggested that the drag coefficient could be correlated with what they called the dynamic parameter which contained inertial, viscous and yield stress components. The dynamic parameter, Q, can be expressed by

$$Q = \frac{Re_{pB}}{1 + KBi} \tag{2.16}$$

$$\textit{where} \qquad Re_{pB} = \frac{dV_{\infty}\rho_f}{\mu_p}, \qquad Bi = \frac{\tau_y d}{\mu_p V_{\infty}} \tag{2.16a}$$

In this expression Re_{pB} is the particle Reynolds number in a Bingham fluid, Bi is the Bingham number and K is a constant which Ansley and Smith evaluated as $7\pi/24$. V_{∞} is

related to the drag coefficient by Equation 2.12.

Atapattu et al. (1988) interpreted Ansley and Smith's results and other data in the literature to give the following correlations between the drag coefficient in a Bingham fluid, C_{DB}, and the dynamic parameter, Q.

$$C_{DB} = \frac{34}{Q} \qquad for\ Q < 20 \tag{2.17a}$$

$$C_{DB} = 0.40 \qquad for\ Q > 200 \tag{2.17b}$$

It was noted that at values of Q below approximately 10, the numerator of Equation 2.17a should more correctly be 24. They reasoned that the yield stresses may have been incorrectly evaluated in the original data. The correlations as reported do not give a smooth transition between ranges of Q. Atapattu et al. also commented on the difficulty of making experimental measurements for small values of Q when the yield stress is high and the settling velocity is low.

Dedegil (1986) suggested that a modified Reynolds number should be used to correlate drag coefficients. The modified Reynolds number included the yield stress and a characteristic shear rate of settling. This modified Reynolds number is identical to the dynamic parameter of Ansley and Smith if the constant K is taken to be unity. Retaining the notation of Ansley and Smith, Dedegil correlated his drag coefficient, C'_{DB}, by

$$C'_{DB} = \frac{24}{Re'_{pB}(1 + Bi)} \qquad for\ Re'_{pB}(1 + Bi) < 8 \tag{2.18a}$$

$$C'_{DB} = \frac{22}{Re'_{pB}(1 + Bi)} + 0.25 \qquad for\ 8 < Re'_{pB}(1 + Bi) < 150 \tag{2.18b}$$

$$C'_{DB} = 0.4 \qquad for\ Re'_{pB}(1 + Bi) > 150 \tag{2.18c}$$

where the new Bingham fluid particle Reynolds number, Re'_{pB} is given by

$$Re'_{pB} = \frac{d V_{\infty B} \rho_f}{\mu_p} \tag{2.19}$$

$V_{\infty B}$ is the single particle settling velocity in a Bingham fluid which is different from that given by Equation 2.12. In his analysis, Dedegil included a yield stress contribution to the settling velocity equation. This additional component represented the particle support provided by the yield stress. He proposed

$$V_{\infty B} = \sqrt{\frac{2}{C'_{DB}\rho_f}\left[\frac{2}{3}(\rho_s - \rho_f) g d - \pi \tau_y\right]} \tag{2.20}$$

The aforementioned work on particle settling in yield stress fluids was restricted to unsheared fluids where particles were observed to settle. Therefore, the yield stress conditions which prevent settling were not satisfied in those studies. In the present work, the yield stresses are high enough for particles to be supported in unsheared fluids. It may not be reasonable to expect that the aforementioned relationships are capable of predicting the settling rates of particles in a sheared fluid.

A.D. Thomas (1979) commented on the settling of coarse particles in a horizontally flowing Bingham fluid. He noted that the resistance to settling changes over the pipe cross sections because of variations in shear rate and that the fluid properties could change as a result of deflocculation. He suggested that particle settling will always occur in a shearing Bingham fluid.

Lockyear et al. (1984) investigated pipe flow of high concentration slurries consisting of coarse coal transported in a fine coal suspension. Viscometry indicated that the carrier fluid could be represented by the Bingham fluid model. Slurry tests were used to infer the yield-gravity number (Equation 2.15) for the carrier fluid above which coarse particle deposition did not occur. The critical yield-gravity number they obtained was 0.1. It should be noted that the high concentration of the slurries in these tests may have also inhibited deposit formation.

Atapattu et al. (1988) suggested that particle settling observed in a high yield stress fluid under shear is due to the time dependent nature of viscoplastic fluids. They remarked that under shear, a new and decreased equilibrium yield stress may exist. Where the yield stress inferred from viscometry or static tests may be adequate to support a particular particle in a stagnant fluid, the equilibrium yield stress of a sheared fluid may not be sufficient.

2.3 Multiparticle systems

Particles immersed in a fluid increase the overall resistance to shear. This increase is often expressed by the relative viscosity, μ_r, which is given by

$$\mu_r = \frac{\mu_m}{\mu_f} \tag{2.21}$$

where μ_m is the mixture viscosity and μ_f is the Newtonian fluid viscosity. The relative viscosity is a function of the volumetric concentration of solids in the mixture and use of this concept has traditionally been restricted to Newtonian fluids.

Einstein (1906) found a theoretical expression for the relative viscosity of a dilute suspension of spheres in laminar flow. The relationship accounts for the distortion in the shear field caused by the presence of the particles but neglects any of the more complex particle behaviour which becomes important at higher concentrations. His expression was

$$\mu_r = 1 + 2.5c \tag{2.22}$$

where c is the solids concentration. Equation 2.22 is probably only valid for values of c less than 10% but provides an important theoretical basis for slurry flow research.

The more complex behaviour at high concentrations is beyond satisfactory theoretical explanation so that it is common to formulate the relative viscosity by including additional terms of a power series to Einstein's equation (2.22). The additional terms might have some theoretical justification but the coefficients are empirically fitted to experimental data. D.G. Thomas (1965) reported an expression based on data for suspensions of spheres taken from numerous sources for cases where particle settling was negligible and particle size effects were minimized. Thomas found

$$\mu_r = 1 + 2.5c + 10.05c^2 + 0.00273 \exp(16.6c) \qquad (2.23)$$

In Equation 2.23 the first two terms are obtained from Einstein's equation, the third term accounts for hydrodynamic particle-particle interactions and the fourth term accounts for the motion of particles from one shear plane to another. Thomas' equation was shown to agree very well with the data he presented up to a solids volume fraction of 0.60.

Gillies et al. (1994) reevaluated the higher order terms using concentric cylinder viscometry of sand particles suspended in oil. They reported

$$\mu_r = 1 + 2.5c + 10c^2 + 0.0019 \exp(20c) \qquad (2.24)$$

The relative viscosities given by this relationship are slightly higher at high concentrations than those determined with Equation 2.23.

At high solids concentrations, the particle-particle interactions in sheared flow are important beyond their contribution to an increased resistance to shear. These interactions contribute to particle dispersion which becomes important to slurry transport. Bagnold (1954) investigated this dispersion using neutrally buoyant spheres in Newtonian fluids. Suspensions of differing concentrations were sheared in an annulus which allowed measurement of the shear stress and normal stress of the mixture on the inner annular wall. The stress measurements allowed the particle shear stress and normal dispersive stress to be quantified.

Bagnold identified two regimes in which either particle inertia or macroviscous behaviour dominated. The two regimes were distinguished by the value of the dimensionless

number which Shook and Roco (1991) referred to as the Bagnold number, B.

$$B = \frac{\rho_s \lambda^{\frac{1}{2}} d^2 \dot{\gamma}_m}{\mu_f} \tag{2.25}$$

where λ is the linear concentration and $\dot{\gamma}_m$ is the shear rate of the mixture. The linear concentration is given by

$$\lambda = \left[\left(\frac{C_{max}}{c} \right)^{\frac{1}{3}} - 1 \right]^{-1} \tag{2.25a}$$

where C_{max} is the maximum volumetric concentration, and c is the local concentration.

In the "macroviscous" regime where the Bagnold number is less that 40, Bagnold suggested that the particle shear stress and normal dispersive stress are proportional to the shear rate and the linear concentration raised to the 3/2 power. For large Bagnold numbers, in the "particle inertial" regime the particle shear stress and normal dispersive stress were found to be proportional to the square of the shear rate and the square of the linear concentration. In both regimes, the exponent of the linear concentration showed some deviation when the linear concentration exceeded 12.

The particle shear stress and the normal particle dispersive stress were related by

$$\tau_{sij} = \tau_{sii} \tan \alpha \tag{2.26}$$

where τ_{sij} is the particle shear stress, τ_{sii} is the normal particle dispersive stress and α is the

characteristic angle of internal friction for the material which is dependent on the flow. Bagnold found experimentally that tan α was 0.32 in the inertial regime and 0.75 in the macroviscous regime.

Leighton and Acrivos (1987) investigated shear-induced particle migration which occurred during viscous flow of concentrated suspensions in a concentric cylinder viscometer. Migration of the neutrally buoyant particles in the suspension was inferred from the change in viscosity of the suspension with time. Two forms of migration were reported, which they proposed were the result of diffusion mechanisms. The first diffusion mechanism occurred in a direction normal to the plane of shear and whose diffusion coefficient was proportional to the square of the particle diameter and to the shear rate. Particles were found to diffuse from the region of high shear in the annular gap to the region of reduced shear in the fluid reservoir of the viscometer. This was observed as a decrease in the suspension viscosity with time of shear. The concentrations in the annular gap and fluid reservoir were initially the same.

The second diffusion mechanism occurred parallel to the velocity gradient which existed across the viscometer gap. This was inferred from changes in the suspension viscosity shortly after shear had begun. It was suggested that the change resulted from a rearrangement of the solids concentration within the gap which may have initially been non-uniform in the radial direction. The diffusion coefficient here was similar to that suggested for the first diffusion mechanism where it is proportional to the shear rate and the square of the particle diameter.

It was suggested that the shear-induced diffusion mechanism would cause a

concentration profile when a variation in shear rate existed such as in a pipe or channel. For flow in a channel where the shear stress is proportional to distance from the wall, the concentration gradient was predicted to be

$$\frac{dc}{dy} = \frac{K_\sigma}{K_1}\left[\frac{1}{\mu_m}\frac{d\mu_m}{dc}\right]^{-1}\frac{1}{y} \qquad (2.27)$$

where c is the local concentration, y is the distance from the centre of the channel and μ_m is the suspension viscosity which may be of the type given by Equation 2.23. The parameters K_σ and K_1 are diffusion related and are weak functions of concentration. Values of 0.6 for both parameters were suggested. Equation 2.27 predicts a region of reduced concentration near the channel wall where the shear rate is highest.

Leighton and Acrivos (1986) used the shear induced diffusion concept to investigate the resuspension of initially settled particles when they were exposed to viscous shear. In the accompanying experiments, particles suspended in a fluid were placed in an annular parallel plate device and the particles were allowed to settle. The lower portion of the annulus held the suspension material and was rotated while the upper surface was held stationary and in contact with the fluid above the settled bed. The relative velocity between the two segments of the device resulted in shear being applied to the fluid which was translated to the settled bed. The force required to hold the upper portion of the device stationary could be measured and the shear quantified. The amount of particle dispersion was quantified by the equilibrium bed height.

It was proposed that the particle dispersion they observed was the result of the shear

induced diffusion they had previously noted (Leighton and Acrivos, 1987) and was believed to oppose the tendency of the particles to settle. The change in bed height was found to be approximately

$$\frac{\Delta h}{d} \approx 2 \frac{\tau}{dg(\rho_s - \rho_f)} \tag{2.28}$$

where Δh is the change in the bed height, d is the particle diameter, τ is the shear stress which is assumed to be constant in the resuspension layer, g is the Acceleration due to gravity and ρ_s and ρ_f are the solid and fluid densities. Experimental evidence was provided which supported their analysis and Equation 2.28.

2.4 Pipe flow of coarse particle slurries

To design a slurry pipeline system, the flow behaviour of the mixture must be predicted in order to assess capital equipment requirements and to specify the optimum operating conditions. A number of modelling approaches can be used to accomplish this.

Durand and Condolios (1952) recognized the importance of distinguishing between homogeneous and heterogeneous slurries in developing design procedures. They undertook experimental testing for a wide range of slurry flow parameters. From these results, they presented a headloss relationship for the flow of non-depositing heterogeneous slurries. Their equation was

$$i = i_w \left[1 + K_D C_v \left(\frac{gD(S_s - 1)}{V^2 \sqrt{C_D}} \right)^{3/2} \right] \tag{2.29}$$

where i is the headloss of the mixture, i_w is the headloss of the carrier fluid, K_D is a constant which can be taken to be 81, C_v is the delivered solids concentration, g is the acceleration due to gravity, D the pipe diameter, S_s is the solid to fluid density ratio, V is the bulk velocity, and C_D is the particle drag coefficient. The particle drag coefficient appears in the equation as a consequence of incorporating the particle settling velocity in order to account for variations in headloss with particle size and fluid viscosity. The headlosses, i and i_w, are expressed in units of meters of water per meter of pipe and are given by

$$i = \frac{(\Delta P/L)}{\rho_w g} \tag{2.30}$$

where $\Delta P/L$ is the pressure gradient, and ρ_w is the density of water.

Equation 2.29 was important because it showed the general relationship between the slurry headloss and parameters such as bulk velocity, delivered concentration, solids density and particle drag coefficient. To illustrate this, Durand and Condolios pointed out that for particles larger than 2 mm, the drag coefficient in water is nearly constant. Their experimental results showed that the slurry headloss did not change significantly when particle size increased above 2 mm.

Newitt et al. (1955) developed an equation for predicting headlosses for heterogeneous suspensions in pipe flow which was similar to Durand's but had a theoretical basis. They began by suggesting that the headloss of the mixture, i, could be considered to be the sum of the fluid, i_w, and solid, i_s, headloss components.

$$i = i_w + i_s \tag{2.31}$$

For flows with a moving bed, the solids headloss component of Equation 2.31 was formulated in terms of sliding friction which is velocity independent. The resulting equation was

$$i = i_w \left[1 + K_N C_v \frac{gD(S_s - 1)}{V^2} \right] \tag{2.32}$$

or

$$i = i_w + 2fK_N C_v (S_s - 1) \tag{2.33}$$

where K_N is a constant reported to be 66 by Newitt and f is the fluid Fanning friction factor. The quantity $2fK_N$ is approximately 0.8. It was noted that although Equation 2.33 was derived for "moving bed" flow, it also worked for flow by saltation. In comparison with Durand's equation (2.29), the exponent of the bulk velocity is now reduced to 2. As a result, Equation 2.33 predicts a headloss curve which is parallel to the water flow curve. This was found to be in agreement with some of the experimental results reported by Newitt.

For pseudohomogeneous flow, particles were assumed to be dispersed throughout the pipe cross-section so that the mixture could be treated as a fluid but with the mixture density. The headloss is then given by

$$i = i_w [1 + C_v (S_s - 1)] \tag{2.34}$$

For these flows, the headloss curves diverge from the water headloss because of the increased mixture density due to the presence of the solids.

The importance of the work of Newitt et al. was the mechanistic approach they used to describe slurry flows and how these descriptions were used to develop predictive equations which did not rely heavily on empirical constants. While their results were similar to those of Durand and Condolios (1952), their approach was more rigorous.

Independent experimental results can be shown which illustrate the "heterogeneous suspension" headlosses which Newitt described. These experimental results are taken from an investigation of the transport of sand in pipelines performed at the Saskatchewan Research Council (Shook et al., 1973). In contrast to the results presented by Durand and Condolios and Newitt et al., the pressure gradients reported here were obtained for slurries with constant in-situ concentrations as opposed to constant delivered concentrations.

Figure 2.1 shows the pressure gradients for heterogeneous suspensions of sand in water. The pressure gradient curves are approximately parallel to the water pressure gradient curves at high velocities. The solids are stratified and roughly follow the behaviour predicted by Equation 2.32.

Figure 2.2 shows the pressure gradient for sand in a moderately viscous fluid (ethylene glycol). For the glycol alone, the flow is laminar below 1.3 m/s. At low and moderate concentrations, the possibility of laminar flow complicates the interpretation of the low velocity data where moving dunes were observed. At high velocities, the pressure gradients diverge from the fluid values. It will be recalled that Newitt had ascribed this behaviour to pseudohomogeneous slurries. At the highest concentration, this

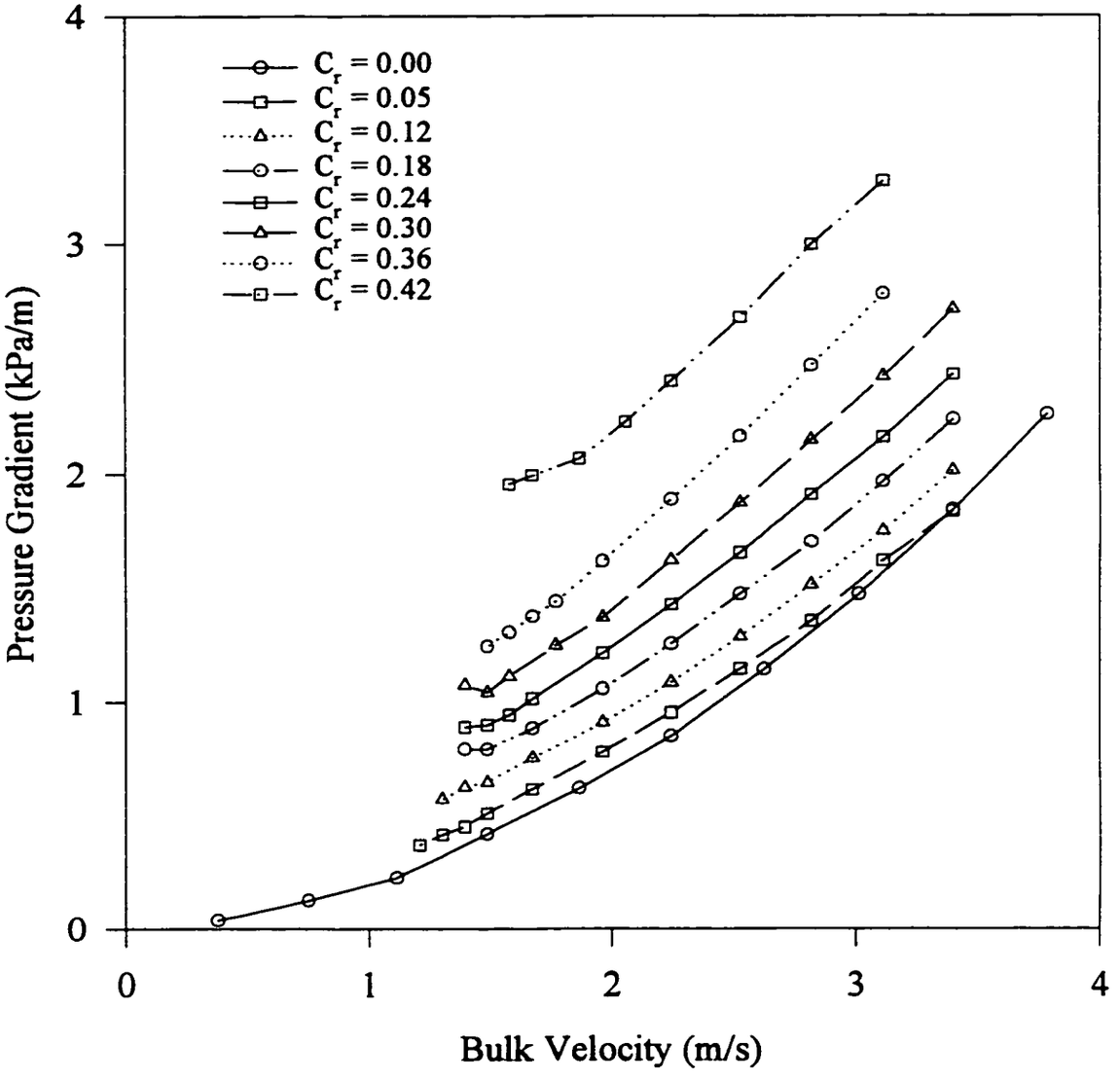

Figure 2.1 : Pressure gradient of 0.18 mm sand in water flowing in a 53 mm diameter pipe (Shook et al., 1973).

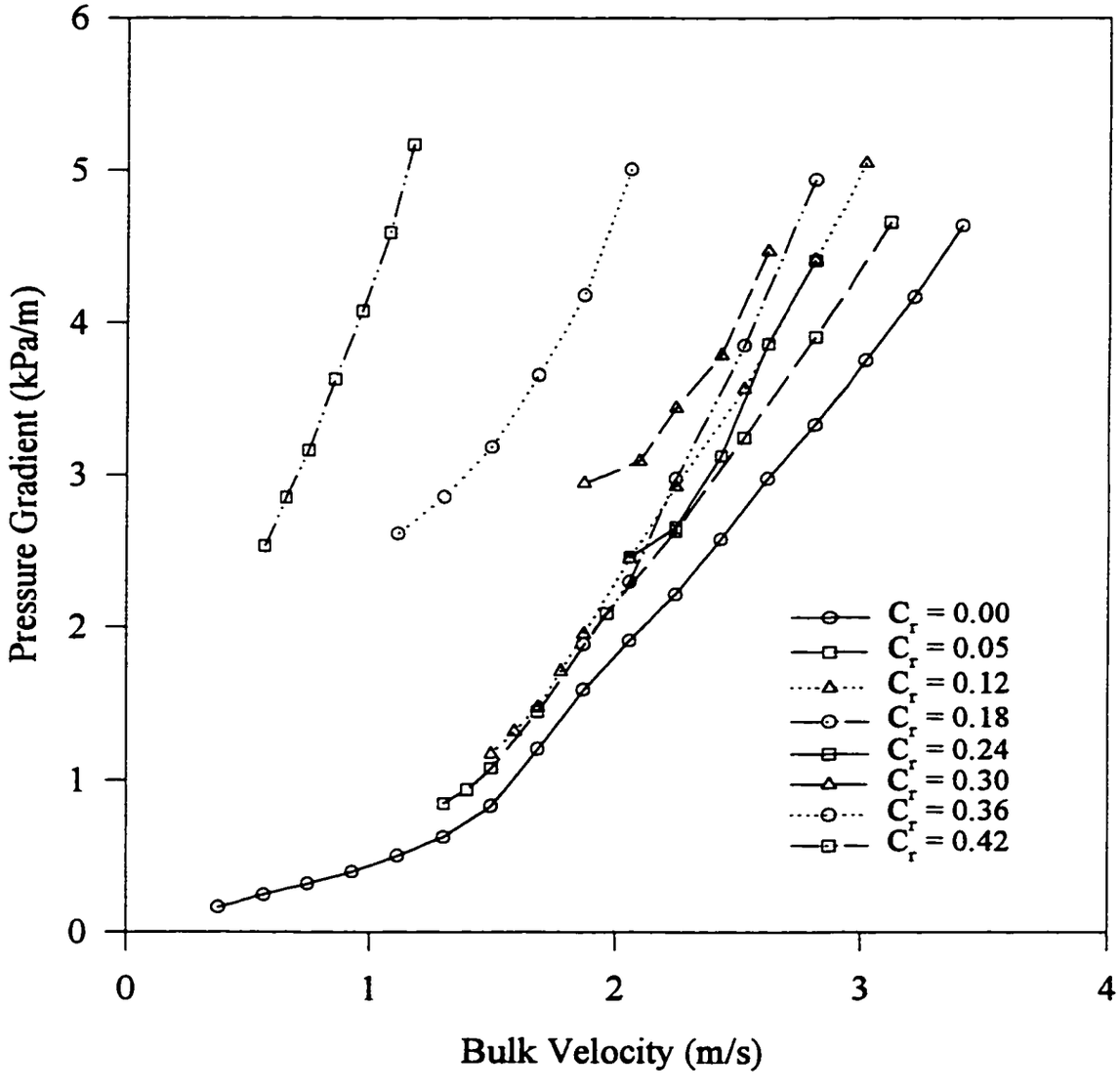

Figure 2.2 : **Pressure gradient of 0.18 mm sand in ethylene glycol flowing in a 53 mm diameter pipe (Shook et al., 1973).**

pseudohomogeneous behaviour seemed to exist in laminar flow where the pressure gradient is nearly directly proportional to the bulk velocity.

2.4.1 Two-layer model

Newitt's equations (2.32 and 2.33) can be viewed as elements of an early version of the so called two-layer model which considers fluid and solids contributions to the overall pressure gradient separately. More recent use of the two-layer concept began with Wilson (1976) and is still actively being pursued by many workers. In this model, material and momentum balances are used to predict pressure gradients and component flowrates for turbulent slurry flows. The success of the two-layer model in describing a wide range of flow conditions is attributed to its mechanistic foundation.

In the two-layer model, the flow is visualized as consisting of two superimposed layers which contain different solid/liquid mixtures. The parameters used in the model are shown in Figure 2.3. The upper layer contains fluid and the solid particles which are suspended by fluid lift forces to produce the in-situ concentration C_1. The lower layer contains fluid, suspended solids and the solid particles which are supported by contact with the wall. The volume fraction of the suspended particles in this layer is also C_1. The fraction of particles supported by contact with the wall is denoted as C_2. In this lower layer, the two solids fractions, C_1 and C_2, combine to give a limiting concentration, C_{lim}. The fraction of the total solids which is supported by the wall in the lower layer is referred to as the contact load fraction, C_c.

An empirical correlation is used to specify the contact load fraction which exists in the lower layer. This fraction is velocity-dependent. Newitt et al. (1955) had considered

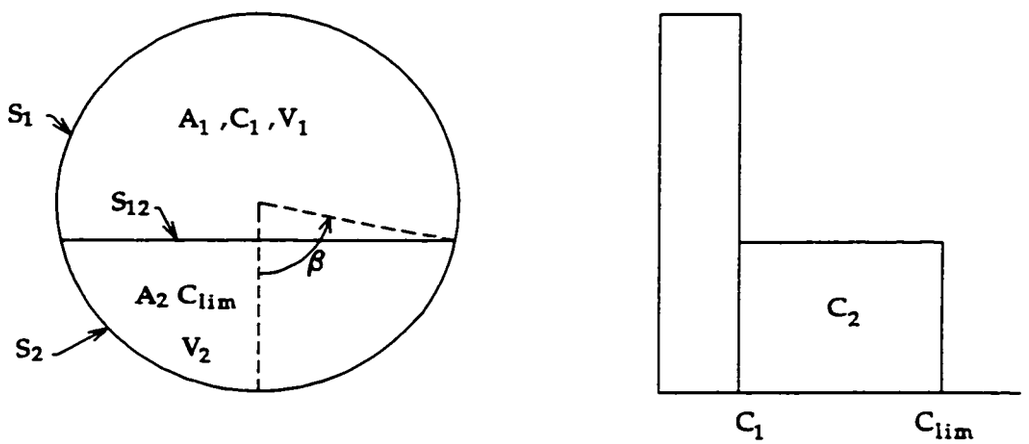

Figure 2.3 : Conceptual representation of the two-layer model.

cases where the slurry headloss curves were observed to converge towards the water headloss with increasing velocity. This behaviour is reflected in the two-layer model by a decrease in the contact load fraction. In cases where the contact load fraction is predicted to be nearly constant with velocity, as with large particles, the headloss is predicted to remain parallel to the water headloss curve. This prediction also agrees with observations of Newitt regarding flows with a "moving bed". The lower layer concentration limit is also determined empirically.

Friction on the upper boundary S_1 is assumed in the model to be pseudohomogeneous friction which resembles fluid friction. Along the lower boundary S_2 friction is assumed to be due to both fluid-like friction and Coulombic friction of the particles supported by contact with the wall. The additional friction component in the lower layer causes the lower layer velocity, V_2, to be less than the upper layer velocity, V_1. This difference provides an impelling force on the lower layer. At the interface, whose position is defined by the angle β, the friction between the layers determines the difference in velocity between the two layers.

Shear stresses on the boundaries are formulated using friction factors and the associated layer velocities. The fluid friction factors are determined using conventional correlations. The friction at the interface is based on a modified Colebrook friction factor for a rough surface. This friction factor is important in determining the relative velocities of the two layers. A correctly specified interfacial friction will give the correct layer velocities and therefore, the correct delivered concentration for the actual in-situ concentration. In practice, it may be difficult to quantify the interfacial friction experimentally since it requires

measuring the delivered concentrations and this can be difficult with large pipelines.

The additional Coulombic friction component in the lower layer is assumed to be velocity independent. This friction is evaluated from the interparticle stress which is due to the immersed weight of the solids. Because the solids concentration is assumed to be constant throughout the lower layer, this stress increases linearly with depth. At the wall, the normal stress is used to calculate the shear stress in terms of a coefficient of sliding friction. The equations which comprise the two-layer model are given in Appendix A.

2.4.2 Laminar flow of coarse particle slurries

When the carrier fluid becomes sufficiently viscous, the flow can become laminar. When this occurs the turbulent lift forces which led to the suspension of a portion of the coarse particles, denoted as C_1 in the two-layer model, do not exist. Any particle dispersion must then occur by a different mechanism.

A.D. Thomas (1979) considered the transport of coarse particles in Newtonian and non-Newtonian carrier fluids where the flows were sometimes laminar. In laminar flow, Thomas suggested that the particles should always settle to a position near the bottom of the pipe so that all the particles should contribute Coulombic friction. At low bulk velocities, the particles would form a stationary bed. At the point of incipient motion, the impelling force from the pressure gradient and the force at the interface balance the Coulombic friction of the particle bed. The pressure gradient for this condition is given by

$$\frac{\Delta P}{L} = 2\eta_s C_{lim} g(\rho_s - \rho_f)\phi \qquad (2.35)$$

where η_s is the coefficient of sliding friction between the particles and the pipe wall, C_{lim} is

the concentration in the lower layer, and ϕ is a geometric function which depends on the height of the lower layer. Thomas remarked that this result shows that the pressure gradient at incipient motion is independent of pipe diameter and so transport by laminar flow can become uneconomical with increasing pipe diameter. As pipe size increases, the bulk velocity needed to produce the pressure gradient required for incipient bed motion becomes quite large.

At pressure gradients above the deposition limit, particle motion was observed to follow some sort of saltation or moving bed mechanism which Thomas believed could also be adequately described by a two-layer model for laminar flow.

Thomas reported that tests using a clay suspension to produce a Bingham plastic carrier fluid showed that slurry behaviour was qualitatively similar for both Newtonian and non-Newtonian carrier fluids. The pressure gradient observed at deposition was lower than was predicted with the Bingham carrier fluid and it was believed that the lower layer concentration was somewhat reduced in this case. Thomas could not be certain that this effect was not the result of an insufficient entry length for the pipeloop but offered an alternative explanation. He suggested that the reduced lower layer concentration resulted from the coarse particles being held apart by the compressive nature of the clay flocs. The lower pressure gradients during flow and at deposition were attributed to this effect. It was also suggested that the deposition pressure gradient with the Bingham carrier fluids may be pipe size dependent since the clay flocs may be destroyed by the high shear rates in small diameter pipes. If this is true, the deposition pressure gradient would be lower in pipes of large diameter.

Laminar flow pressure gradient predictions for stratified slurries were made by Shook (1980) using a distributed viscosity and a two-layer model approach. The distributed viscosity method assumed the particles settle to form a high concentration region near the bottom of the pipe which could be treated as a shearing continuum and whose viscosity was increased by the concentration of particles. Pressure gradients for these flows were obtained using a finite element method. At low velocities, observed pressure gradients were higher than predicted by this method. The higher friction losses were assumed to be the result of a contact load mechanism like that in the two-layer model discussed previously.

To apply the two-layer model to laminar flow, the fluid friction factors at the pipe wall for each of the layers and at the interface were derived for Newtonian fluids using a least squares solution of the Navier-Stokes equations for flow in segmental channels. The friction factors were given as:

$$f_1 Re_1 = 15.375 - (1.676 + 0.007416\ \beta)\frac{V_{12}}{V_1} \tag{2.36a}$$

$$f_{12} Re_1 = 17.964 - 0.0154\ \beta - (9.981 + 0.0242\ \beta)\frac{V_{12}}{V_1} \tag{2.36b}$$

$$f_{2m} Re_2 = \left(\frac{\mu_f}{\mu_m}\right)\left[15.375 - (1.676 + 0.007416\ (180 - \beta))\frac{V_{12}}{V_2}\right] \tag{2.36c}$$

where f_1 is the friction factor on the upper pipe boundary, f_{12} is the friction factor at the interface, f_{2m} is the friction factor for the fluid component of the friction along the lower pipe boundary, Re_1 and Re_2 are the Reynolds numbers for the upper and lower layers, V_1, V_{12}, and V_2 are the velocities of the upper layer, at the interface and in the lower layer respectively, μ_f is the Newtonian fluid viscosity, μ_m is the mixture viscosity in the lower layer and β is the angle defining the position of the interface. β is measured in degrees for these equations. The Reynolds numbers for the two layers are given by

$$Re_1 = \frac{D_{eq1} V_1 \rho_1}{\mu_1}, \qquad Re_2 = \frac{D_{eq2} V_2 \rho_1}{\mu_m} \tag{2.37}$$

where D_{eq1} and D_{eq2} are the hydraulic equivalent diameters of the two layers, ρ_1 is the density and μ_1 the viscosity of the mixture of fluid and suspended particles. To simplify the solution of these equations, V_{12} was assumed to be 1.5 V_2 and the concentration in the lower layer was taken to be 0.50.

The distributed viscosity and two-layer model predictions were compared to observed results for sand in ethylene glycol slurries in terms of relative effective viscosities. It was shown that the two-layer model gave higher pressure drops or effective viscosities than the distributed viscosity predictions for the same in-situ concentration. At low velocities, the observed effective viscosities were higher than the distributed viscosity predictions. Some observed pressure drops were even higher than the two-layer model predicted. As the velocity was increased, the observed effective viscosity decreased and

eventually became lower than the distributed viscosity predictions. This suggested that a change in the flow regime occurred, such as particle migration away from the pipe wall.

Maciejewski et al. (1993) used the two-layer model to interpret results for transport of large rocks in clay suspensions with yield stresses in a 263 mm diameter pipeline. They commented on the possibility of a clay suspension being viscous enough for laminar flow to arise and that the interfacial friction factor and the contact load fraction could be quite different from those in turbulent flow. The situation is further complicated by the existence of a yield stress in the suspension which has an unknown effect on these parameters.

In these experiments, concentration profiles were available which allowed the layer concentrations and the interface location to be specified empirically. This removed the need to use a correlation to calculate the lower layer limiting concentration. Use of a magnetic particle to determine the velocity of the lower layer allowed the interfacial friction factor to be inferred. These values showed substantial scatter but indicated that an increase in yield stress caused a decrease in the difference in velocity between the layers or, alternatively, an increase in the interfacial friction factor. Maciejewski et al. suggested that the increase may follow the form proposed by Dedegil (1986) for settling of a single particle. They suggested correlating the friction factor with the modified Reynolds number to include the Bingham number as in Equation 2.18. They noted that the interfacial friction factor appeared to be higher in fluids with yield stresses in both laminar and turbulent flow, suggesting that the yield stress remains an important parameter in both flow regimes.

Frankiewicz et al. (1991) studied the laminar and turbulent transport of concentrated fine coal in oil slurries. Both laminar and turbulent pressure gradient measurements indicated

lower effective viscosities in pipe flow than were measured in a concentric cylinder viscometer. This was believed to be the result of a layer of decreased particle concentration at the pipe wall. This was supported indirectly by pitot tube measurements which showed flatter velocity distributions in laminar flow. The turbulent velocity profiles were symmetrical about the pipe axis as would be expected for uniformly distributed particles. However, there was a distinct asymmetry in the laminar flow velocity profiles implying increased resistance to motion in the lower part of the pipe. No concentration variation was detected in these flows.

In another study, Ghosh and Shook (1989) interpreted experimental results for coarse particles transported in power law fluids using the two-layer model. The contact load fractions at a number of flow conditions were inferred from laminar and turbulent headloss measurements. These fractions were found not to change abruptly at the laminar to turbulent transition and seemed largely insensitive to increases in the fluid effective viscosity.

The two-layer model was found to be useful for predicting pressure gradients in the laminar and turbulent flow regimes for particles transported by these power law fluids. At low bulk velocities, negative values of the lower layer velocities were predicted and these indicated that the interfacial friction factor used in the predictions was incorrect for viscous fluids.

2.4.3 Alternative flow models

Other methods have been used to make predictions for coarse particle slurry flows and therefore warrant consideration. A simple method, which allows pressure drop and pipe size scale-up calculations to be made, is to characterize the slurry with a fluid model such

as the Bingham model and use pipe flow equations developed for that fluid model. This method can often be used with homogeneous, or nearly homogeneous slurries where the solid particles are fine and uniformly dispersed in the pipe. There have been some attempts to extend this method for use with coarse particle slurries. This may be appropriate for highly concentrated slurries where the coarse particles are distributed fairly uniformly during flow but since Coulombic friction is insensitive to pipe diameter there is a large degree of uncertainty about the reliability of scale-up predictions.

Laminar pipe flow of highly concentrated coal slurries was investigated by Lockyear et al. (1984). The slurries consisted of coarse coal in a fine coal suspension carrier. The fine coal suspensions in these tests were characterized by concentric cylinder viscometry and were found to follow the Bingham fluid model. The yield stresses and plastic viscosities of the carrier fluids were correlated with the fine coal volume fractions.

Pipeline pressure gradients of the coarse coal slurries, which were measured over a range of velocities, showed considerable scatter which was attributed to the heterogeneous nature of these slurries. The overall behaviour of the data appeared to follow the Bingham fluid model as predicted by the Buckingham equation (2.6). This observation led Lockyear et al. to express the observed behaviour of the different slurries in terms of apparent yield stresses and apparent plastic viscosities. Equations were obtained which correlated the apparent model parameters with the carrier fluid parameters and the solids volume fractions of the mixtures and the carrier fluids. It was remarked that the apparent parameters exhibited a great deal of scatter and the correlations did not reduce to the carrier fluid parameters when extrapolated to a coarse solids fraction of zero.

Pressure gradient predictions made using the correlated model parameters with the Buckingham equation (2.6) were compared to the observed pressure gradients. Differences varied between ±20% in most cases but even larger variations were seen in some cases. Use of this simple fluid model would be even less appropriate at lower solid concentrations where the flow would likely be more stratified.

The opposite extreme of the simple fluid models are complex numerical flow simulations which require computers to obtain a solution. One such method is described by Hsu et al. (1989). Hsu used a finite element method to predict velocity and concentration distributions of non-colloidal slurries in horizontal pipelines. While this method is based on the continuity and momentum equations for the elements within the solution domain, their solution required the use of many correlations involving numerous empirical coefficients. Numerical simulation results were compared to experimental results found in the literature and the agreement was very good for the cases shown.

3 EXPERIMENTAL PROCEDURES AND CONDITIONS

3.1 52 mm diameter pipeloop tests

The 52 mm diameter pipeloop used for most of the experimental work was used previously in various configurations (Ghosh, 1989 and Sumner, 1992). The present layout (Figure 3.1) was selected to promote flow stabilization upstream of the sensing equipment. This was important because particle settling might not be rapid in the fluids to be studied. The loop was constructed primarily from 2 inch (nominal) aluminum pipe with acrylic pipe being used for the observation section of the loop.

Flow was provided by a 3"x2" rubber lined centrifugal pump (Linatex Canada Inc., Montreal, PQ). Power came from a 7.5 horsepower electric motor which rotated at a fixed speed of 1150 rpm. The electric motor was connected to a Roto-Cone variable diameter pulley (Dana Corporation, Elgin, IL) which drove the pump. Downstream of the pump outlet was a two-inch pinch valve which allowed the operator to produce velocities lower than could be achieved by the variable cone drive alone. This was followed by a bypass valve and hose which allowed short circuiting of the flow through the stand tank just upstream of the pump for solids loading. This bypass hose was also used during clean-out. The pump outlet was 0.55 m below the elevation of the rest of the pipeloop so a short vertical section was needed. A two-inch magnetic flowmeter (Foxboro Company Ltd., Montreal, PQ) was located 1.3 m downstream of the vertical section.

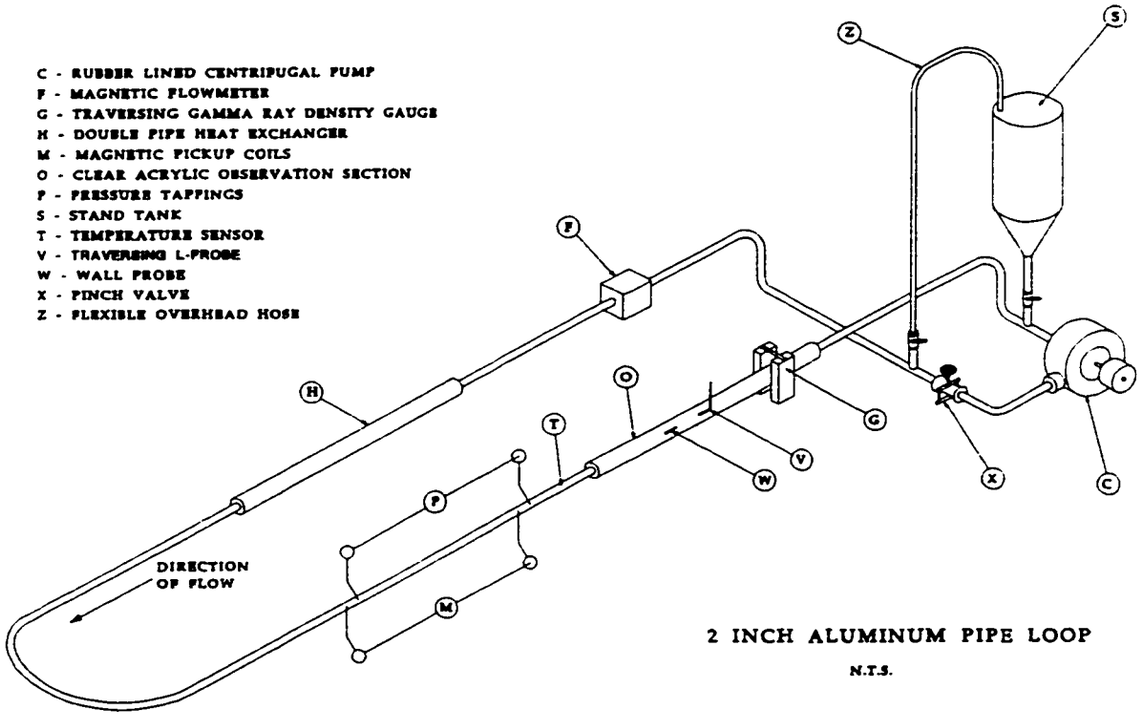

Figure 3.1 : 52 mm diameter test pipeloop.

Following the flowmeter was a double pipe heat exchanger used to maintain isothermal operation of the loop. Friction losses were expected to be substantial so heat removal was considered to be essential. A long return bend then directed flow back along the front of the loop where most of the sensing equipment was located. The pressure loss pipe section was located 4.4 m or 83 pipe diameters downstream of the long return bend. Flow stabilization was expected to occur primarily along the initial 10.8 m leg of the pipeloop with only minimal disturbance caused by the 0.65 m radius long return bend.

The entrance length needed for laminar flow of a Newtonian fluid to develop in a pipe can be taken to be (Shook and Roco, 1991)

$$\frac{L_e}{D} = 0.062\,Re \tag{3.1}$$

Where L_e is the necessary entrance length, D is the pipe diameter and Re is the pipe Reynolds number. Chen et al. (1970) suggested that with Bingham fluids, the entrance length can be correlated using the plastic viscosity to determine the pipe Reynolds number. They also suggested that the coefficient on the right hand side of Equation 3.1 decreases as the ratio of the yield stress to the wall shear stress increases and the velocity profile becomes flatter.

A conservative estimate of the entrance length can be made for the test pipeline using Equation 3.1 and the transition Reynolds number (2100) for a Newtonian fluid. The required entrance length is estimated to be 6.9 m. Therefore, the initial approach length, the long return bend and the final approach length of the pipeloop used here probably ensured

that the flow was fully developed at the pressure drop and observation sections.

Pressure losses were measured using a variable reluctance differential pressure transducer (Validyne International Inc., Northridge, CA). The transducer was connected to two pressure tappings on the pipe placed 2.69 m apart. Changes to the transducer's reluctance were converted into a direct current voltage with a signal demodulator. The diameter of this section of pipe was measured volumetrically and found to be 52.4 mm.

An acrylic pipe section containing two conductivity probes was placed downstream of the pressure drop section. The first probe was an L-shaped intrusive probe capable of being positioned along the vertical pipe axis with a traversing mount. The second probe was embedded in the wall at the bottom of the pipe. A 1.13 m approach section was located between the inlet to the acrylic section and the conductivity probes. The diameter of the acrylic pipe was slightly smaller than the rest of the pipe used at 50.4 mm.

A vertically traversing gamma ray densitometer was located downstream of the conductivity probes. The position of the gamma ray device relative to the pipe was measured using a precision dial depth gauge (Mitutoyo Corporation, Tokyo, Japan).

Following the gamma ray device, an elevation change was required to return the flow to the pump inlet. A stand tank was located just upstream of the pump to provide net positive suction head and to allow loading of the pipeloop.

Voltage signals from the magnetic flowmeter and pressure transducer demodulator were monitored with a computer (Digital Equipment Corporation, LSI-11, Maynard, MA) and an analog to digital converter (Data Translation Inc., Marlboro, MA). The data acquisition program is given in Appendix B. Three measurements, each consisting of one

thousand individual readings, were averaged to obtain the recorded values for pressure drop and velocity. The time needed to complete each measurement was approximately one minute.

The temperature of the pipeloop was monitored using a digital thermistor (Fisher Scientific Limited, Ottawa, ON) attached to the outside of the aluminum pipe and covered with insulation.

3.2 Magnetic particle velocity

To determine the mean particle velocity, and thereby the delivered solids concentration, a number of small magnets were encapsulated with epoxy resin and ground as nearly spherical as possible. Brass filings were blended with the epoxy to increase the bulk density of the particles. The particle average diameters were between 3.7 mm and 4.7 mm and their densities ranged between 2.33 g/cc and 2.92 g/cc. These particles resembled closely the 4.4 mm spheres used in the experiments.

To detect the passage of a single magnetic particle, two short wire sensor coils were wound over the pressure drop pipe section of the test pipeloop. The location of these coils is shown in Figure 3.1. The separation between coils was 3.06 m. These coils each contained 150 turns of copper wire.

Figure 3.2 shows the equipment used to measure the magnetic particle velocities. Passage of the magnetic particle through a coil induced a small voltage which was then amplified. The amplifiers were constructed in the Chemical Engineering department electronics shop. Each amplifier input included a low pass filter to reduce the high frequency noise that existed in the laboratory. The amplifier gain was approximately 100. The resulting

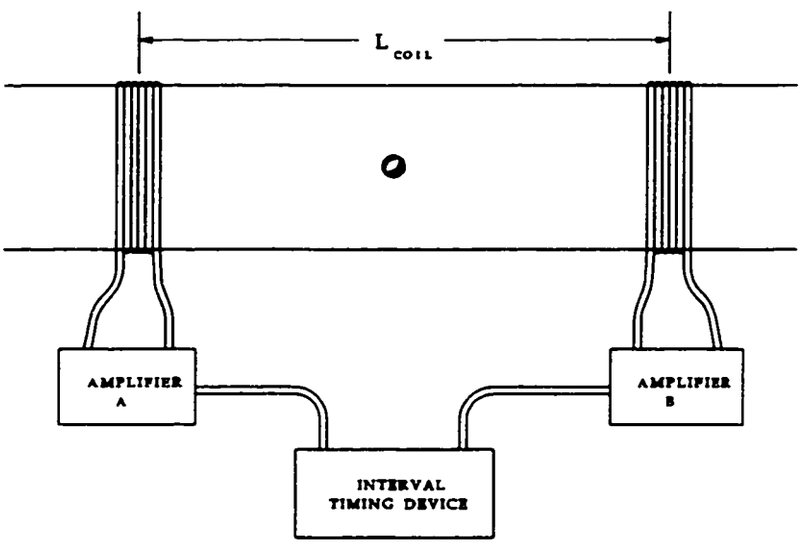

Figure 3.2 : Magnetic particle detection and timing system.

signals were in the one to three volt range and depended on the position of the magnetic particle in the pipe cross section, the orientation of the magnet poles and the velocity of the particle. The amplified signals started and stopped a counter/timer (Model CM-52, Analog Digital Research). The coil separation, L_{coil}, and the interval time, t_{int}, allowed calculation of the time-average axial velocity of the magnetic particle.

3.3 Velocity probe

The electrical conductivity of a two phase mixture depends on the local concentration of the two phases and their individual conductivities (Perry and Green, 1984). This property has been exploited previously to measure local particle velocities in flowing mixtures (Sumner, 1992) . An electrical field is established between relatively large electrodes and two pairs of sensor electrodes are placed in the field. Changes to the local conductivity which result from the passage of particles in close proximity to the sensor electrodes result in a variation in the potential between these electrodes.

Because the two pairs of sensor electrodes are located a small axial distance apart, the two electrical signals are quite similar. The signals will exhibit a small time difference owing to the time required for the particles to travel the distance between them. The signals also have some random variation due to the changes in the positions of the particles relative to one another. Provided the electrodes are close to one another and flow is predominantly in the axial direction this random variation should be small. To determine the time difference in the signals and to reject the random variation, a cross-correlation of the two signals is performed.

In the present work, two conductivity probes were used. The first was the L-shaped

intrusive probe which was constructed from 4.8 mm diameter stainless steel tubing. This probe was mounted on a vertical traversing assembly (United Sensor & Control Corp., Watertown, MA) which allowed the determination of particle velocity profiles on a vertical axis of the pipe. This probe and the associated electronics are shown in Figure 3.3. The two sensor electrode pairs of the L-probe were embedded in epoxy resin for electrical isolation from the probe body. The electrode pairs had an axial separation of 9.6 mm with the first electrode pair being located 45.8 mm from the probe tip. The sensor electrodes were spaced approximately 1 mm apart. The electric field is generated by applying a direct current potential (5-8 volts) between the field electrode and the probe body which acted as the grounding electrode. Signals from the sensor electrodes were amplified and observed using an oscilloscope (Advance Electronics Ltd., Essex, England). These amplified signals were then cross-correlated using a digital signal analyzer (Model 5830B, Rockland Scientific Corp., Rockleigh, NJ).

The second probe was embedded in the wall at the bottom of the acrylic pipe. The sensor electrode pairs of the wall-probe were separated axially by 9.75 mm. Field and ground electrodes were also embedded in the wall on either side of the sensor electrode pairs. The electronic signal processing circuit required for this probe was the same as for the L-probe. The acrylic pipe which contained these probes was slightly smaller in diameter (50.4 mm) than the rest of the pipeloop. Bulk velocities were corrected for this diameter difference and also for the presence of the L-probe in the cross section.

3.4 Gamma ray densitometer

The gamma ray densitometer uses a Cesium 137 source with a collimated beam to

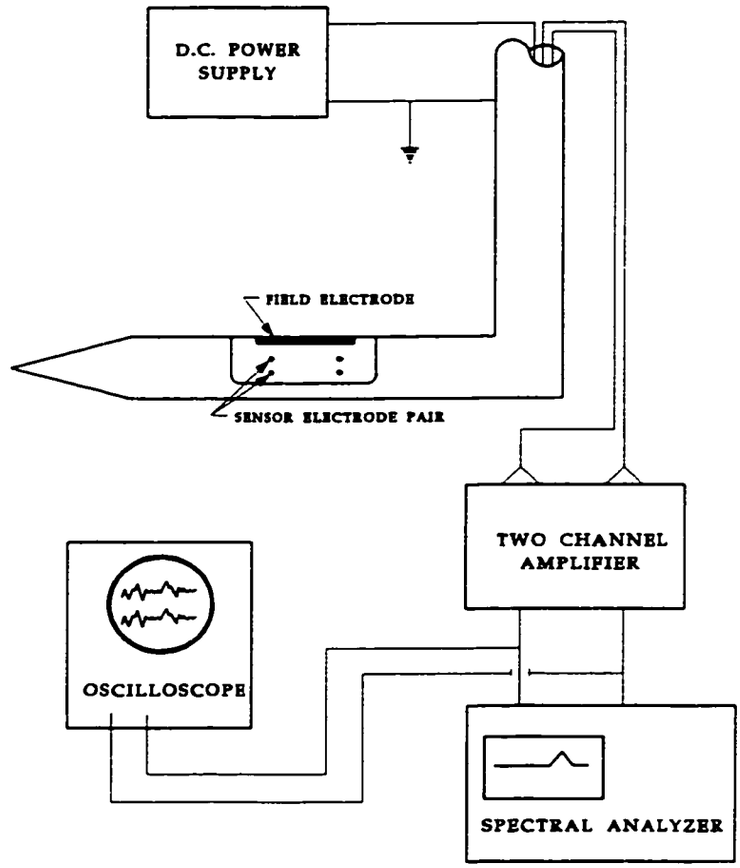

Figure 3.3 : Conductivity L-probe and associated electronics.

detect changes in the total absorbance along the path between the source and a scintillation counter. Total absorbance along the path is dictated by Lambert's law. For a two phase mixture in pipe flow, Lambert's law can be stated as:

$$\frac{N}{N_o} = \exp\left[- \kappa_w x_w - \kappa_f x(1 - c) - \kappa_s x c \right] \qquad (3.2)$$

In Equation 3.2, N is the measured intensity, N_o is the unattenuated intensity, κ_w, κ_f and κ_s are the wall, fluid and solid absorption coefficients, x_w denotes the path length of the beam through the pipe wall, and x denotes the path length through the pipe interior. Both x_w and x are functions of position. The wall absorbance contribution $\kappa_w x_w$ is determined by performing a traverse with an empty pipe. The path length of the chord inside the pipe is determined from another traverse with the pipe full of a fluid of known absorption coefficient. The mean concentration of solid particles along the chord can then be determined from the above relationship using the absorption coefficients of the two phases (Shook and Roco,1991). These coefficients must be measured independently using a sample cell of known dimensions.

A schematic drawing of the gamma ray densitometer and its associated electronic equipment is shown in Figure 3.4. The scintillation crystal and photomultiplier tube were manufactured by Ekco Electronics Ltd. The remaining electronic components were obtained from EG&G Ortec (EG&G Canada Ltd., Markham, ON). The scintillation counter photomultiplier requires a high voltage bias supply to generate a signal which can be detected. The signal occurs as a number of discrete pulses and is amplified further

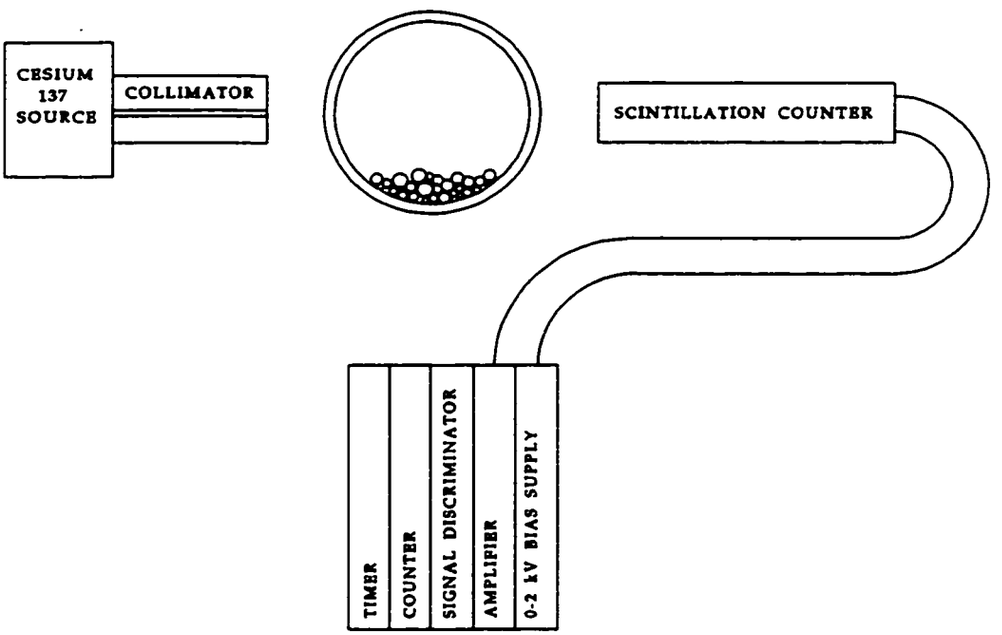

Figure 3.4 : Gamma ray densitometer and associated electronics.

electronically. This signal is then discriminated to remove event levels which are outside the range associated with the gamma rays of interest. The events which are within the acceptable range are reproduced at a standard voltage level and pulse width. These pulses are then counted for the time duration selected with the timer.

3.5 Magnetic flowmeter

Bulk velocities were determined with a Foxboro magnetic flowmeter. The meter consists of two components; a flowtube and a transmitter. The flowtube is a section of non-conducting pipe surrounded by an electromagnet which generates a magnetic field perpendicular to the pipe axis. A pair of sensor electrodes embedded in the pipe wall detects the small voltage generated by the flow of the conductive medium through the magnetic field. The transmitter demodulates and amplifies the sensor electrode signal into a direct current voltage which is proportional to the mean velocity over the pipe cross section (Shercliff, 1962). The voltage produced was recorded by computer and converted into a velocity using a linear relationship. The slope and intercept of this relationship were determined by calibration of the flowtube and transmitter. The transmitter was calibrated using a Foxboro E96 calibrator which simulates the output of a flowtube in operation. Once the transmitter had been calibrated, the flowtube was calibrated by measuring the volume of water which passed through it over a given time period. Flow was maintained steady over this period and the flowmeter output was monitored.

3.6 Concentric cylinder viscometer

In order to characterize the fluid during the experiments, a Haake Rotovisco RV 3 concentric cylinder viscometer (Haake, Inc., Saddle Brook, NJ) was used. The system

included an MK 50 measuring head and an MV I sensor. Output from the device was recorded graphically on a Hewlett-Packard 7040A X-Y Recorder. The viscometer included a temperature cell surrounding the sample cup. The temperature cell was connected to a circulating water bath thermostat.

3.7 Test conditions

3.7.1 Kaolin/Bentonite suspensions

A Kaolin clay suspension was chosen for the transport fluid because it was known to follow the Bingham fluid model closely (Xu et al. 1993). It was planned to vary the fluid parameters by changing the Kaolin content of the suspension. The Kaolin suspension was obtained from the Saskatchewan Research Council following tests they had performed with it. It had been made by the addition of dry Kaolin clay to tap water. The suspension was diluted until it contained 17.5% solids by volume and had a density of 1300 kg/m^3. At this concentration, concentric cylinder viscometry indicated the yield stress was 16 Pa and the plastic viscosity was 18 mPa.s. This suspension was stable when circulated alone in the pipe but problems were encountered following the addition of spheres in the first slurry tests.

To minimize air entrainment, the glass beads were wetted with some of the suspension prior to addition. Nevertheless, some air entrainment occurred and this air was difficult to remove because of the high yield stress of the slurry. Air collected in the pump cavity and decreased its efficiency to the point where the flowrate of the slurry was reduced. Increasing the pump speed in an attempt to flush the air from the pump led to pump cavitation and higher gas contents. High pump speeds at reduced efficiency dispersed the gas into fine bubbles which resisted coalescence in the viscous suspension. Significant air

content in the suspension was evident visually after the fluid was allowed to sit for a day.

The dispersed air also appeared to increase the effective viscosity of the suspension significantly. However it was found that the shear produced by flow at low velocities released the air slowly to the top of the pipe where it could be removed from a bleed port.

At this point the pipeloop was left standing for two and one half months while other work was performed. At the end of this time, the suspension had a low yield stress and plastic viscosity. Significant amounts of dry Kaolin clay were then added to increase these parameters. When the suspension contained 30% solids by volume, and a density of 1500 kg/m^3, the yield stress was still lower than required (3 Pa).

In order to induce a significant change in the slurry, small amounts of Bentonite clay were then added. This produced significant increases in the yield stress and the plastic viscosity. The resulting Kaolin/Bentonite suspension had a yield stress that was able to support the smaller (1.7 mm) of the coarse particles when the fluid was stationary. However, the fluid characteristics were found to change gradually with time. These changes were probably due to the high shear produced by flow in the pipe and repeated passage through the pump. In subsequent tests, Bentonite was added when necessary to increase the yield stress. Suspension density, solid content, and rheology were monitored carefully during the experiments.

3.7.2 Solid material

Large glass spheres were chosen for several reasons: their simple geometry, their resistance to wear, their relatively uniform size, and their high settling velocities. Two sizes were used in these experiments. The larger spheres were −4+5 mesh (4.4 mm median

diameter) and the smaller ones were -10+12 mesh (1.7 mm median diameter). Their density was measured as 2470 kg/m^3.

Experiments were also conducted using narrowly screened gravel obtained locally. The gravel was all -4+6 mesh (4.1 mm median diameter) before the tests. Particle degradation was evident from a shift in the size measured after the tests and also by an increase in the fines content of the suspension. Following the tests, a sample of the transported gravel was washed over a No. 70 mesh screen and then air dried. The size distribution obtained from dry screening of the washed gravel is shown in Table 3.1. The degradation of the large particles to the smaller sizes and the generation of fine material resembles that which was reported by Gillies (1993) and indicates the difficulty of conducting prolonged tests with relatively large angular particles in small diameter test loops.

3.7.3 Test matrix

The two phase tests performed in the two inch diameter test pipeloop at the University of Saskatchewan are listed in Table 3.2.

Table 3.1 : Particle size distribution of gravel following tests.

Mesh No.	Opening Size (mm)	Percent Retained (w/w)	Cumulative Retained (w/w)
4	4.76	0.3	0.3
6	3.36	66.8	67.1
8	2.38	27.1	94.2
12	1.68	2.8	97.0
18	1.00	1.8	98.8
35	0.50	0.7	99.5
-35		0.4	99.9

Table 3.2 : Test conditions for two inch diameter pipeloop.

Solid Component			Fluid Component		
Material	Median Size (mm)	In-situ Volume Fraction	Material	Yield Stress (Pa)	Plastic Viscosity (mPa.s)
-10+12 mesh glass spheres	1.7	0.15	Water	0	1
		0.25			
		0.15	Kaolin/ Bentonite	6.5	110
		0.25		5.6	110
-4+5 mesh glass spheres	4.4	0.15	Water	0	1
		0.25			
		0.15	Kaolin/ Bentonite	4.1	65
				17	62
				25	80
		0.25		3.4	59
-4+6 mesh gravel	4.1	0.15	Kaolin/ Bentonite	5.3	97
		0.25		6.3	120

4 EXPERIMENTAL RESULTS AND DISCUSSION

4.1 Concentration profiles for large spheres in water

The slurries composed of the glass spheres in water were always in turbulent flow. Settling velocities of the particles in water were calculated using Equations 2.12 and 2.13 to be 0.44 m/s for the 4.4 mm spheres and 0.23 m/s for the 1.7 mm ones. These high settling velocities led to stratified flows which can be seen in the concentration profiles shown in Figures 4.1 and 4.2. These settling velocities can be used with the correlation proposed by Gillies et al. (Equation A.6) to determine the contact load fraction used in the two-layer model. Gillies' correlation was based on data gathered with angular particles. At a bulk velocity of 1.0 m/s, the contact load fractions for the 4.4 mm and 1.7 mm spheres are predicted to be 0.96 and 0.92 respectively. At 2.5 m/s, the contact load fractions are 0.90 and 0.82 for the two sizes.

The concentration profiles, measured using the gamma ray densitometer, all exhibit the same general shape with a nearly constant high concentration near the bottom of the pipe and a falling concentration region above that. This will be seen more clearly as individual cases are considered. At the lower concentrations, the concentration distribution is approximately exponential. In the transition region the gradient was nearly linear for the cases studied here.

It is observed that the concentration profiles do not change significantly in the

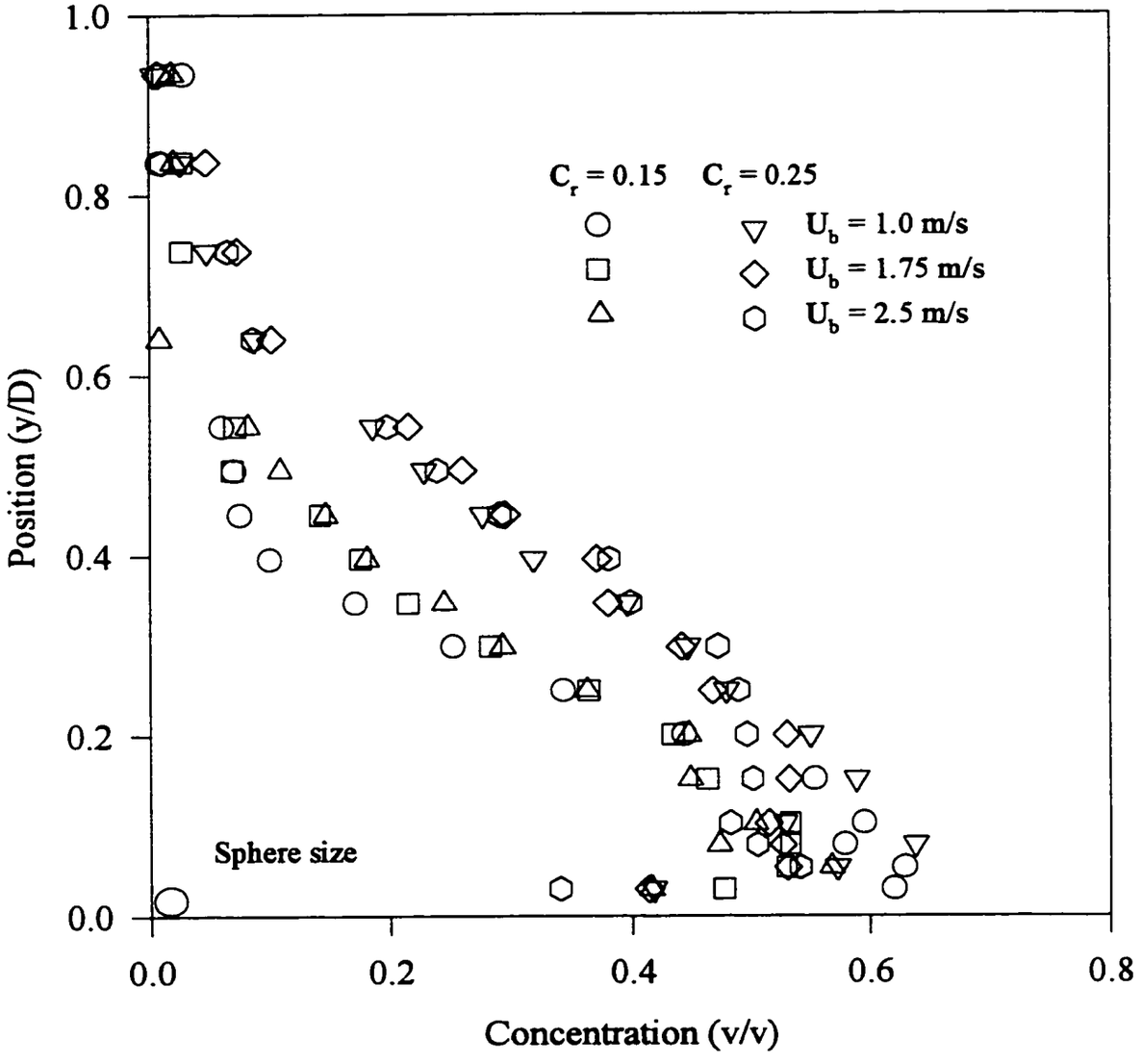

Figure 4.1 : Concentration profiles in a 53 mm pipe for 1.7 mm glass spheres in water.

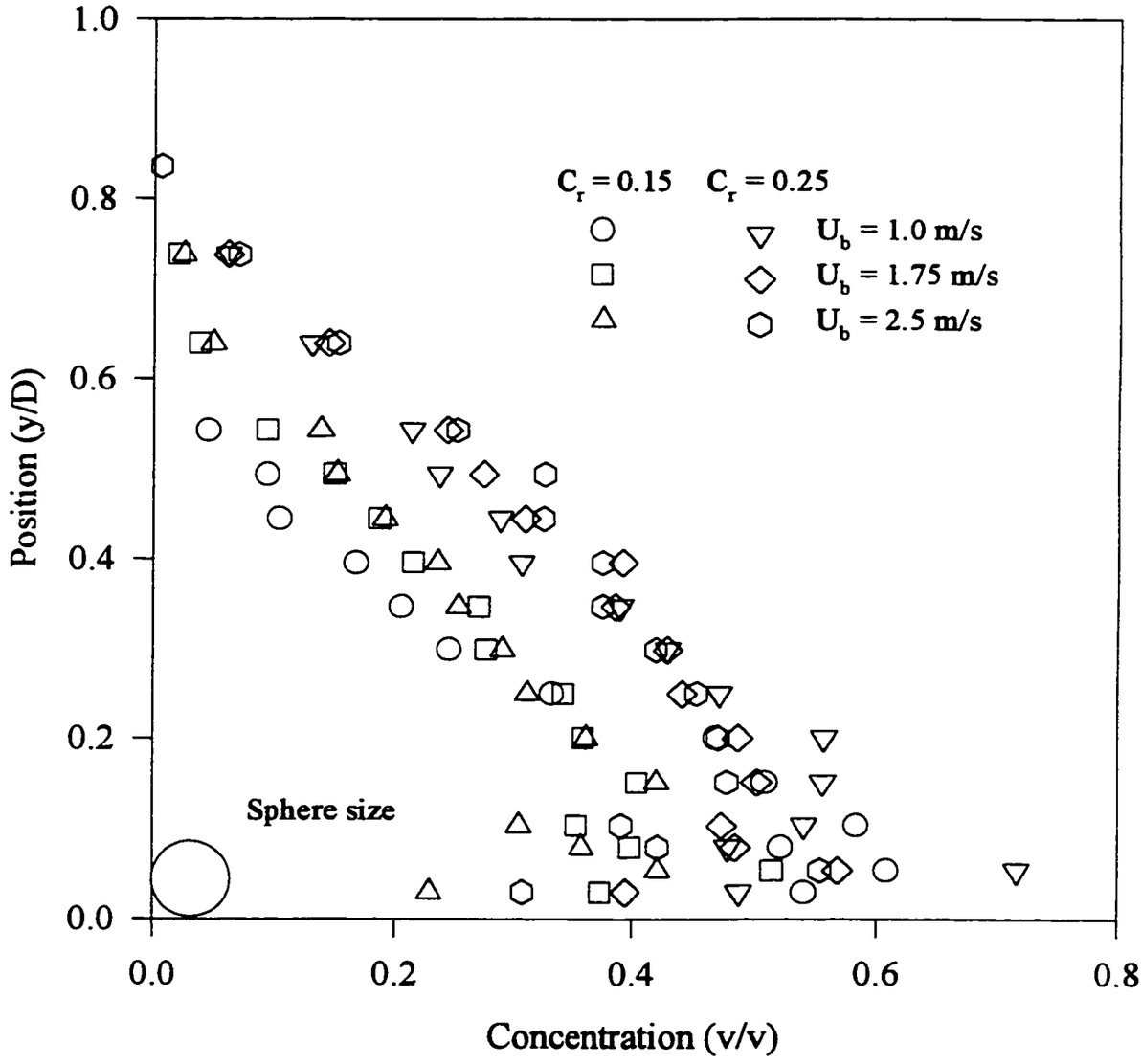

Figure 4.2 : Concentration profiles in a 53 mm pipe for 4.4 mm glass spheres in water.

velocity range of 1.75 m/s to 2.5 m/s. The highest concentrations are slightly lower in the 2.5 m/s profiles than in the 1.75 m/s ones. The profiles obtained at 1.0 m/s show still higher concentrations near the bottom of the pipe. The concentration decreases more rapidly with elevation at 1.0 m/s than at the higher velocities at an in-situ concentration of 0.15. The concentration gradients at all velocities were about the same when the in-situ concentration was increased to 0.25.

Near the bottom of the pipe, the concentration distributions are not monotonic. A zone of high concentration (hereafter called a moving bed) is present in this region. The apparent scatter in the measurements is due to the large size of the particles, as indicated by the inset circles, and to the short gamma ray path length. A distinct concentration variation, which is roughly sinusoidal in shape, can be seen for the first few particle diameters above the bottom of the pipe. This variation is similar to that found when large particles are placed in containers (Shook and Roco, 1991). Since these concentrations are time averaged measurements it suggests that the particle arrangement in the layer near the wall is highly stable. The high concentrations at the lowest positions decrease only slightly with increasing velocity suggesting that the bottom layer moves as a sheet.

4.1.1 Particle size and in-situ concentration effects

Particle size effects on the concentration profiles are most evident in the moving bed region. This is seen in Figure 4.3 for a bulk velocity of 1.75 m/s with an in-situ concentration of 0.15. The larger 4.4 mm spheres show a lower concentration in the bed. In the dispersion region, the 4.4 mm particles had a slightly higher concentration at the same elevation. The two particle sizes showed similar concentration gradients in the dispersion

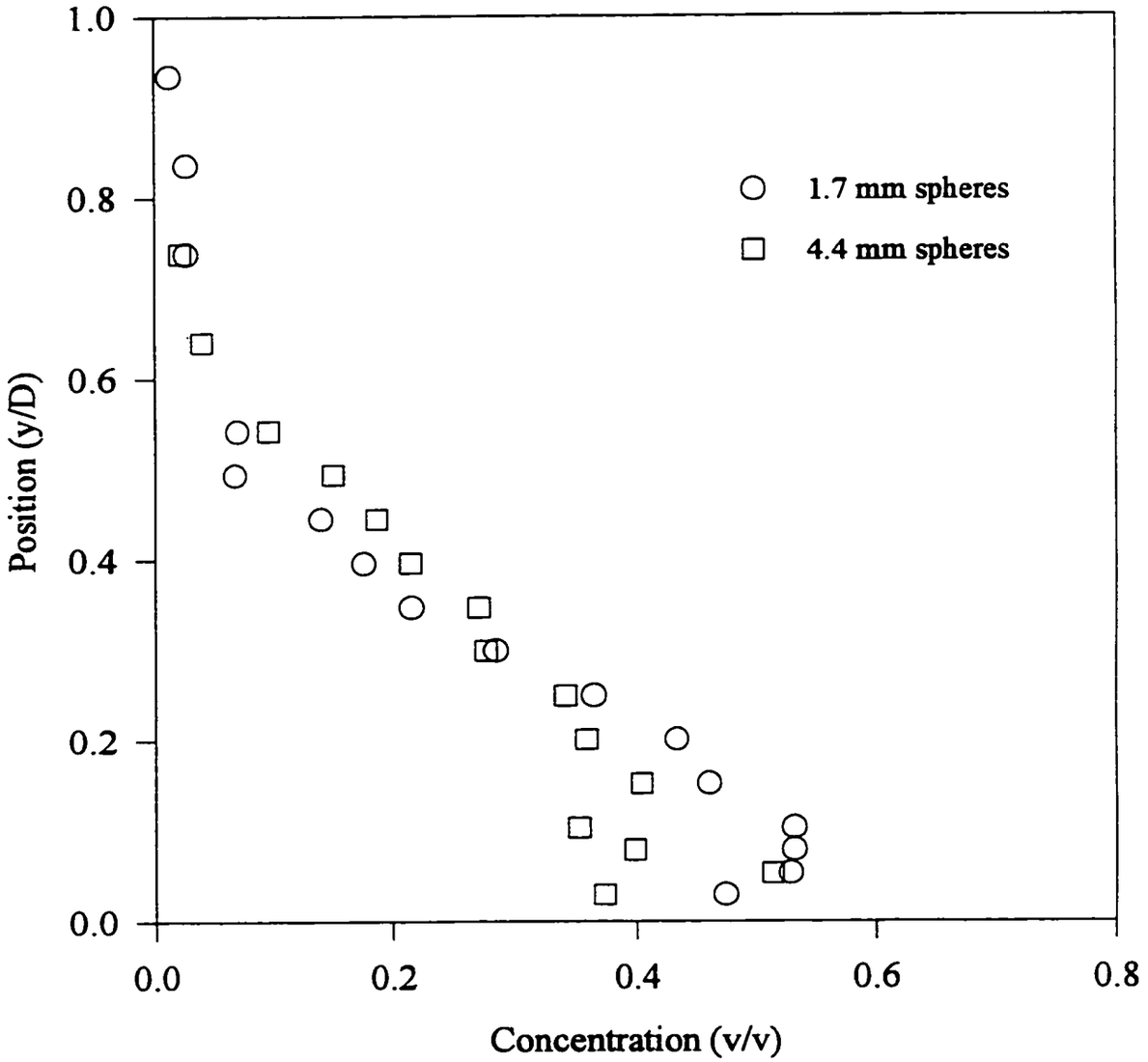

Figure 4.3 : **Concentration profiles for spheres in water at an in-situ concentration of 0.15 and a bulk velocity of 1.75 m/s.**

region.

Similar observations were made for an in-situ concentration of 0.25 at a bulk velocity of 1.75 m/s but the effects were less pronounced. The concentration profiles for the two particle sizes are shown in Figure 4.4 for this condition. The profiles are nearly the same with only a slight decrease in bed concentration for the larger 4.4 mm particles.

Figure 4.5 shows the effect of increasing the particle concentration from 0.15 to 0.25 with the 1.7 mm spheres. The decreasing concentration regions above y/D = 0.2 appear to have similar slopes for the two mean concentrations. The slurry with an in-situ concentration of 0.25 has a thicker high concentration region of particles near the bottom of the pipe. The additional thickness is approximately 0.12 pipe diameters and the two cases have the same maximum concentration of 0.53.

The effect is similar for the 4.4 mm spheres as illustrated in Figure 4.6. Again the high concentration region is thicker for the larger in-situ concentration. The dispersion regions for the two bulk concentrations have nearly the same concentration gradient. However, with these larger particles, the maximum concentration near the bottom of the pipe was higher for the larger in-situ concentration. Figures 4.5 and 4.6 were obtained at a bulk velocity of 1.75 m/s.

4.2 Water slurry pressure gradients in turbulent flow

Coarse particle slurries in turbulent flow display frictional losses which are quite different from those of pure fluids. The particle-wall friction mechanism is considered to be Coulombic, i.e. it is velocity independent. This produces a nearly constant increase in the pressure gradient compared to that of the fluid alone, provided the solids are completely

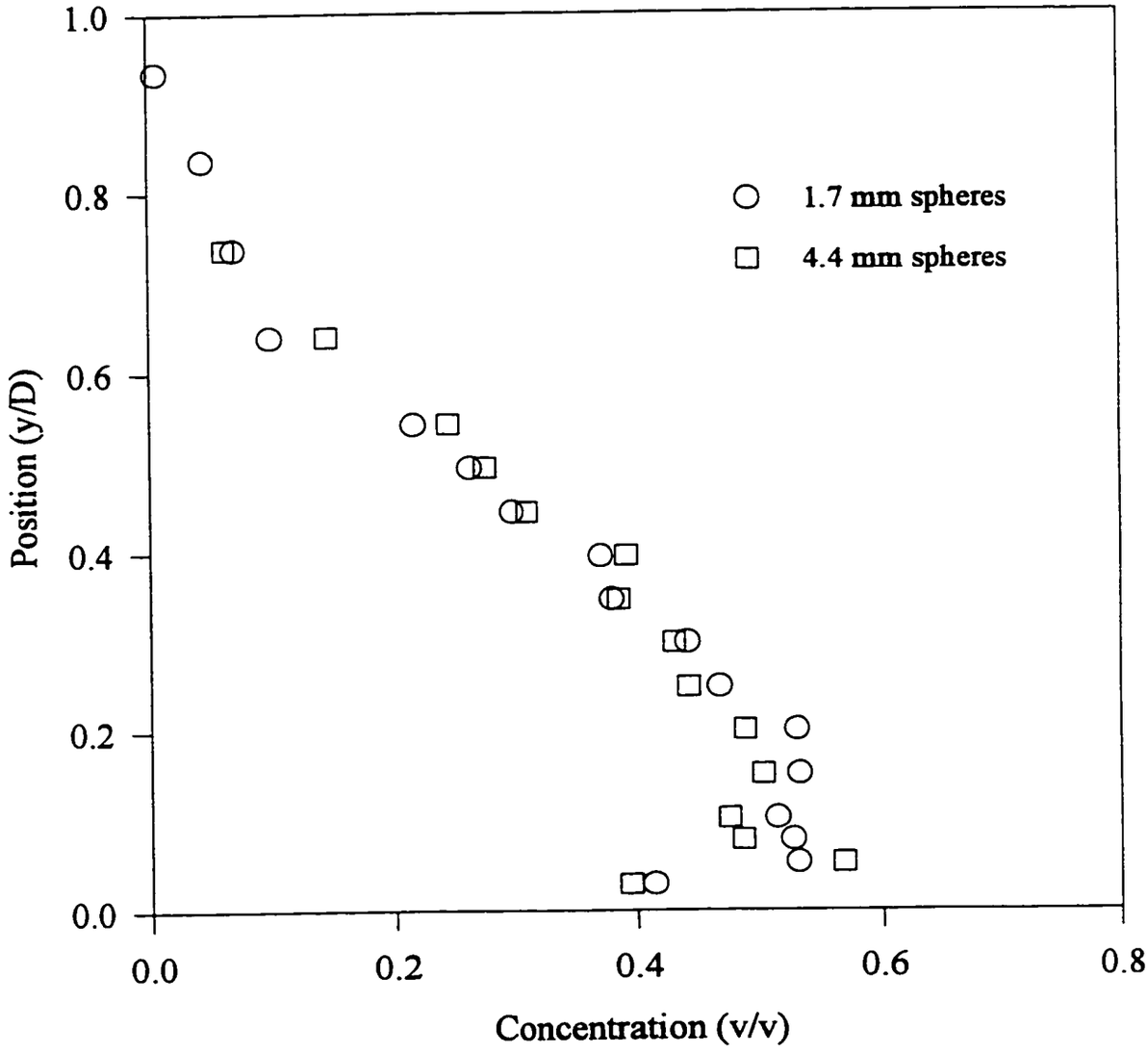

Figure 4.4 : **Concentration profiles for spheres in water at an in-situ concentration of 0.25 and a bulk velocity of 1.75 m/s.**

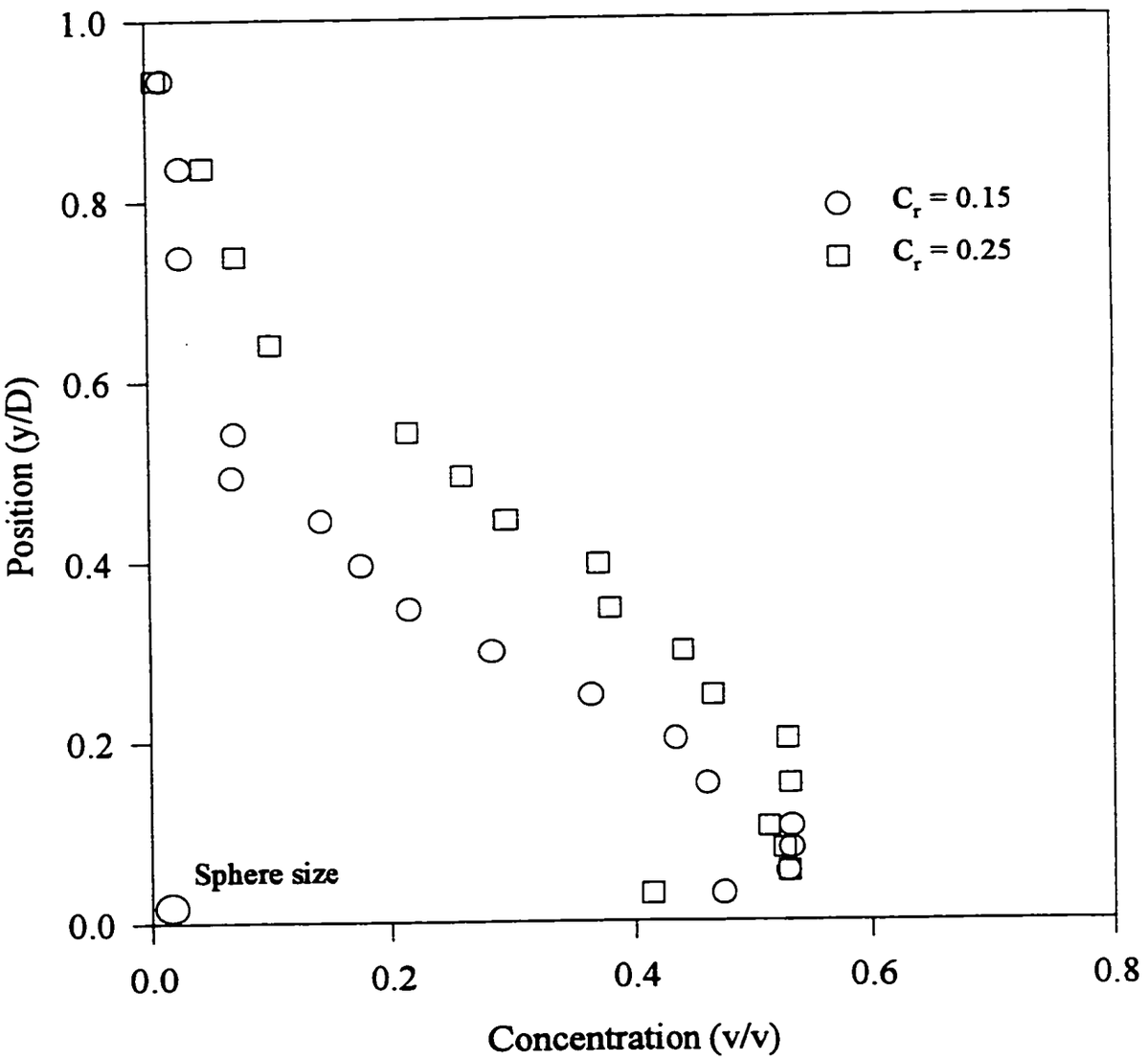

Figure 4.5 : **Concentration profiles for 1.7 mm spheres in water at a bulk velocity of 1.75 m/s.**

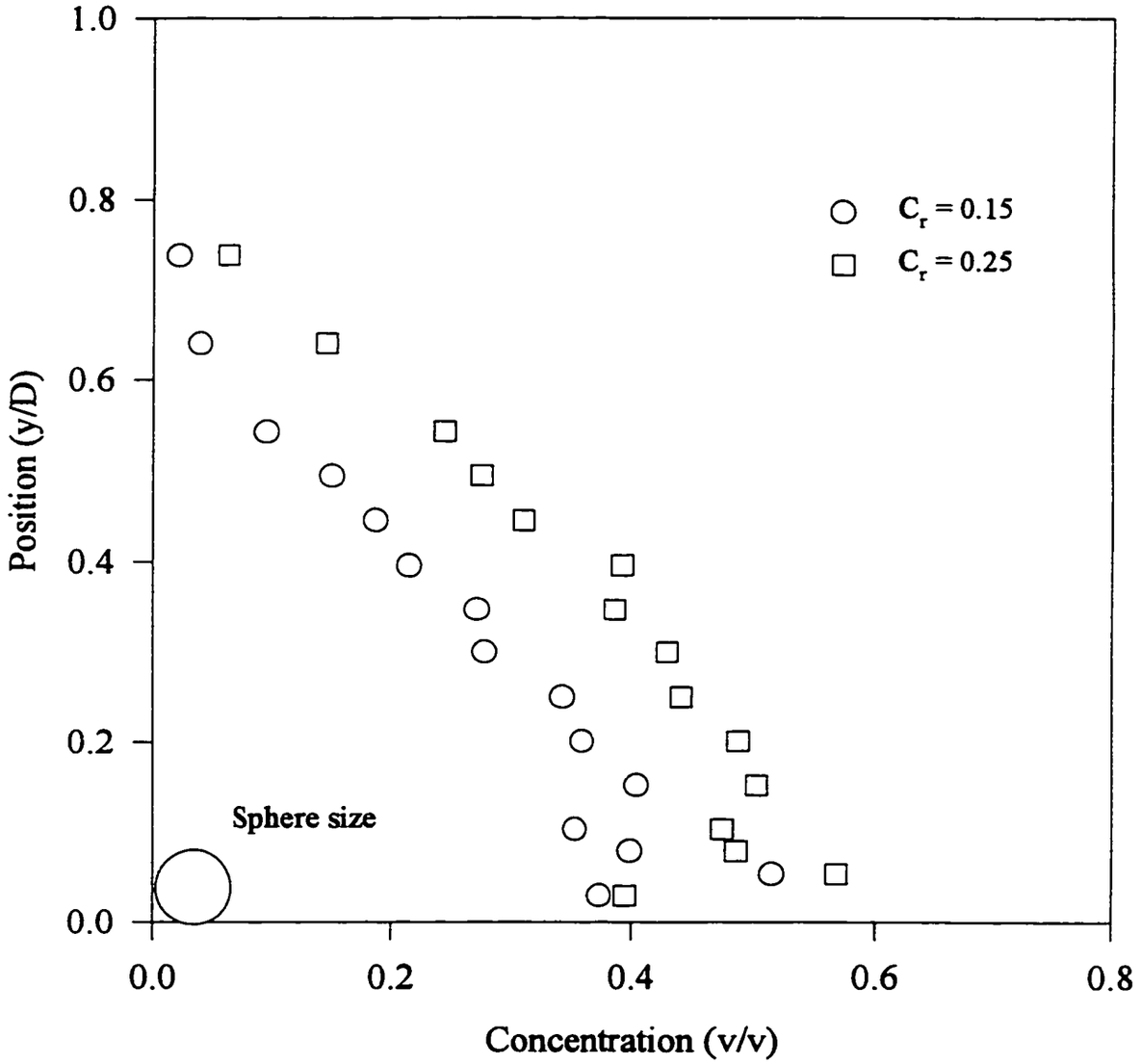

Figure 4.6 : Concentration profiles for 4.4 mm spheres in water at a bulk velocity of 1.75 m/s.

mobile. This behaviour was discussed previously in Section 2.4.

Figure 4.7 shows the pressure gradients observed for the 1.7 mm glass spheres in water at in-situ concentrations of 0.15 and 0.25 by volume. The pressure gradient for water flowing alone in the pipe is included for comparison. Water flow predictions were made using the Fanning friction factor as correlated by Churchill (1977). This was found to give excellent agreement with water tests made prior to the slurry tests.

At velocities below 0.8 m/s, a significant portion of the particles forms a stationary bed. The rapidly increasing pressure gradients observed at these low velocities correspond to water flow through a partially blocked pipe. As the velocity is increased above 0.8 m/s, rolling dunes form and travel above a stationary layer of particles. Occasionally the stationary layer was observed to slide forward before becoming stationary again. Above 1.6 m/s the particles were in motion at all times with rolling dunes evident. Particles at higher elevations were observed to pass their lower neighbours so that a condition of particle shear existed. There also appeared to be some axial variation in particle velocity since the particles were visually observed to surge forward at times. This may have been the result of the dunes remaining intact. At velocities in excess of 2.6 m/s, there was no axial velocity variation detectable.

Figure 4.8 shows the pressure gradients observed for the 4.4 mm glass spheres transported by water at in-situ concentrations of 0.15 and 0.25. Two sets of data are presented for each concentration and these will be discussed further in the next section. With these larger particles, duning was less pronounced. At velocities below 0.5 m/s the bed was stationary with a few layers of particles in saltating flow. Above this velocity, the bed began

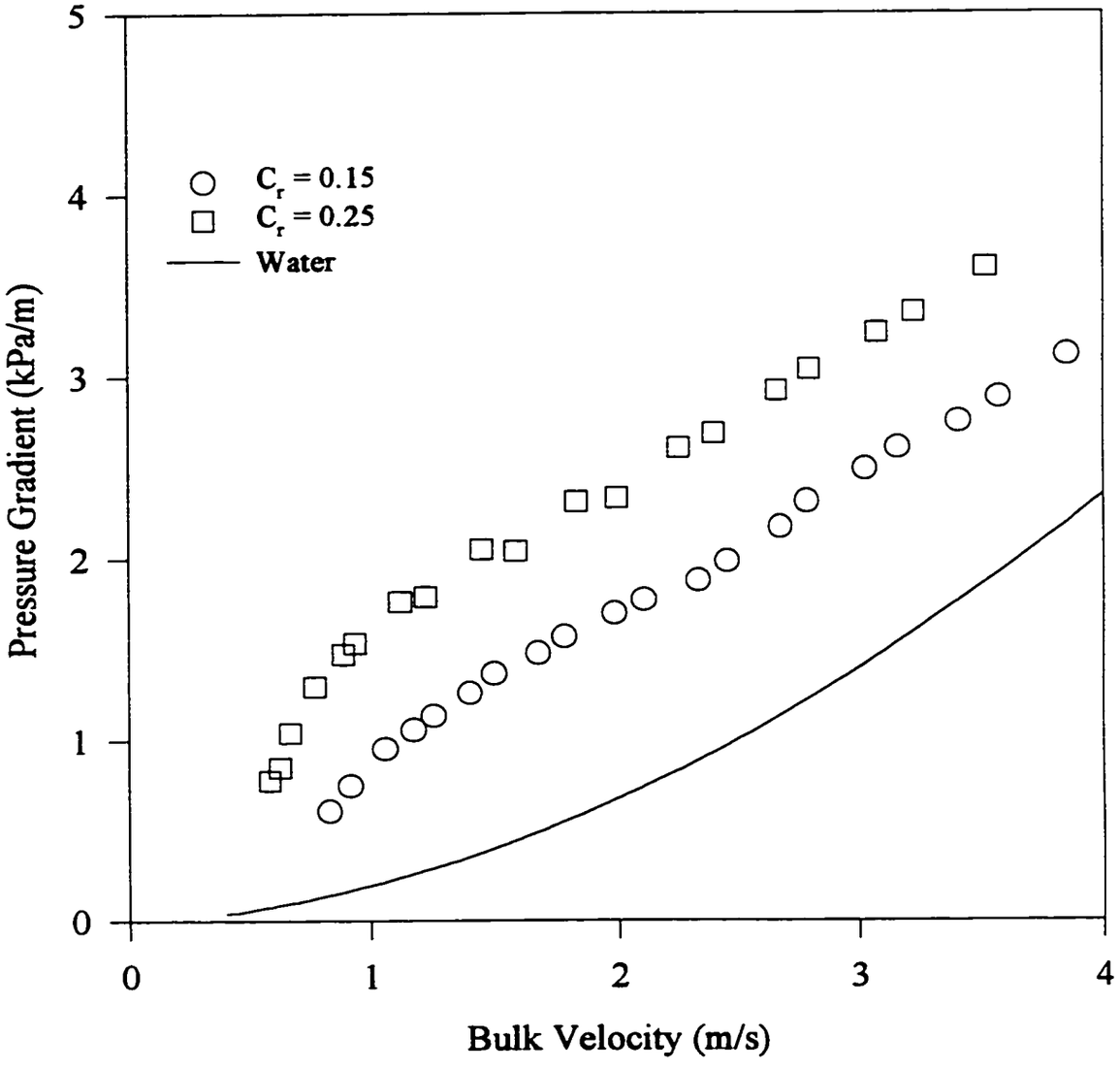

Figure 4.7 : Pressure gradients in a 53 mm pipe for 1.7 mm glass spheres in water.

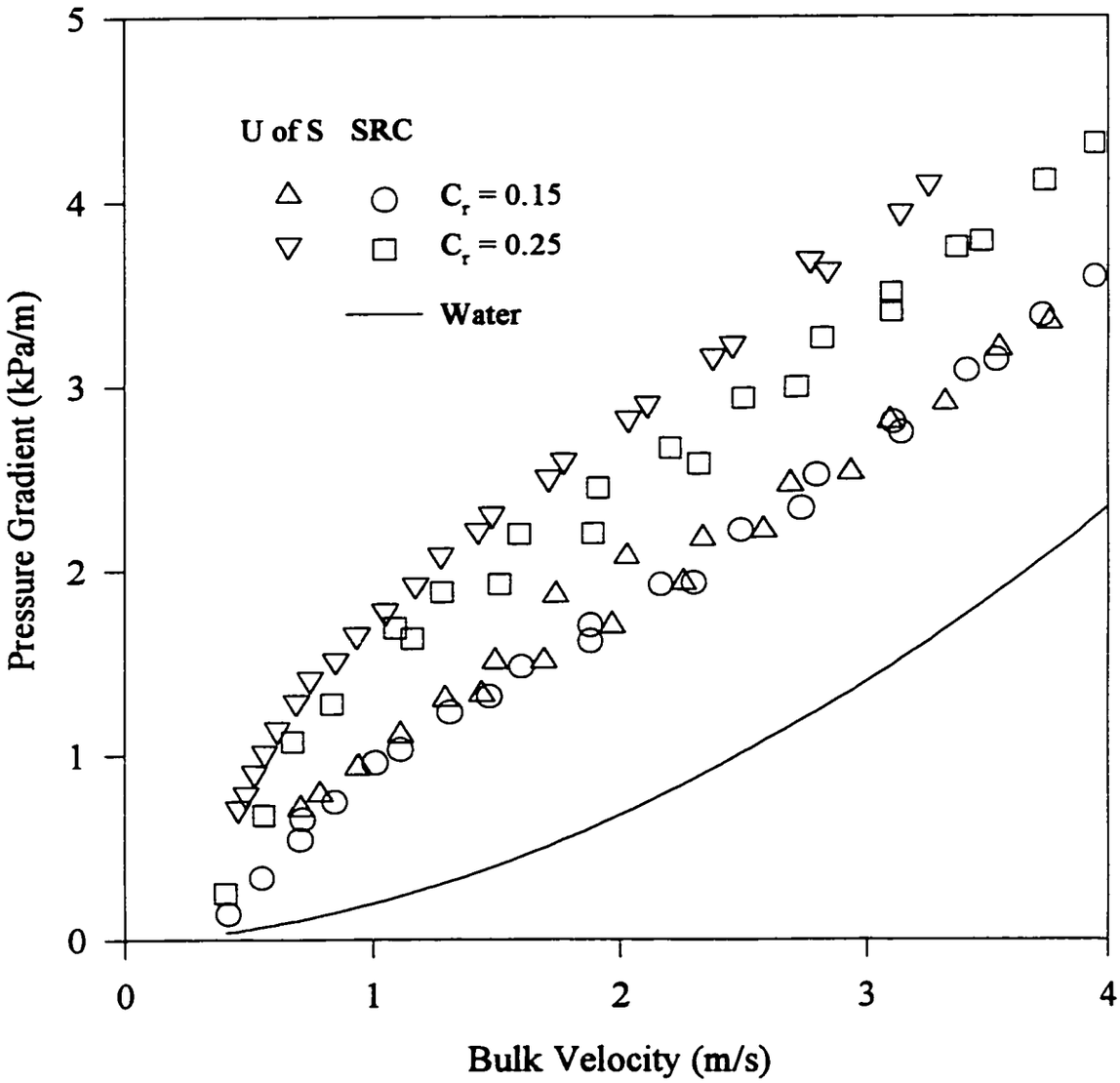

Figure 4.8 : **Pressure gradients in a 53 mm pipe for 4.4 mm glass spheres in water.**

to slide en masse with a few particle layers continuing to travel by saltation. No clear evidence of shearing layers was observed, in contrast with the smaller 1.7 mm glass spheres.

4.2.1 Two-layer model predictions for water slurries

After some minor adjustments the two-layer model used here (Appendix A) was found to be capable of predicting the pressure gradients associated with the water slurries examined here. It was found that the existing contact load correlation (Equation A.6) gave predictions which were unsatisfactory for these large particles in the small diameter pipe. The correlation predicted that the contact load fraction should decrease significantly over the experimental velocity range. However, the observed concentration profiles and pressure gradients suggested that no significant decrease occurred. The contact load fractions for the two particle sizes calculated at a bulk velocity of 1.0 m/s seemed reasonable. These fractions, 0.96 for the 4.4 mm and 0.92 for the 1.7 mm spheres, were assumed to be constant throughout the velocity range in the use of the two-layer model to predict pressure gradients. The sliding friction coefficient, η_s, was taken to be 0.45 for both particle sizes. The maximum bed concentration was taken to be 0.60 as suggested by the concentration profiles obtained at 1.0 m/s.

Figure 4.9 shows the pressure gradients observed with the 1.7 mm spheres and those predicted by the two-layer model used here. The agreement above 1.6 m/s is quite good. Below this velocity, particle flow was unsteady and the lower observed pressure gradient represents the incomplete transition to bed free flow in the pipe. Since a partial flow of solids is not included in this version of the model, this transitional flow can not be predicted accurately. The deposition velocity indicated by the discontinuity was predicted fairly well

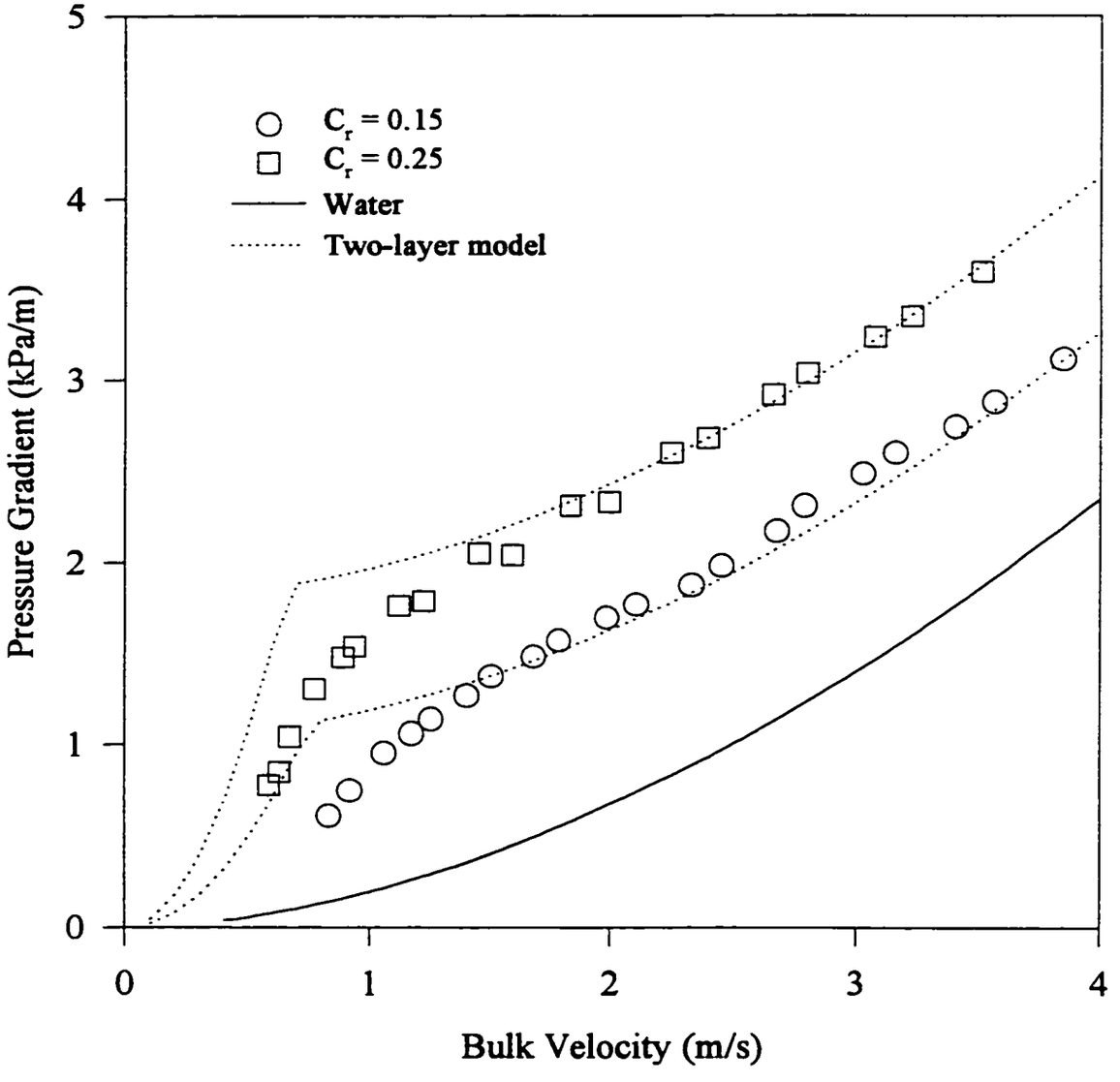

Figure 4.9 : **Pressure gradients predicted by two-layer model for 1.7 mm spheres in water.**

by the model. Below deposition, the fluid friction losses in the partially blocked pipe were not predicted well. The interfacial friction factor used in the model to express momentum transfer between the fluid region and the particle bed does not seem to be appropriate for use with a largely stationary but deformable bed interface.

As mentioned previously, the two-layer model used here was simplified by neglecting any variation in contact load. This simplification was useful for illustrating the physical mechanisms involved in coarse particle transport. Here, the excess pressure gradient is defined as the difference between the pressure gradient for the slurry and for that of the fluid alone at the same bulk velocity. This excess pressure gradient is shown in Figure 4.10 for the 1.7 mm particle slurries.

At low velocities, the excess pressure gradient results from fluid flow in a partially blocked pipe. The increase in pressure gradient with bulk velocity in this region is very rapid. When the excess pressure gradient reaches that associated with the Coulombic friction of the entire bed mass, particle motion is predicted. However, the experiments show that the transition is gradual. If the contact load fraction decreases with increased turbulence, a corresponding decrease in the excess pressure gradient should occur. With the slurries studied here, it was found that the contact load fraction did not change significantly over the velocity range so the model was modified as described previously. The observed excess pressure gradient does remain quite constant above 1.6 m/s when the bed is fully mobile.

Figure 4.11 shows the observed values and model predictions of the pressure gradient for the 4.4 mm spheres in water. At bulk velocities above 1.6 m/s, where the bed is fully mobile, the observed pressure gradient is seen to exceed the two-layer model

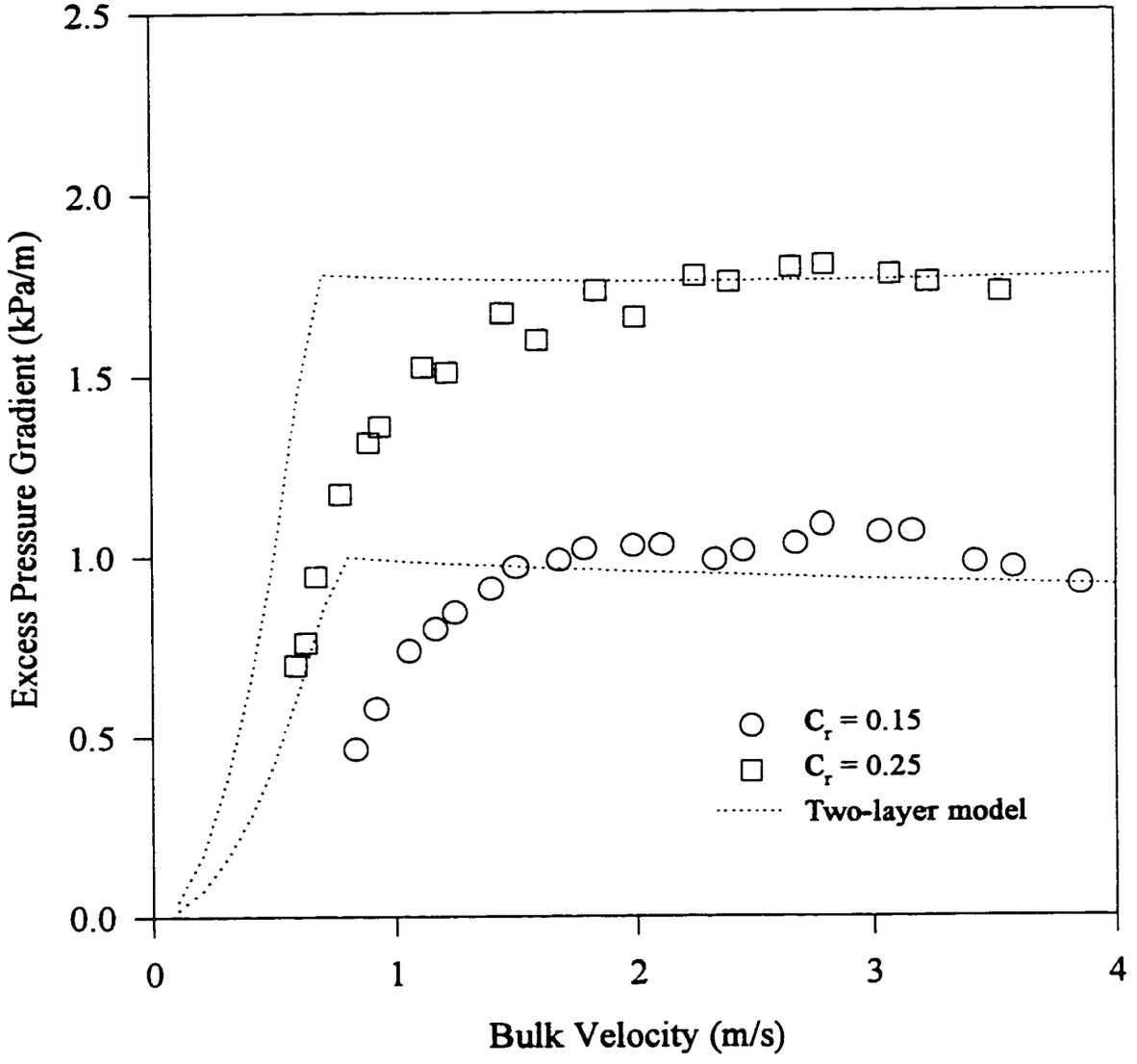

Figure 4.10 : Excess pressure gradients predicted by two-layer model for 1.7 mm spheres in water.

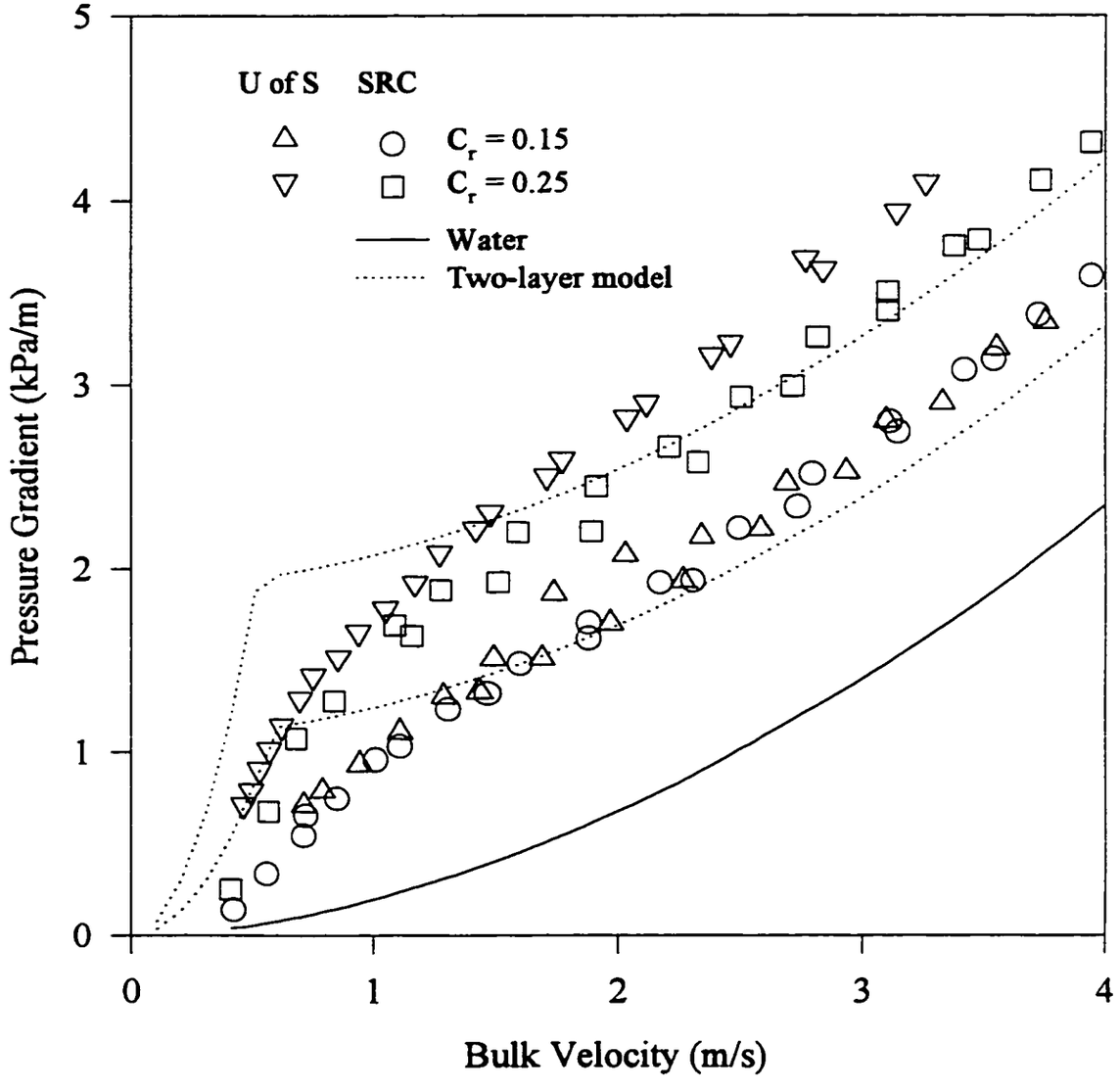

Figure 4.11 : **Pressure gradients predicted by two-layer model for 4.4 mm spheres in water.**

prediction. The deviation from the model increases with velocity. This apparent velocity-dependent component at the higher velocities was unexpected and justified repeating the experiments. The first set of measurements performed at the University of Saskatchewan (denoted as U of S) are shown with the triangle and inverted triangle data points for the two in-situ concentrations. The duplicate experiment was performed in a different, but similar, 53 mm diameter pipeloop at the Saskatchewan Research Council (denoted as SRC). The corresponding data points are shown as circles and squares for the two concentrations.

The two data sets at in-situ concentrations of 0.15 agree very well with one another. The two-layer model prediction at the higher velocities assumes a constant contact load fraction of 0.96. The observed pressure gradient was found to exceed even that of 100% contact load at the higher velocities in both tests at this concentration.

The results at the higher bulk concentration of 0.25 did not agree with one another. The first data set (U of S) showed higher pressure gradients and no hysteresis in comparison to the replicate. Particle degradation may have been partially responsible for the disagreement between the two tests because some spheres were observed to fracture during the tests at the Saskatchewan Research Council facility. Above the velocity where the bed was observed to became fully mobile, the pressure gradient was found to exceed the value which would be predicted if all the particles were supported by contact with the wall. Also, the deviation between the observed and predicted pressure gradient was found to increase with velocity.

Figure 4.12 shows the excess pressure gradient for the slurries containing the 4.4 mm spheres. This shows more clearly the deviation from the model which was not found

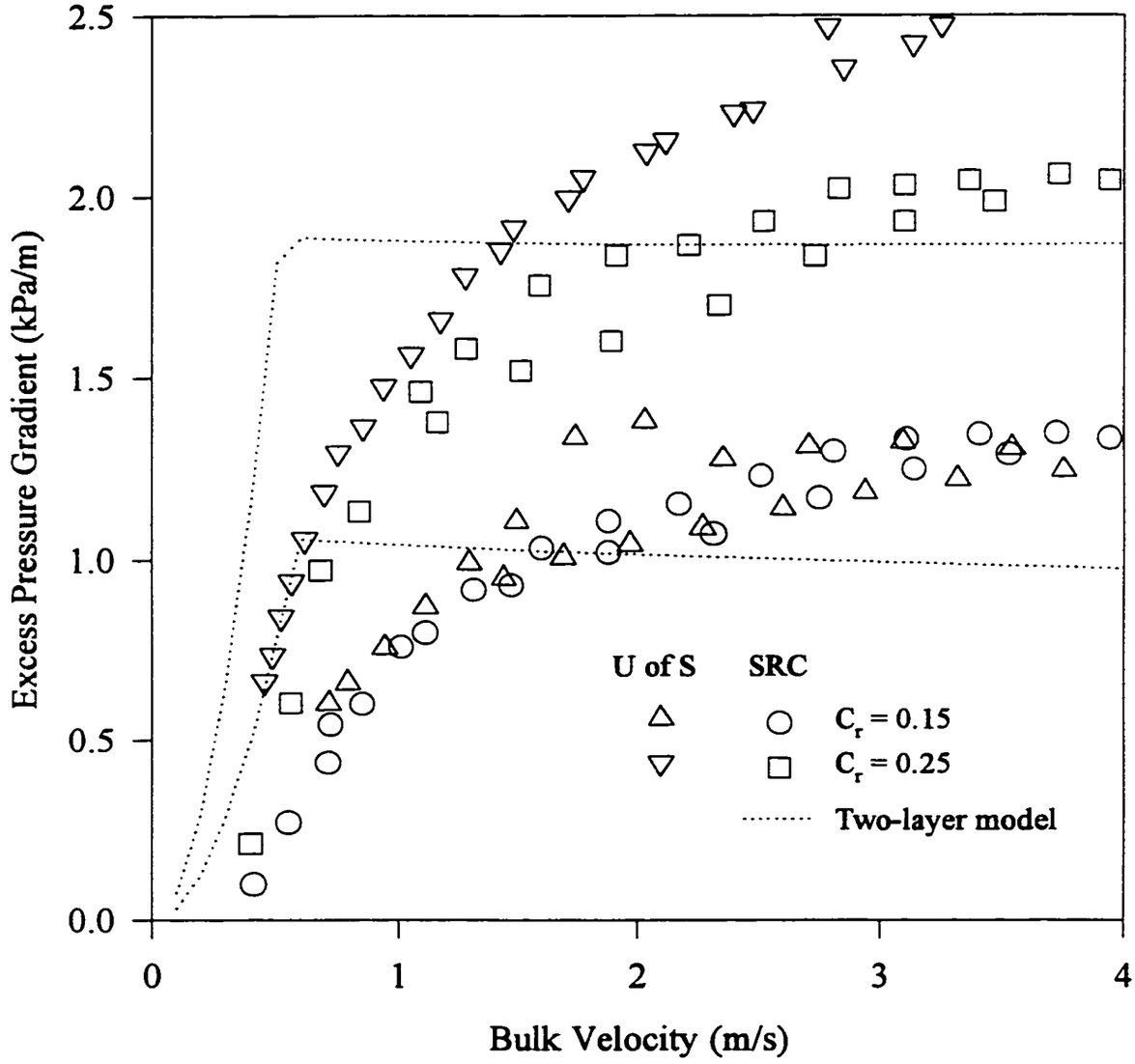

Figure 4.12 : Excess pressure gradients predicted by two-layer model for 4.4 mm spheres in water.

with the 1.7 mm spheres. The particles were observed to become fully mobile at about the velocity where the excess pressure gradient reached the Coulombic friction component predicted by the model. Beyond this point the excess pressure gradient continued to increase slightly with velocity.

The cause of the velocity dependent behaviour of the 4.4 mm particle slurries is unclear, especially when the concentration profiles are considered. Figure 4.12 shows that a significant difference in excess pressure gradient exists between 1.75 m/s and 2.5 m/s. Figure 4.2 shows that the chord averaged concentration profiles do not change between these velocities for the two concentrations. It would have been reasonable to expect that the increase in excess pressure gradient would cause a visible change in the internal structure of the slurry such as increased particle dispersion. However no significant changes in the chord averaged concentrations were observed and changes to the concentration distribution in the lateral direction would not have been detected with the gamma ray device.

The slight hysteresis observed in the pressure gradient, which was reproducible at the lower bulk concentration, would suggest a structural change in the bed of these large particles. Each data point was collected over approximately three minutes so that the slurry had passed through the loop, including the pump, a minimum of four times at velocities above 2 m/s. Therefore, any changes to the structure of the slurry were stable enough to withstand the resulting mixing of particles. This behaviour can not be reconciled easily.

In summary, the two-layer model can be used to interpret the different flow regimes of the settling slurries investigated here. When modelling flow with a stationary bed, the use of the Colebrook friction factor (Equation A.14) at the bed interface seems to lead to an

overprediction of the pressure gradient. At the velocity where the excess pressure gradient resulting from the reduced cross section meets the Coulombic friction associated with the immersed weight of the entire bed, the bed can be seen to become fully mobile. When the bed is mobile, the pressure gradient is largely the sum of the fluid friction losses and the Coulombic friction losses resulting from the contact load component. The quantitative results obtained could be improved with better interfacial friction and contact load correlations for these large particles in small pipes.

4.3 Magnetic particle velocities in water slurries

At each bulk velocity, between five and fifteen interval times, t_{int}, were recorded for the passage of the magnetic particle between the sensor coils. The particle velocities thus obtained were averaged. Figure 4.13 shows the magnetic particle velocities obtained for the 1.7 mm spheres in water at both concentrations. Linear regression lines are included to indicate the nearly linear relationship between the bulk velocity and the magnetic particle velocities. The slopes of the lines for the two concentrations are similar. At the lowest bulk velocities where the particle bed approaches a stationary condition, the magnetic particle velocity begins to drop below the regression line. The lower stationary deposit velocity observed with the higher concentration slurry can be inferred from the existence of magnetic particle velocities at lower bulk velocities.

It was observed that magnetic particle velocities were recorded at low velocities where only a portion of the particles in the loop were travelling at appreciable velocities. These magnetic particle velocities were nearly as high as the bulk velocities although the flow was clearly segregated and the particle velocity was probably below the bulk velocity

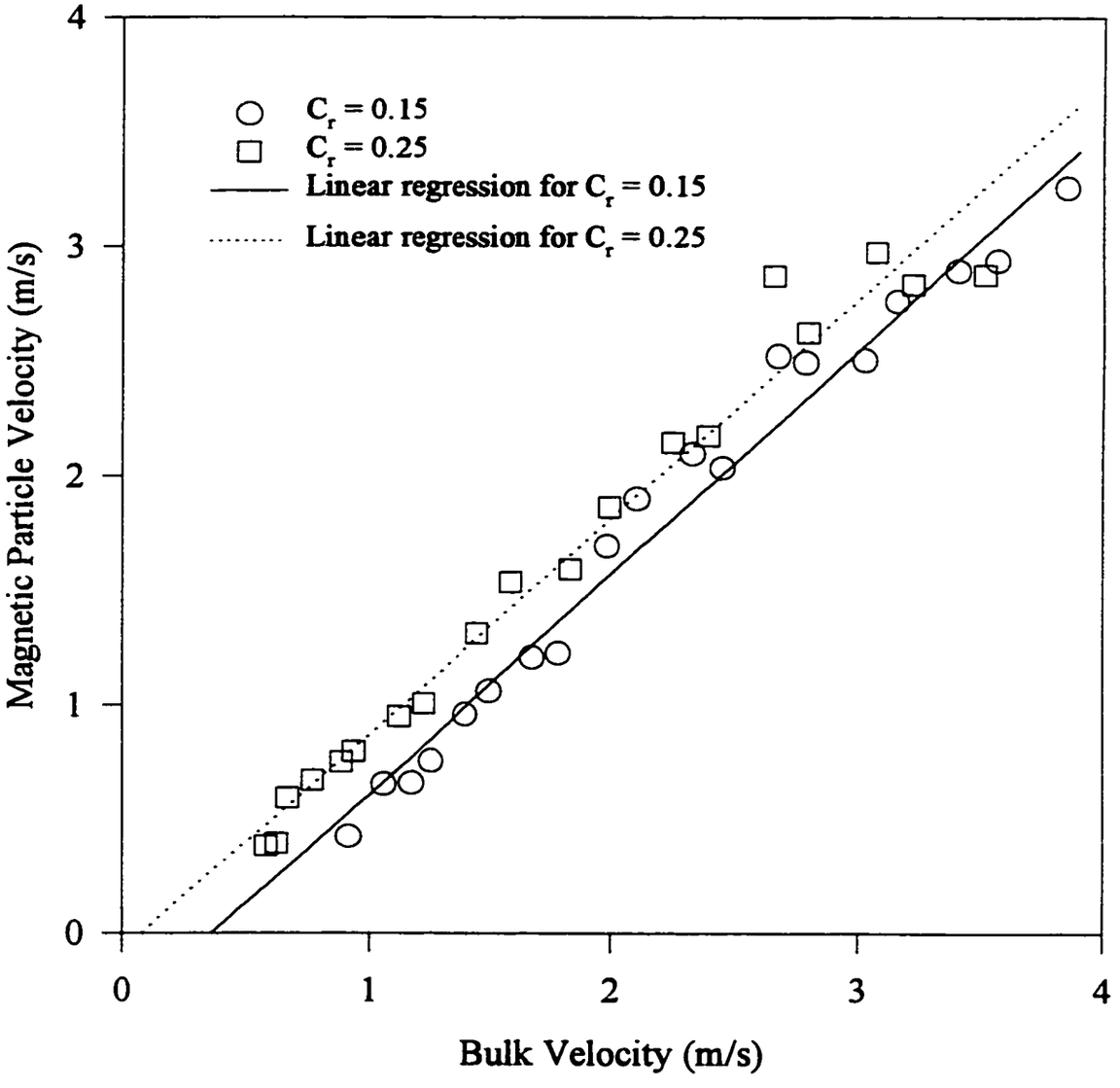

Figure 4.13 : Magnetic particle velocities in water and 1.7 mm sphere slurries.

in most of the bed. This suggests that the magnetic particles travelled preferentially near the bed interface where the velocity was high and particle movement continued down to the lowest velocities. Similar results were obtained with the larger 4.4 mm spheres.

Figures 4.14 and 4.15 show that the magnetic particle velocities were not influenced very strongly by particle size. Figure 4.14 shows the particle velocities for both the 4.4 mm and 1.7 mm spheres at an in-situ concentration of 0.15. The linear regression line applies to all of the data points. At the highest bulk velocities, the magnetic particle velocities are slightly higher with the 4.4 mm particle slurry. At the lowest bulk velocities, the magnetic particle velocities are nearly the same for both particle sizes. Figure 4.15 shows the same behaviour at an in-situ concentration of 0.25.

Figures 4.14 and 4.15 also include lines which represent the two-layer model predictions for the upper and lower layer velocities. The magnetic particle velocities are seen to fall within this fairly narrow band. This supports the idea that the size and density of the magnetic particle led to its preferential location at the bed interface and that the particle velocities are interface velocities.

4.4 Flow of Kaolin/Bentonite suspensions

4.4.1 Couette flow of Kaolin/Bentonite suspensions

The Kaolin/Bentonite suspensions used in these experiments were found to follow the Bingham fluid model very well. Figure 4.16 shows the data obtained from the concentric cylinder viscometer for two typical Kaolin/Bentonite suspensions. In this diagram, shear stresses and shear rates are calculated from the viscometer deflection and spindle speed using multipliers supplied by the viscometer manufacturer. Linear regressions of the shear

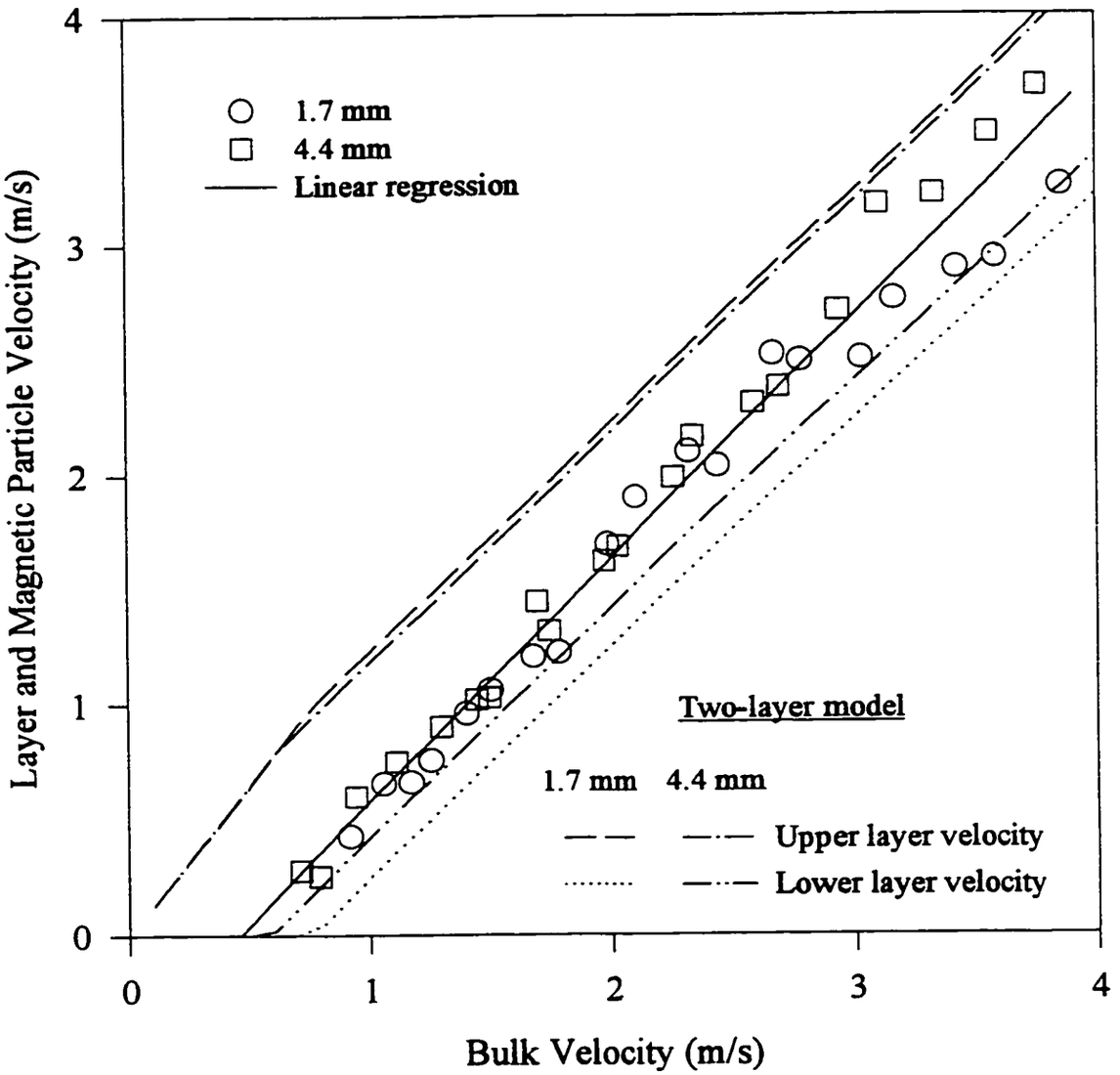

Figure 4.14 : Magnetic particle velocities in water and glass sphere slurries with in-situ concentrations of 0.15.

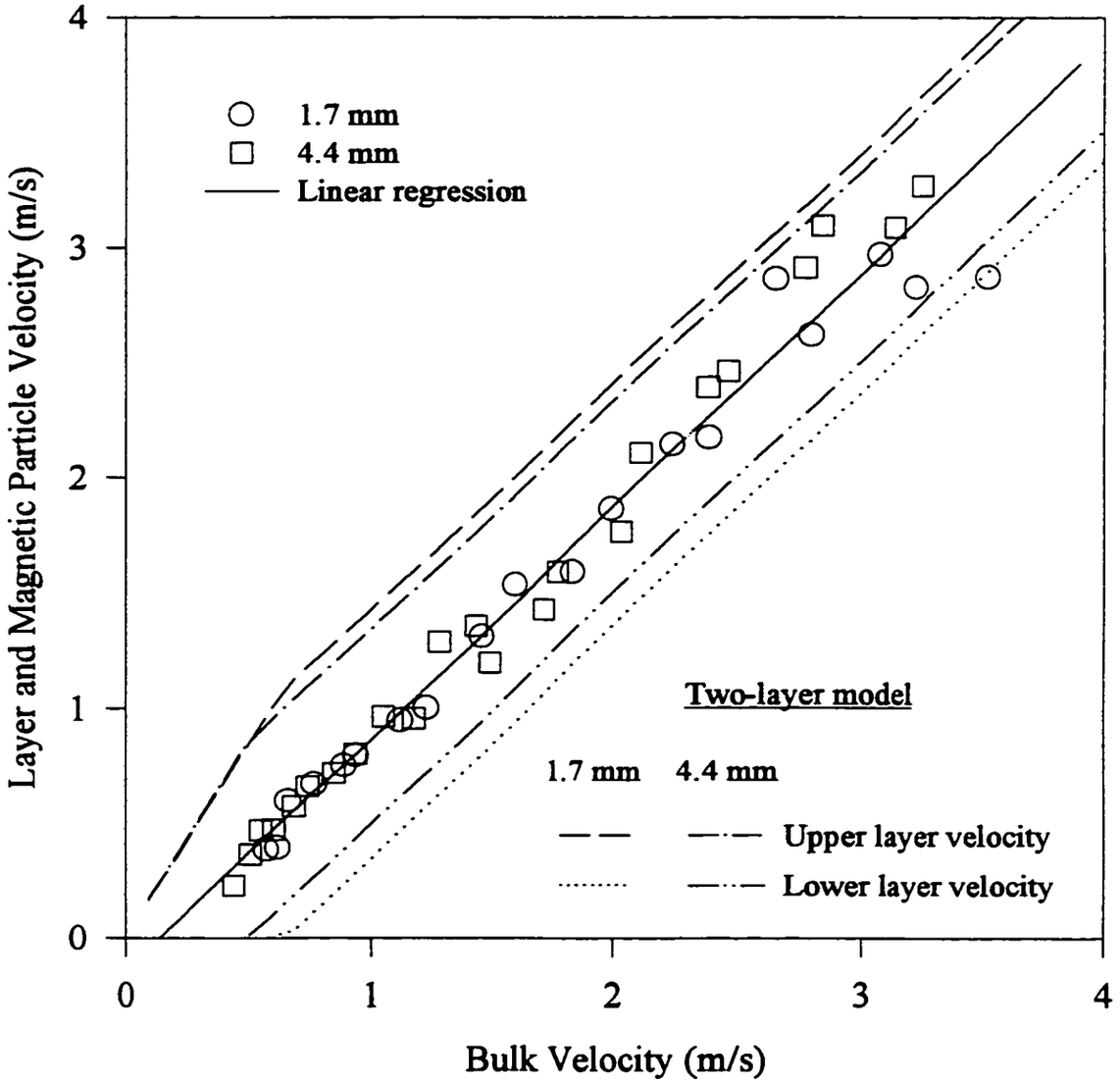

Figure 4.15 : Magnetic particle velocities in water and glass sphere slurries with in-situ concentrations of 0.25.

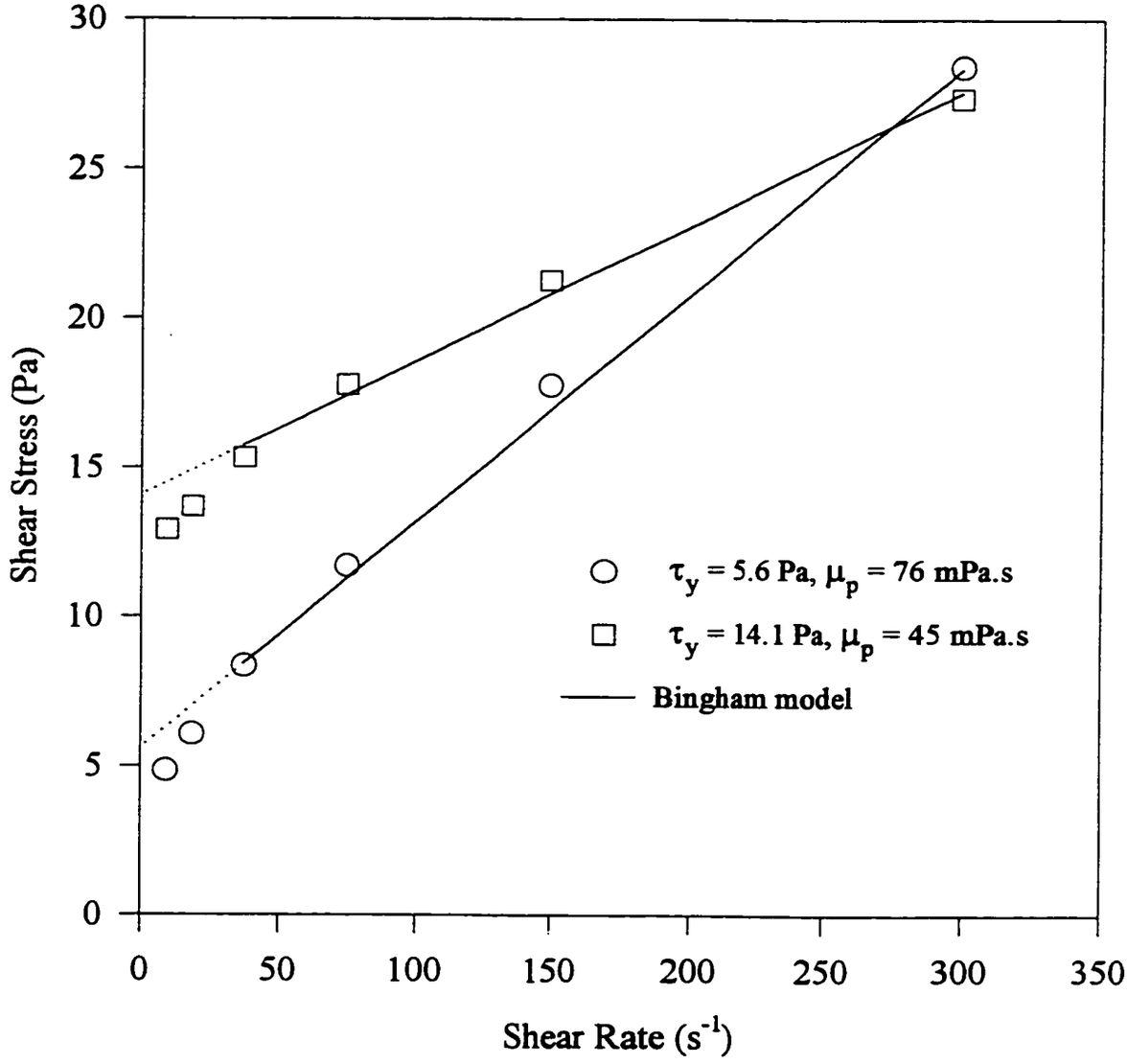

Figure 4.16 : Use of the Bingham fluid model to characterize Kaolin/Bentonite suspensions.

stress and shear rate values give the model parameters of yield stress, τ_y, and plastic viscosity, μ_p for the two fluids.

A concern when using a concentric cylinder viscometer to characterize a Bingham fluid is that a condition of incomplete shear can occur as the applied shear stress approaches the yield stress. When this occurs the fluid is not sheared across the entire gap between the spindle and the cup. This is a concern primarily with viscometers which have a large gap. With the viscometer used in the present work, the gap was physically small (0.96 mm). For each viscometer spindle speed used with a given fluid, a test for complete shear across the gap was made and the incomplete shear data were rejected from the linear regression. The model parameters were re-evaluated until all data points were acceptable. The Bingham model fits for the data reported in Figure 4.16 are included as straight lines. The dotted portions are extrapolated for low shear rates since the lowest two points of each data set are not used in the regression due to the possibility of incomplete shear.

4.4.2 Pipe flow of Kaolin/Bentonite suspensions

Bingham model parameters obtained for clay suspensions at low shear rates often deviate from those obtained from higher shear conditions, possibly because of deflocculation. For this reason, the shear stress range used to characterize a suspension in a concentric cylinder viscometer should match the pipe wall shear stress anticipated for the velocity range of interest. Extrapolation should be avoided when attempting to characterize these suspensions with a viscometer.

Ideally the fluid behaviour should remain stable throughout the experimental work. However it was observed that the rheology of the suspensions gradually changed with time.

Observed pressure losses for the Kaolin/Bentonite slurries often showed a slight hysteresis as a result of gradual deflocculation of the clay slurry. Therefore, fluid parameters were evaluated for each experiment using the concentric cylinder viscometer. To determine if the viscometer was able to characterize fluid flow accurately, the model parameters obtained from the concentric cylinder viscometer were compared to those obtained from pipe flow for a number of Kaolin/Bentonite mixtures.

This comparison of model parameters identified the range of fluid behaviour where the viscometer could be used to determine model parameters reliably. Figure 4.17 shows the observed pressure gradient for the original Kaolin suspension as a function of bulk velocity. There was no Bentonite in this suspension. Also shown are Buckingham equation (2.6) predictions fitted by least squares to the pipe flow data and the parameters from the concentric cylinder viscometry. Agreement is quite good in the laminar flow region. This fluid exhibited a significant yield stress and a moderate plastic viscosity. Turbulent pressure gradient predictions using the model of Wilson and Thomas (Equation 2.11) are seen to be rather unsatisfactory although the transition does occur at about the right velocity. The deviation is similar to that which was observed by Xu et al. (1993). Horizontal lines show the range of pipeline pressure gradients which correspond to the shear stresses which could be achieved in the concentric cylinder viscometer. It is seen that the viscometer shear stresses cover essentially the entire range of wall shear stresses encountered in laminar pipe flow.

Figure 4.18 shows the pressure gradient for a Kaolin/Bentonite suspension with a lower yield stress and increased plastic viscosity. Again the concentric cylinder and pipe

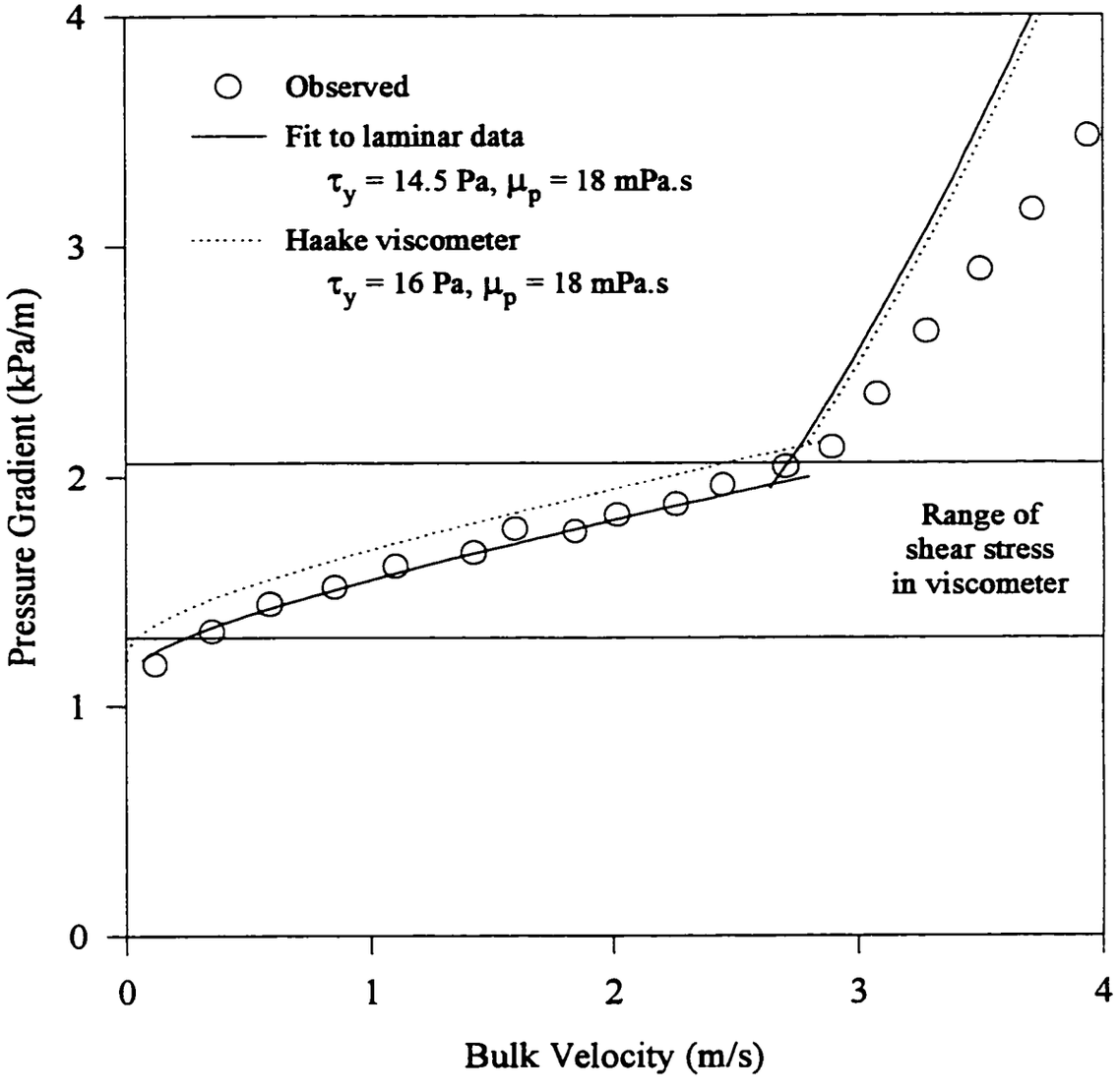

Figure 4.17 : Comparison of Bingham model parameters for a Kaolin suspension.

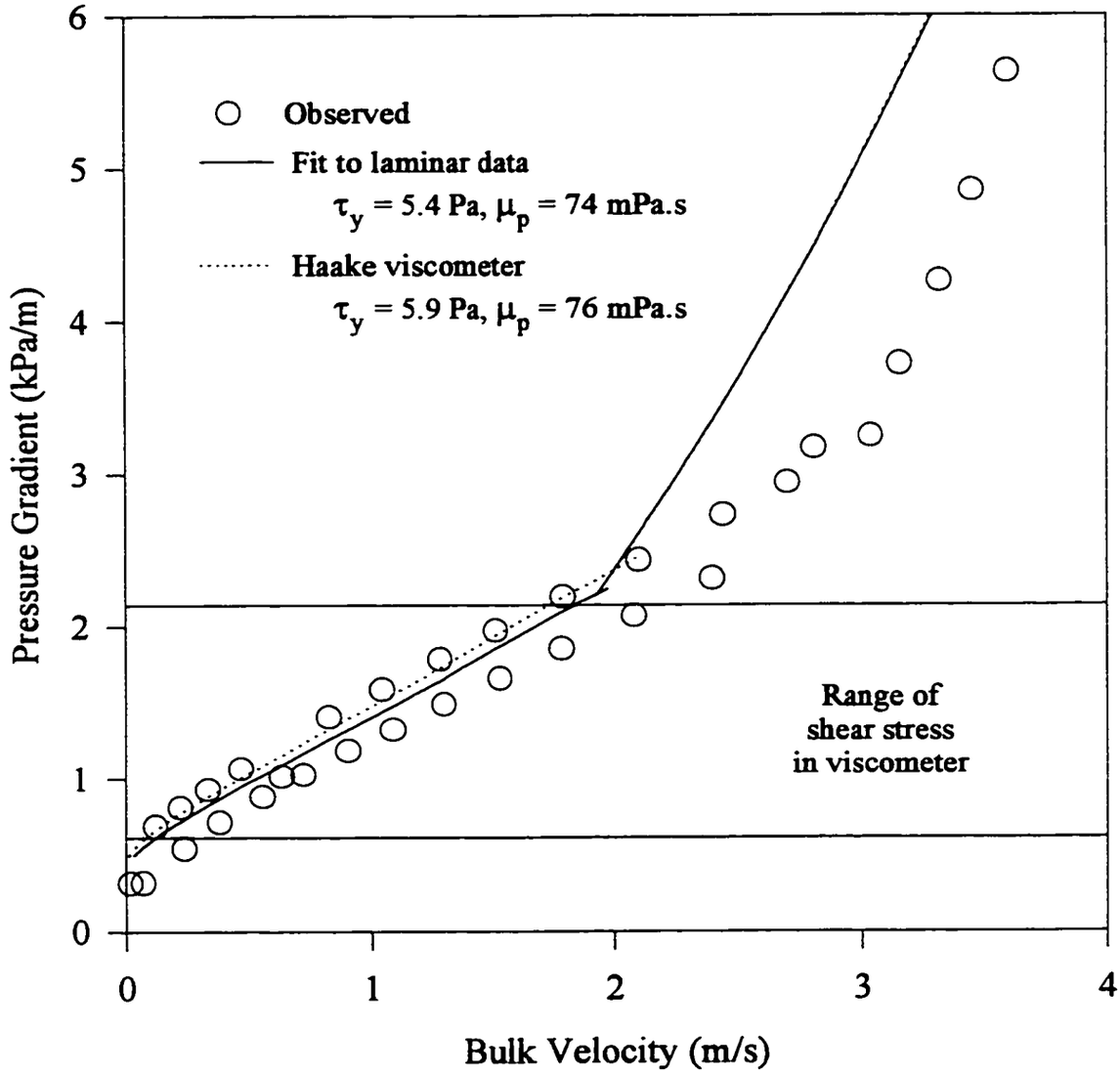

Figure 4.18 : Comparison of Bingham model parameters for a Kaolin/Bentonite suspension with a low yield stress.

flow model parameters are in good agreement in laminar flow. However the turbulent region predictions are unsatisfactory and the transition velocity is underpredicted by about 1 m/s. Again the shear stress range achieved in the viscometer covers most of the range of wall shear stresses encountered in laminar pipe flow.

Figure 4.19 shows data for a Kaolin/Bentonite suspension with a substantial yield stress and moderate plastic viscosity. This suspension contained a higher fraction of Bentonite than the previous cases. The viscometry shear stresses covered the range of wall shear stresses in the pipe. The yield stress values obtained from the concentric cylinder viscometer and pipe flow are in good agreement but a discrepancy between the plastic viscosities exists.

A similar result is seen in Figure 4.20. This is another Kaolin/Bentonite suspension which had high yield stress and plastic viscosity values. This suspension had a still higher fraction of Bentonite. The shear stress range in the viscometer only included a portion of the shear stress range encountered in the pipe. The yield stress obtained from the viscometer is in good agreement with that obtained from the pipe flow. The plastic viscosity from the viscometer is much higher than that obtained from the pipe flow.

Differences in the plastic viscosities obtained from the two flow geometries may partially be due to the limited shear stresses which could be applied with this viscometer. The limited shear stress in the viscometer has the effect of limiting the shear rate which can be applied. Thus the lower shear rates in the viscometer do not provide the same shear condition which is encountered in pipe flow. For the more viscous suspensions, the Bingham model parameters obtained from the low shear condition in the viscometer were not

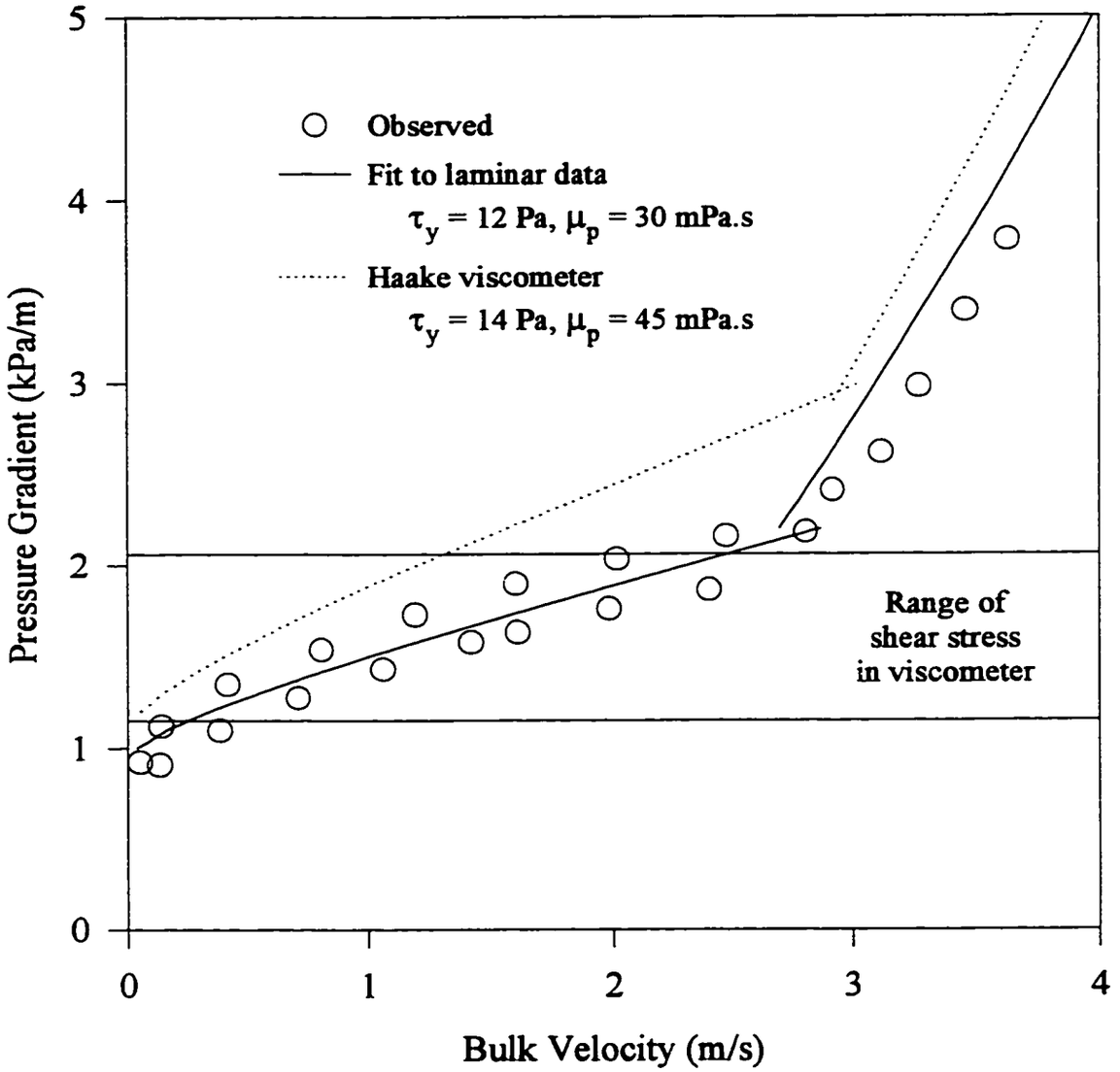

Figure 4.19 : Comparison of Bingham model parameters for a Kaolin/Bentonite suspension with a moderate yield stress.

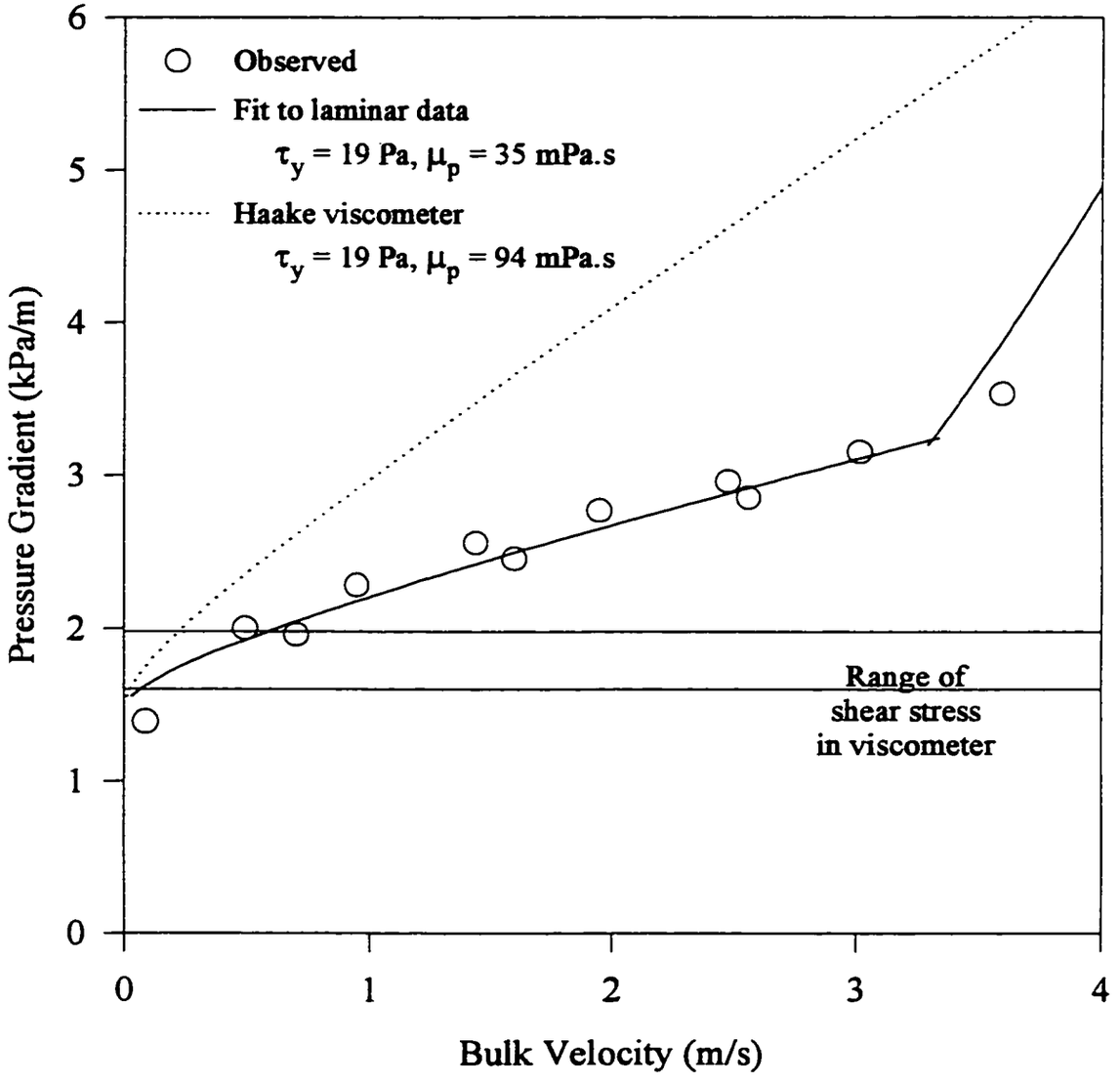

Figure 4.20 : **Comparison of Bingham model parameters for a Kaolin/Bentonite suspension with a high yield stress.**

representative of the high shear conditions encountered with pipe flow.

In the present work, differences in model parameters resulting from non-representative shear levels in the viscometer cannot be corrected but can be identified. To do this, the spindle shear stress in the viscometer is compared to the wall shear stress in the pipe. Table 4.1 shows the linear regression model parameters from the concentric cylinder viscometer. It also shows the ranges of shear stresses produced in the viscometer. The ranges of average pipe wall shear stresses observed in pipe flow are determined from the pressure gradients and Equation 2.5. The higher limit reflects the fact that additional losses result from the presence of solid particles.

Viscometry results become less reliable when the lowest pipe wall shear stresses become comparable to the maximum value obtained in the viscometer. The viscometer plastic viscosity values marked with an asterisk may be higher than would be representative of the fluid behaviour in the pipe since shear stresses are below those which were observed in the pipe. The observations made with suspensions containing a high fraction of Bentonite indicate that the plastic viscosities of those fluids may also differ between the two geometries. The yield stresses are likely to be correct in all cases.

4.5 Concentration profiles in Kaolin/Bentonite slurries

Table 4.2 lists the fluid properties and theoretical yield stresses required to support the solid particles, calculated from Equation 2.14. Four sets of experiments met or exceeded this criterion. Visual observations through the transparent pipe section showed that the flow was always highly stratified with particles travelling in a bed-like structure at the bottom of the pipe. This stratification always occurred, despite the fact that the solid particles would

have had a very low or negligible settling velocity under static conditions. The concentration profiles which follow illustrate the degree of stratification observed.

Table 4.1 : Concentric cylinder viscometry results.

Description	Yield Stress (Pa)	Plastic Viscosity (mPa.s)	Range of Spindle Stress (Pa)	Range of Wall Shear Stress (Pa)
Original Kaolin (Fig. 4.17)	16	18	17-27	15-30
Kaolin/Bent. (Fig. 4.18)	5.9	76	8-28	4-29
Kaolin/Bent. (Fig. 4.19)	14	45*	15-27	12-29
Kaolin/Bent. (Fig. 4.20)	19	94*	21-26	18-46
15% 1.7 mm spheres	6.5	110	8-22	13-82
25% 1.7 mm spheres	5.6	110	7-22	11-70
15% 4.4 mm spheres	4.1	65	5-23	11-49
25% 4.4 mm spheres	3.4	59	4-21	13-53
15% 4.4 mm spheres	17	62*	18-26	24-71
15% 4.4 mm spheres	25	80*	26-28	29-82
15% 4.1 mm gravel	5.3	97	7-20	13-70
25% 4.1 mm gravel	6.3	120	8-24	12-90
* may not be representative of pipe flow				

4.5.1 Concentration profiles for 1.7 mm sphere slurries

The Kaolin/Bentonite suspensions used with the 1.7 mm spheres had a density of 1460 kg/m^3. The theoretical yield stress required to support these particles in stationary fluid is calculated from Equation 2.14 to be 3.6 Pa. Concentric cylinder viscometry measurements

Table 4.2 : Slurry test conditions and required particle support yield stress.

	Description	Material	Median Diameter (mm)	Density (kg/m^3)
Solid Components	-10+12 mesh	Glass spheres	1.7	2470
	-4+5 mesh	Glass spheres	4.4	2470
	-4+6 mesh	Gravel	4.1	2650
Slurry Description	Yield Stress (Pa)	Plastic Viscosity (mPa.s)	Density (kg/m^3)	Required Yield Stress (Pa)
15% 1.7 mm	6.5	110	1460	3.6
25% 1.7 mm	5.6	110	1460	3.6
15% 4.4mm #1	4.1	65	1500	8.9
25% 4.4mm	3.4	59	1500	8.9
15% 4.4mm #2	17	62*	1150	12.1
15% 4.4mm #3	25	80*	1170	11.9
15% 4.1 mm	5.3	97	1470	10.1
25% 4.1 mm	6.3	120	1500	9.8
* may not be representative of pipe flow				

indicate the yield stress of the suspensions used for these slurries to be in excess of this minimum value. The Bingham model parameters and the concentration profiles for the 1.7

mm sphere slurries are shown in Figures 4.21 and 4.22 for in-situ concentrations of 0.15 and 0.25 respectively. Conditions are always laminar.

The profiles for a bulk concentration of 0.15 (Figure 4.21) show stratification with moving beds which have blunted noses of nearly uniform concentration near the bottom of the pipe. This occurred in spite of the fact that the fluid yield stress is 80% higher than the theoretical support yield stress. Above these uniform regions, the concentration decreases to zero in an approximately linear fashion. Visual observations of the flow at 0.8 m/s revealed the bottom third of the bed to be sliding as a unit. The middle third contained particles which appeared to shear in layers and the top third where particles appeared to move in a dune-like fashion.

A doubling of the bulk velocity from 0.8 m/s to 1.6 m/s causes a decrease in the concentration of the uniform layer. The elevation at which the concentration begins to decrease below the uniform layer concentration is higher for the 1.6 m/s case since the in-situ concentration remained constant. The concentration gradient appears to be lower at this higher velocity. The 0.0 m/s profile was obtained after the flow was stopped quickly from a bulk velocity of 1.6 m/s. The short period of time that flow persisted in the pipeloop due to inertia was long enough for most of the spheres to re-establish their loose packed arrangement at the bottom of the pipe.

Figure 4.22 shows the concentration profiles for an in-situ concentration of 0.25. Again the flows are highly stratified with blunted noses of nearly uniform concentration near the bottom of the pipe. The concentration of this region is reduced when the bulk velocity was increased from 0.8 m/s to 1.6 m/s. Above this region the concentration drops quickly

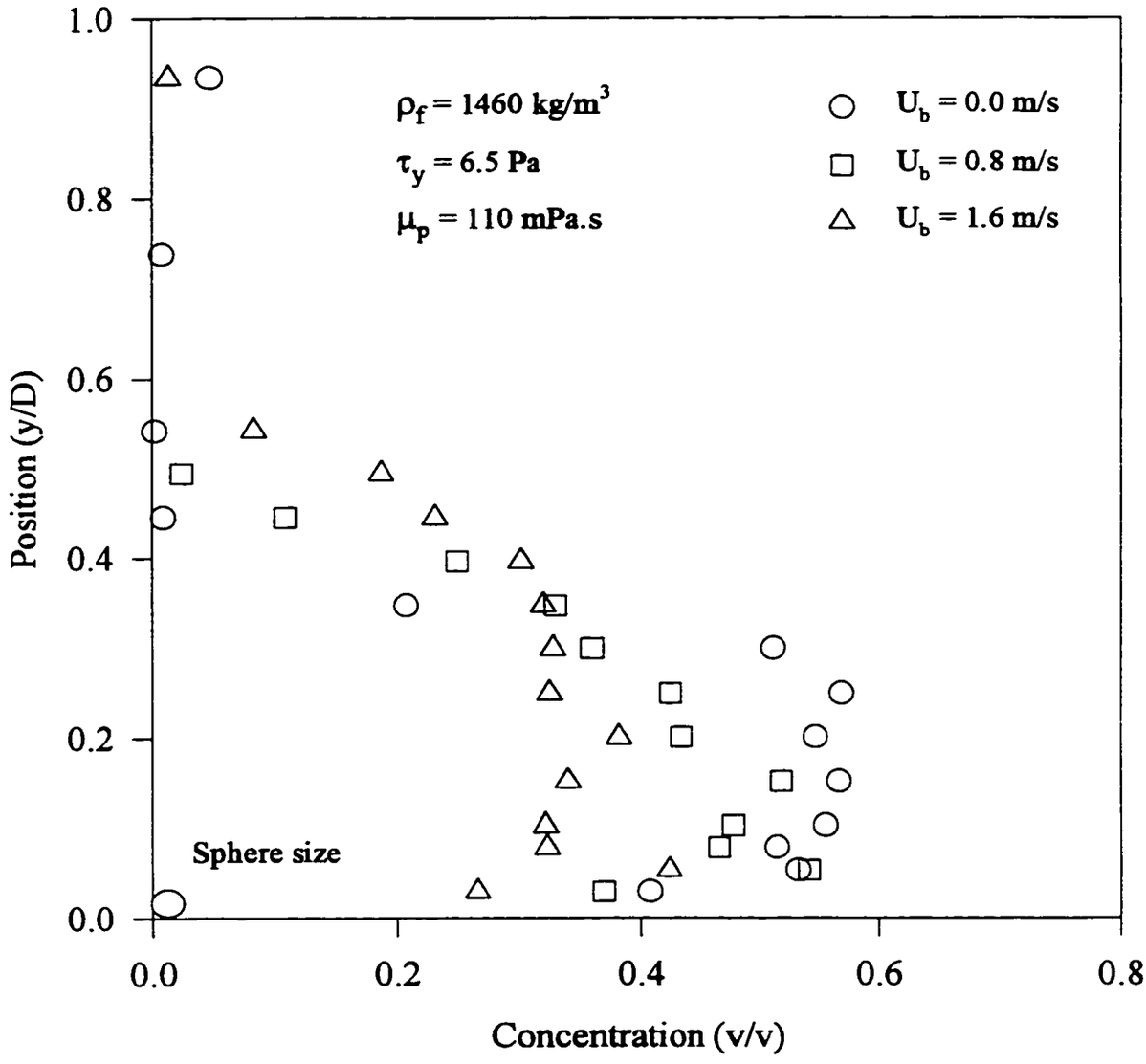

Figure 4.21 : Concentration profiles for 15% 1.7 mm spheres in a Kaolin/Bentonite suspension.

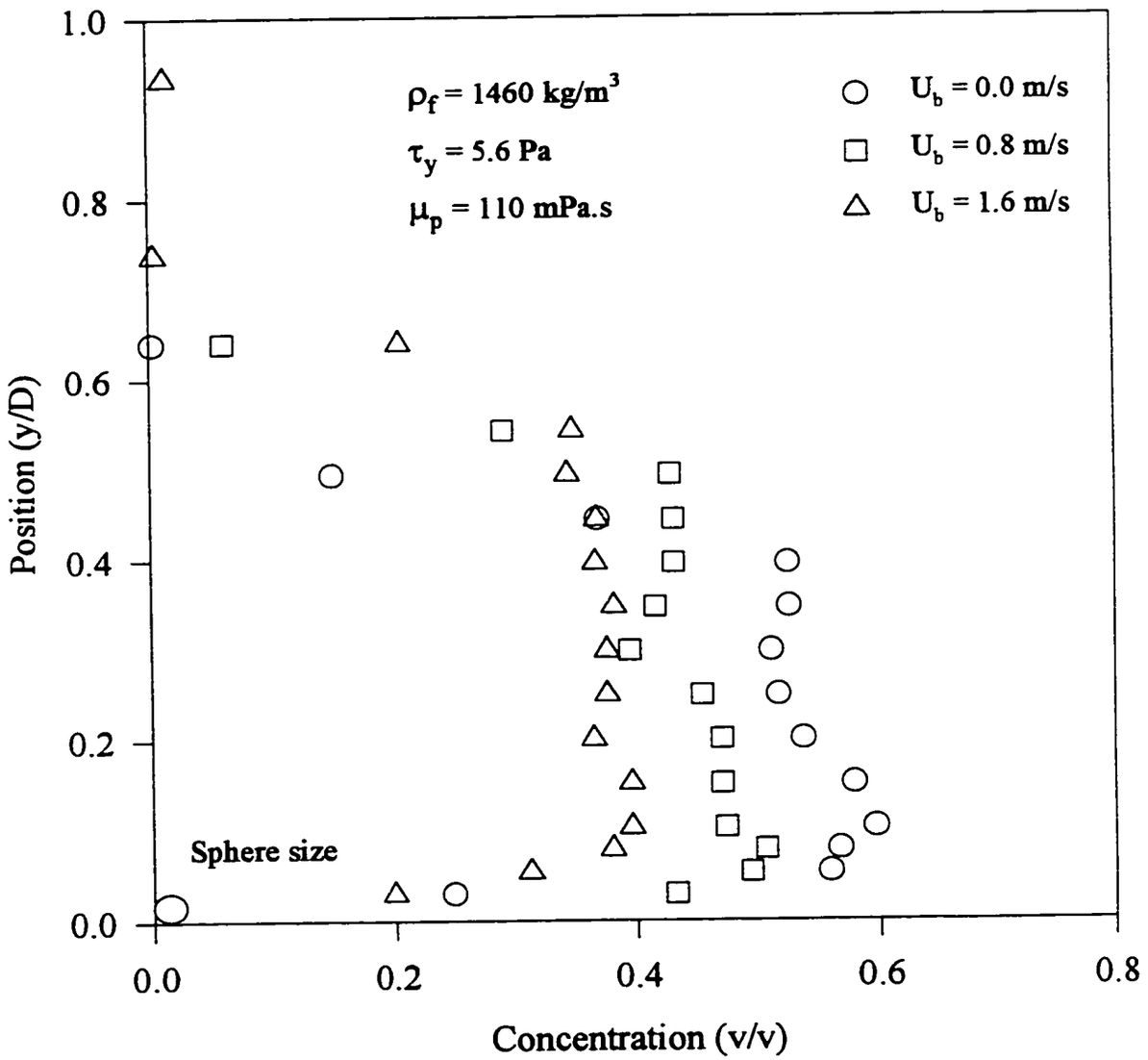

Figure 4.22 : **Concentration profiles for 25% 1.7 mm spheres in a Kaolin/Bentonite suspension.**

towards zero. Particle flow at 0.8 m/s appeared to be largely sliding with some shear in the bottom half of the bed and noticeably more relative motion in the top half. The particles reached their loose packed arrangement once flow was stopped from the 1.6 m/s velocity.

Figures 4.23 and 4.24 show the concentration profiles for the 0.15 and 0.25 slurries at bulk velocities of 0.8 m/s and 1.6 m/s respectively. At 0.8 m/s, Figure 4.23 shows the two in-situ concentrations had approximately the same concentration of 0.45 in the uniform region along the pipe bottom. This uniform region was thicker for the higher in-situ concentration case. The concentration gradients above this were similar for both concentrations.

Figure 4.24 shows similar results at a bulk velocity of 1.6 m/s. Here the uniform region concentration was slightly higher for the higher in-situ concentration of 0.25. The concentration gradients for the two bulk concentrations were again similar.

4.5.2 Concentration profiles for 4.4 mm spheres in low yield stress fluids

The theoretical yield stress required to support the 4.4 mm spheres in a fluid with a density of 1500 kg/m^3 is 8.9 Pa. The Kaolin/Bentonite suspension used here had less than half the required yield stress but did, however, have a moderate plastic viscosity. The low yield stress and moderate plastic viscosity of these slurries led to transitional or turbulent flow at a bulk velocity of 1.6 m/s. Flow was laminar at a bulk velocity of 0.8 m/s.

Figure 4.25 shows the concentration profiles for the two in-situ concentrations at a bulk velocity of 0.8 m/s where flow was laminar. The concentration of the uniform region along the bottom of the pipe was higher for the bulk concentration of 0.25. This effect is more substantial here than was observed with the smaller 1.7 mm spheres. With these

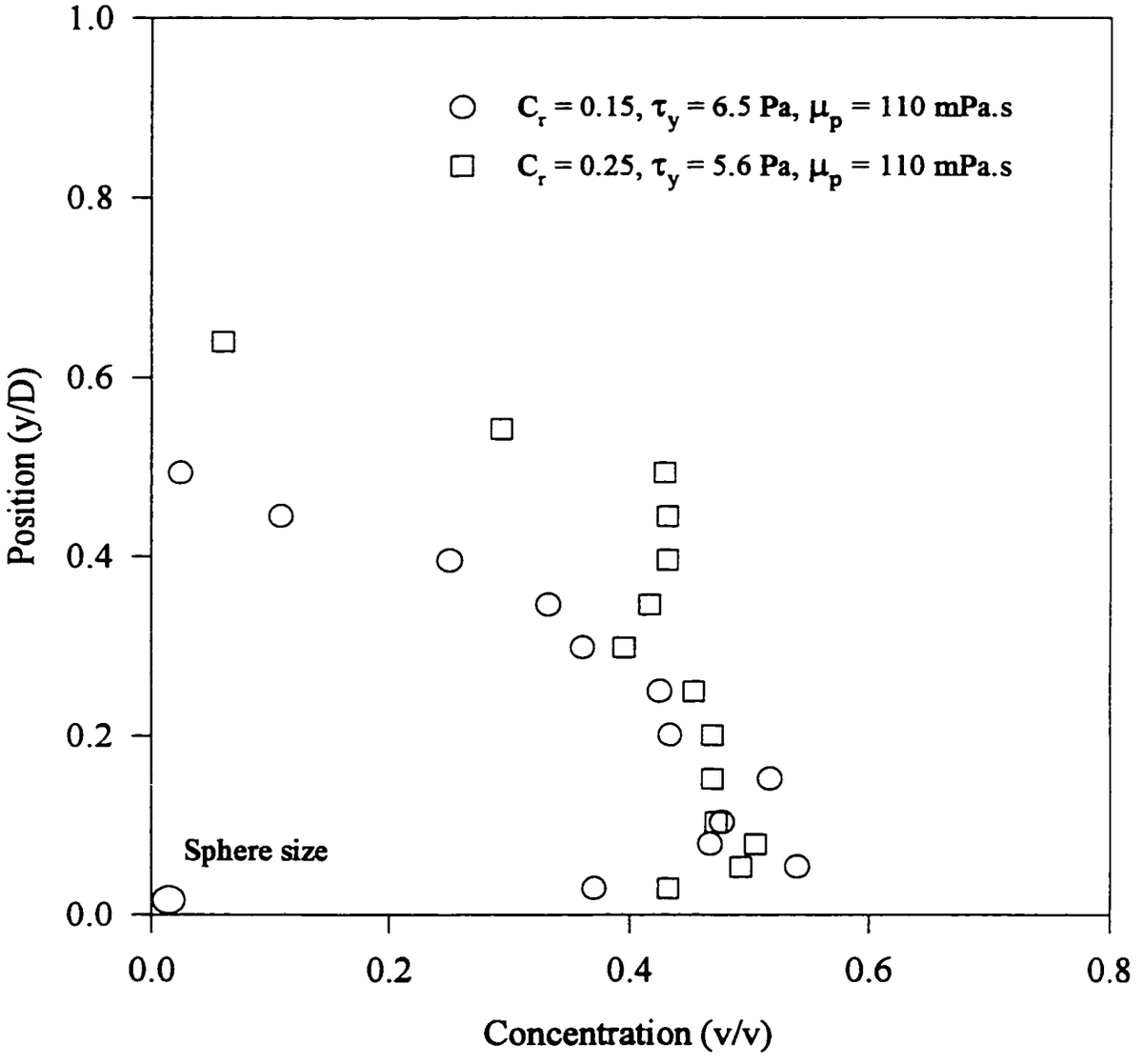

Figure 4.23 : Concentration profiles for 1.7 mm spheres in Kaolin/Bentonite suspensions at a bulk velocity of 0.8 m/s.

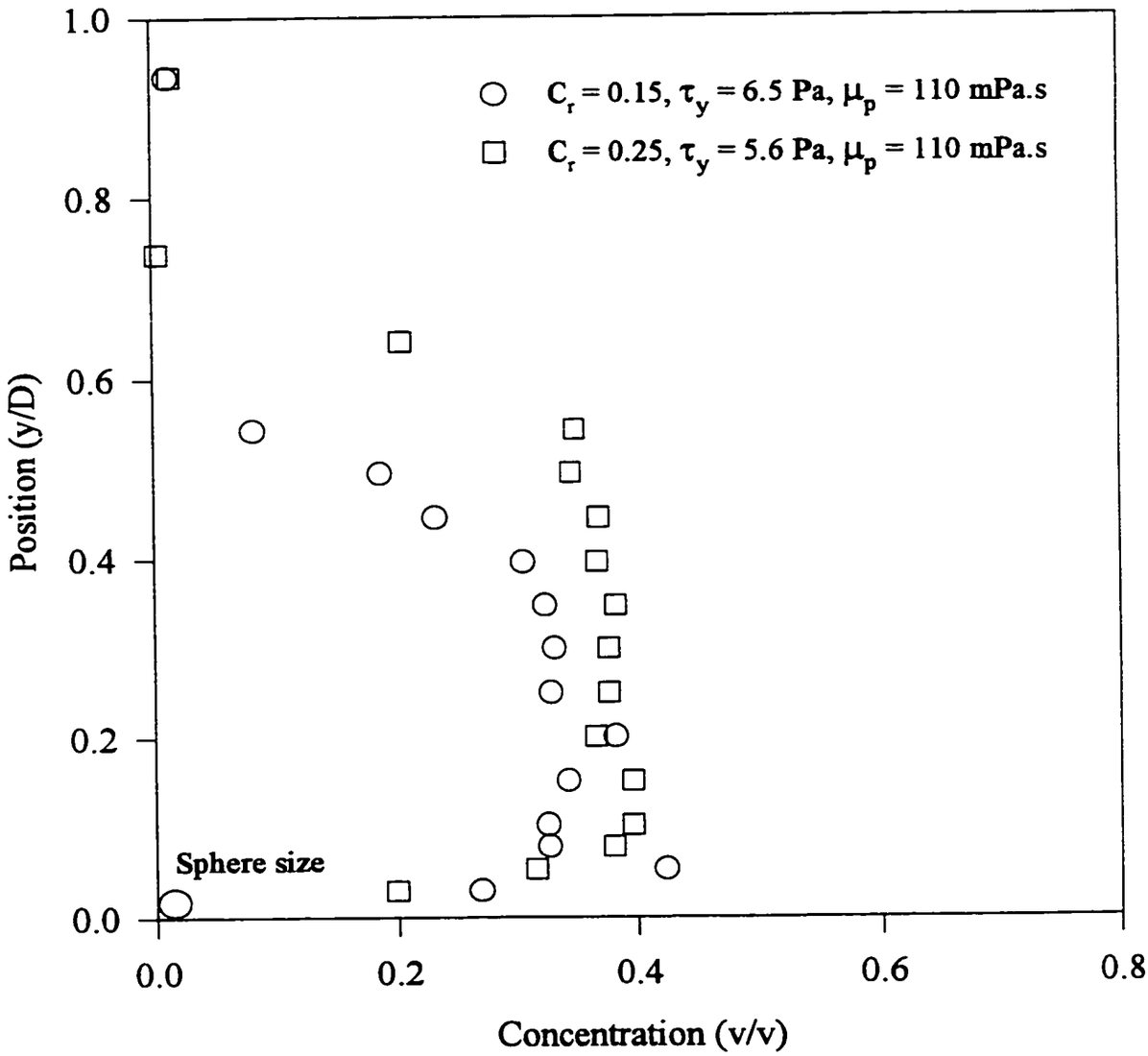

Figure 4.24 : Concentration profiles for 1.7 mm spheres in Kaolin/Bentonite suspensions at a bulk velocity of 1.6 m/s.

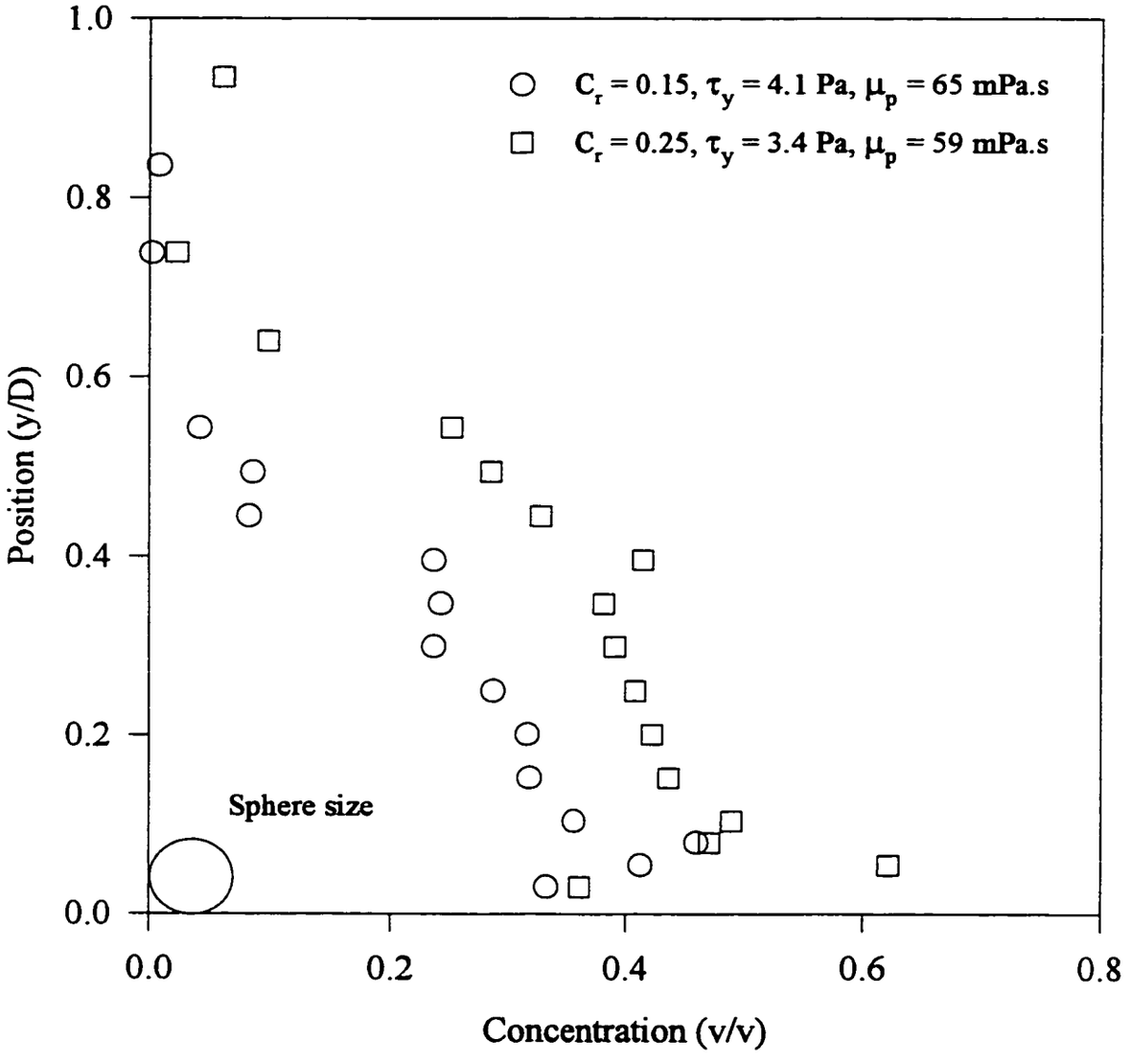

Figure 4.25 : **Concentration profiles for 4.4 mm spheres in Kaolin/Bentonite suspensions with low yield stresses at a bulk velocity of 0.8 m/s.**

slurries, the uniform concentration layers seem to have about the same thickness for the two concentrations.

Figure 4.26 shows the concentration profiles at a bulk velocity of 1.6 m/s where the flow is turbulent and further particle dispersion is observed. There still appears to be a region of nearly constant concentration near the bottom of the pipe but with a lower concentration than in the laminar flow case. Particles are carried higher in the flow at this higher velocity. In the upper regions of the flow where the concentration decreases, the decrease is much more gradual than was observed with the laminar cases so that some particle are found high in the pipe.

4.5.3 Concentration profiles for 4.4 mm spheres in high yield stress fluids

The high yield stress clay suspensions used here had lower densities but higher fractions of Bentonite. This resulted in the glass spheres having a larger immersed weight than in the high density/low yield stress suspensions. The theoretical minimum yield stress required to suspend the 4.4 mm spheres in this fluid was 12 Pa. Negligible particle settling rates were confirmed by particle settling trials in a stationary fluid. Two slurries were made from two Kaolin/Bentonite suspensions whose yield stresses exceeded the theoretical minimum. Both slurries had in-situ concentrations of 0.15.

The suspensions used in these slurries were too viscous to characterize reliably with the concentric cylinder viscometer. The shear stress required to characterize these fluids properly with the viscometer exceeded the range of the instrument. Based on experience with these suspensions, the measured yield stress was probably fairly accurate while the indicated plastic viscosity may have been too high. Thus the fluid model parameters for

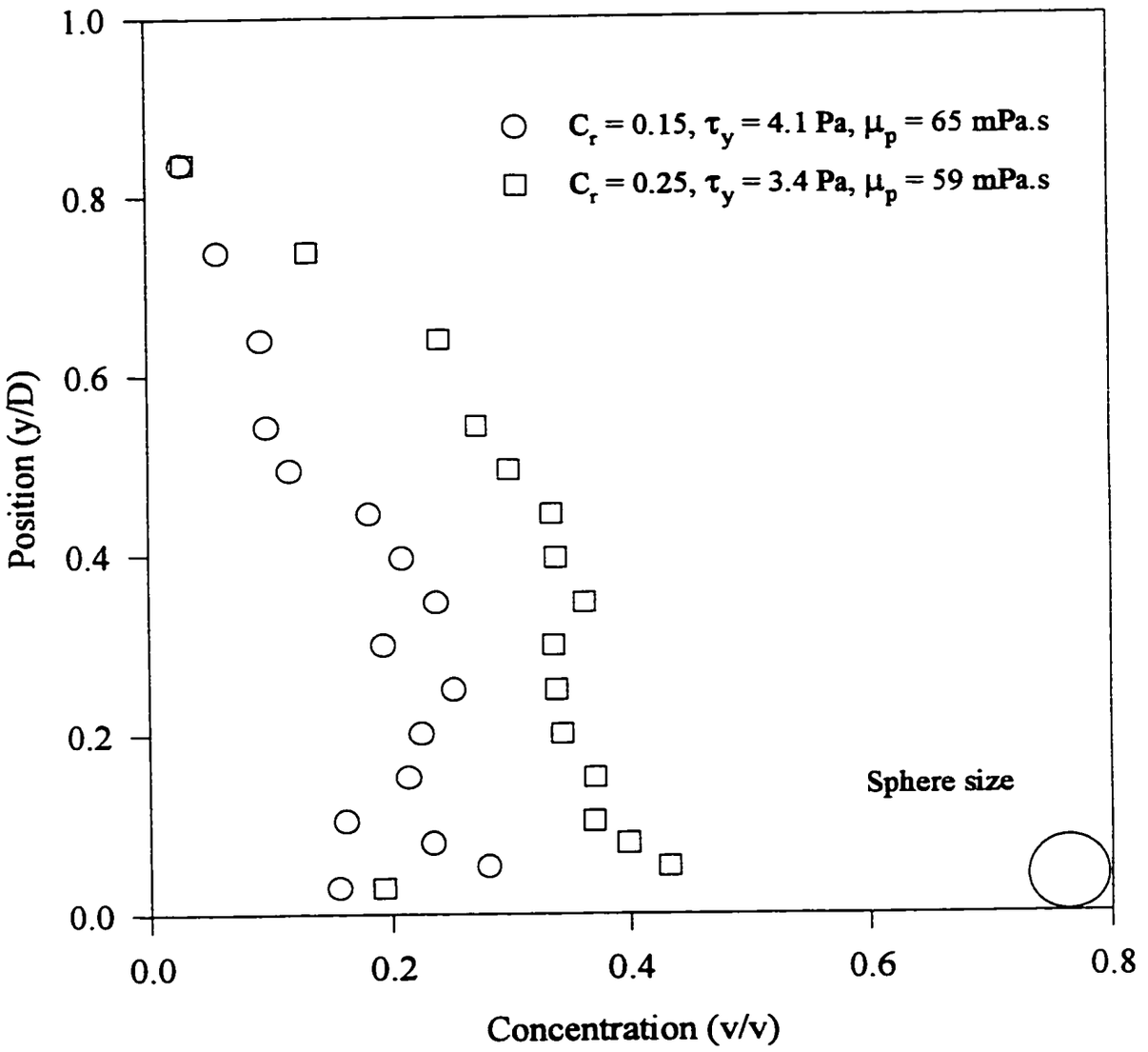

Figure 4.26 : Concentration profiles for 4.4 mm spheres in Kaolin/Bentonite suspensions with low yield stresses at a bulk velocity of 1.6 m/s.

these suspensions should be viewed with some scepticism.

The first suspension had a yield stress of 17 Pa and a plastic viscosity of 62 mPa.s as determined from concentric cylinder viscometry. The second suspension was produced by an addition of Bentonite to the first slurry. Viscometry of this suspension indicated a yield stress of 25 Pa and a plastic viscosity of 80 mPa.s.

Figure 4.27 shows the concentration profiles measured with the Kaolin/Bentonite suspension whose yield stress was 17 Pa. While the yield stress exceeded the theoretical value for particle suspension in a static fluid, the profiles show stratified flow for bulk velocities of 0.8 and 1.6 m/s. Both velocities produced laminar flow but show a marked difference from the profiles observed in the low yield stress fluid cases. In the high yield stress fluids, the concentration profile displayed a smaller region of nearly uniform concentration and a larger region of decreasing concentration. The concentration at the pipe bottom was observed to be high and decreased as the velocity increased. When the flow of the 17 Pa slurry was stopped abruptly from a velocity of 1.6 m/s, the particles settled to form a loosely packed bed. With the 25 Pa yield stress fluid, the particles did not settle completely when flow was stopped from 1.6 m/s. With the more viscous slurry, the flow stopped quickly and the dispersed particles became supported in a partially dispersed state in the stationary fluid. This observation may be indirect evidence that the yield stress of a shearing fluid is different from its value when stationary as suggested by Atapattu et al. (1988).

Figures 4.28 and 4.29 show the concentration profiles for the two high yield stress slurries at bulk velocities of 0.8 and 1.6 m/s respectively. In both cases, the concentrations

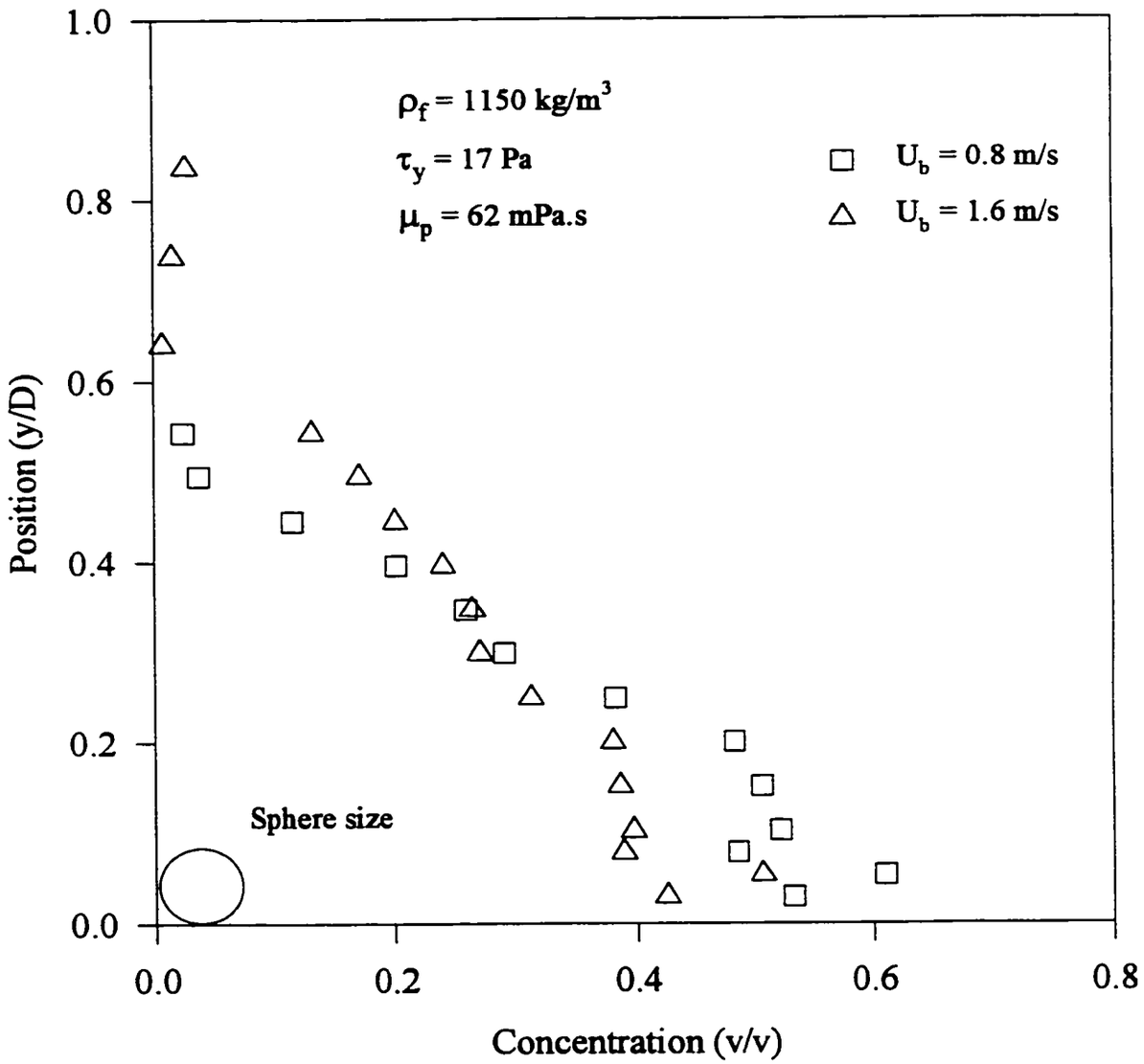

Figure 4.27 : Concentration profiles for 15% 4.4 mm spheres in a Kaolin/Bentonite suspension with a high yield stress.

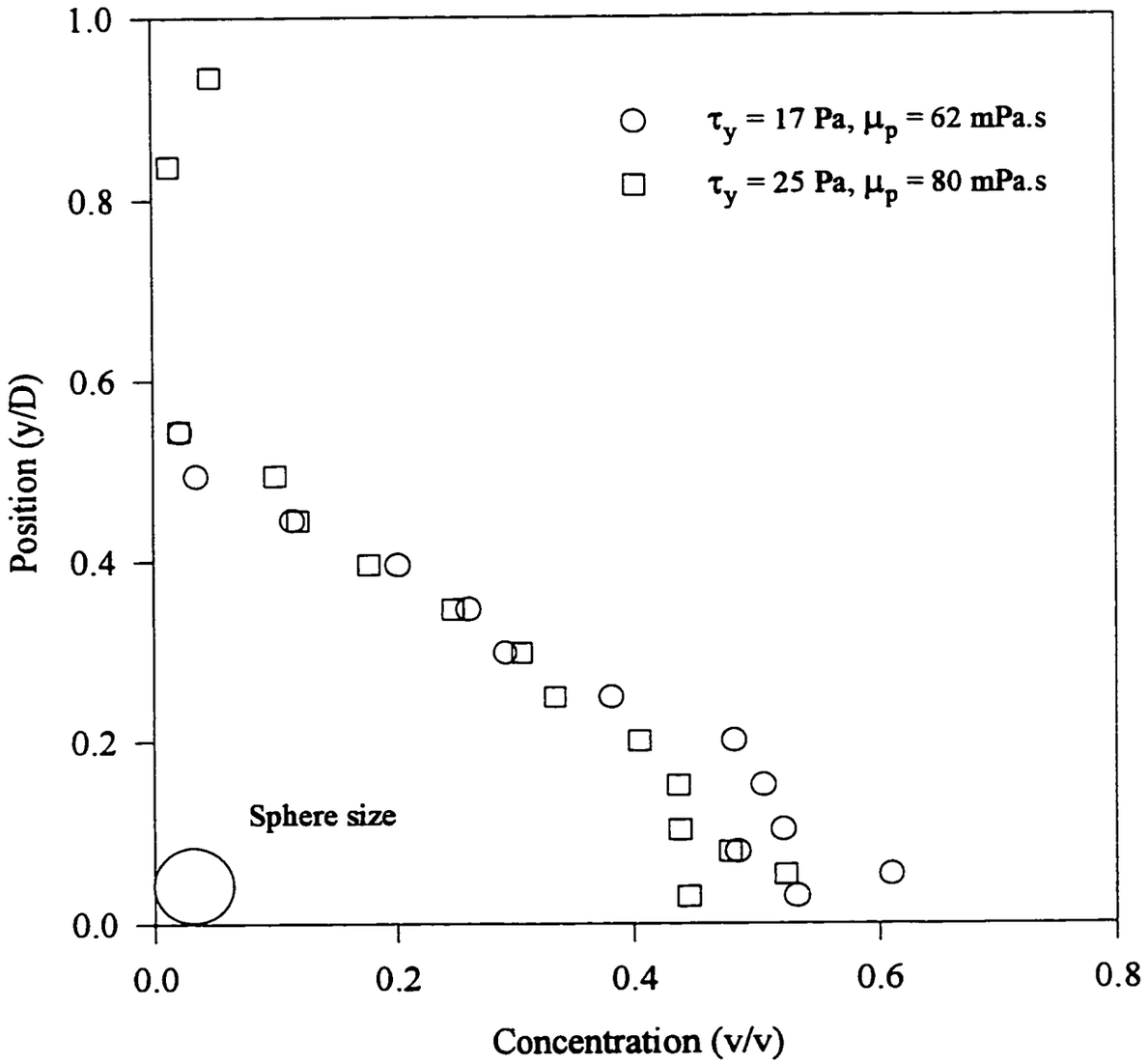

Figure 4.28 : Concentration profiles for 15% 4.4 mm spheres in Kaolin/Bentonite suspensions with high yield stresses at a bulk velocity of 0.8 m/s.

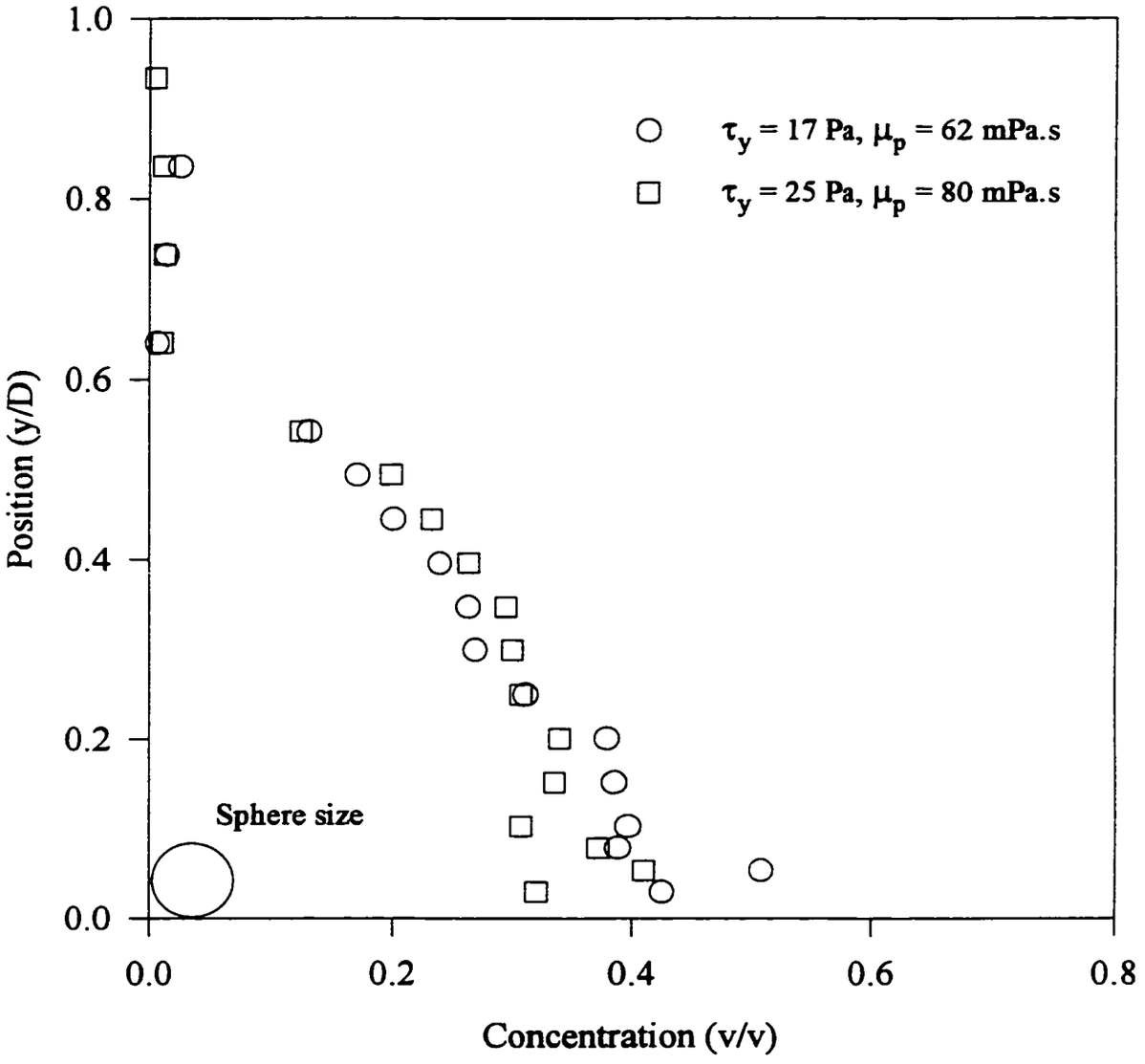

Figure 4.29 : Concentration profiles for 15% 4.4 mm spheres in Kaolin/Bentonite suspensions with high yield stresses at a bulk velocity of 1.6 m/s.

between the pipe bottom and y/D = 0.2 are slightly higher with the less viscous fluid. Above y/D = 0.2, the concentrations are approximately the same.

4.5.4 Concentration profiles for 4.1 mm gravel slurries

The concentration profiles for 4.1 mm gravel in a high density Kaolin/Bentonite suspension are shown in Figure 4.30 at an in-situ concentration of 0.15. Flow was always laminar for these profiles. At a velocity of 0.8 m/s the concentration decreases from a high value at the pipe bottom in a nearly linear fashion. At the higher bulk velocity, the uniform concentration layer near the bottom of the pipe is more clearly seen.

The concentration profiles for a gravel slurry with an in-situ concentration of 0.25 are shown in Figure 4.31. The profiles show regions of nearly uniform concentration in the lower half of the pipe. The concentrations of these uniform regions are slightly lower at this bulk concentration when compared to the lower in-situ concentration profiles (Figure 4.30). Above this region, the concentration falls. The concentrations in the uniform concentration region are slightly lower at the higher velocity. The fluid was slightly more viscous, as indicated by the Bingham model parameters, than the lower in-situ concentration case shown in Figure 4.30. This is probably due to an increase in the quantity of fine solids resulting from degradation of these large angular particles. Degradation of these particles was discussed in Section 3.7.2.

Concentration profiles for gravel slurries with in-situ concentrations of 0.15 and 0.25 at a bulk velocity of 0.8 m/s are shown in Figure 4.32. Concentrations near the bottom of the pipe are similar as are the concentration gradients above the uniform concentration layers. The higher plastic viscosity of the high concentration case resulting from the particle

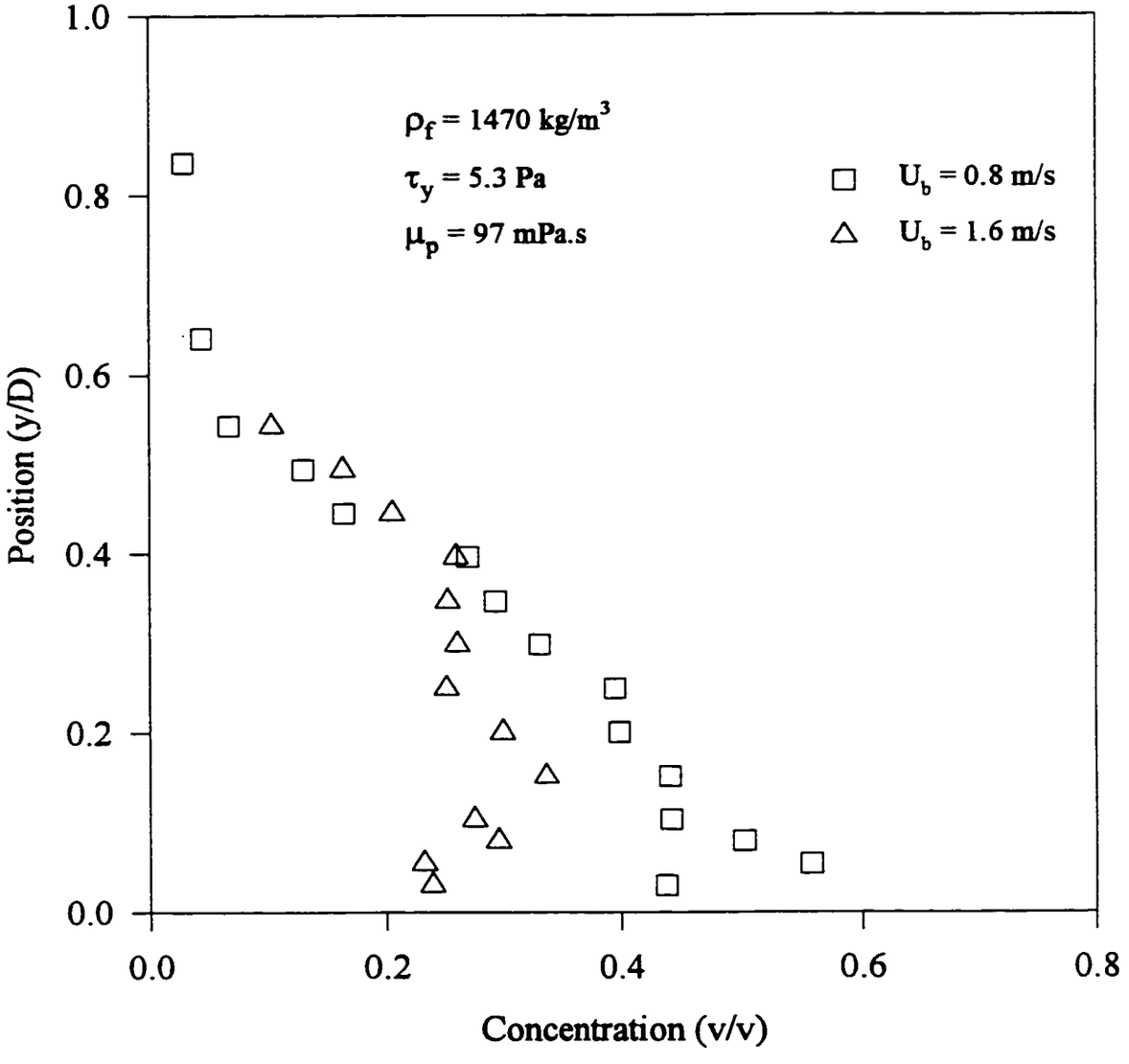

Figure 4.30 : Concentration profiles for 15% 4.1 mm gravel in a Kaolin/Bentonite suspension.

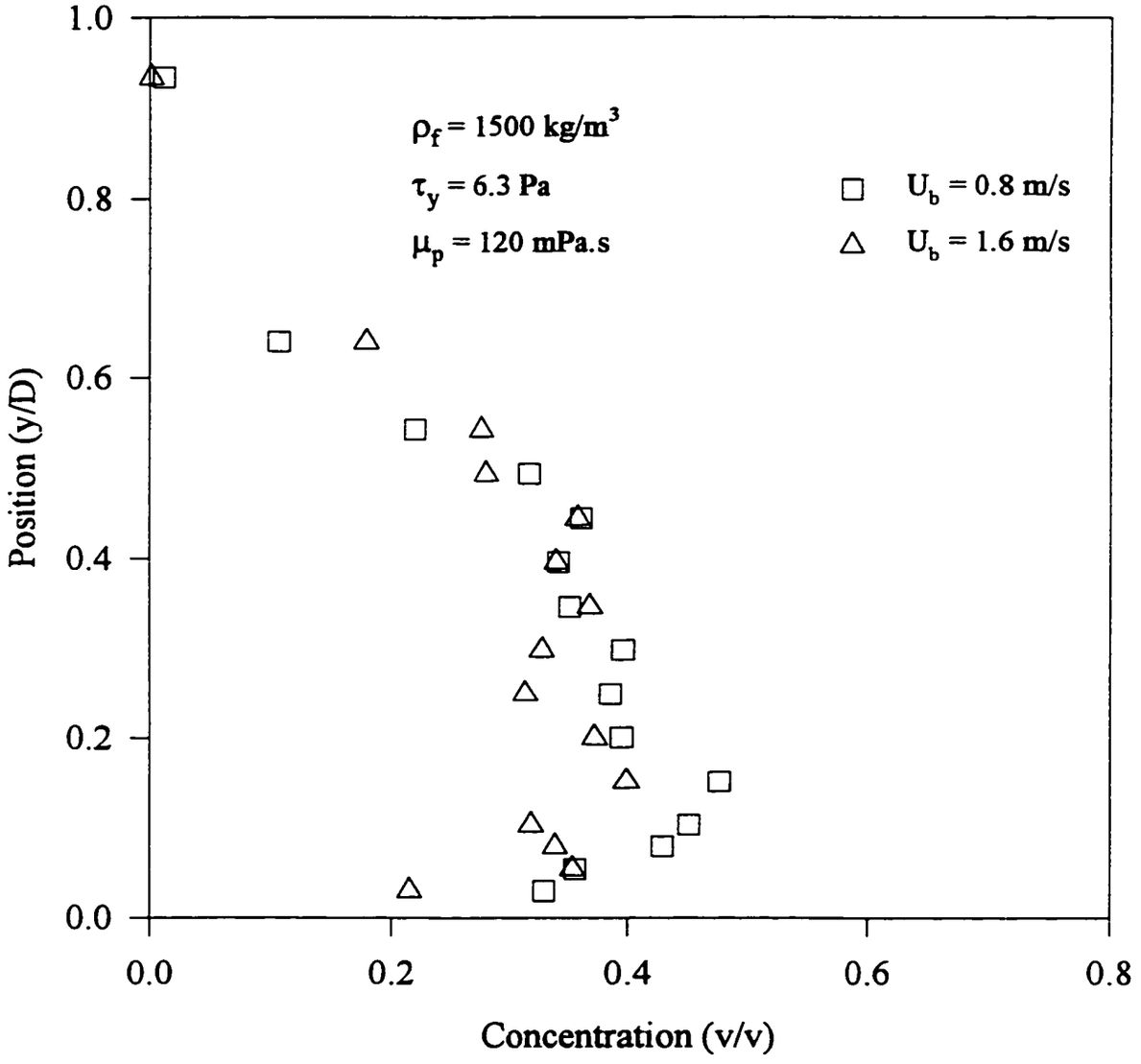

Figure 4.31 : Concentration profiles for 25% 4.1 mm gravel in a Kaolin/Bentonite suspension.

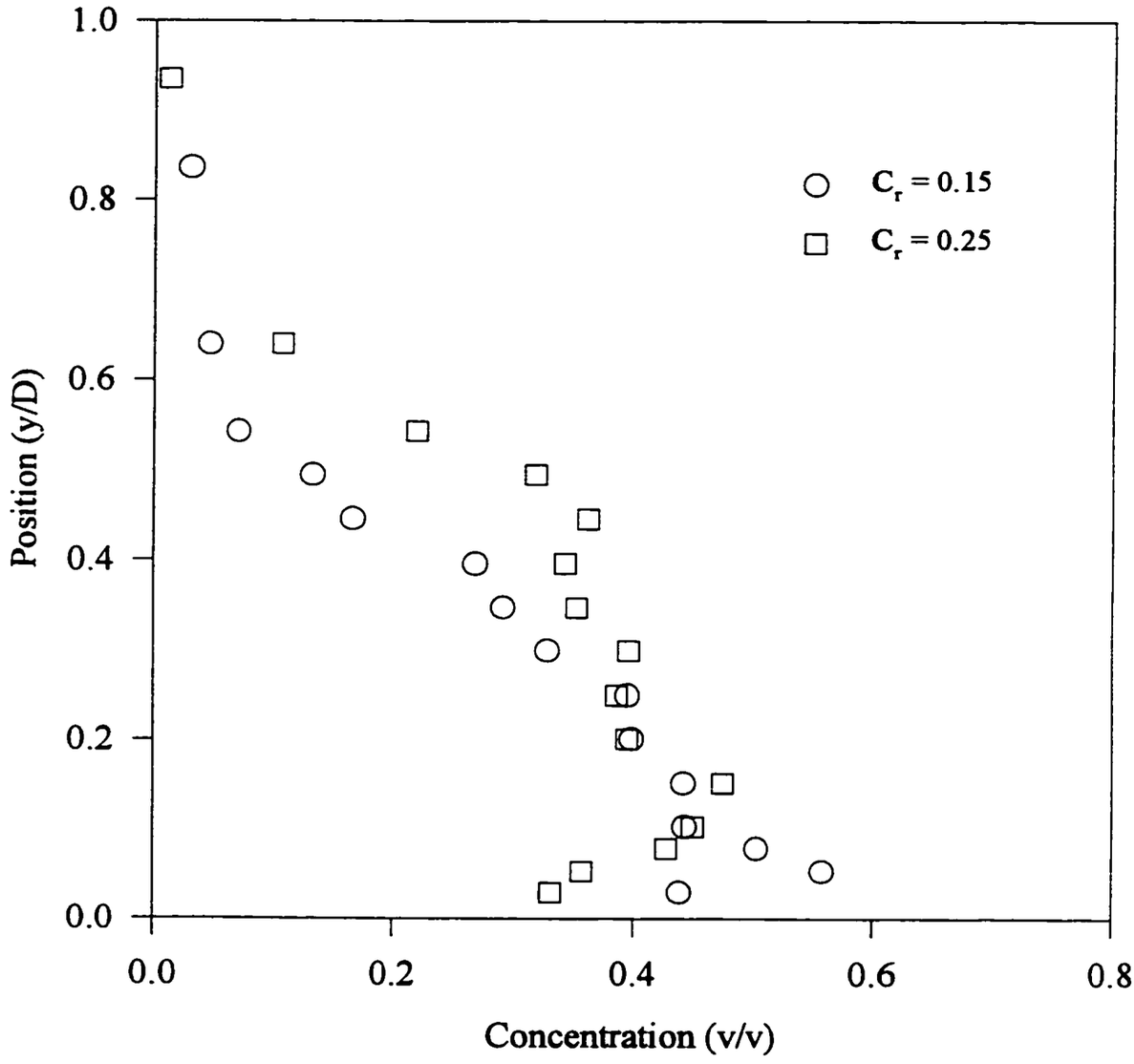

Figure 4.32 : Concentration profiles for 4.1 mm gravel in Kaolin/Bentonite suspensions at a bulk velocity of 0.8 m/s.

degradation makes a direct comparison of the two slurries a little uncertain.

Figure 4.33 shows the concentration distribution for gravel at in-situ concentrations of 0.15 and 0.25 at a bulk velocity of 1.6 m/s. The profiles are similar in shape with the higher bulk particle concentration being reflected in the local concentration at all positions, in contrast with the lower velocity observations.

4.5.5 Comparison of concentration profiles in Kaolin/Bentonite suspensions

The concentration profiles for coarse particles in Kaolin/Bentonite suspensions which were measured included two sizes of glass spheres and gravel at two bulk velocities and two in-situ concentrations. The fluids all had significant plastic viscosities which varied by a factor of two. Fluid yield stresses were, in some cases, high enough to support the particles under static conditions. In all cases, the slurries were found to be highly stratified.

Figures 4.34 and 4.35 show the concentration profiles for laminar flow cases with an in-situ concentration of 0.15 at bulk velocities of 0.8 m/s and 1.6 m/s respectively. Data obtained when the yield stresses were large enough to support particles are distinguished in the inset tables. While there is some variation in local particle concentrations, the similarity between cases is evident in spite of the variation in particle size and fluid properties.

Figures 4.36 and 4.37 show the concentration profiles for in-situ concentrations of 0.25 at the same two bulk velocities. Again there is only a marginal difference between the local concentrations. It appears that the variations in particle and fluid properties in the cases investigated here were of secondary importance to the in-situ concentration and the bulk velocity in determining the concentration profiles for these slurries. The yield stress did not

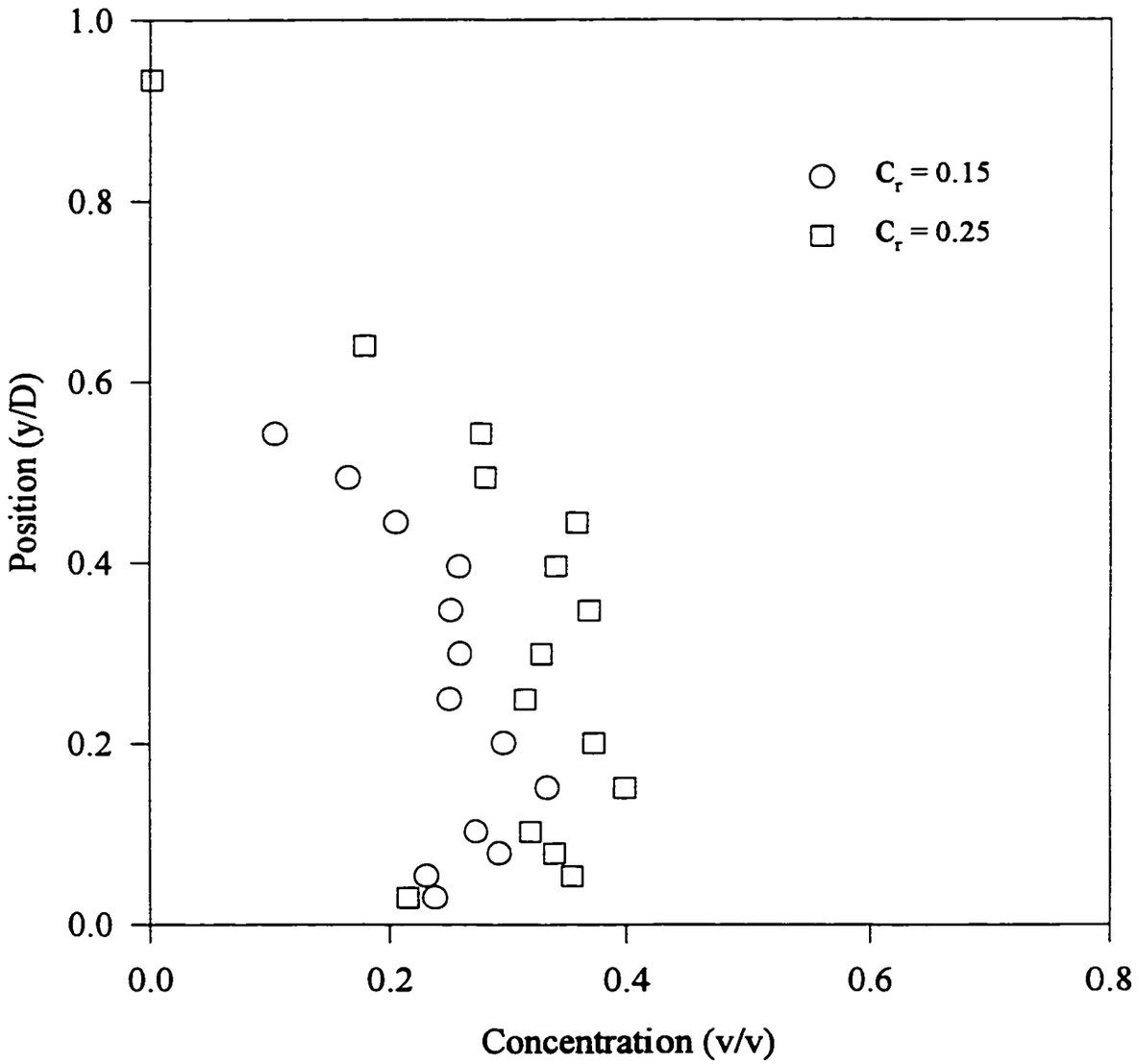

Figure 4.33 : Concentration profiles for 4.1 mm gravel in Kaolin/Bentonite suspensions at a bulk velocity of 1.6 m/s.

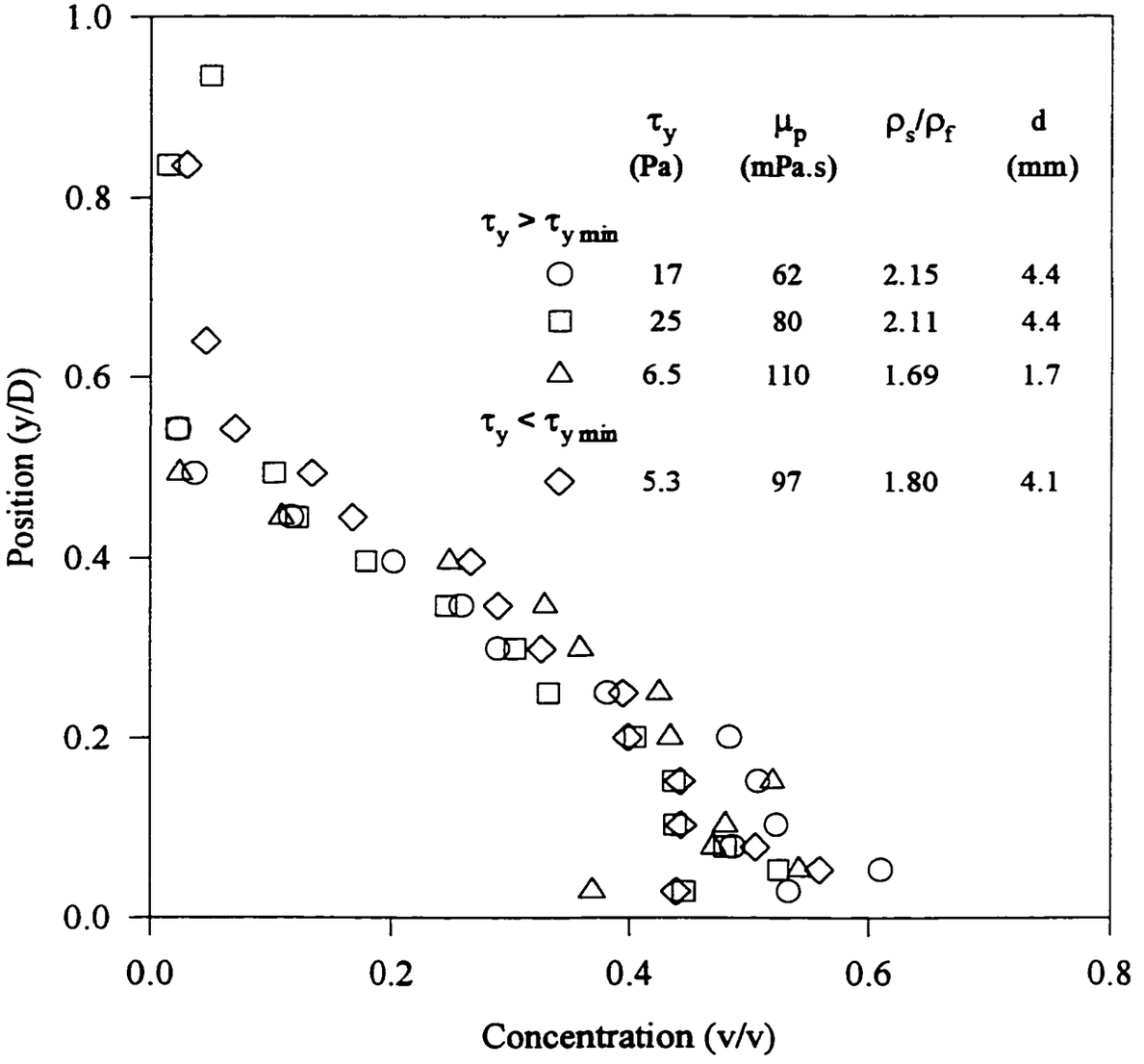

Figure 4.34 : Concentration profiles for 15% coarse particles in Kaolin/Bentonite suspensions at a bulk velocity of 0.8 m/s.

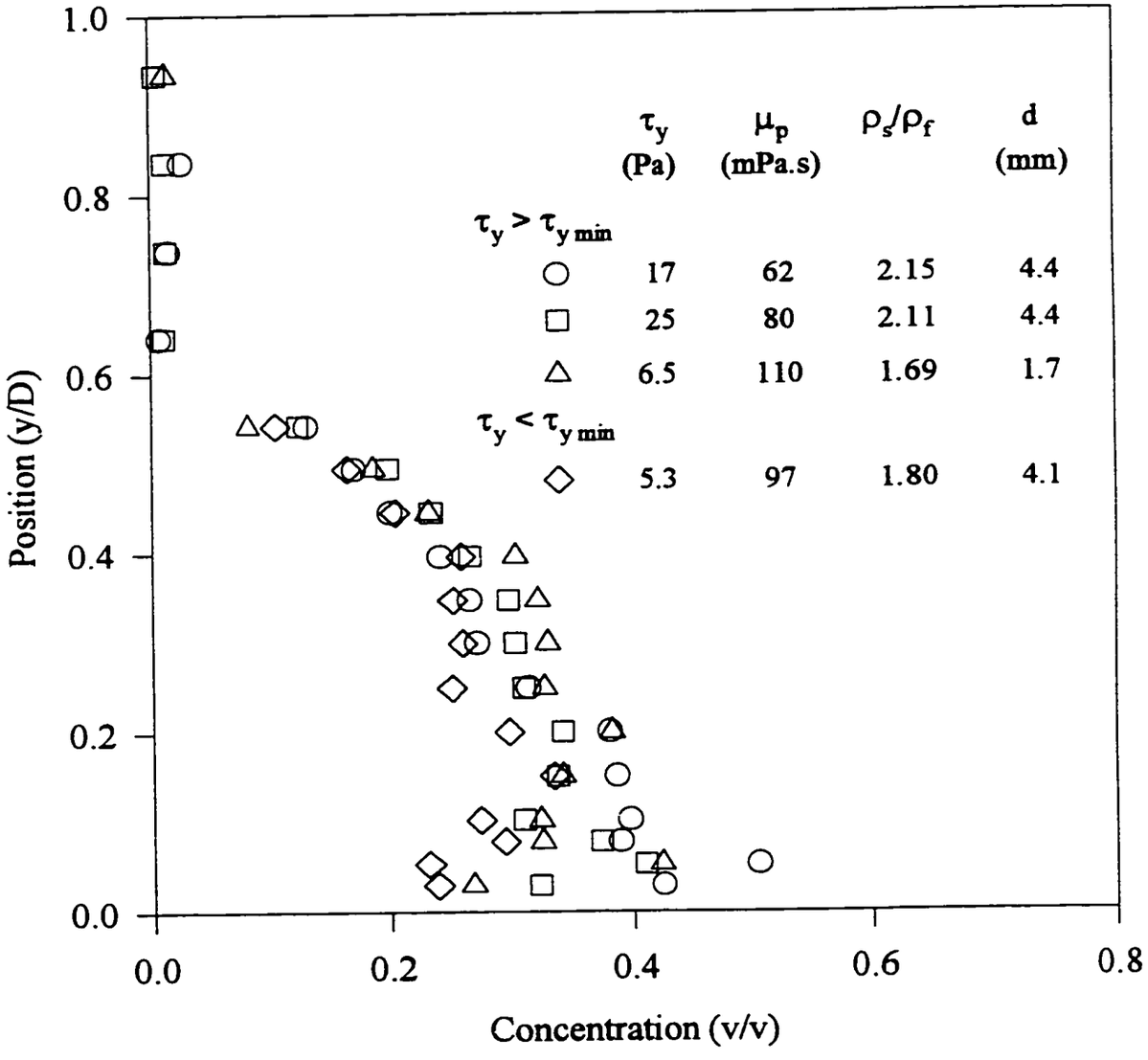

Figure 4.35 : Concentration profiles for 15% coarse particles in Kaolin/Bentonite suspensions at a bulk velocity of 1.6 m/s.

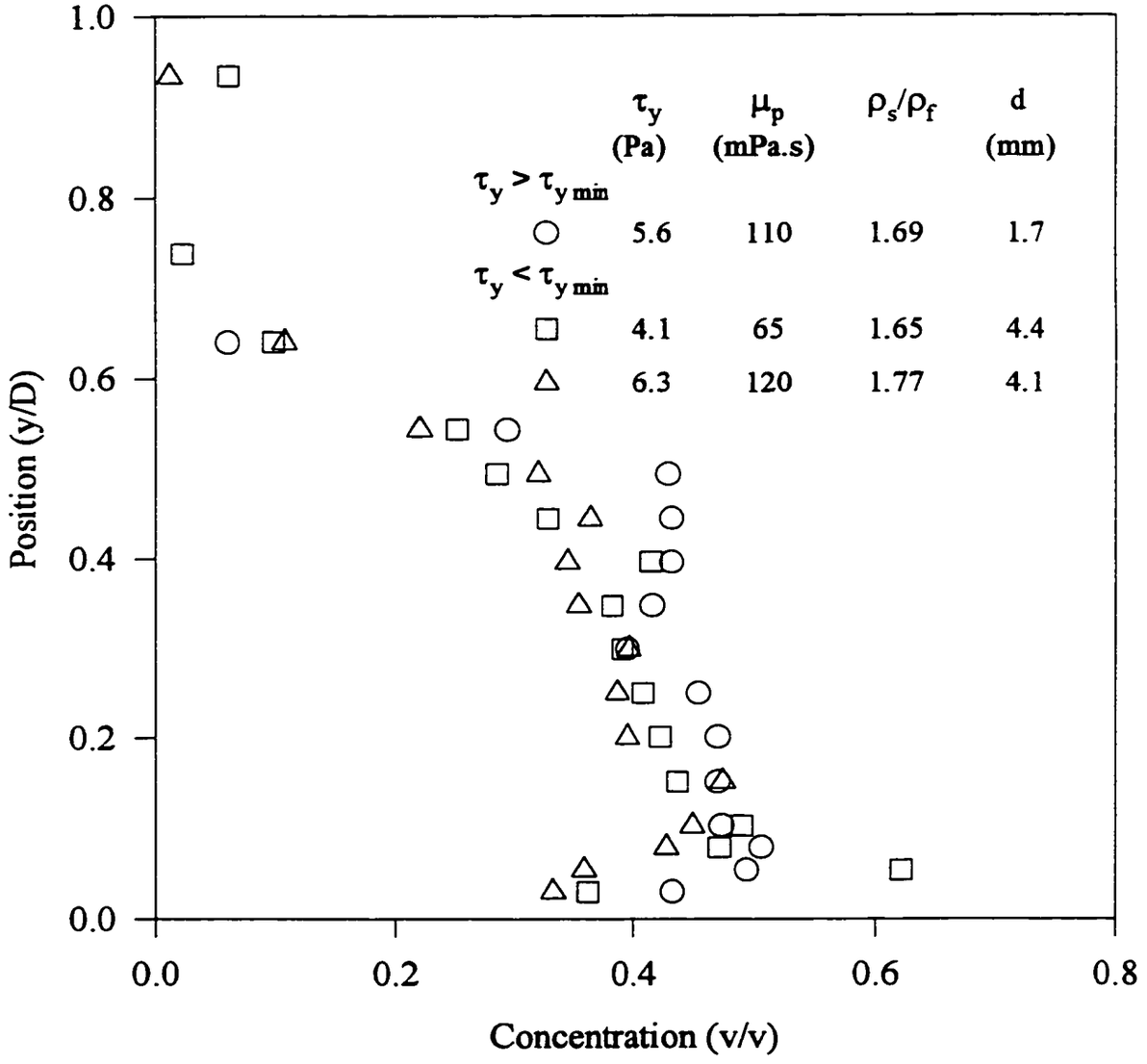

Figure 4.36 : Concentration profiles for 25% coarse particles in Kaolin/Bentonite suspensions at a bulk velocity of 0.8 m/s.

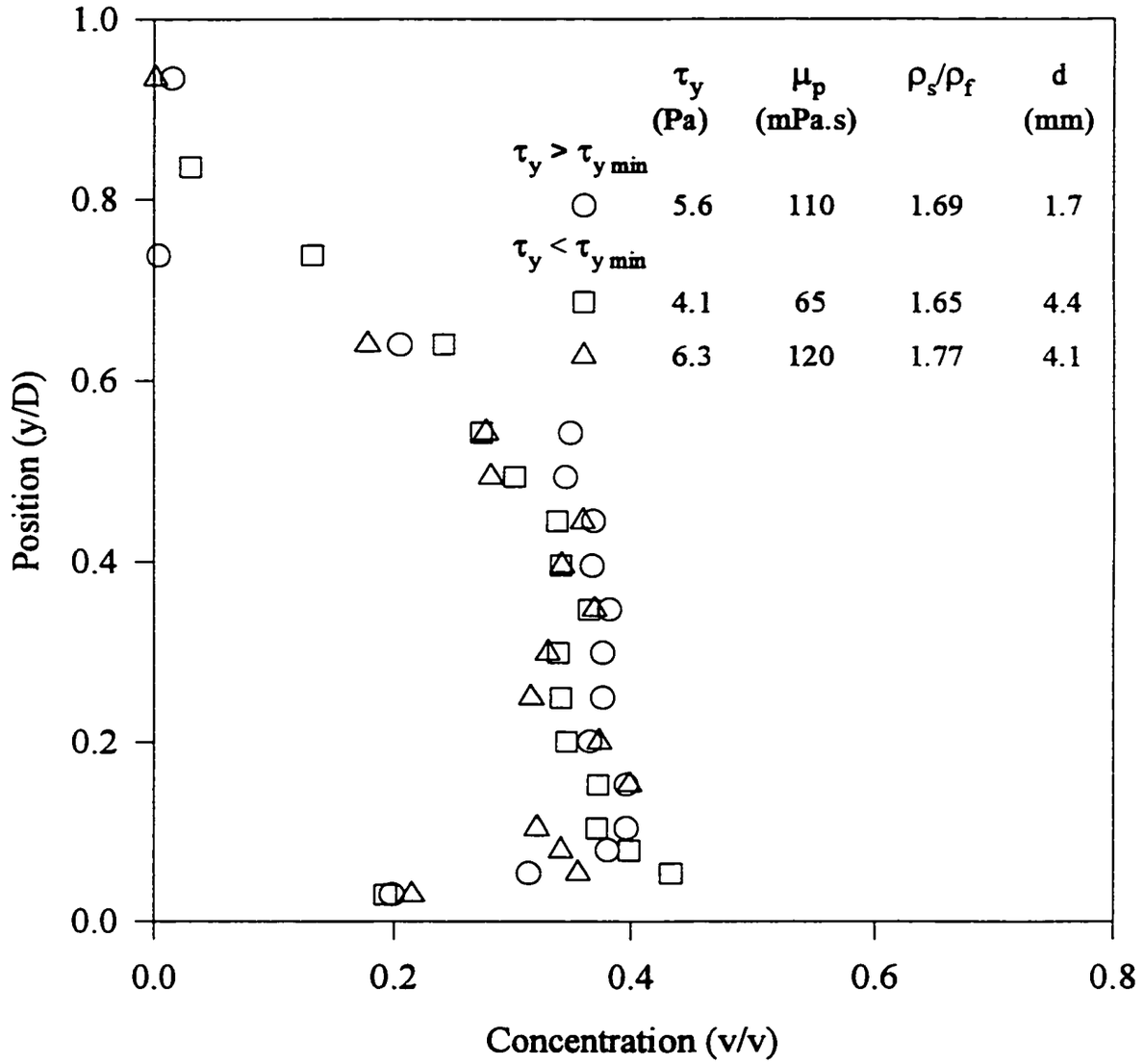

Figure 4.37 : Concentration profiles for 25% coarse particles in Kaolin/Bentonite suspensions at a bulk velocity of 1.6 m/s.

seem to contribute significantly to particle suspension in horizontally flowing slurries.

4.6 Particle velocity profiles in Kaolin/Bentonite slurries

Particle velocity profiles were recorded along the vertical axis of the pipe for each of the slurries at two bulk velocities. The measured velocities are believed to be significantly below their true values because of a boundary layer effect on the probe. The indicated velocities in the lower layer are such that the corresponding velocities in the upper particle free region would have to be unrealistically high for the bulk velocity to be correct. The existence of a boundary layer is further supported by comparison of the velocity profiles for the two particle sizes. The effect of a boundary layer would be expected to be more severe for the smaller particles and it is seen that the measured velocities for these particles are indeed significantly lower than those for the larger particles at the same bulk velocity. However, the shapes of the velocity profiles are probably qualitatively correct. The velocities at the lowest elevations were measured using the wall probe with the elevation taken as one half the particle diameter.

Figure 4.38 shows the velocity profiles for the 1.7 mm spheres. The profiles are nearly linear for most of their range but at the higher elevations the velocities seem to increase more rapidly. At these positions the particle concentration has decreased and this should lead to a decrease in the local resistance to shear. This less viscous mixture produces the higher local shear rates or velocity gradients at these locations. The profiles for the two concentrations are similar for the two bulk velocities.

Figure 4.39 shows the particle velocity profiles for the 4.4 mm spheres in the low yield stress fluid. The flow at 0.87 m/s is laminar while the flow at 1.74 m/s is turbulent or

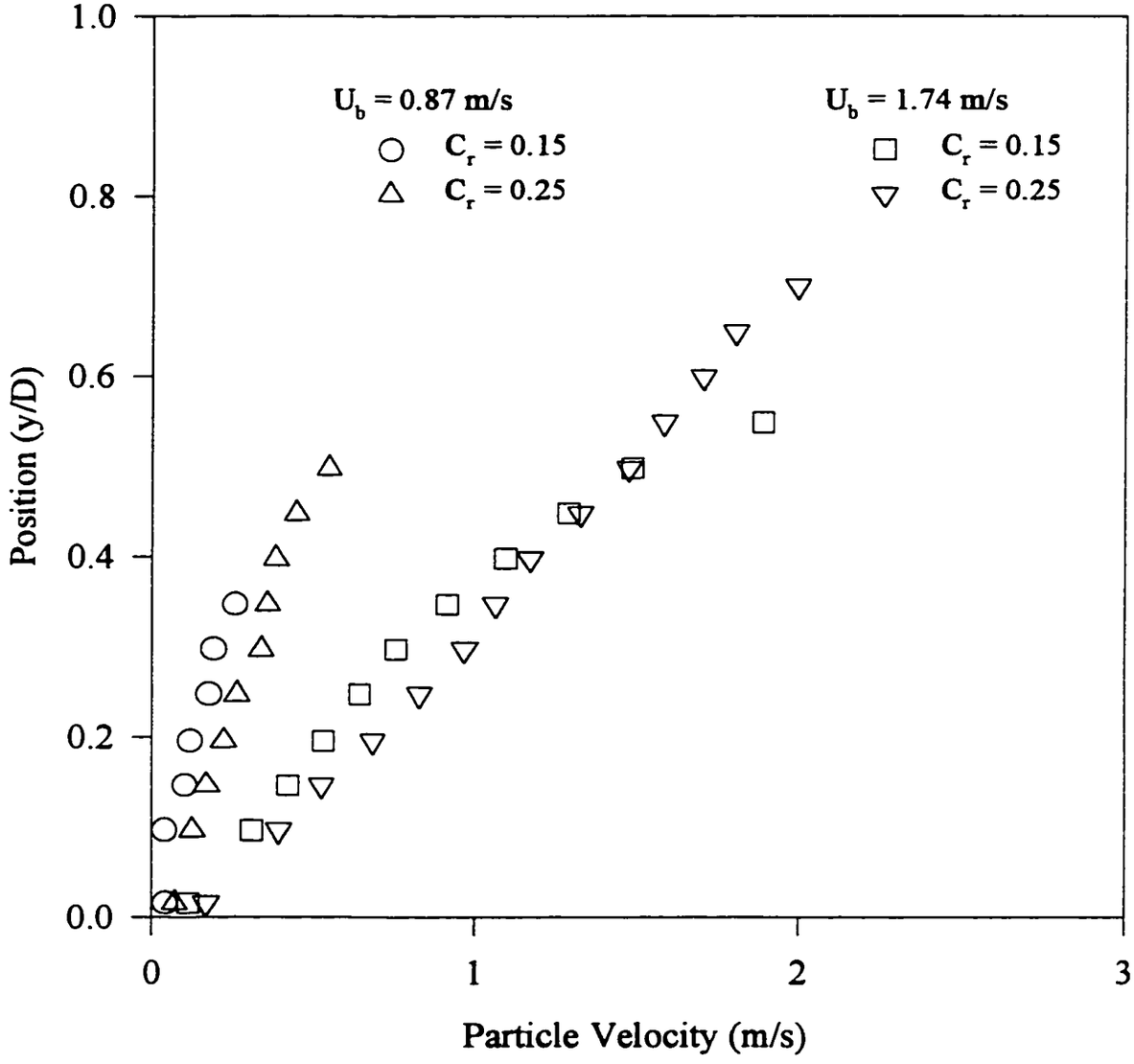

Figure 4.38 : Particle velocity profiles for 1.7 mm spheres in Kaolin/Bentonite suspensions.

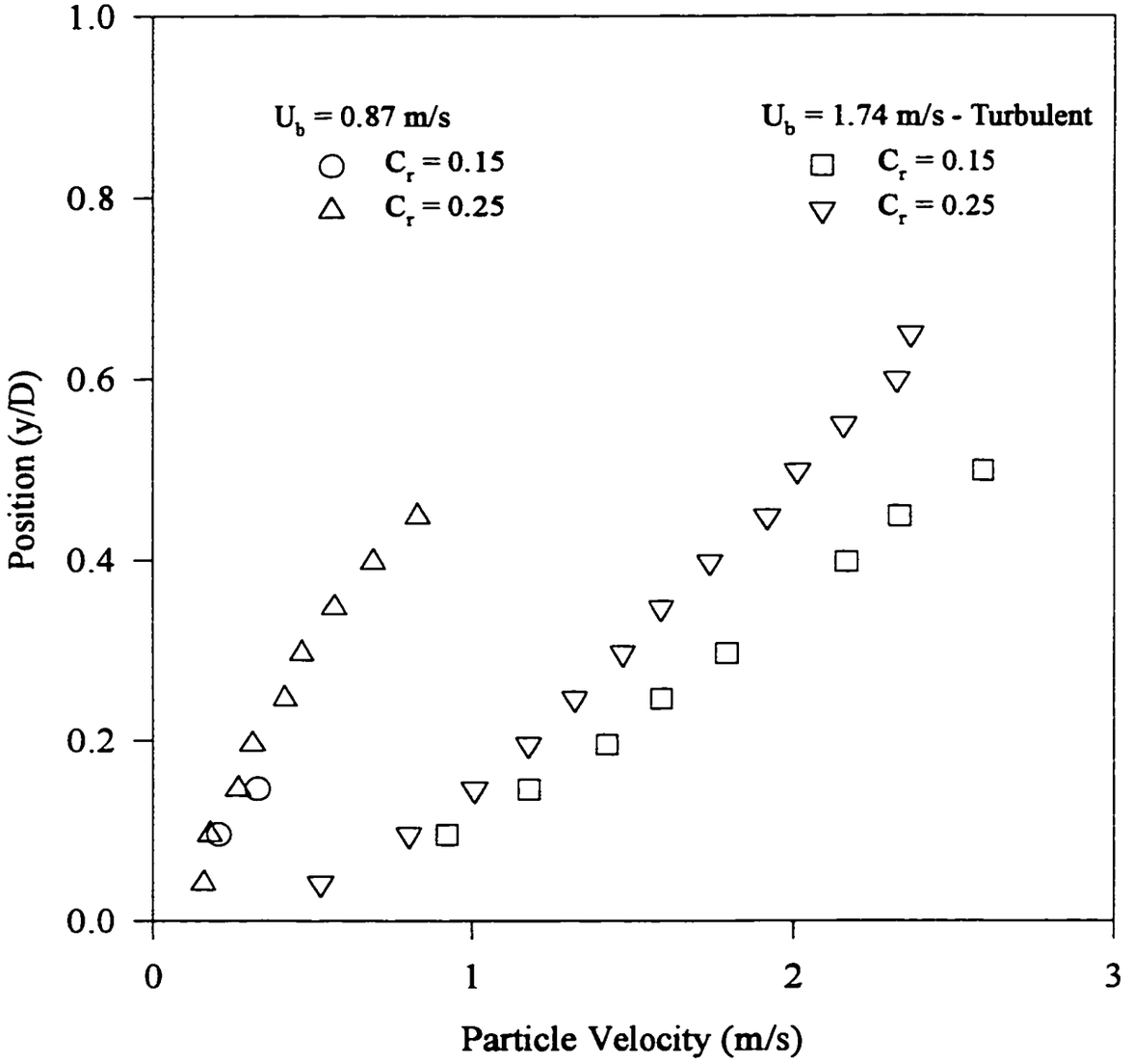

Figure 4.39 : Particle velocity profiles for 4.4 mm spheres in Kaolin/Bentonite suspensions with low yield stresses.

transitional. Again the profiles are nearly linear but with the turbulent flow, the particle velocity gradient is slightly steeper close to the wall.

Figure 4.40 shows the particle velocities for the 4.4 mm spheres in the two high yield stress suspensions. Both slurries have in-situ concentrations of 0.15 and the flow is laminar. The profiles with the two fluids are similar at the two bulk velocities. The particle velocities measured in the more viscous fluid were higher near the wall than those in the other fluid. This corresponds to the slightly lower near wall particle concentration which was measured with the more viscous fluid as was shown previously in the concentration profiles (Figures 4.28 and 4.29).

The velocity profiles for the 4.1 mm gravel are shown in Figure 4.41. As with the previous velocity profiles, they appear nearly linear over most of their length. Curvature occurs at elevations which correspond to significantly reduced concentrations as was seen in Figures 4.32 and 4.33. Flow was laminar in each case.

4.7 Kaolin/Bentonite slurry pressure gradients

In the slurry tests, both laminar and turbulent flows could be obtained with the less viscous fluids but only laminar flow could be produced with the more viscous fluids because of the pump head limitation. Turbulent flow seemed to cause degradation of the clay suspension so that some hysteresis appeared in the pressure drop measurements when turbulent flow was achieved. Partial deflocculation of clay suspensions in turbulent flow has been reported by D.G. Thomas (1964) and by Xu et al. (1993).

4.7.1 Pressure gradients of 1.7 mm sphere slurries

The pressure gradient for the flow of 1.7 mm sphere slurries at in-situ concentration

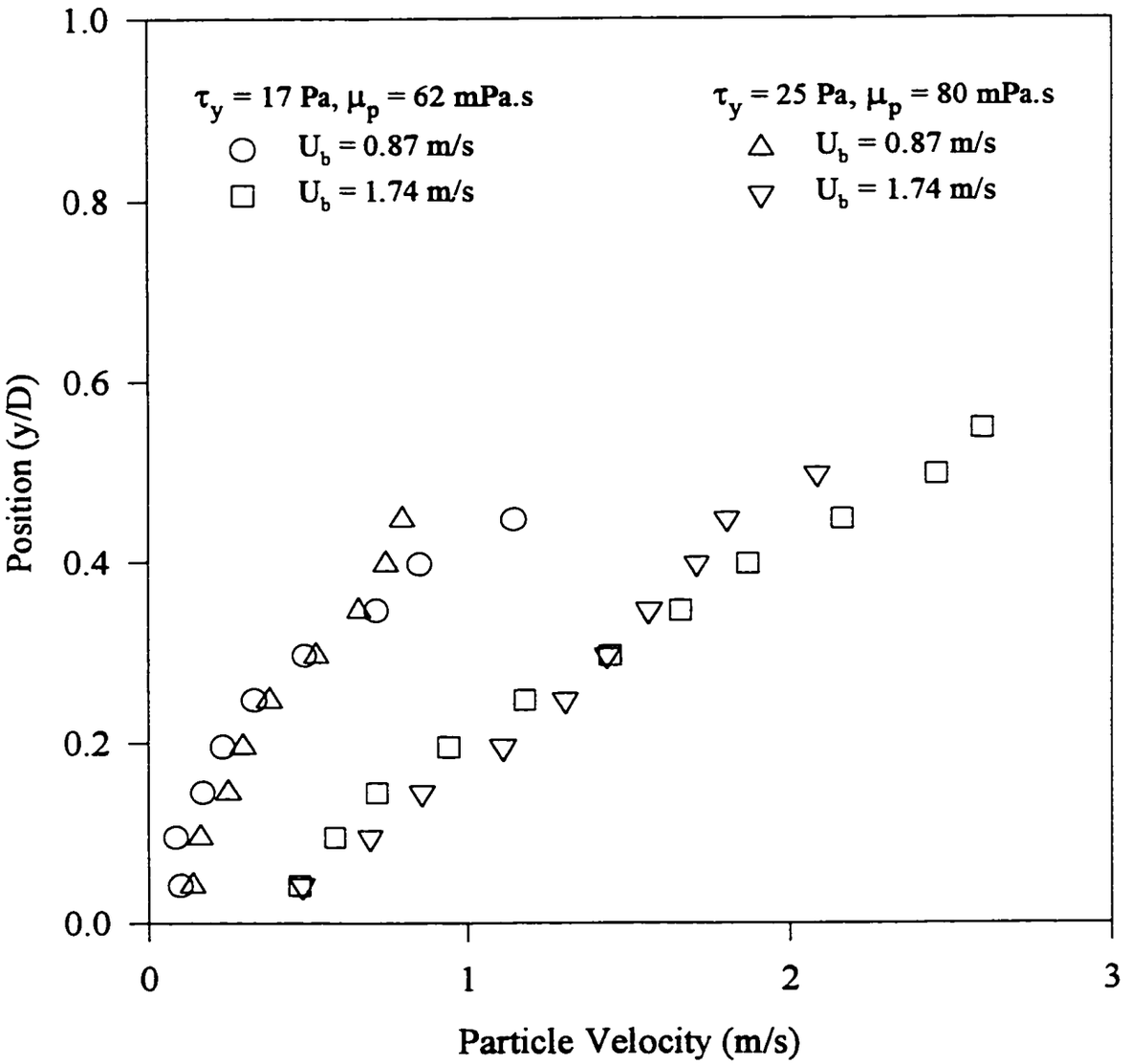

Figure 4.40 : Particle velocity profiles for 4.4 mm spheres in Kaolin/Bentonite suspensions with high yield stresses.

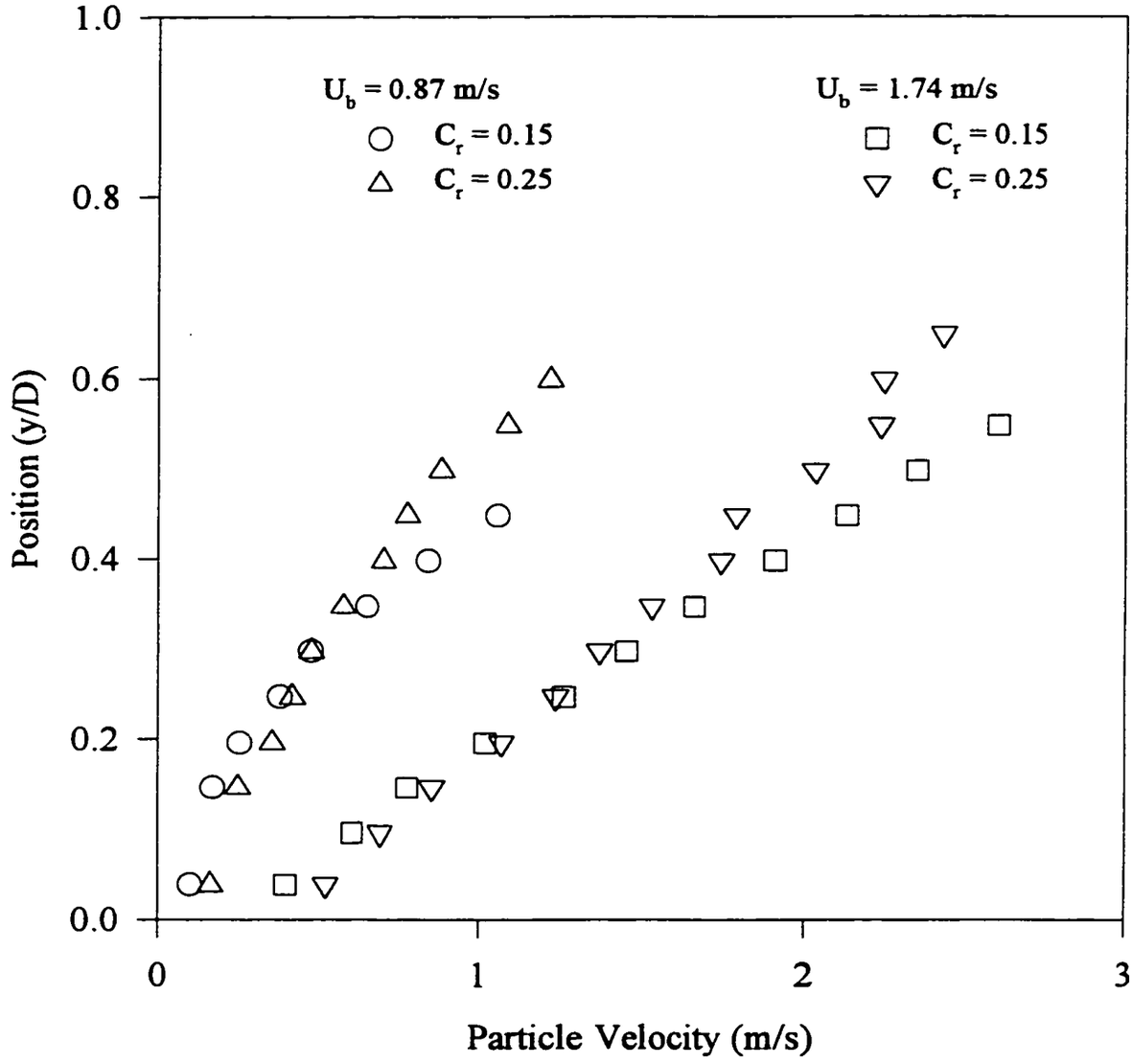

Figure 4.41 : Particle velocity profiles for 4.1 mm gravel in Kaolin/Bentonite suspensions.

of 0.15 and 0.25 are shown in Figure 4.42. The data points are shown in comparison with the predicted pressure gradients for pipe flow of the clay suspension carriers using Bingham parameters determined by viscometry and Equations 2.6 and 2.11. The yield stresses determined from viscometry was in excess of the theoretical value needed to support these particles (Equation 2.14). The effect of fluid parameter differences between the two slurries was not significant.

The shapes of the two sets of data are similar. At very low velocities, the pressure gradient increases rapidly since flow occurs through a reduced cross section above a stationary or nearly stationary bed. When all the particles are moving at a rate comparable to the bulk velocity, the pressure gradient becomes nearly a linear function of bulk velocity, resembling a Newtonian fluid in laminar flow. The apparent slope of the pressure gradient for the slurries in this region is higher than for the fluid alone and increases with bulk concentration.

At the lower concentration of 0.15, velocities were probably high enough to produce turbulent flow. These highest velocities exceed the fluid transition velocity predicted by the intersection of Equations 2.6 and 2.11. The possibility of turbulent flow is supported by the deflocculation of the clay suspension as indicated by the hysteresis in the data.

Between 0.2 m/s and 0.5 m/s, particle flow was observed to be predominantly a slowly sliding bed with some saltating particles forming small rolling dunes along the upper surface of the bed. At 1.0 m/s, the entire particle bed was moving much more quickly and was quite active with rolling dunes and particle shear evident.

At a concentration of 0.25, turbulent flow did not occur and hysteresis was not

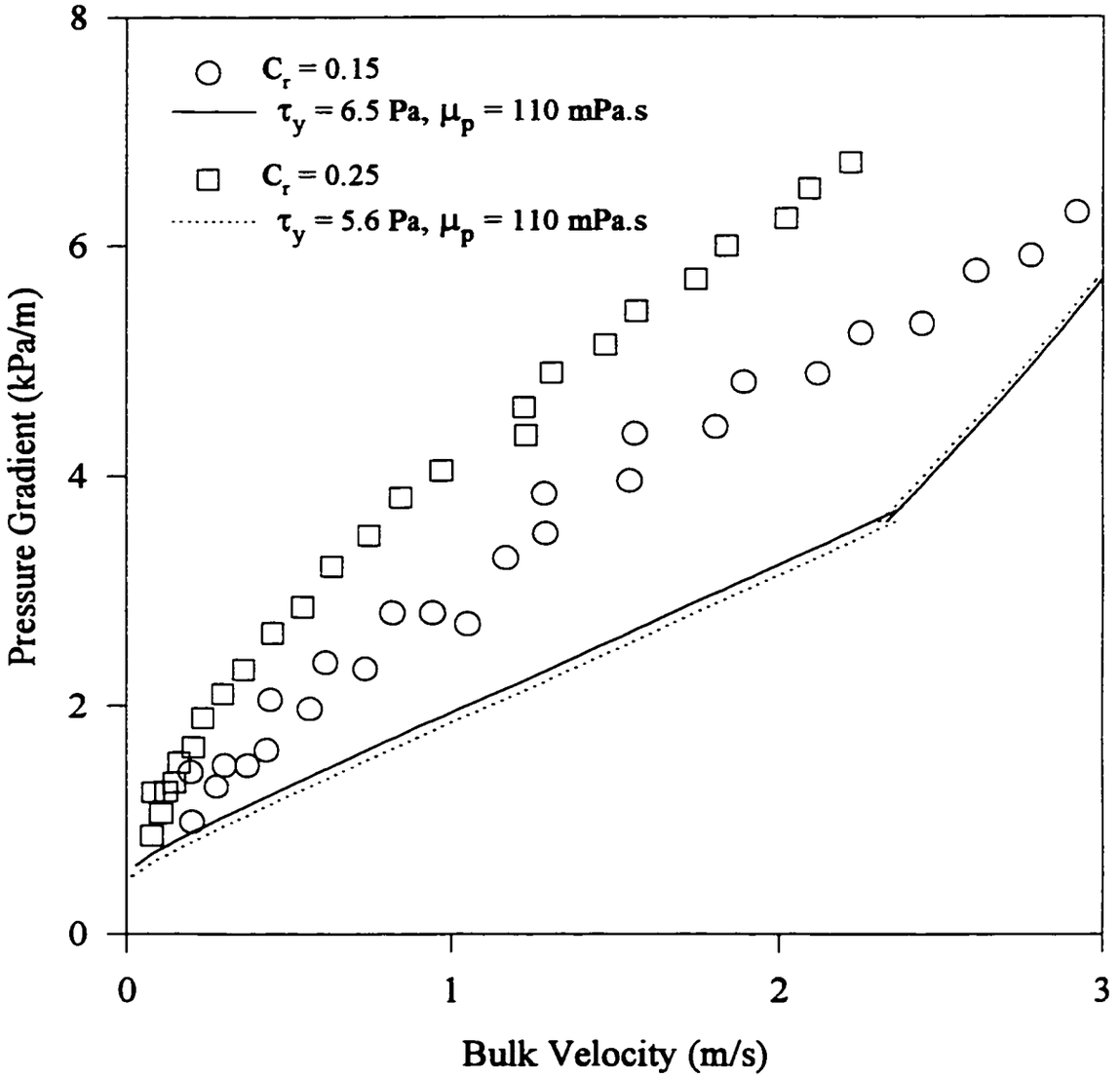

Figure 4.42 : Pressure gradients for 1.7 mm spheres in Kaolin/Bentonite suspensions.

observed. A stationary bed was observed at velocities below 0.1 m/s. Then, up to 0.4 m/s, the bed slid slowly with some particle shear in its upper portion and saltating particles at the top. At 1.2 m/s, the entire bed was sheared.

4.7.2 Pressure gradients for 4.4 mm spheres in low yield stress fluids

The pressure gradients observed with the two concentrations of 4.4 mm spheres in low yield stress Kaolin/Bentonite suspensions are shown in Figure 4.43. The yield stress determined from viscometry was less than the theoretical value required to support these particles. Because of the less viscous nature of these suspensions, both laminar and turbulent flow conditions were observed with these slurries. Hysteresis in both sets of data suggests that deflocculation occurred during turbulent flow. Both sets of data show the pressure gradient increases nearly linearly with bulk velocity over the laminar flow region but with a slope which is significantly higher than would be observed with the fluid alone. The increased slope appears to be a function of concentration. The pressure gradient increases non-linearly in the turbulent flow region. The turbulent behaviour follows that which is typical for coarse particle slurries which are stratified and have a portion of the solid particles being supported by contact load. It is difficult to determine whether the laminar to turbulent transition velocity of the slurry is different from that predicted for the fluid alone.

At the lowest velocities, the particle beds were observed to slide en masse with only a few particles saltating along the top. Within the sliding bed, there was little relative motion between particles. As the bulk velocity was increased, the bed velocity increased and it appeared that particle separation also increased. With this increase in distance between particles, their individual movement increased but seemed insufficient to produce layers of

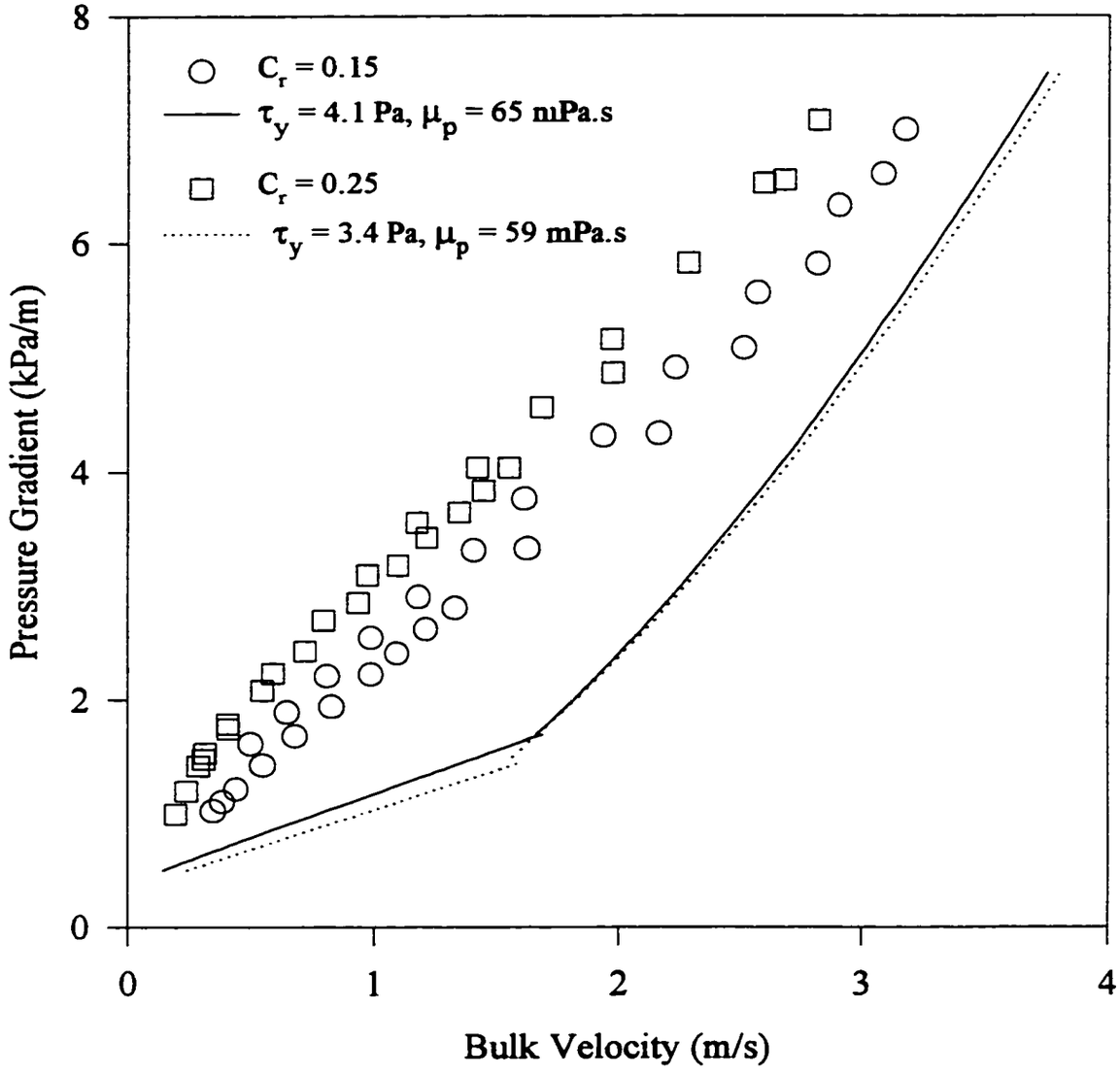

Figure 4.43 : Pressure gradients for 4.4 mm spheres in Kaolin/Bentonite suspensions with low yield stresses.

shearing particles as was observed with the smaller 1.7 mm particles. This is similar to the observations made with these particles with water as the carrier fluid.

It was not possible to reduce the bulk velocity sufficiently with these slurries to form a stationary particle bed. At a concentration of 0.15, a particle bed was observed to be sliding slowly at a bulk velocity of 0.34 m/s with a few saltating particles along the top. At the higher concentration of 0.25, the bed was still moving at the lowest bulk velocity of 0.20 m/s.

4.7.3 Pressure gradients for 4.4 mm spheres in high yield stress fluids

Figure 4.44 shows the pressure gradient observations made with two different high yield stress fluids with a coarse particle in-situ concentration of 0.15. In both cases, the fluids had yield stresses which were higher than the theoretical value needed to support the particles under static conditions. The pressure gradients predicted for the carrier fluids suggest that the flow was laminar for this range of velocities. However, as mentioned in Section 4.4.2, the viscometer may indicate a plastic viscosity which is higher than the true value when inadequate shear is used to determine the model parameters with a concentric cylinder viscometer. The plastic viscosities of these fluids have therefore been treated with some scepticism. The appearance of deflocculation in these results would suggest that some turbulent flow may have occurred and that the fluids may be slightly less viscous than the viscometry results indicated. However there is an added complication in that these suspensions have a higher fraction of Bentonite in the Kaolin/Bentonite mixture. The additional Bentonite was needed to produce the higher yield stresses. Bentonite slurries are typified as having greater time dependence due to their weaker floc structures. This, and not

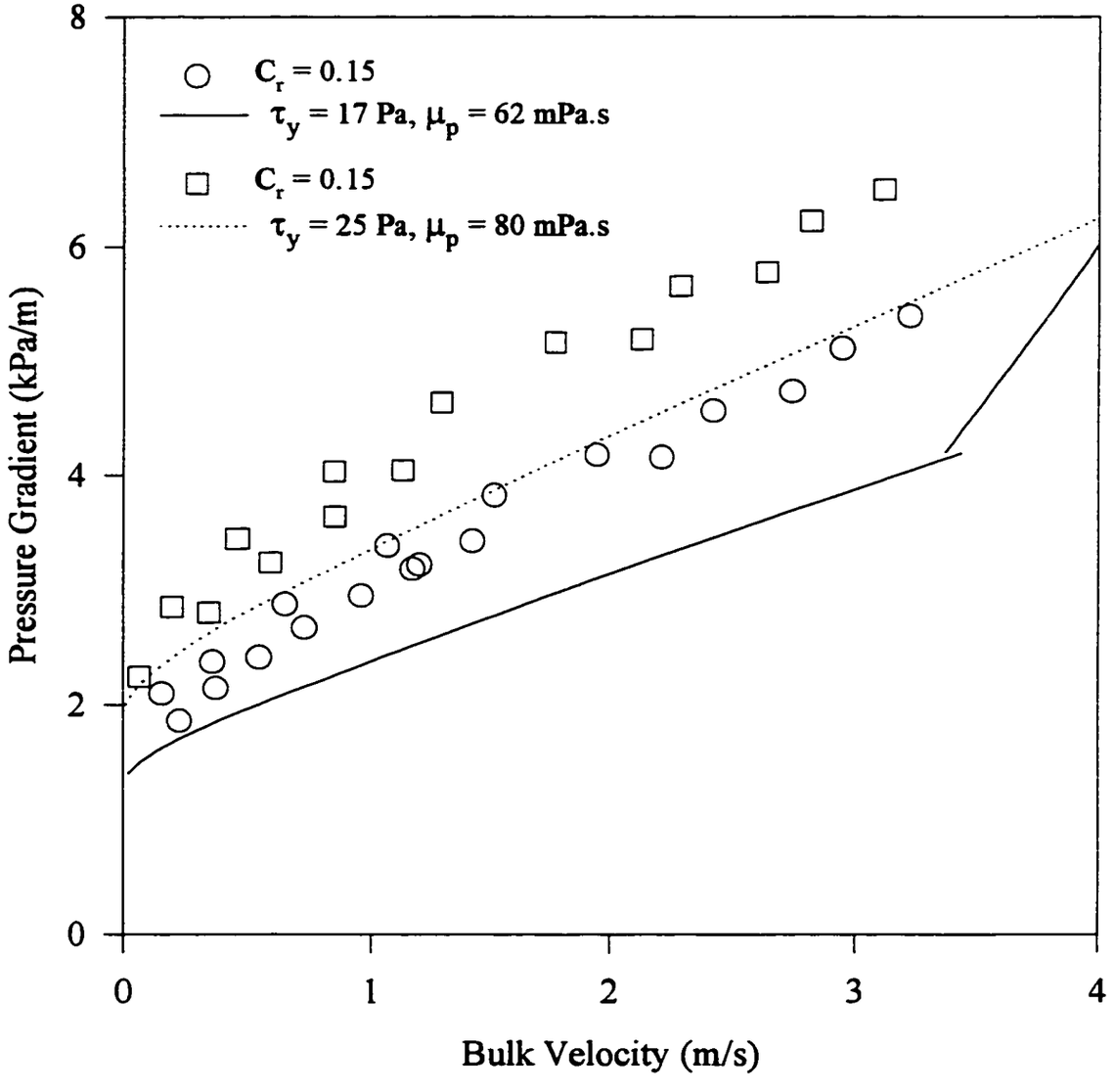

Figure 4.44 : Pressure gradients for 4.4 mm spheres in Kaolin/Bentonite suspensions with high yield stresses.

turbulence, may be the cause of the deflocculation.

The shapes of the curves here are similar to those discussed in the previous two subsections (4.7.1 and 4.7.2). A slight curvature in the pressure gradient is observed at the lower velocities where particle velocities are low. This curvature decreases as the velocity increases. The observed data and the fluid model predictions extrapolate to approximately the same pressure gradient at the no flow condition. This suggests that the value of the yield stress inferred from viscometry agrees with the pipe flow behaviour.

4.7.4 Pressure gradients for 4.1 mm gravel slurries

The pressure gradients for the two concentrations of gravel in the Kaolin/Bentonite suspension are shown in Figure 4.45. The model parameters determined from viscometry for the two cases indicate yield stresses lower than the theoretical support value. Figure 4.45 also shows the predicted fluid pressure gradients based on these model parameters. The difference between the two fluids is the result of degradation of the angular particles which increased the amount of fine material in the carrier fluid.

At an in-situ concentration of 0.15, a stationary bed existed below a bulk velocity of 0.25 m/s. Only a few particles were saltating at the top of the bed at this velocity. Above 0.25 m/s, the particles moved as a sliding bed. There was more relative motion between the particles of the bed here than was observed with the large glass spheres in a similar flow condition. By 0.60 m/s, the entire bed appeared to be mobile with particle mixing within the bed. At about this point the pressure gradient is observed to increase linearly with further increases in bulk velocity. The slope in this linear region is greater than for the fluid alone. At the highest velocities, turbulent flow may have occurred.

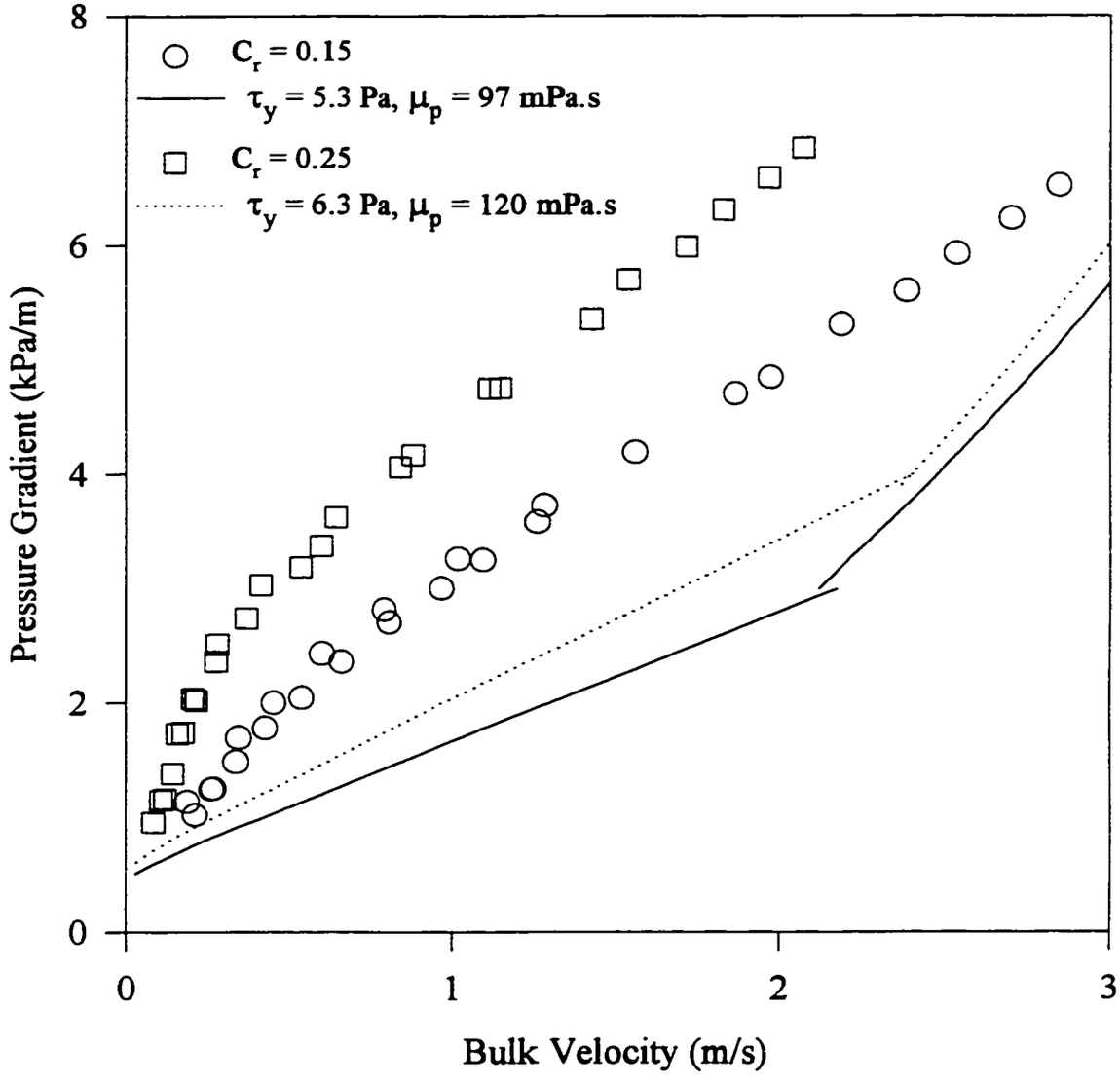

Figure 4.45 : Pressure gradients for 4.1 mm gravel in Kaolin/Bentonite suspensions.

At an in-situ concentration of 0.25, the behaviour was similar. A stationary bed existed below 0.20 m/s. Above this velocity, the bed began to slide with only small amounts of relative motion within it. The entire bed became active at about 0.60 m/s. Above 6.0 m/s the pressure gradient was linearly related to bulk velocity with a slope greater than that for the fluid alone.

4.7.5 Pressure gradient estimates in laminar flow

Visual observations and concentration profile measurements of the slurries studied here would support the use of a two-layer model. Alternatively, the increased slope of the velocity-pressure gradient curves resulting from the presence of the particles suggests a modified viscosity model.

4.7.5.1 Flow in a partially blocked pipe

At the low bulk velocities, where a stationary bed exists or a sliding bed exists which is nearly stationary, the pressure gradient can be estimated by considering fluid flow in a partially blocked pipe. The increased pressure gradient resulting from the reduced cross-section can be approximated for laminar flow of the Kaolin/Bentonite suspension using the hydraulic equivalent diameter and the Buckingham equation (2.6). This method of approximation gives fairly good results at the lowest velocities as indicated in Figure 4.46 for the 1.7 mm spheres and Figure 4.47 for the 4.1 mm gravel. The discrepancy is probably due mostly to the use of the equivalent diameter in laminar flow. Pipe roughness is not important in laminar flow so the rough surface at the bed interface is assumed to not affect flow losses.

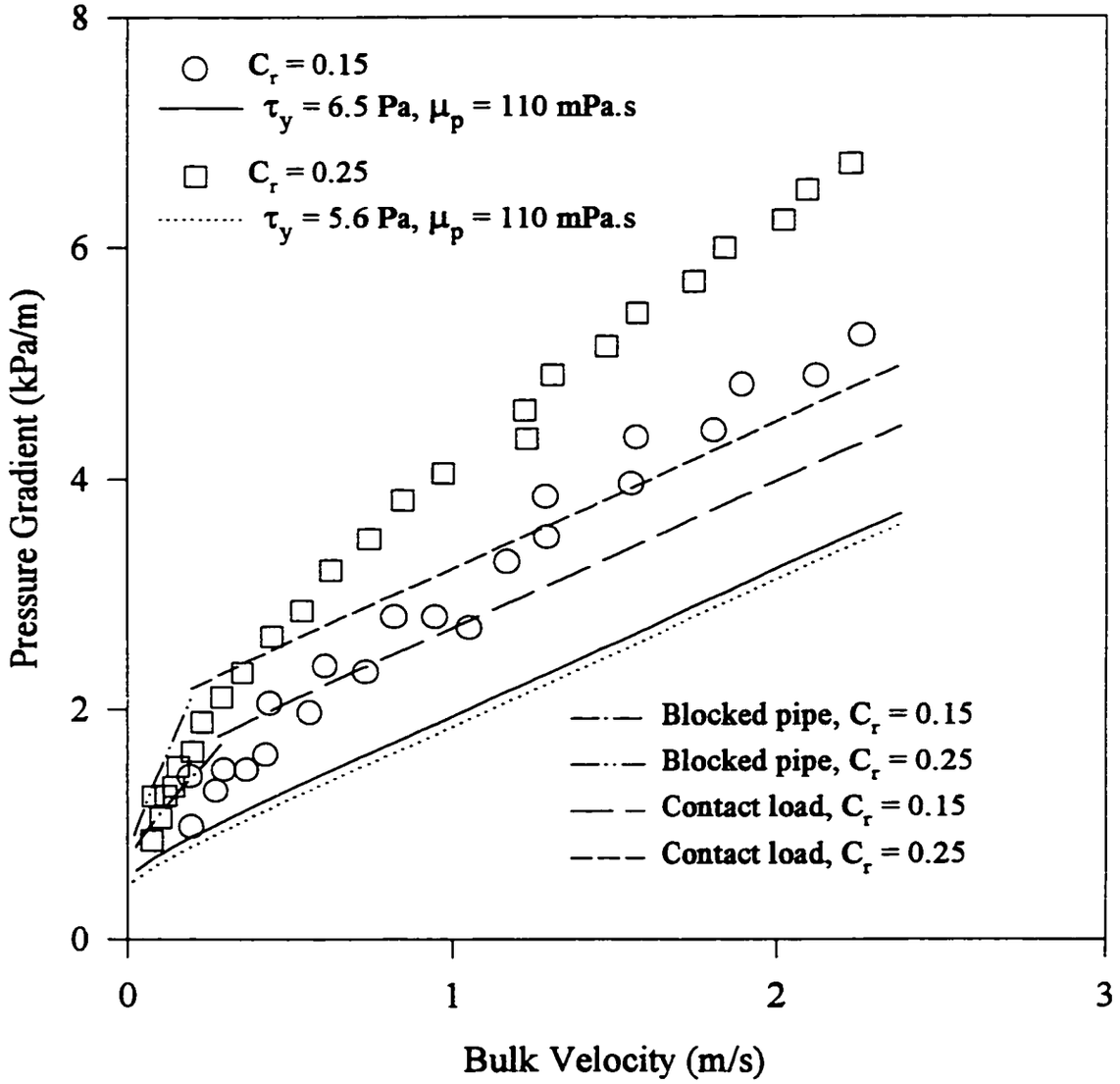

Figure 4.46 : **Pressure gradient estimates for 1.7 mm spheres in Kaolin/Bentonite suspensions in laminar flow.**

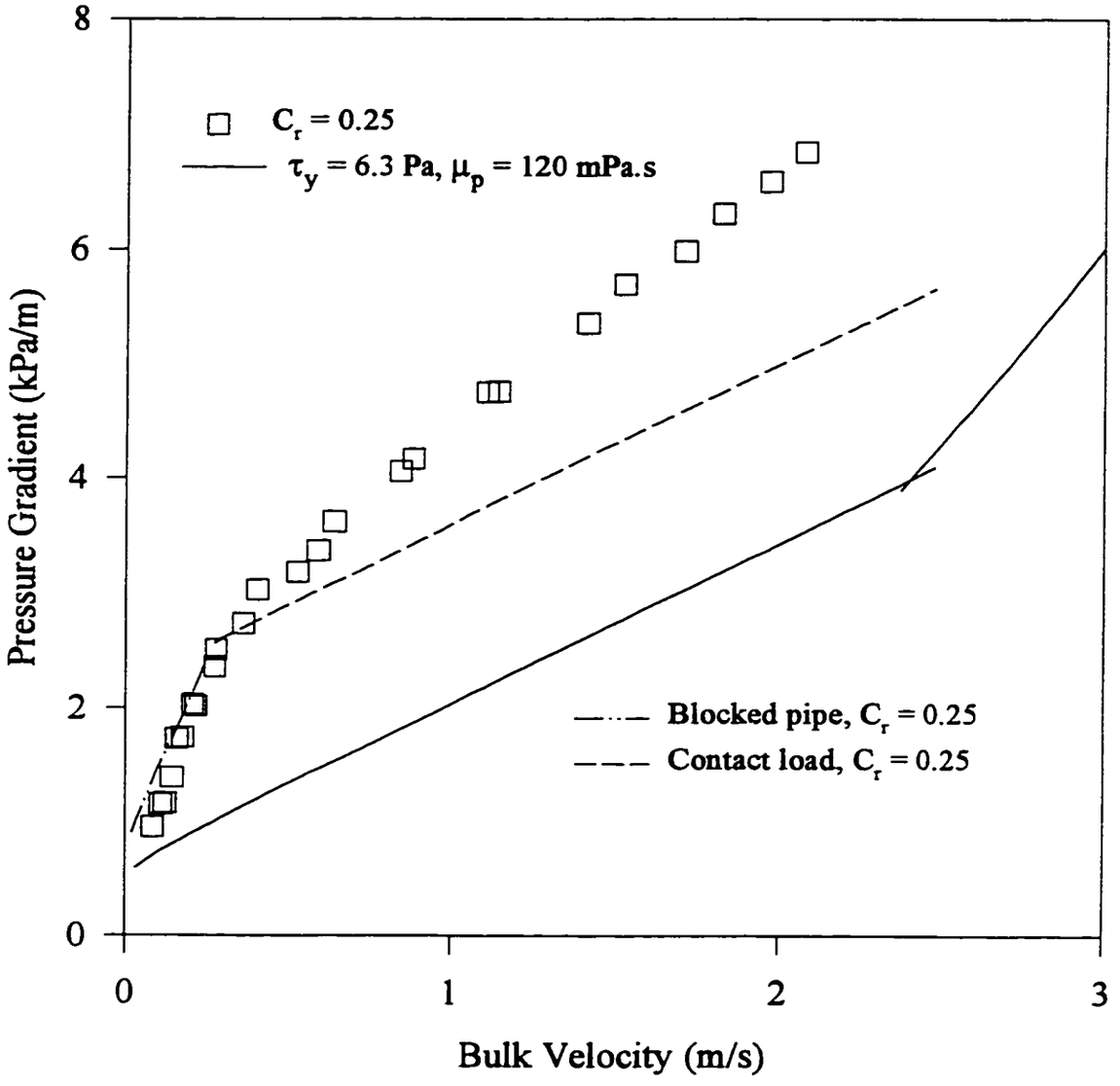

Figure 4.47 : **Pressure gradient estimates for 25% 4.1 mm gravel in a Kaolin/Bentonite suspension in laminar flow.**

4.7.5.2 Contact load contributions to pressure gradients

The pressure drop results show that at low velocities, fluid drag forces acting on the particle bed are not sufficient to cause the bed to slide. As the fluid drag on the particle bed increases with bulk velocity, it eventually overcomes the particle-wall friction which opposes bed motion. Since there is no turbulent suspension, the entire bed must be supported by something like contact load in laminar flow.

Using Equation A.17 and assuming complete contact load, a coefficient of friction of 0.45, and a bed concentration of 0.60, the pressure gradient due to Coulombic friction for each of the cases reported can be calculated. The results are given in Table 4.3. The bulk velocity where the blocked pipe pressure gradient prediction intersects the combined fluid and Coulombic friction line is found to be close to the velocity where the particle bed was observed to become mobile in each case. This is shown in Figures 4.46 and 4.47 for the 1.7 mm spheres and 4.1 mm gravel respectively.

Once the particle bed is completely mobile, there appears to be an additional friction loss beyond the Coulombic component for laminar flow. This additional frictional loss is velocity dependent as indicated by the increase in slope of the pressure gradient of the slurry when compared to the fluid line. Particle concentration has a significant affect on this velocity dependent component of the slurry pressure gradient. This is seen in Figure 4.46 where the pressure gradients of two slurries with different solids concentrations but similar carrier fluids are shown.

4.7.5.3 Pseudohomogeneous pressure gradients

It is clear that there is a higher rate of viscous energy loss in these flows than can be

accounted for solely by a simple combination of fluid friction and Coulombic friction. An additional component exists which is velocity dependent and this suggests it may be viscous in nature.

Table 4.3 : Coulombic friction pressure gradients.

Solid Component	Coarse Solids Fraction	Fluid Density (kg/m^3)	Coulombic Pressure Gradient (kPa/m)	Estimated Deposit Velocity (m/s)
1.7 mm spheres	0.15	1460	0.76	0.90
	0.25	1460	1.37	0.73
4.4 mm spheres low τ_y	0.15	1500	0.73	1.60
	0.25	1500	1.31	1.41
4.4 mm spheres high τ_y	0.15	1150	1.00	1.56
	0.15	1170	0.98	0.80
4.1 mm gravel	0.15	1470	0.89	1.29
	0.25	1500	1.56	0.76
sphere density : 2470 kg/m^3				
gravel density : 2650 kg/m^3				

Friction losses for pseudohomogeneous slurries can be predicted using the relative viscosity which was determined for the bulk particle concentration as correlated by D.G.

Thomas (1965) or Gillies et al. (1994). The relative viscosity predicted by Thomas' equation (2.23) for the glass spheres at concentrations of 0.15 and 0.25 are 1.63 and 2.43 respectively. Using Gillies' equation (2.24) for the gravel, the relative viscosities are 1.64 and 2.53 for the two bulk concentrations.

At the higher bulk velocities, the particles become dispersed and more uniformly distributed within the pipe. While a truly uniform concentration condition is not likely to develop with these large particles, laminar flow of a well dispersed slurry may approach the pressure gradient predicted for a pseudohomogeneous fluid using the relative viscosity.

Figure 4.48 shows the observed pressure gradients for the 1.7 mm spheres again. Included in the figure are the predicted pressure gradients using the pseudohomogeneous fluid assumption. The bulk concentrations were used to determine the relative viscosity with Thomas' equation. The Buckingham equation (2.6) was then used to predict the pressure gradient based upon the original fluid yield stress and the plastic viscosity after it had been scaled by the relative viscosity. The agreement is fairly good at the higher velocities where the particles were fairly well dispersed.

When the flow is highly stratified, the local viscosity will vary significantly with position in the pipe. Modelling of this flow requires a finite element approach and will be discussed in Chapter 5. However it can be stated that the nonlinear nature of the relative viscosity functions lead to higher overall pipe average viscosity and therefore overall friction losses when the particles become stratified. So at lower velocities where the flow becomes more stratified, the friction losses are expected to be higher than the uniformly distributed solids (pseudohomogeneous) case. As the velocity increases and particle dispersion

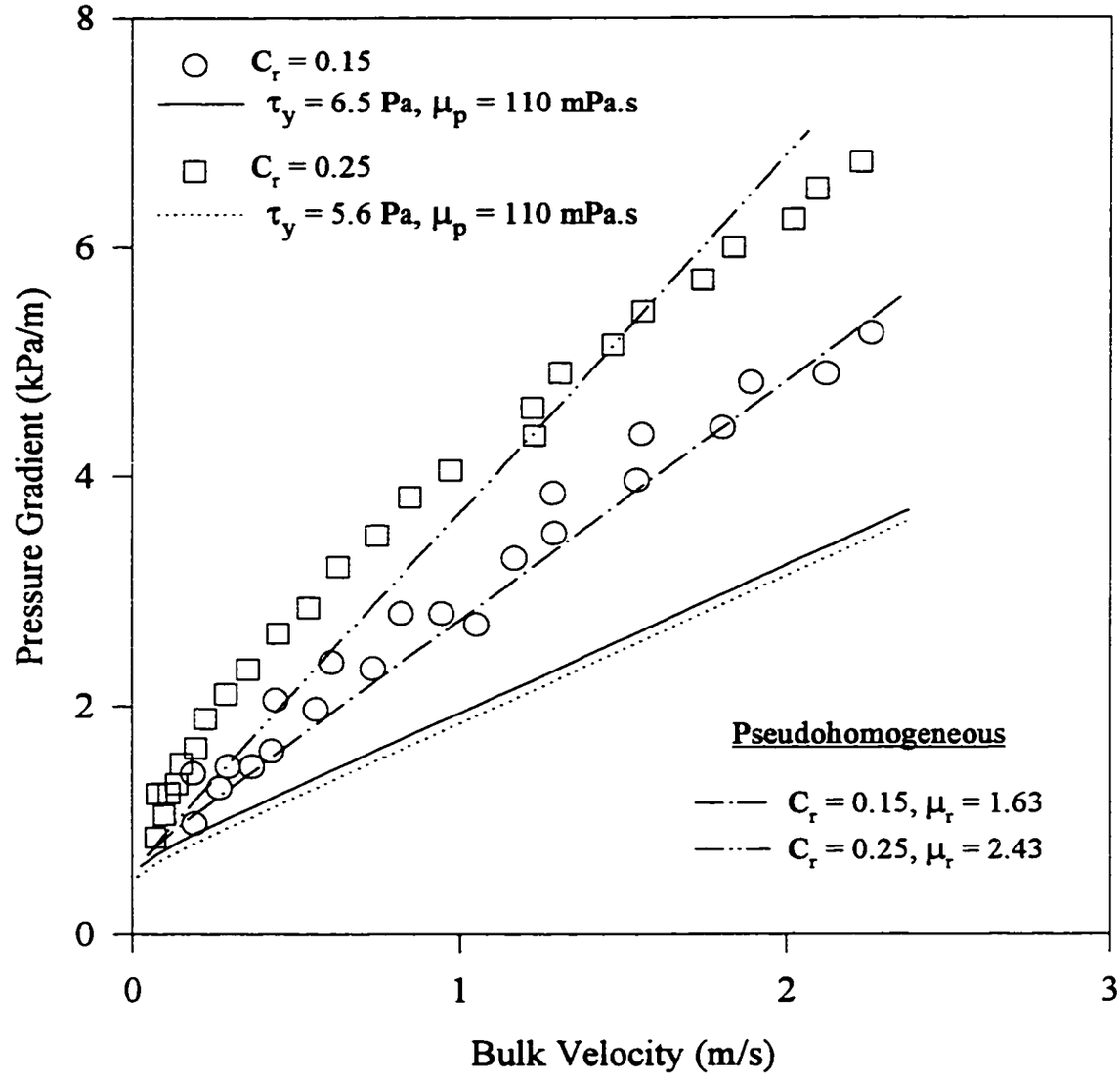

Figure 4.48 : **Pseudohomogeneous pressure gradient estimates for 1.7 mm spheres in Kaolin/Bentonite suspensions in laminar flow.**

increases, the pipe average effective viscosity decreases towards the pseudohomogeneous value. This change with bulk velocity provides a possible explanation for the curvature in the pressure gradients observed in Figure 4.48

4.8 Magnetic particle velocities in Kaolin/Bentonite slurries

Magnetic particle velocities were recorded for the Kaolin/Bentonite slurries as an indication of the bulk particle flow behaviour. It was originally hoped that the magnetic particle would be representative of the average particle behaviour and could be used to estimate particle flowrates and delivered concentrations. However, it was found that in both turbulent water flows and laminar flows of the clay suspensions the magnetic particle had an affinity for the top of the particle bed. This was inferred from the high values of the magnetic particle velocities. The diagonal lines on Figures 4.49 to 4.52 show that the magnetic particle velocities were usually equal to or greater than the bulk velocity. These high velocities would be expected to occur in the upper portion of the bed.

It is not entirely clear why these particles travelled so high in the bed. In the 1.7 mm particle slurries, this may have been due to the magnetic particle being larger (3.8 mm). It was not possible to make a smaller particle which would still be sensed when passing through the coils.

For the 4.4 mm spheres and the 4.1 mm gravel, the magnetic particle was 4.4 mm in diameter which was close to the median sizes. However, this particular magnetic particle had a density of 2080 kg/m^3 which was slightly lower than that of the glass and the gravel. In this case, it would seem the density may have been responsible for the higher elevation of the particle.

The average axial velocity of the magnetic particles, determined from between five and fifteen passages through the test coils, was determined at each bulk velocity in the pressure gradient flow tests. The results obtained with the two in-situ concentrations of 1.7 mm spheres are shown in Figure 4.49. There was very little difference between the particle velocities for the two concentrations. Below 0.2 m/s, where a particle bed exists, the magnetic particle is observed to be moving along what must be the top of the bed. The particle velocity is slightly lower than the bulk velocity. Once the bed is fully mobile, the velocity of the magnetic particle is seen to increase linearly with the bulk velocity. Flow is laminar for all points shown here. At the high bulk velocities, the particle velocity is significantly above the bulk value.

The magnetic particle velocities observed with the 4.4 mm spheres covered both laminar and turbulent flow regions and are shown in Figure 4.50. In the laminar flow region, there appears to be a linear relationship between the magnetic particle velocity and the bulk velocity. The magnetic particle velocity is higher than the bulk velocity in this region. When the flow becomes turbulent, the magnetic particle velocity still appears to increase linearly with bulk velocity but the constant of proportionality is lower than was observed in the laminar case.

Magnetic particle velocities for the 4.4 mm spheres in two significantly different fluids are shown in Figure 4.51. In both cases, the in-situ concentration was 0.15 and only laminar flow is considered. The first suspension had a low yield stress and a high density while the second had a high yield stress and a low density. Figure 4.51 shows that the bulk velocity at which the magnetic particle begins to move is about the same for the two cases.

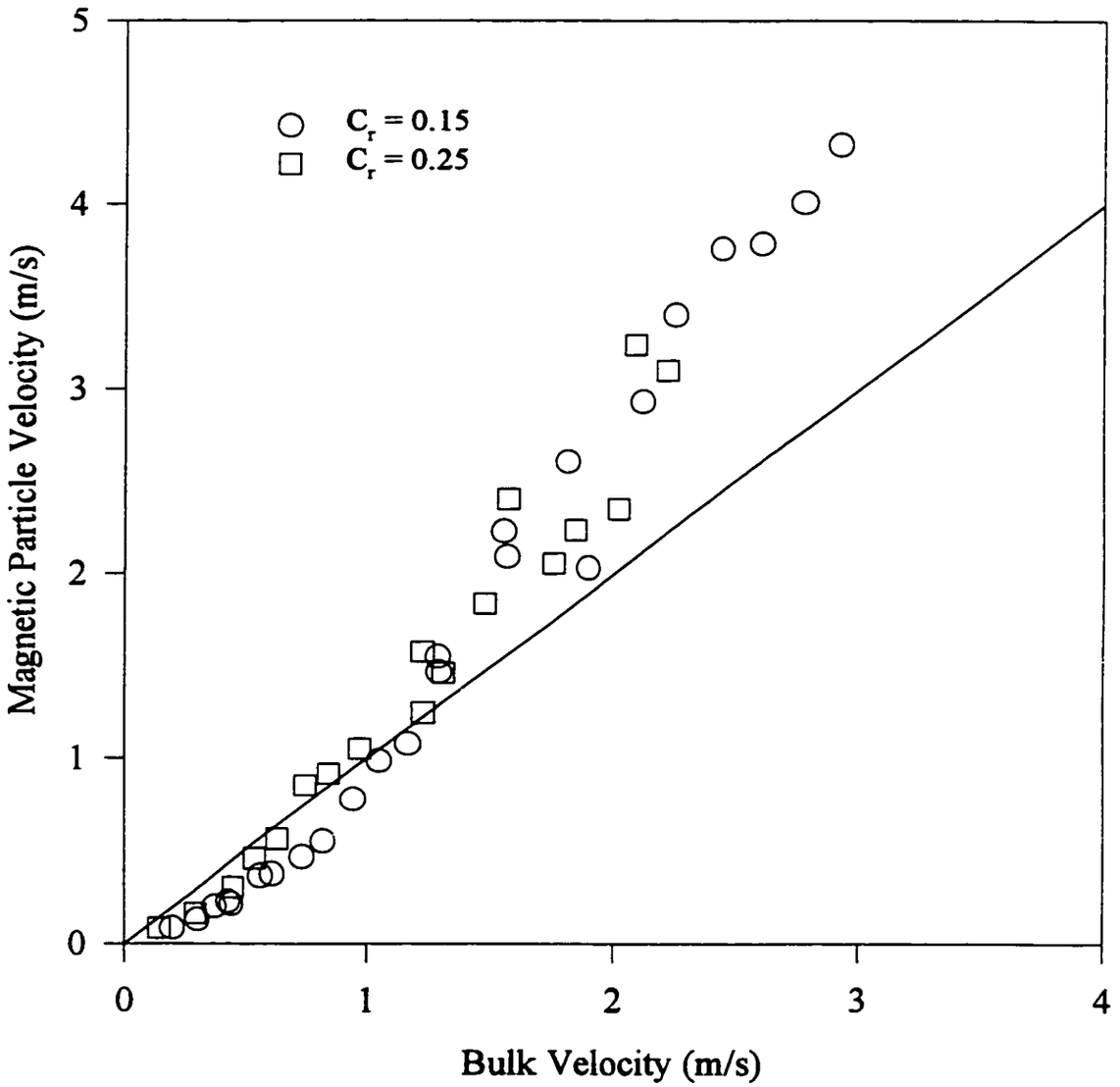

Figure 4.49 : Magnetic particle velocities in Kaolin/Bentonite suspensions with 1.7 mm spheres.

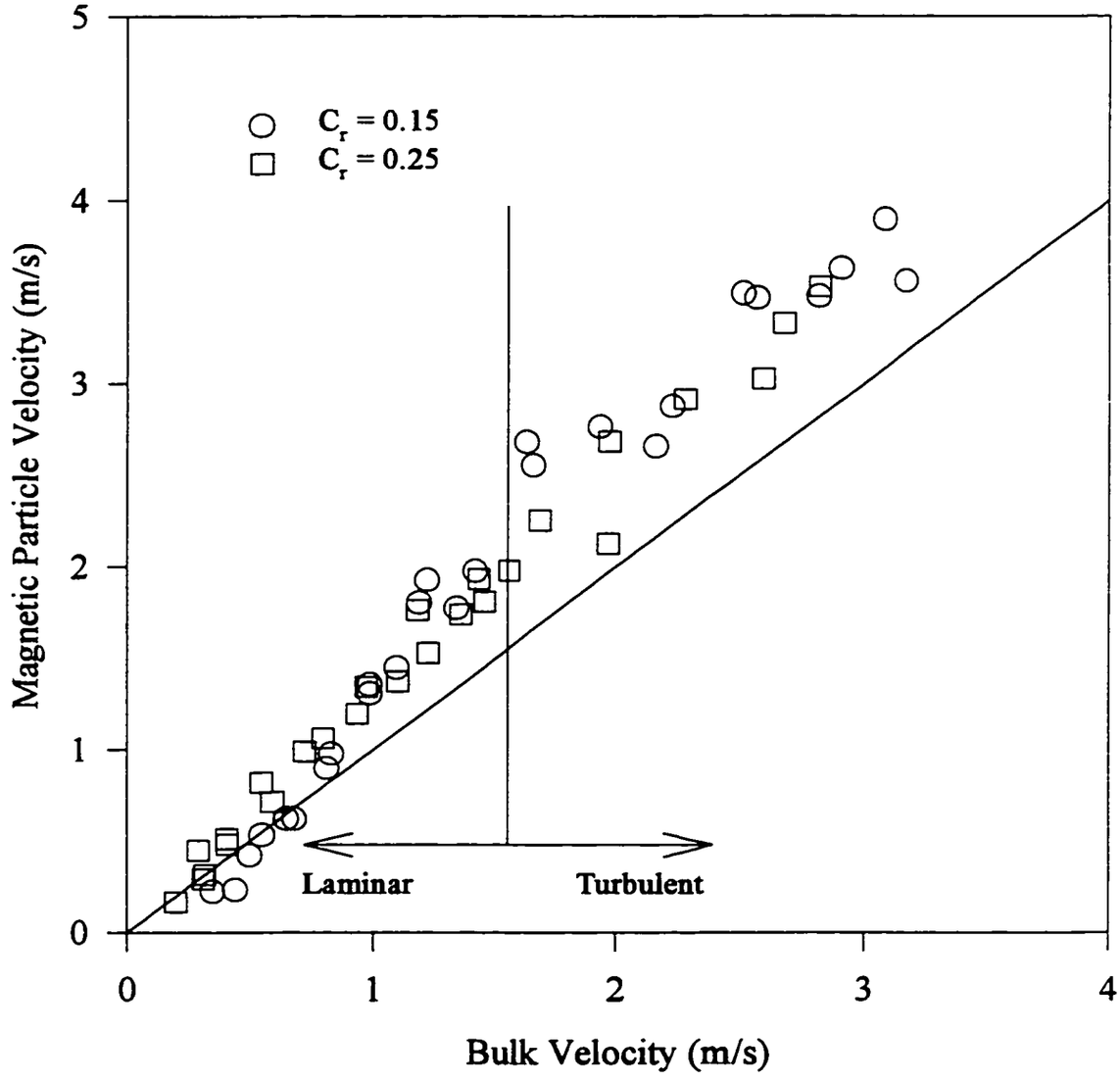

Figure 4.50 : Magnetic particle velocities in low yield stress Kaolin/Bentonite suspensions with 4.4 mm spheres.

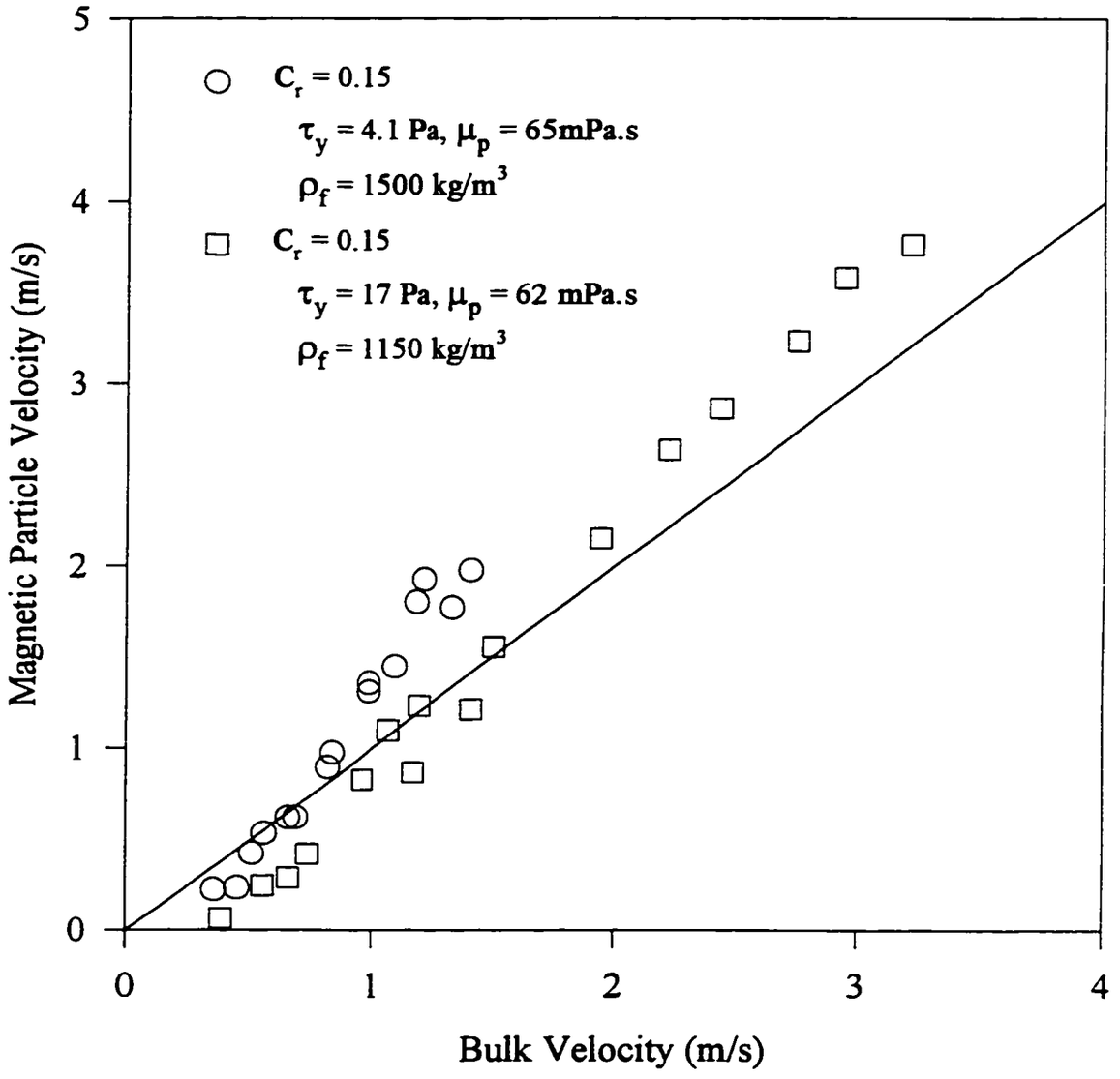

Figure 4.51 : Magnetic particle velocities in two significantly different Kaolin/Bentonite suspensions with 15% 4.4 mm spheres.

The constant of proportionality relating the particle velocity to the bulk velocity is lower with the high yield stress fluid. This agrees with the velocity profiles which indicated higher particle velocities at the top of the bed with the lower yield stress fluids.

The magnetic particle velocities were roughly linearly related to bulk velocities with the 4.1 mm gravel slurries but more scatter was observed in the data. The results are shown in Figure 4.52. Magnetic particle velocities were close to the bulk values at and below 1.5 m/s. At higher bulk velocities, the magnetic particle velocities were significantly higher than the bulk values.

4.9 Particle velocities near the wall for Kaolin/Bentonite slurries

The velocities of the large particles along the bottom of the pipe were measured using the conductivity probe embedded in the pipe wall. Velocities were recorded over the range of bulk velocities during the pressure gradient measurements for each slurry.

The velocities measured with the 1.7 mm spheres were quite low. The size of these particles is such that within one particle diameter of the wall, local velocities would be expected to be low in laminar flow. These low velocities are evidence of the boundary layer effect which was noticed with the probe. Figure 4.53 shows the results for the two Kaolin/Bentonite slurries with 1.7 mm particles at in-situ concentrations of 0.15 and 0.25. In both cases, flow was laminar below 2.4 m/s. The higher in-situ concentration slurry has higher wall velocities at all bulk velocities.

Figure 4.54 shows results for the larger 4.4 mm spheres in the low yield stress carriers. Here the wall velocities were only slightly higher at the higher in-situ concentration. The wall velocities are seen to increase with the bulk velocity in an approximately quadratic

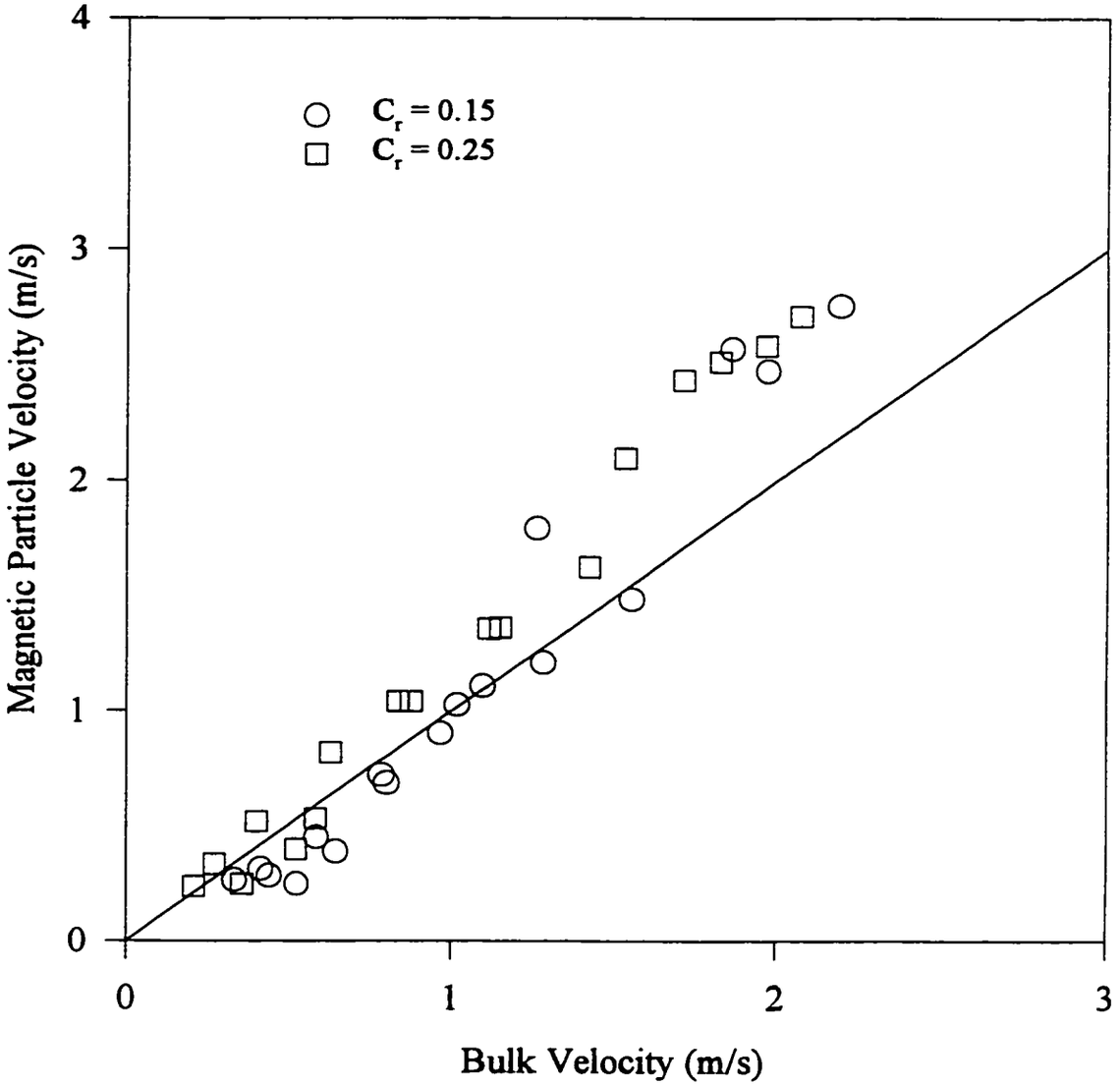

Figure 4.52 : Magnetic particle velocities in Kaolin/Bentonite suspensions with 4.1 mm gravel.

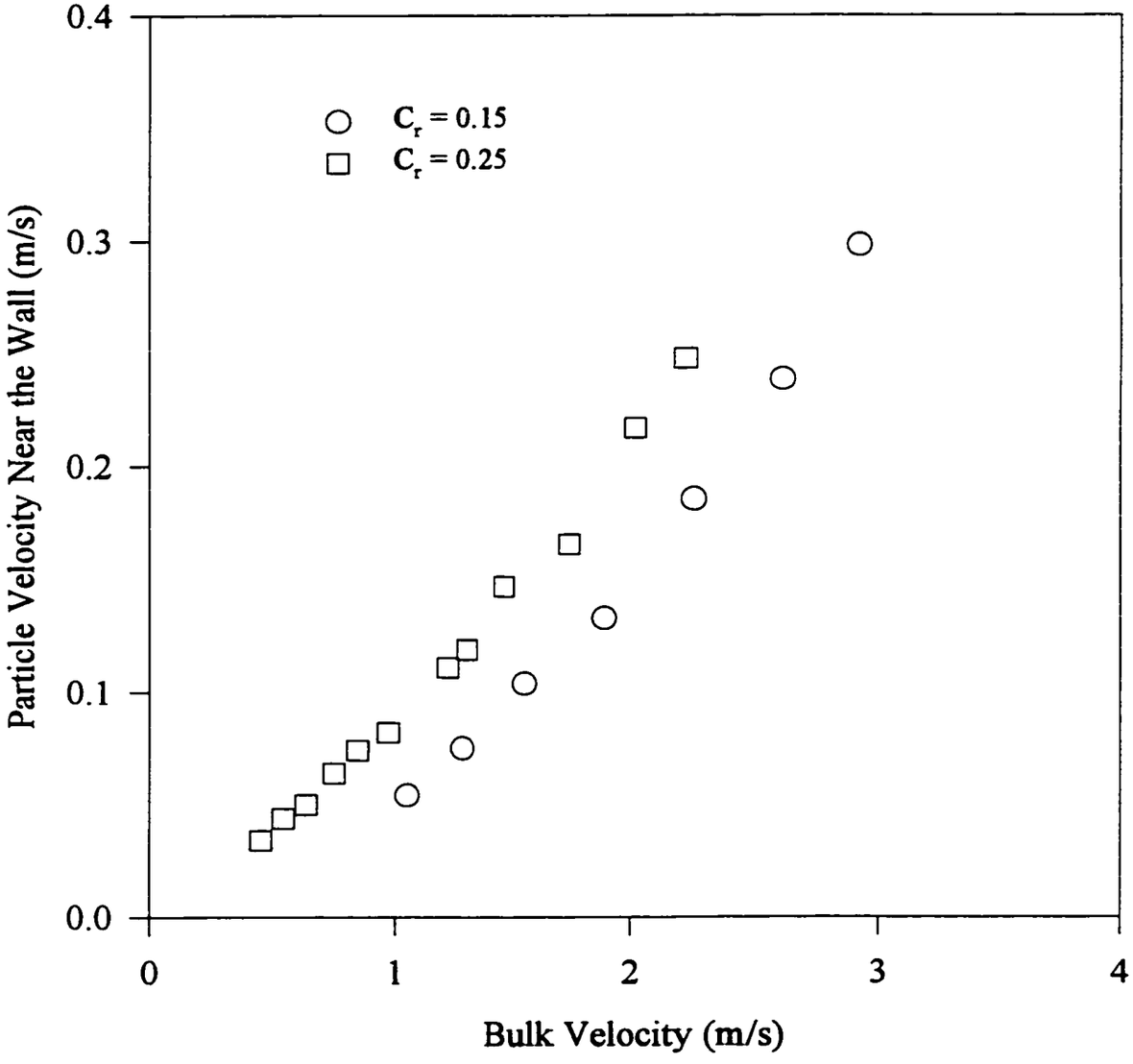

Figure 4.53 : Particle velocities near the wall for 1.7 mm spheres in Kaolin/Bentonite suspensions.

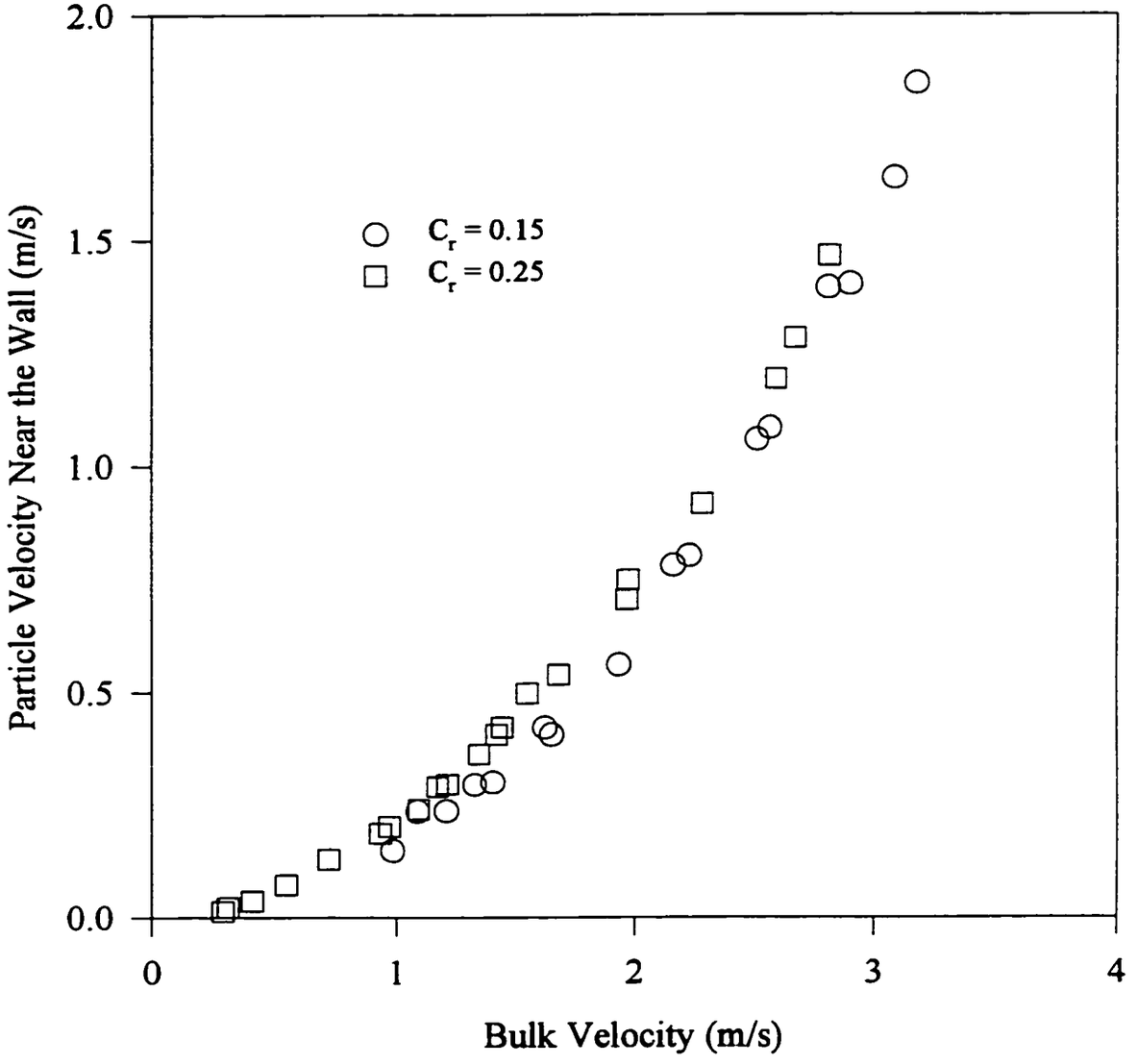

Figure 4.54 : Particle velocities near the wall for 4.4 mm spheres in Kaolin/Bentonite suspensions with low yield stresses.

fashion. The data includes points which are in turbulent flow. The laminar to turbulent transition velocity for the suspensions is approximately 1.8 m/s.

The wall velocities measured for the 4.4 mm spheres in the high yield stress suspensions are shown in Figure 4.55. Both slurries had in-situ concentrations of 0.15. The Bingham model parameters determined from viscometry are shown to distinguish the two slurries. The wall velocities for the two slurries are nearly the same throughout the velocity range studied. Again a quadratic relationship is evident.

The wall velocities observed with the 4.1 mm gravel are shown in Figure 4.56. The wall velocities for the higher in-situ concentration are higher for a given bulk velocity by an amount which appears similar to that observed with the 4.4 mm spheres. Flow is laminar below 2.2 m/s at the lower concentration and for all data at the higher concentration.

Combining the results for the 4.4 mm spheres and 4.1 mm gravel on a single figure shows very little variation. Figure 4.57 contains the data for both these spherical and angular particles. These experimental conditions include laminar and turbulent flow, two bulk concentrations and a significant variation in fluid properties. The relationship between wall velocity and bulk velocity does not appear to be very sensitive to these variations.

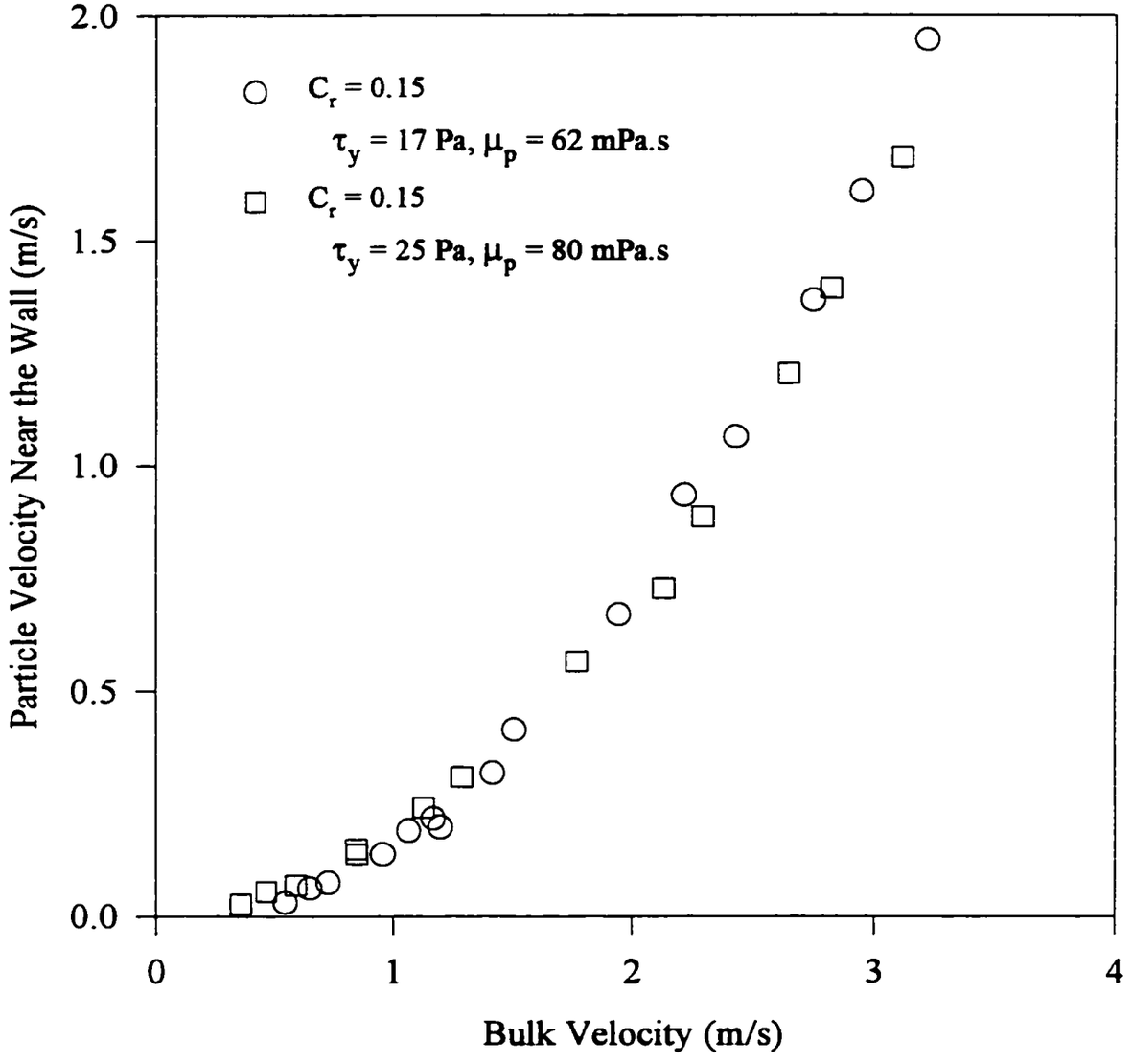

Figure 4.55 : Particle velocities near the wall for 4.4 mm spheres in Kaolin/Bentonite suspensions with high yield stresses.

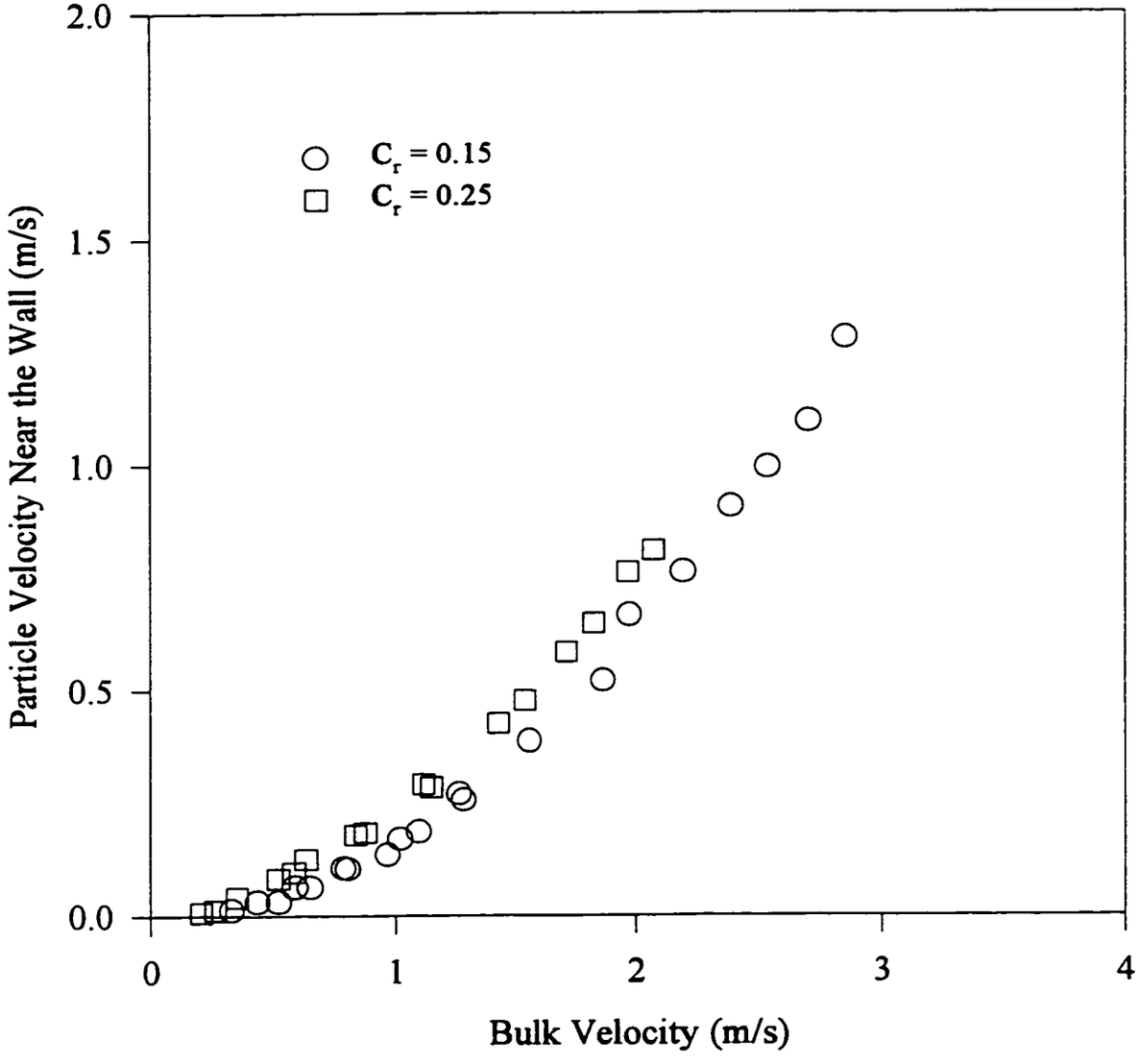

Figure 4.56 : **Particle velocities near the wall for 4.1 mm gravel in Kaolin/Bentonite suspensions.**

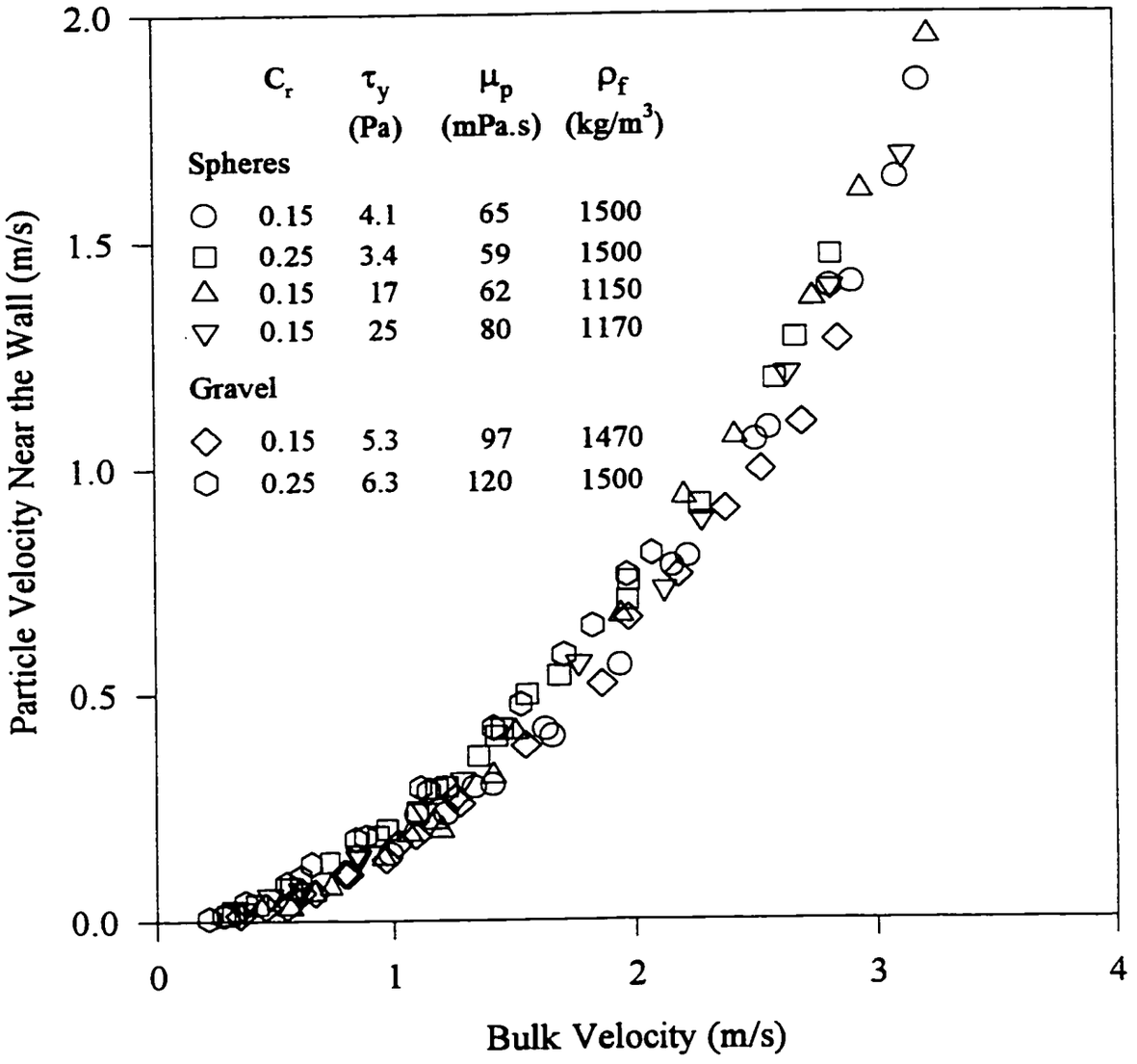

Figure 4.57 : **Particle velocities near the wall for 4 mm particles in Kaolin/Bentonite suspensions.**

5 NUMERICAL SIMULATION OF SLURRY FLOW

5.1 Finite element model

The flow which is to be simulated is unidirectional viscous flow in a horizontal pipe. The finite element solution allows the use of an arbitrary coordinate system provided the true geometry can be represented by a large number of elements using the chosen coordinates. In this case Cartesian coordinates are selected for their simplicity. The governing equation for fully developed, steady horizontal laminar flow of a fluid is (Bird et al., 1960)

$$\frac{\partial}{\partial x}\left(\mu\frac{\partial w}{\partial x}\right) + \frac{\partial}{\partial y}\left(\mu\frac{\partial w}{\partial y}\right) - \frac{dP}{dz} = 0 \qquad (5.1)$$

where μ is the viscosity and w is the z-wise velocity. In Equation 5.1, both viscosity and velocity may vary over the pipe cross section. Solution of this equation over the pipe cross section will provide a prediction of the fluid velocity distribution due to the pressure gradient in the pipe. Use of a finite element method to obtain a solution for Equation 5.1 will give a velocity at each of the element nodes within the solution domain for a specified pressure gradient.

The finite element technique used to solve Equation 5.1 is commonly described as Galerkin's method. A more thorough description of the application of this method can be

found in Segerlind (1984). Galerkin's method uses a weighted residual formulation which requires finding the solution to the weighted residual integral equation:

$$I = - \iint_A \Phi_i(x,y)\ R(x,y)\ dA = 0 \tag{5.2}$$

In Equation 5.2, $\Phi_i(x,y)$ is the weighting function at each node i and R(x,y), the residual, is the differential equation (5.1) to be solved. In Galerkin's method, the weighting function is chosen to be the same as the shape function which is used to approximate the solution within each element. If a linear shape function, ϕ_i, is used within each element and also as the weighting function then

$$\Phi_i(x,y) = \phi_i = a_i + b_i x + c_i y \tag{5.3}$$

and in this case, Equation 5.2 can be rewritten as

$$I = - \iint_A [\phi_i]^T \left[\frac{\partial}{\partial x}\left(\mu \frac{\partial w}{\partial x} \right) + \frac{\partial}{\partial y}\left(\mu \frac{\partial w}{\partial y} \right) - \frac{dP}{dz} \right] dA = 0 \tag{5.4}$$

where $[\phi_i]^T$ is a column vector of shape functions.

In the flows to be considered here, the viscosity will vary throughout the cross section since it will be a function of local shear rate and particle concentration. In the finite element method, the local shear rate will also be assumed to be constant for each element. To obtain a solution the effective viscosity will be assumed constant within any particular element. This allows the viscosity to be replaced by the element viscosity, μ_i, and taken

outside the derivatives in Equation 5.4. The product of the shape function and the first term of Equation 5.1 can then be rearranged to give

$$\mu_t[\phi_t]^T\frac{\partial}{\partial x}\left(\frac{\partial w}{\partial x}\right) = \mu_t\frac{\partial}{\partial x}\left([\phi_t]^T\frac{\partial w}{\partial x}\right) - \mu_t\left(\frac{\partial[\phi_t]^T}{\partial x}\right)\left(\frac{\partial w}{\partial x}\right) \tag{5.5}$$

This same procedure can also be applied to the second term in Equation 5.1. Thus the weighted residual integral can be rewritten as

$$I = -\iint_A\left[\mu_t\frac{\partial}{\partial x}\left([\phi_t]^T\frac{\partial w}{\partial x}\right) + \mu_t\frac{\partial}{\partial y}\left([\phi_t]^T\frac{\partial w}{\partial y}\right)\right]dA$$

$$-\iint_A\left[-\mu_t\left(\frac{\partial[\phi_t]^T}{\partial x}\right)\left(\frac{\partial w}{\partial x}\right) - \mu_t\left(\frac{\partial[\phi_t]^T}{\partial y}\right)\left(\frac{\partial w}{\partial y}\right)\right]dA$$

$$-\iint_A\left[-[\phi_t]^T\frac{dP}{dz}\right]dA = 0 \tag{5.6}$$

The first integral of Equation 5.6 can be replaced using Green's theorem.

$$\iint_A\left[\mu_t\frac{\partial}{\partial x}\left([\phi_t]^T\frac{\partial w}{\partial x}\right) + \mu_t\frac{\partial}{\partial y}\left([\phi_t]^T\frac{\partial w}{\partial y}\right)\right]dA = \oint_S\left[\mu_t[\phi_t]^T\frac{\partial w}{\partial x}\cos\theta + \mu_t[\phi_t]^T\frac{\partial w}{\partial y}\cos\theta\right]dS \tag{5.7}$$

where θ is the angle of the outward normal at the domain boundary. This replacement is

needed to allow the application of the boundary conditions. It also simplifies Equation 5.6 so that it contains only first order derivatives of w.

What remains is to express the second integral of Equation 5.6 with a system of linear equations which can be solved. This will be done beginning with a single triangular element. Following Equation 5.3, the continuous z-wise fluid velocity is replaced by a linear approximation within each element using the shape function and the velocity at the element nodes. The element shape functions are expressed as a row vector $[\phi_i]$ and the velocities at the element nodes by a column vector. The nodes of the element are denoted by the subscripts i, j, and k. Thus the velocity, w, within the element being considered is given by

$$w = \begin{bmatrix} \phi_i & \phi_j & \phi_k \end{bmatrix} \begin{bmatrix} w_i \\ w_j \\ w_k \end{bmatrix} \tag{5.8}$$

The velocity gradient with respect to the x direction is

$$\frac{\partial w}{\partial x} = \begin{bmatrix} \frac{\partial \phi_i}{\partial x} & \frac{\partial \phi_j}{\partial x} & \frac{\partial \phi_k}{\partial x} \end{bmatrix} \begin{bmatrix} w_i \\ w_j \\ w_k \end{bmatrix} \tag{5.9}$$

Equation 5.6 can be rewritten for a single element with the node velocities represented by their column vector, $[w_i]$, and the weighting function, $[\phi_i]^T$ being a column vector which is the transpose of the shape vector, $[\phi_i]$.

$$I = -\oint_S \left[\mu_t [\phi_i]^T \frac{\partial w}{\partial x} \cos\theta + \mu_t [\phi_i]^T \frac{\partial w}{\partial y} \cos\theta \right] dS$$

$$- \iint_A \left[- \mu_t \left(\frac{\partial [\phi_t]^T}{\partial x} \right) \left(\frac{\partial [\phi_t]}{\partial x} \right) - \mu_t \left(\frac{\partial [\phi_t]^T}{\partial y} \right) \left(\frac{\partial [\phi_t]}{\partial y} \right) \right] dA \quad [w_t]$$

$$- \iint_A \left[- [\phi_t]^T \frac{dP}{dz} \right] dA = 0 \tag{5.10}$$

This equation can be expanded to include the entire solution domain and written in the more compact form

$$[I] = [B] + [K]\ [w] - [F] = [0] \tag{5.11}$$

where [I] is the weighted residual integral vector, [B] is the boundary vector, [w] is the nodal velocity vector, [F] is the force vector, [0] is the zero vector and [K] is the stiffness matrix such that

$$[B] = - \oint_S \left[\mu_t [\phi_t]^T \frac{\partial w}{\partial x} \cos\theta + \mu_t [\phi_t]^T \frac{\partial w}{\partial y} \cos\theta \right] dS \tag{5.11a}$$

$$[K] = - \iint_A \left[- \mu_t \left(\frac{\partial [\phi_t]^T}{\partial x} \right) \left(\frac{\partial [\phi_t]}{\partial x} \right) - \mu_t \left(\frac{\partial [\phi_t]^T}{\partial y} \right) \left(\frac{\partial [\phi_t]}{\partial y} \right) \right] dA \tag{5.11b}$$

$$[F] = - \iint_A \left[[\phi_t]^T \frac{dP}{dz} \right] dA \tag{5.11c}$$

The dimensions of these column vectors and square matrix are determined by the number of nodes in the solution domain.

5.1.1 Solution domain for laminar flow in a pipe

The physical domain which is to be modelled is the pipe cross section. A vertical axis of symmetry exists so that the finite element mesh only needs to include half the pipe cross section. The mesh used here contained 25 equal width concentric rings with these rings being further subdivided to form rows of isosceles triangles. The mesh is shown in Figure 5.1.The linear shape function used (Equation 5.3) imposes a condition of constant strain rate for each of the triangular elements. A coarser grid was also used (15 rings) and was found not to have any substantial effect on the results generated.

The boundary conditions for the domain are mixed. An essential boundary condition existed along the pipe wall where the velocity was known to be zero. Along the central axis, natural boundary conditions existed because of symmetry. That is, the velocity gradient normal to the central axis is zero.

Solution of Equation 5.11 was obtained using a Gauss-Seidel technique. An iterative solution was necessary since non-Newtonian fluids give rise to a velocity dependent effective viscosity in the overall stiffness matrix, [K]. This effective viscosity had to be updated as the solution proceeded. An over-relaxation factor of 1.75 was used in the solution.

5.1.2 Local viscosity

The distribution of particles in the pipe is assumed to cause a variation in the local resistance to shear which can be described by the relative viscosity. The relative viscosity

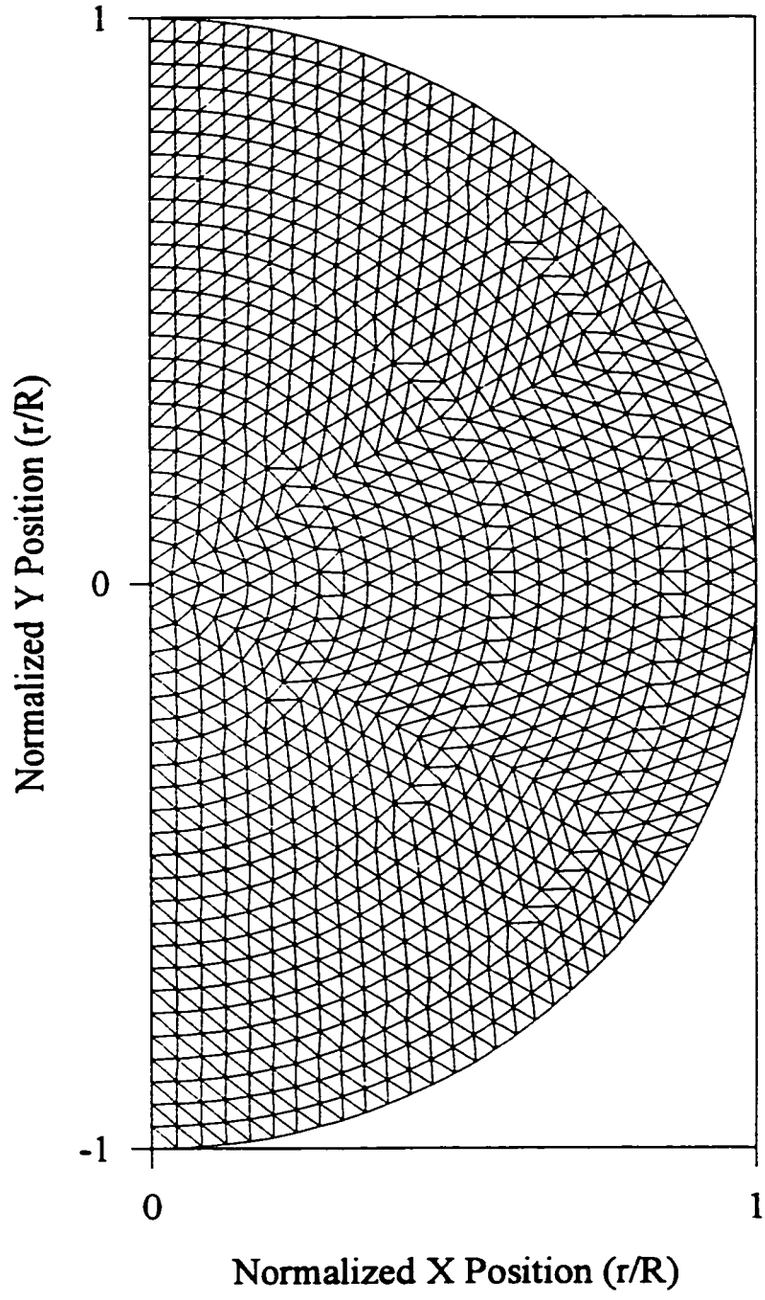

Figure 5.1 : Finite element solution mesh.

of each element, μ_{ri}, is determined by rewriting Equations 2.23 and 2.24 with the average solids concentration for each element, c_i, to give

$$\mu_{rt} = 1 + 2.5 c_t + 10.05 c_t^2 + 0.00273 \exp(16.6 c_t) \tag{5.12}$$

and

$$\mu_{rt} = 1 + 2.5 c_t + 10 c_t^2 + 0.0019 \exp(20 c_t) \tag{5.13}$$

where Equation 5.12 is used with spherical particles and 5.13 is used with sand particles. The element mixture viscosities are then given by Equation 2.21 as

$$\mu_{mt} = \mu_{rt} \mu_f \tag{5.14}$$

where μ_{mi} is the element mixture viscosity and μ_f is the Newtonian fluid viscosity. The element mixture viscosities are used in Equation 5.11 to solve for the velocity distribution over the pipe cross section.

Concentration variations in the lateral direction are assumed to be small (Shook et al., 1979) so that the concentration profiles determined with the traversing gamma ray device can be used to provide the concentration distributions. Use of Equations 5.12 to 5.14 to determine the velocity distribution of the two-phase mixture imposes the assumption that particle size does not affect the solution.

5.1.3 Modification for non-Newtonian fluids

In the simulation of particle-free flow of a non-Newtonian fluid in a pipe, the effective viscosity of each element is used in finding a solution. The effective viscosity of an

element is evaluated using the shear rate of the element from the previous iteration. The shear rate, and therefore the effective viscosity, of each element converge towards a final value as the solution proceeds.

When particles are present, it is assumed that a relationship similar to the relative viscosity (Equation 5.14) applies to non-Newtonian fluids. It would seem that the Newtonian fluid viscosity in Equation 5.14 should be replaced by some form of the effective viscosity of the non-Newtonian fluid. For a homogeneous Bingham fluid the effective viscosity is given by

$$\eta = \frac{\tau_y}{|\sqrt{\tfrac{1}{2}(\Delta:\Delta)}|} + \mu_p \qquad \textit{for } \tfrac{1}{2}(\tau:\tau) > \tau_y^2 \tag{2.2a}$$

$$\Delta = 0 \qquad \textit{for } \tfrac{1}{2}(\tau:\tau) < \tau_y^2 \tag{2.2b}$$

However it is not immediately apparent how the local particle concentration should be used to modify the local effective viscosity of a non-Newtonian fluid. The second term of Equation 2.2a is associated with shear and it would seem reasonable to assume that this term is affected by particle concentration in a manner similar to that observed with Newtonian fluids. The first term of Equation 2.2a contains the yield stress which is due to fine particle flocculation and there is little physical justification for this term to increase with coarse particle concentration.

In the finite element simulations performed here, the element effective viscosity was

modified to account for the local particle concentration by using the relative viscosity equations (5.12 and 5.13) as multipliers for the second term of Equation 2.2a so that

$$\eta_m = \frac{\tau_y}{|\sqrt{\tfrac{1}{2}(\Delta:\Delta)}|} + \mu_r\mu_p \qquad \textit{for } \tfrac{1}{2}(\tau:\tau) > \tau_y^2 \tag{5.15}$$

where η_m is the effective viscosity of the mixture. Equation 2.2b was not modified.

In terms of the Bingham fluid model, the plastic viscosity is increased by the relative viscosity as determined by the local solids concentration and Equation 5.12 or 5.13. The yield stress is not adjusted for the local concentration. The effect of the solids concentration on a rheogram relating shear stress to shear rate (e.g. Figure 4.16), is to increase the slope of the plot but the intercept with the ordinate stays the same.

The shear rate dependence of the effective viscosity with the Bingham fluid required an iterative solution to be used. At the start of the solution procedure, an initial guess of the velocity distribution was required. For this the velocity distribution for one-dimensional pipe flow of the fluid alone was used. After the solution had proceeded a few iteration cycles, the updated velocities in the solution domain were used to calculate the updated shear rate for each element. These were then used with the local solids concentrations to calculate the modified effective viscosity for the elements.

5.1.4 Concentration distribution prediction

In the absence of lift forces, the particles are supported by contact with other particles and ultimately the wall. The force associated with this support can be expressed through an interparticle normal stress, τ_{syy}, which increases with depth in the bed. If the

upward vertical direction is denoted as y, the interparticle normal stress can be expressed by (Roco and Shook, 1983)

$$- \frac{\partial \tau_{syy}}{\partial y} = c(\rho_s - \rho_f) g_y \qquad (5.16)$$

In the horizontal direction, g_x is zero so that

$$- \frac{\partial \tau_{sxx}}{\partial x} = 0 \qquad (5.17)$$

According to Bagnold (1954), the interparticle stress can be related to the shear stress, τ_{sij}, and the angle of internal friction of the solids, α, for inertial interparticle contact by Equation 5.18.

$$\tau_{sii} = \frac{\tau_{sij}}{\tan \alpha} \qquad \textit{where } i = x, y \textit{ and } j = z \qquad (5.18)$$

Although Bagnold distinguished between inertial and "viscous" shear processes, Equation 5.18 should also apply in laminar flow if Bagnold's reasoning is valid. Unfortunately, Equations 5.16 and 5.18 do not provide a satisfactory description of the laminar flow concentration profiles so equations 5.12 and 5.13 must be reconsidered. The first two terms of these relative viscosity equations are the result of the presence of the particles in the shear field (Einstein, 1906). The remaining two terms of each equation are probably the result of particle interactions. It is reasonable to assume that it is these

interactions which contribute the dispersive stress. For the one dimensional flow of a Newtonian fluid the normal component of the interparticle shear stress should then obey an equation of the form

$$\tau_{sij} = - \mu_d \mu_f \dot{\gamma}_{ij} \tag{5.19}$$

where μ_d is a "dispersive viscosity" which is due to the particle interactions. From Thomas' equation (5.12) for spheres it seems that a suitable expression for μ_d should be

$$\mu_d = K_v(10.05\, c^2 + 0.00273 \ \exp(16.6\, c)) \tag{5.20}$$

where the coefficient K_v reflects the fact that τ_{sij} is proportional to the higher order term effect. In the absence of other evidence, K_v will be taken as unity.

Equations 5.16 through 5.20 can be combined to produce a differential equation for pipe flow describing the variation of the interparticle stress in terms of the dispersive viscosity, the viscosity of the fluid, and shear rate. To account for Bingham fluid behaviour, the effective viscosity given by Equation 2.2 will be used in place of μ_f.

$$- \frac{\partial}{\partial x}\left(\frac{\mu_d \eta_f \dot{\gamma}_{xz}}{\tan \alpha} \right) - \frac{\partial}{\partial y}\left(\frac{\mu_d \eta_f \dot{\gamma}_{yz}}{\tan \alpha} \right) = c(\rho_s - \rho_f) g_y \tag{5.21}$$

This equation can be rearranged to describe the variation of solids concentration within the pipe.

$$\left(\dot{\gamma}_{xz} \frac{d\mu_d}{dc} \right) \frac{\partial c}{\partial x} + \left(\dot{\gamma}_{yz} \frac{d\mu_d}{dc} \right) \frac{\partial c}{\partial y} + \left(\frac{(\rho_s - \rho_f) g_y \tan \alpha}{\eta_f} \right) c$$

$$+ \mu_d\left(\frac{\partial \dot{\gamma}_{xz}}{\partial x} + \frac{\partial \dot{\gamma}_{yz}}{\partial y}\right) + \frac{\mu_d}{\eta_f}\left(\dot{\gamma}_{xz}\frac{\partial \eta_f}{\partial x} + \dot{\gamma}_{yz}\frac{\partial \eta_f}{\partial y}\right) = 0 \qquad (5.22)$$

Equation 5.22 can be used as R(x,y) in the weighted residual integral (5.2) to develop a system of equations which can be solved to produce a finite element solution for the concentration distribution.

It is noted that the final two terms of Equation 5.22 contain the partial derivatives of shear rate and effective viscosity which are constant for the constant strain rate elements being used here. Therefore, to remain consistent with the finite element solution for velocity, only the first three terms of Equation 5.22 need to be considered. Thus the weighted residual integral becomes

$$[I] = \left[Q\ [\phi]^T \frac{\partial[\phi]}{\partial x} + R\ [\phi]^T \frac{\partial[\phi]}{\partial y} + S\ [\phi]^T [\phi]\right][c] = [0] \qquad (5.23)$$

where

$$[Q] = \eta_f \dot{\gamma}_{xz}\frac{\partial \mu_d}{\partial c}\ , \qquad [R] = \eta_f \dot{\gamma}_{yz}\frac{\partial \mu_d}{\partial c}\ , \qquad [S] = (\rho_s - \rho_f) g_y \tan\alpha \qquad (5.23a)$$

The coefficients are velocity and concentration dependent and require an iterative solution.

A natural boundary condition for the concentration exists along the central axis of symmetry where the derivative normal to the boundary is zero. However, a problem arises in specifying the essential boundary conditions which exist on the pipe wall and where the

concentration must be specified. Since the variation of concentration on the pipe wall can not be predicted independently, a finite element solution is not possible without making assumptions about the conditions near the wall.

It would seem reasonable to assume that lateral variations of concentration are small with these particles. With no variation with respect to x, Equation 5.22 can be simplified to become an ordinary differential equation and the concentration profile equation is now

$$\left(\dot{\gamma}_{yz} \frac{d\mu_d}{dc} \right) \frac{dc}{dy} + \left(\frac{(\rho_s - \rho_f) g_y \tan \alpha}{\eta_f} \right) c = 0 \qquad (5.24)$$

Equation 5.24 has been solved using an adaptive step size, fourth order Runge-Kutta method (Press et al., 1989). An initial concentration is specified at the bottom of the pipe and the solution is advanced in the y direction using the local values of the shear rate, dispersive viscosity and the effective fluid viscosity from the results of the finite element velocity solution.

Once the concentration profile in the y-direction has been found, the concentration at each node in the pipe cross section is set to the predicted value at that elevation. The nodal point concentrations are then used to calculate mean element concentrations which are integrated over the domain to obtain the overall mean in-situ concentration. The concentration at the pipe bottom which was used to start the Runge-Kutta solution is then adjusted in proportion to the deviation between the integrated concentration and the specified in-situ concentration and another solution is sought. This process is repeated until the integrated mean concentration matches the specified value.

An attempt was made to couple the finite element and ordinary differential equation solutions to obtain predictions for both velocity and concentration profiles which were independent of any experimental measurements. However it was found that the velocity and concentration distributions are too interdependent in most cases and that convergence frequently could not be obtained.

5.2 Finite element simulations

A number of simulations were performed in order to test the ability of the proposed numerical method to predict velocity and concentration distributions for slurries with Newtonian and non-Newtonian carriers. These tests include experiments conducted in other investigations to clarify the usefulness of the simulation in its present state. A summary of the simulation cases is listed in Table 5.1.

The experimental tests with ethylene glycol and oil carrier fluids were performed at the Saskatchewan Research Council as part of a multiclient study on the flow behaviour in horizontal well bores (Gillies et al. 1993, 1994).

In each simulation, the velocity distribution was calculated with the finite element method using a specified pressure gradient and concentration profile. The required concentration profile was specified by using a two part linear profile which approximated an experimentally measured profile. Once the velocity profile was determined, the concentration profile was then calculated using the Runge-Kutta integration method. The computer program is listed in Appendix C.

5.2.1 Glycol slurry simulations

The ethylene glycol slurries were tested at 6 °C which gave a fluid viscosity of 46

mPa.s. These flows were laminar. Sand with a median diameter of 0.43 mm was used as the solids phase at an in-situ concentration of 0.20. The pipeloop used had an internal diameter of 53 mm. The comparison between experimental and simulation results are made at two bulk velocities.

Table 5.1 : Numerical simulation test cases.

Fluid (model)	Plastic Viscosity (mPa.s)	Yield Stress (Pa)	Bulk Velocity (m/s)	In-situ Concentration
glycol (Newtonian)	46	0	0.93	0.2
	46	0	1.15	0.2
oil (Newtonian)	1440	0	0.11	0.2
	2360	0	0.06	0.2
Kaolin/ Bentonite (Bingham)	110	6.5	1.6	0.15
	65	4.1	0.8	0.15
	62	17	1.6	0.15
	80	25	1.6	0.15

The first case simulated the glycol slurry at a bulk velocity of 0.93 m/s. At this velocity, there was a stationary deposit in the pipe below 0.1 y/D and the observed pressure gradient was 1.82 kPa/m. With the simulation, the predicted bulk velocity for this pressure gradient was 1.19 m/s. The pressure gradient was then adjusted and the simulation was repeated until a bulk velocity of 0.93 m/s was obtained. The pressure gradient which gave a velocity of 0.93 m/s was 1.35 kPa/m. The predicted velocity profile and the specified and

calculated concentration profiles along the pipe centreline are shown in Figure 5.2 for the bulk velocity of 0.93 m/s. Also shown are the measured concentration profile and the velocity profile measured with a pitot tube.

The shape of the predicted velocity profile and that obtained with the pitot tube agree reasonably well although the measured velocities are greater than the predicted ones. The pitot tube velocities were probably all high since a screw pump was used for these tests and the mean velocity was known to be correct.

The concentration profile calculated using Equation 5.24 agrees reasonably well with the observed distribution of solids. It underpredicts the concentration at the wall and also the amount of dispersion higher in the pipe. The calculated delivered concentration is 0.065 v/v compared to a measured value of 0.064 v/v. Thus the largest discrepancy between the model and the observed flow behaviour is that the predicted pressure gradient is 26% below the observed value.

Figure 5.3 shows the observed and model results for the glycol-sand slurry at a bulk velocity of 1.15 m/s. Here the predicted velocity profile gives excellent agreement with the values measured with the pitot tube. Once again the pressure gradient is underpredicted by the model. With the observed pressure gradient of 2.06 kPa/m and specified concentration profile, the predicted velocity was 1.45 m/s. The pressure gradient was adjusted to 1.60 kPa/m in order to give the correct bulk velocity of 1.15 m/s.

The calculated concentration profile did not agree with the measured values nearly as well in this experiment. The predicted concentration was high for most of the profile but suggested no solids would travel above y/D = 0.53. It is possible that the measured

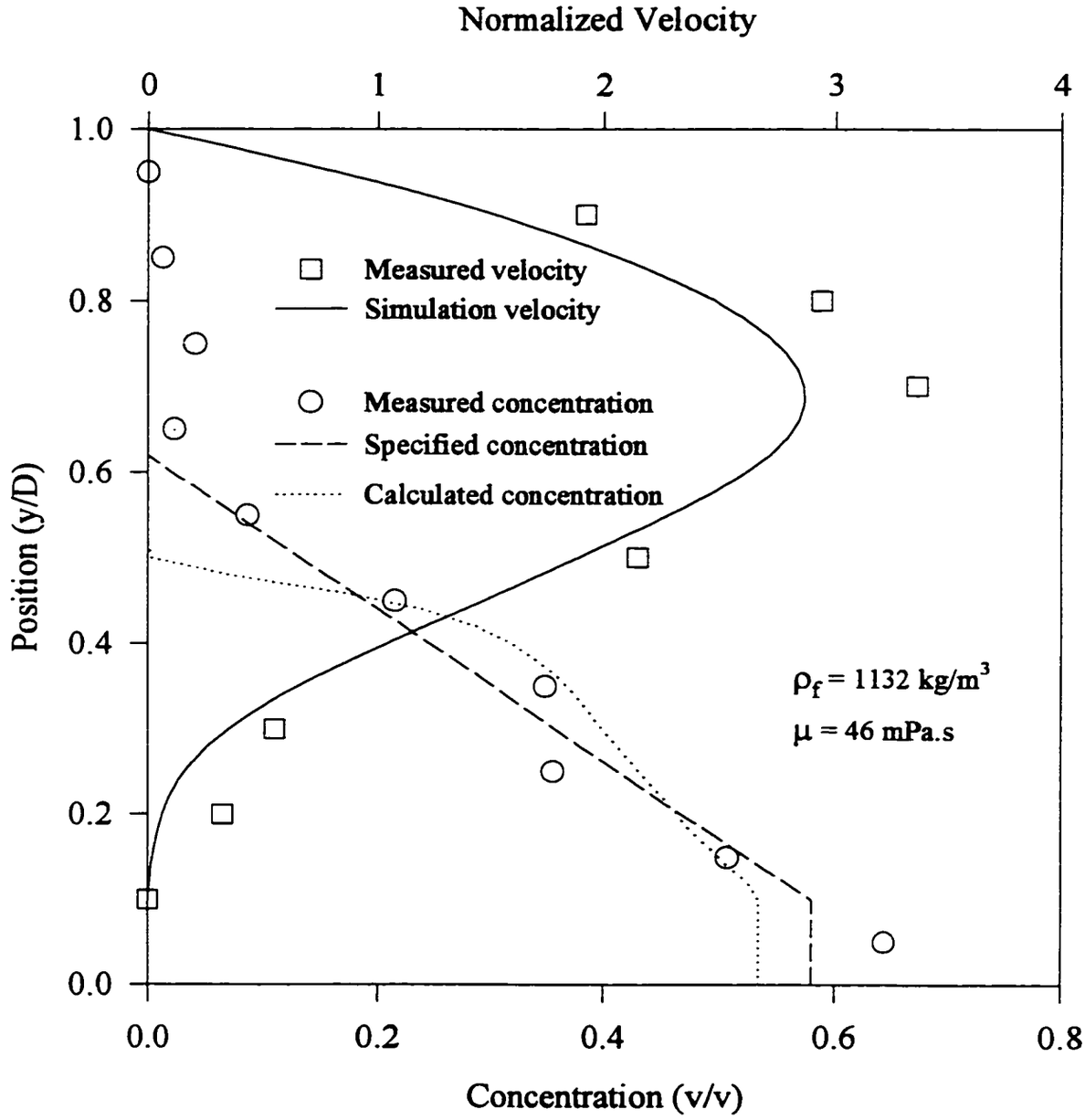

Figure 5.2 : Predicted velocity and concentration profiles for 20% 0.43 mm sand in ethylene glycol at a bulk velocity of 0.93 m/s.

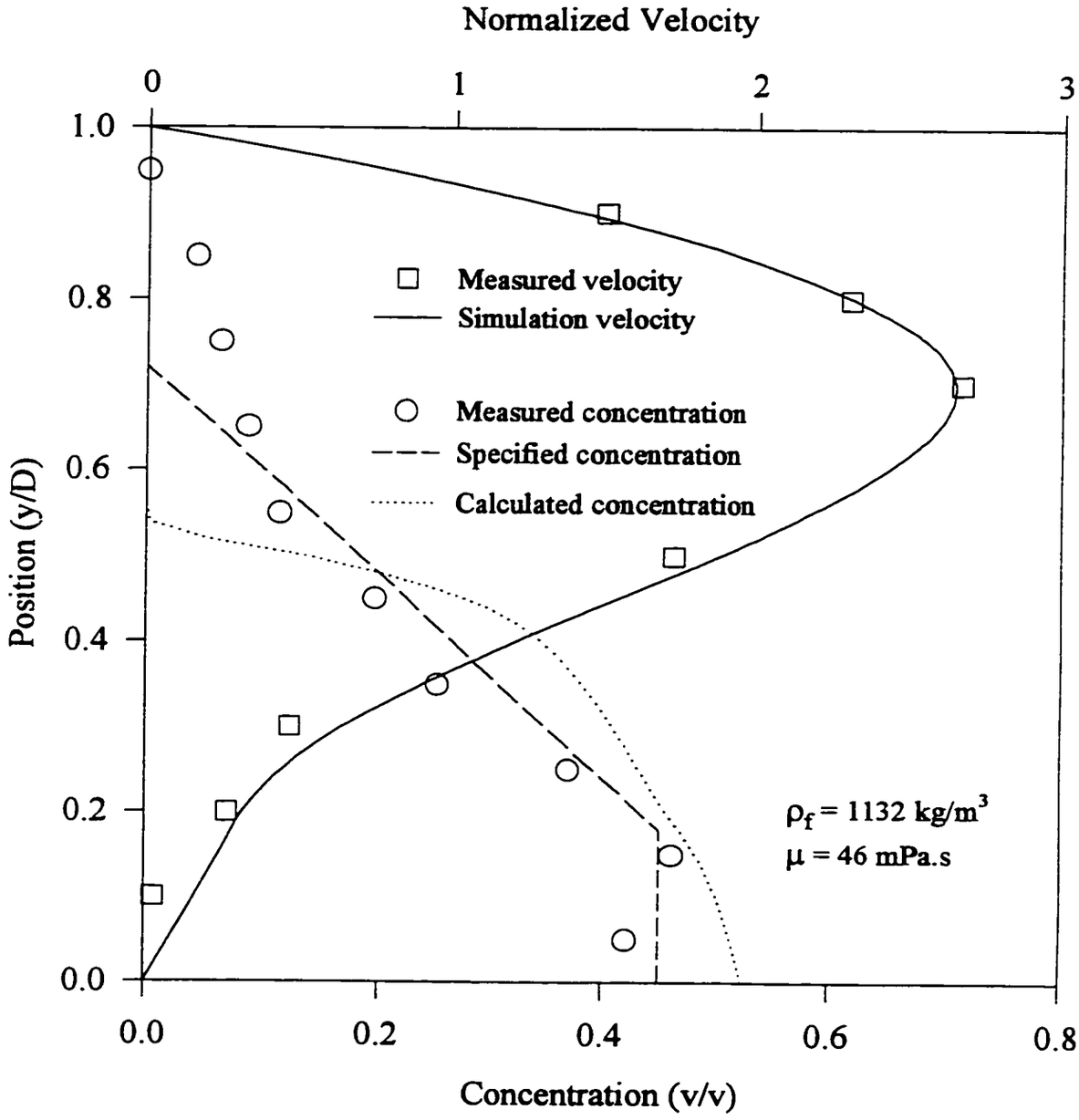

Figure 5.3 : **Predicted velocity and concentration profiles for 20% 0.43 mm sand in ethylene glycol at a bulk velocity of 1.15 m/s.**

concentration distribution was not quite at an equilibrium condition at this high velocity. The calculated delivered concentration was 0.113 compared to the measured value of 0.114. This agreement is rather surprising given the difference in the concentration profiles.

5.2.2 Oil slurry simulations

The oil slurries contained sand with a median size of 0.43 mm and an in-situ concentration of 0.20. Simulation results are compared to results obtained with two different fluid viscosities in a 53 mm pipe. The same oil was used for both tests but the temperature was changed to give fluid viscosities of 1440 and 2360 mPa.s. At the low bulk velocities here it was not possible to measure point velocities with the pitot tube,

Comparisons of observed and simulated results for a fluid viscosity of 1440 mPa.s are shown in Figure 5.4 for a bulk velocity of 0.11 m/s. The observed pressure gradient was 4.74 kPa/m while the simulation pressure gradient which gave this bulk velocity was determined to be 5.02 kPa/m.

The calculated concentration profile follows the observed profile closely. The concentration predicted at the bottom is, however, slightly higher than the measured value. The calculated delivered concentration was 0.103 compared to the measured value which was 0.146. This suggests that the predicted velocity in the particle-rich region may be lower than actually exists in the pipe.

For the oil slurry whose fluid viscosity was 2360 mPa.s, the bulk velocity was 0.06 m/s. At this velocity, the pressure gradient was observed to be 4.34 kPa/m while the simulation pressure gradient was 4.53 kPa/m.

The velocity and concentration profiles are shown in Figure 5.5 for the higher

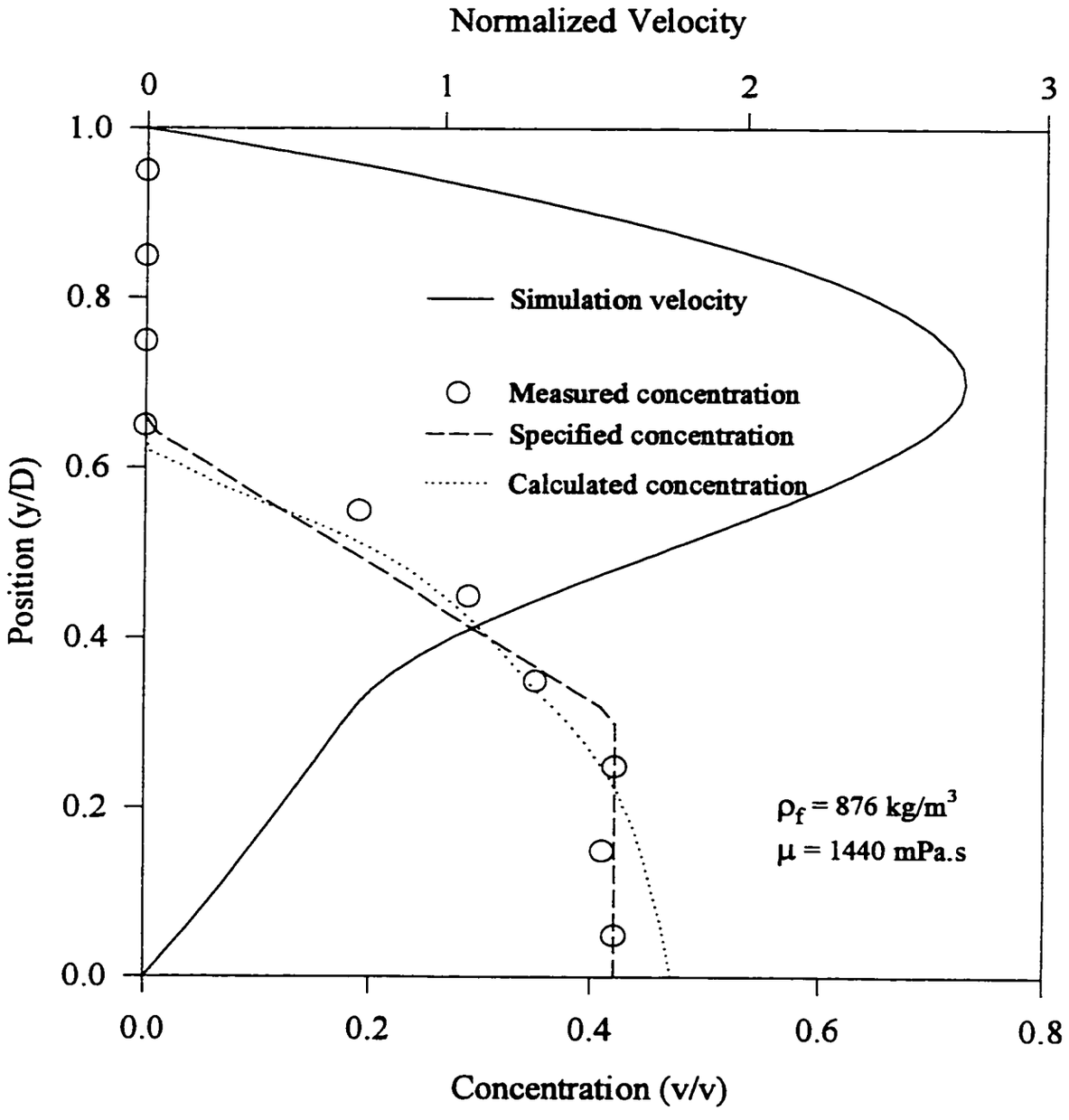

Figure 5.4 : Predicted velocity and concentration profiles for 20% 0.43 mm sand in a 1440 mPa.s oil at a bulk velocity of 0.11 m/s.

viscosity oil. The calculated concentration profile agrees well with the measured profile. However the delivered concentration calculated from the numerical simulation was again low. The calculated value was 0.088 compared to the measured value of 0.136. This difference indicates that the velocities in the high concentration layer are underpredicted.

With these slurries and their high viscosity carrier fluids, the calculated pressure gradients exceed the observed values for the same bulk velocity. This is in contrast to the lower viscosity glycol results where the observed values were higher than the calculated values. The concentration profiles predicted with these more viscous flows agree well with the measured profiles. There is, however, a discrepancy between the measured and calculated delivered concentrations.

The observations made with the glycol and the oil slurries would seem to suggest that the viscous and dispersive mechanisms used here describe the flows fairly well but do not specify them completely. There may be additional effects whose importance varies with the fluid viscosity.

5.2.3 Kaolin/Bentonite slurry simulations

Four test cases are presented from the results obtained from the present investigation which used Kaolin/Bentonite suspensions as carrier fluids. The first case is a slurry containing the 1.7 mm glass spheres at an in-situ concentration of 0.15. The next three cases consider 4.4 mm glass spheres at in-situ concentrations of 0.15 in three different fluids.

The Kaolin/Bentonite suspension used with the 1.7 mm spheres had a yield stress which was sufficient to support the particles if the fluid were stationary, according to Equation 2.14. The measured concentration and local particle velocity profiles and the

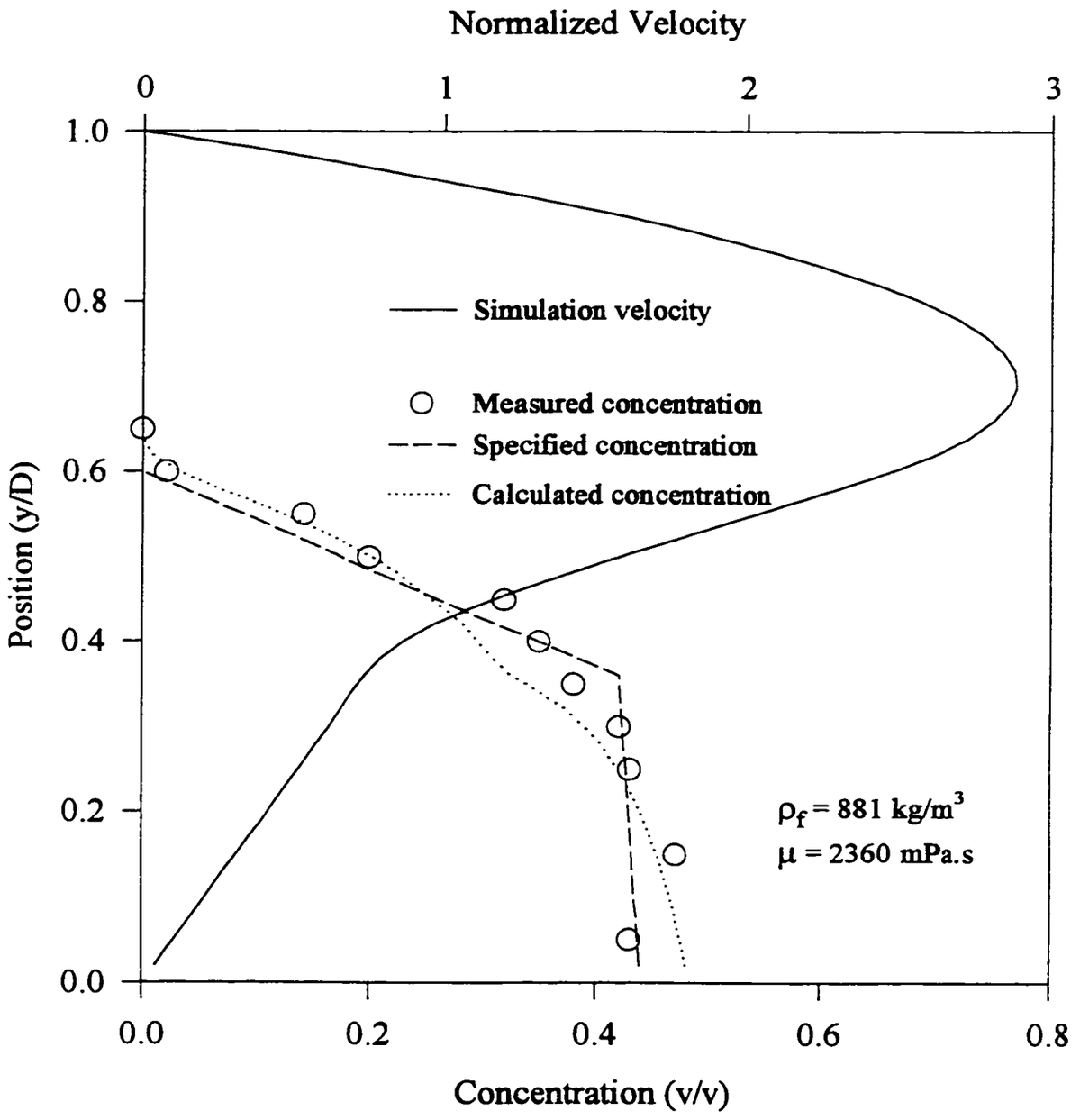

Figure 5.5 : **Predicted velocity and concentration profiles for 20% 0.43 mm sand in a 2380 mPa.s oil at a bulk velocity of 0.06 m/s.**

predicted velocity, specified and calculated concentration profiles are shown in Figure 5.6. The bulk velocity of the slurry was 1.6 m/s.

The local particle velocities observed with the probe are significantly lower than the simulated values. This discrepancy illustrates the magnitude of the velocity error which results from the boundary layer on the probe in laminar flow. Thus the measured local velocities give only qualitative indications of the shape of the velocity distribution. The blunt profile predicted by the simulation is a result of the effect of the yield stress. It is this blunting which causes the maximum velocity to be lower than the value observed with Newtonian fluids.

The measured pressure gradient for this mixture was 4.37 kPa/m in comparison to the simulation prediction of 4.29 kPa/m. As in the case of the Newtonian carrier fluid simulations, the predicted concentrations near the pipe wall are higher than the observed values. The difference is more noticeable in the present case. The delivered concentration predicted by the simulation is 0.117.

The first simulation made with the slurry of 4.4 mm spheres considered the high density and low yield stress carrier. The yield stress was not capable of supporting the particles in a stationary fluid according to Equation 2.14. The results with a bulk velocity of 0.8 m/s were used since this flow was laminar. These results are shown in Figure 5.7.

Only two points on the velocity profile could be measured because of equipment problems but they also suggest the influence of the boundary layer on the probe. The measured pressure gradient at this velocity was 2.20 kPa/m. The simulation suggested a pressure gradient of only 1.50 kPa/m in this case. The predicted concentration profile also

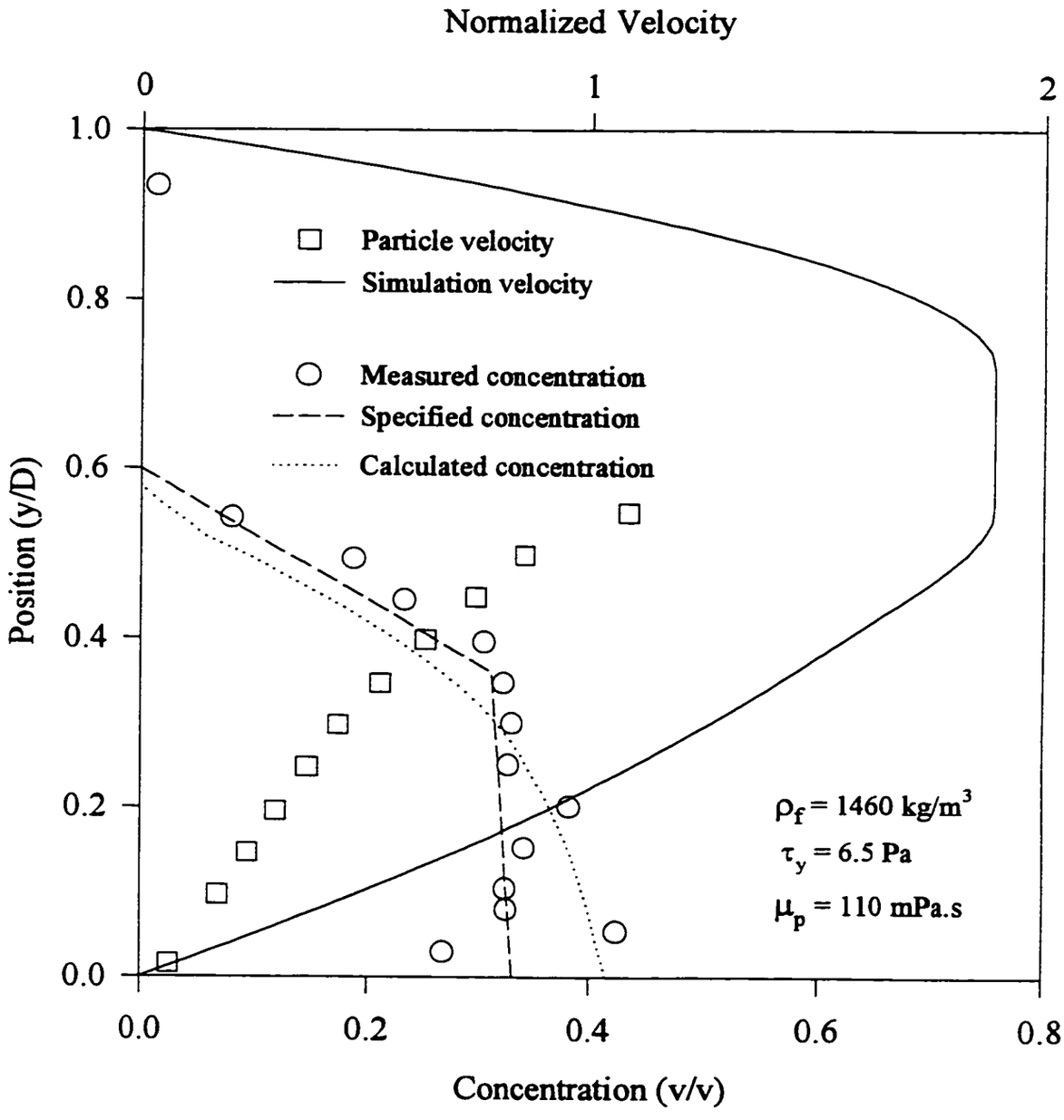

Figure 5.6 : **Predicted velocity and concentration profiles for 15% 1.7 mm spheres in a Kaolin/Bentonite suspension at a bulk velocity of 1.6 m/s.**

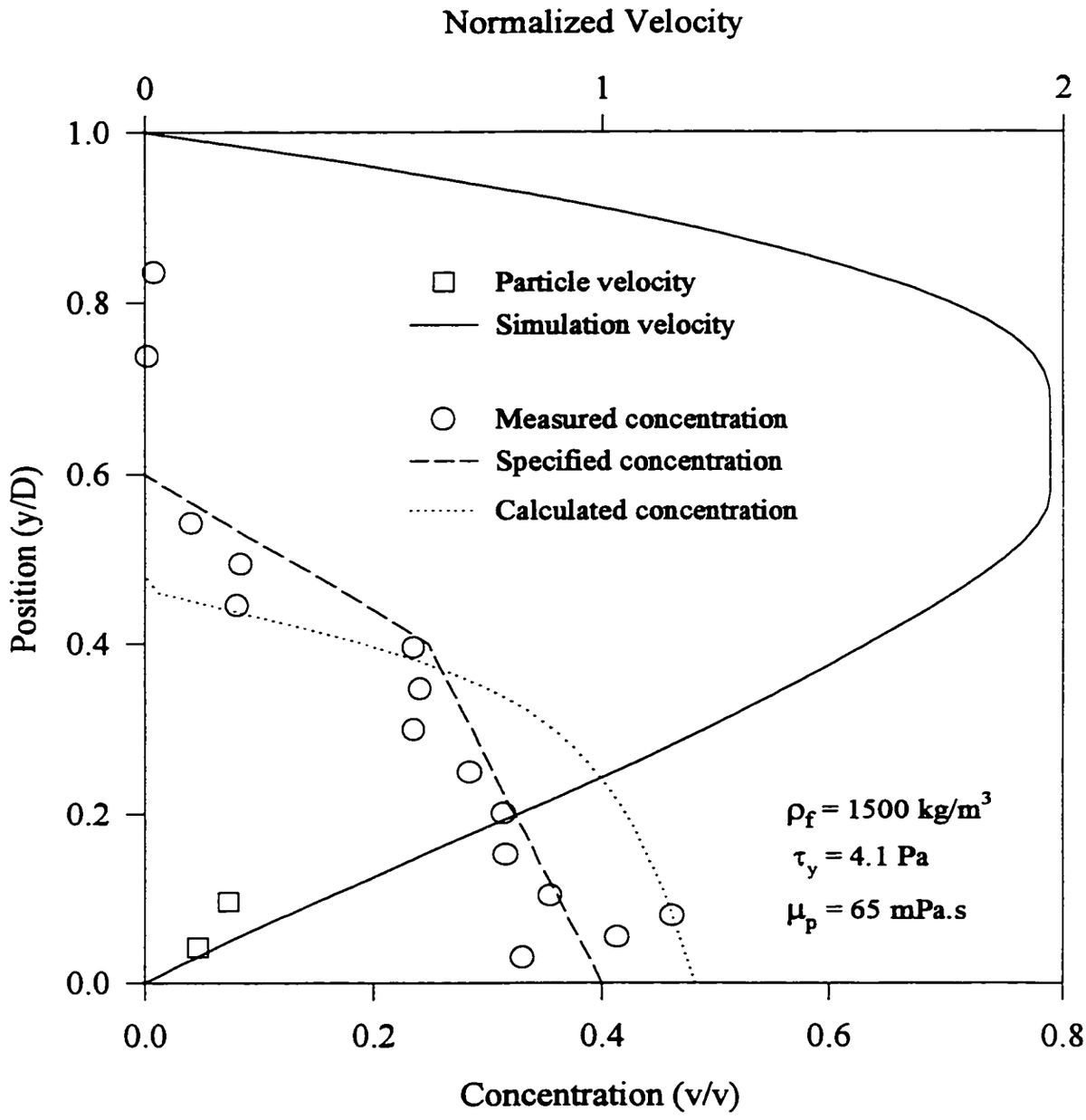

Figure 5.7 : **Predicted velocity and concentration profiles for 15% 4.4 mm spheres in a Kaolin/Bentonite suspension with a low yield stress at a bulk velocity of 0.8 m/s.**

shows a significant departure from the measured values throughout the pipe. The delivered concentration was calculated to be 0.109.

Using the more viscous low density and high yield stress suspension, the simulation results compare more favourably to the measured values. In this case, the particles would have been suspended if the fluid were stationary. The measured and simulated results at a bulk velocity of 1.6 m/s are shown in Figure 5.8. The particle velocity measurements are still lower than the simulation prediction but the shapes are in agreement. It is interesting that the predicted velocity at the bottom of the pipe is actually lower than the measured value. It is noted that one particle diameter corresponds to y/D = 0.08. The measured and simulated pressure gradients are in good agreement. The measured value is 3.90 kPa/m and the simulation value is 3.73kPa/m. The calculated concentration profile also agrees well with the specified profile. The delivered concentration was calculated to be 0.105.

The next simulation was with the highest yield stress suspension and the 4.4 mm spheres at a bulk velocity of 1.6 m/s. The measured and simulated results are shown in Figure 5.9. The predicted concentration profile agrees well with the specified profile. The measured and calculated pressure gradients are 4.97 and 4.92 kPa/m respectively. The calculated delivered concentration was 0.124.

5.2.4 Summary

Simulations of slurries with Newtonian or Bingham model fluids agree best with observed pipe flow behaviour when viscous carrier fluids are used. The predicted concentration profiles and pressure gradients agree reasonably well with the measured values. The calculated values of the delivered concentrations were low, however. This

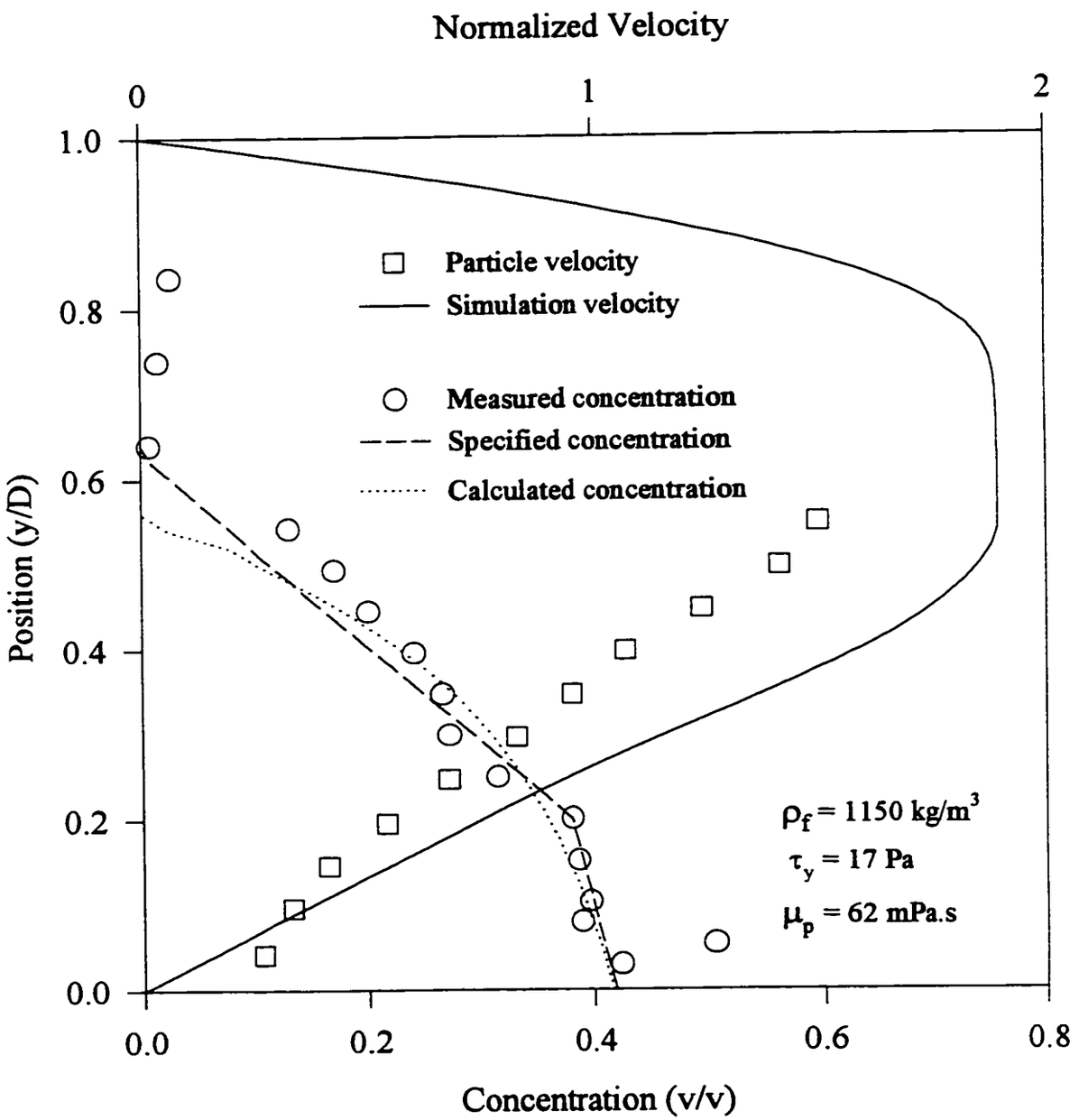

Figure 5.8 : **Predicted velocity and concentration profiles for 15% 4.4 mm spheres in a Kaolin/Bentonite suspension with a 17 Pa yield stress at a bulk velocity of 1.6 m/s.**

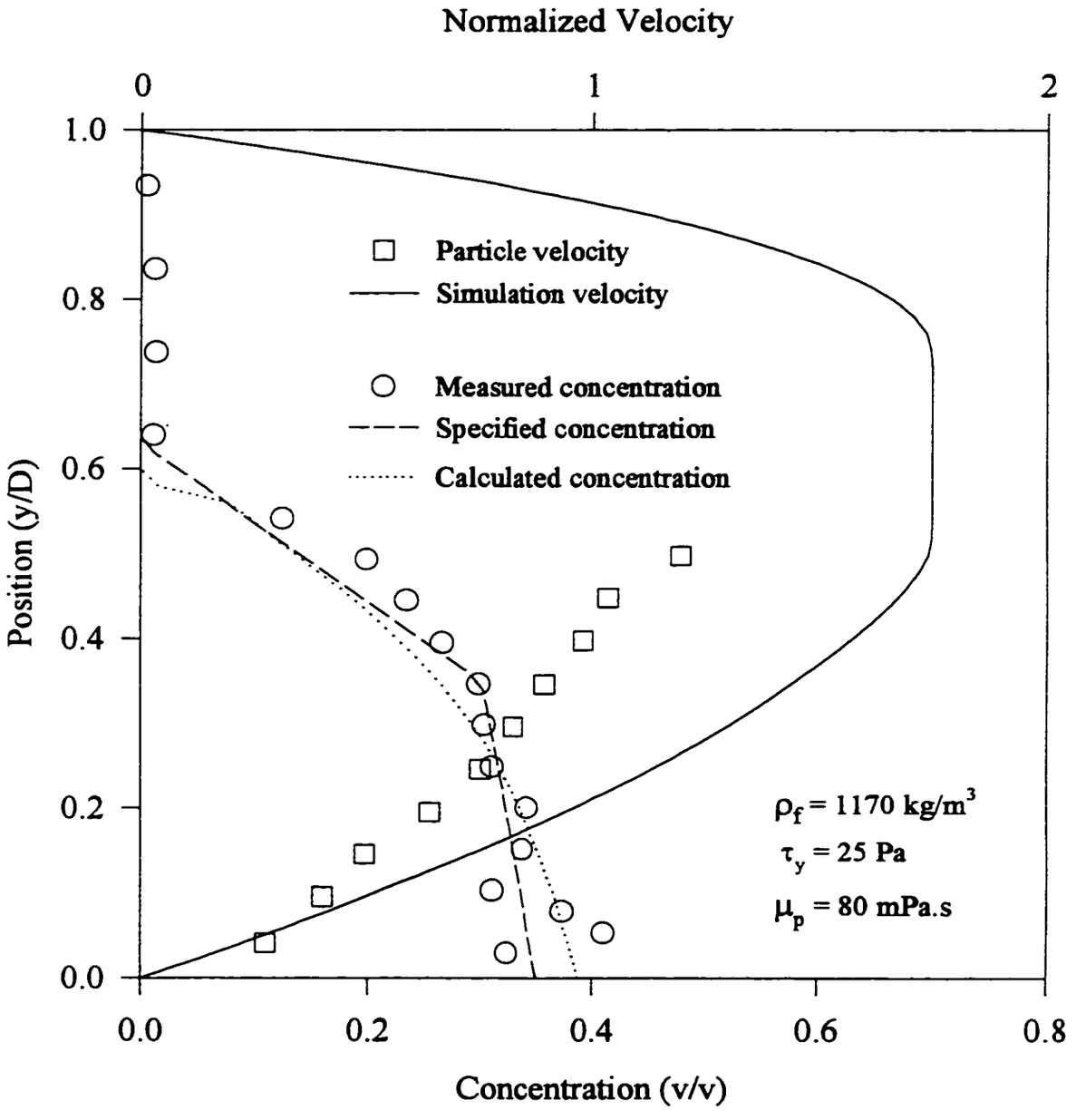

Figure 5.9 : **Predicted velocity and concentration profiles for 15% 4.4 mm spheres in a Kaolin/Bentonite suspension with a 25 Pa yield stress at a bulk velocity of 1.6 m/s.**

would suggest that the velocity profiles were under predicting the velocities in the lower portions of the pipe for these flows.

With less viscous carrier fluids, the pressure gradient was under predicted and the amount of particle dispersion near the bottom of the pipe was also under predicted. The velocity profile and delivered concentration appear to be about right.

These observations suggest that the modified viscosity in the particle rich lower layer is too high so that the velocity in that layer is underpredicted. Also, in this case the dispersive mechanism represented by Equation 5.24 under predicts particle dispersion. The dispersive viscosity, as described by Equation 5.20, was derived from the relative viscosity Equation 5.12. It is possible that the factor K_v varies with some particle-related parameter such as the Bagnold number (Equation 2.25) or that there is an additional stress contribution not described by Equation 5.24.

5.2.5 Sensitivity analysis of model

The response of the finite element and Runge-Kutta models was evaluated by performing additional simulations based on the glycol-sand and oil-sand test cases. Of particular interest was the effect of the specified concentration profile used in solving the finite element model. This concentration distribution determines the variation of the effective viscosity of the elements in the solution domain. Also of interest is the effect of the calculated velocity distribution and the resulting element shear rates on the Runge-Kutta solution of Equation 5.24.

Figure 5.10 shows the effect of a change in the specified concentration profile on the finite element simulated velocity profile. The simulations use the same glycol-sand mixture

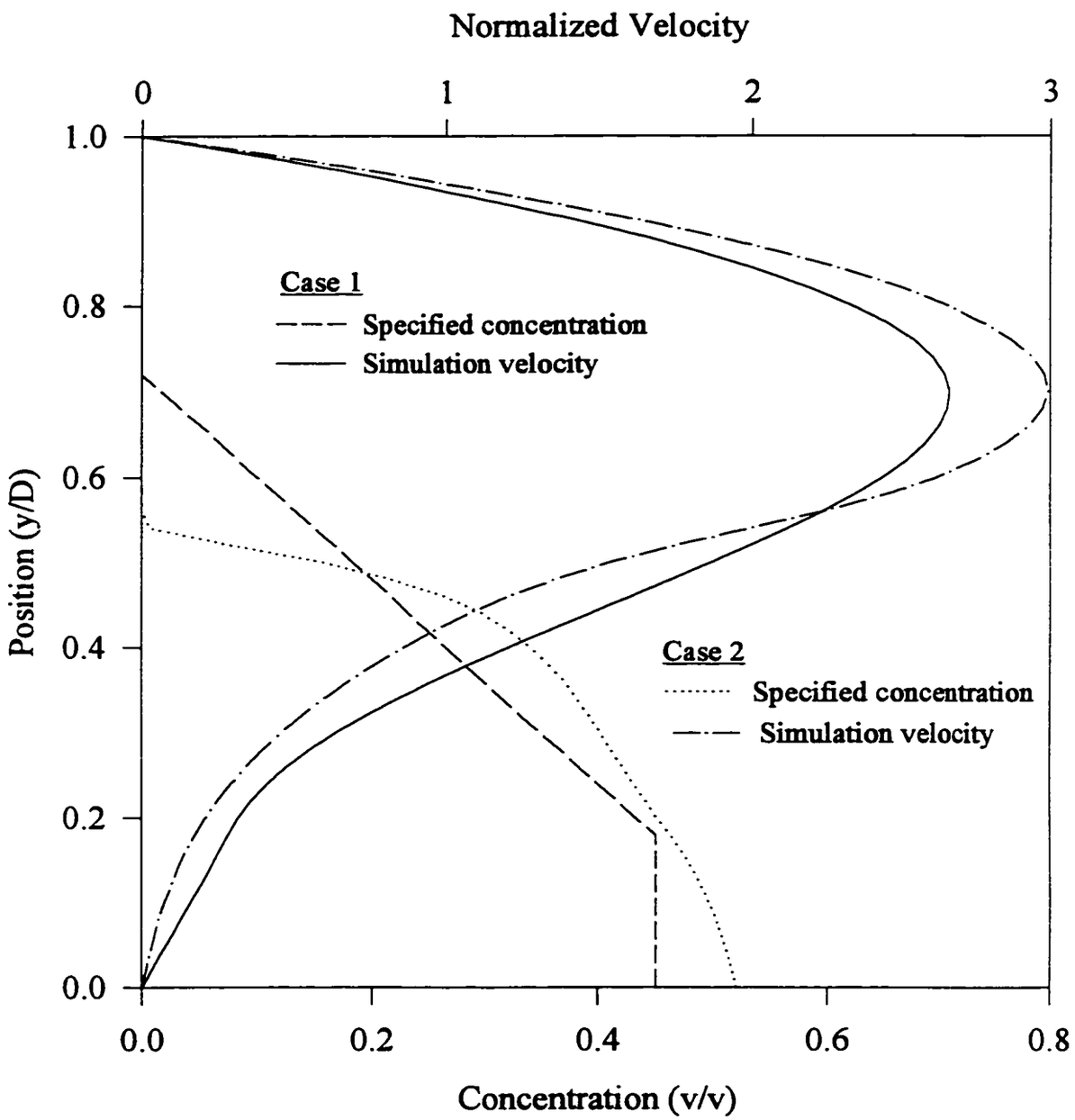

Figure 5.10 : The sensitivity of finite element velocity predictions to the specified concentration distribution with a low viscosity fluid.

discussed in Section 5.2.1 where the bulk velocity was 1.15 m/s. In case 1, the original specified concentration profile was used and the velocity distribution was determined. It is recalled that the predicted velocity profile agreed very well with measurements made with a pitot tube. The simulated pressure gradient in this case was 1.60 kPa/m.

The numerically predicted concentration distribution from case 1 was used as the specified concentration in the second simulation case of this slurry. This concentration profile produced a substantial change in the simulated velocity profile. The velocities were reduced throughout the particle-containing region and increased in the particle-free region. Consider the strong concentration dependence of the relative viscosity function (Equation 5.12) in the high concentration region near the bottom of the pipe. Significant changes to the velocity profile would be expected in this region for even modest changes in concentration. The simulated pressure gradient had to be increased to 1.88 kPa/m in order to maintain a bulk velocity of 1.15 m/s.

The effect of changes to the velocity distribution on the concentration profile prediction are shown in Figure 5.11 for the same glycol-sand mixture and bulk velocity. The numerically predicted concentration profiles for the two velocity profiles are shown. The substantial variation in the velocity profile had only a modest effect on the concentration profile.

Figure 5.12 shows the specified concentration, simulated velocity and predicted concentration profiles for an oil-sand mixture at a bulk velocity of 0.11 m/s. This is the same mixture discussed in Section 5.2.2. The first case shown in Figure 5.12 uses the original concentration specification for which the velocity simulation and concentration predictions

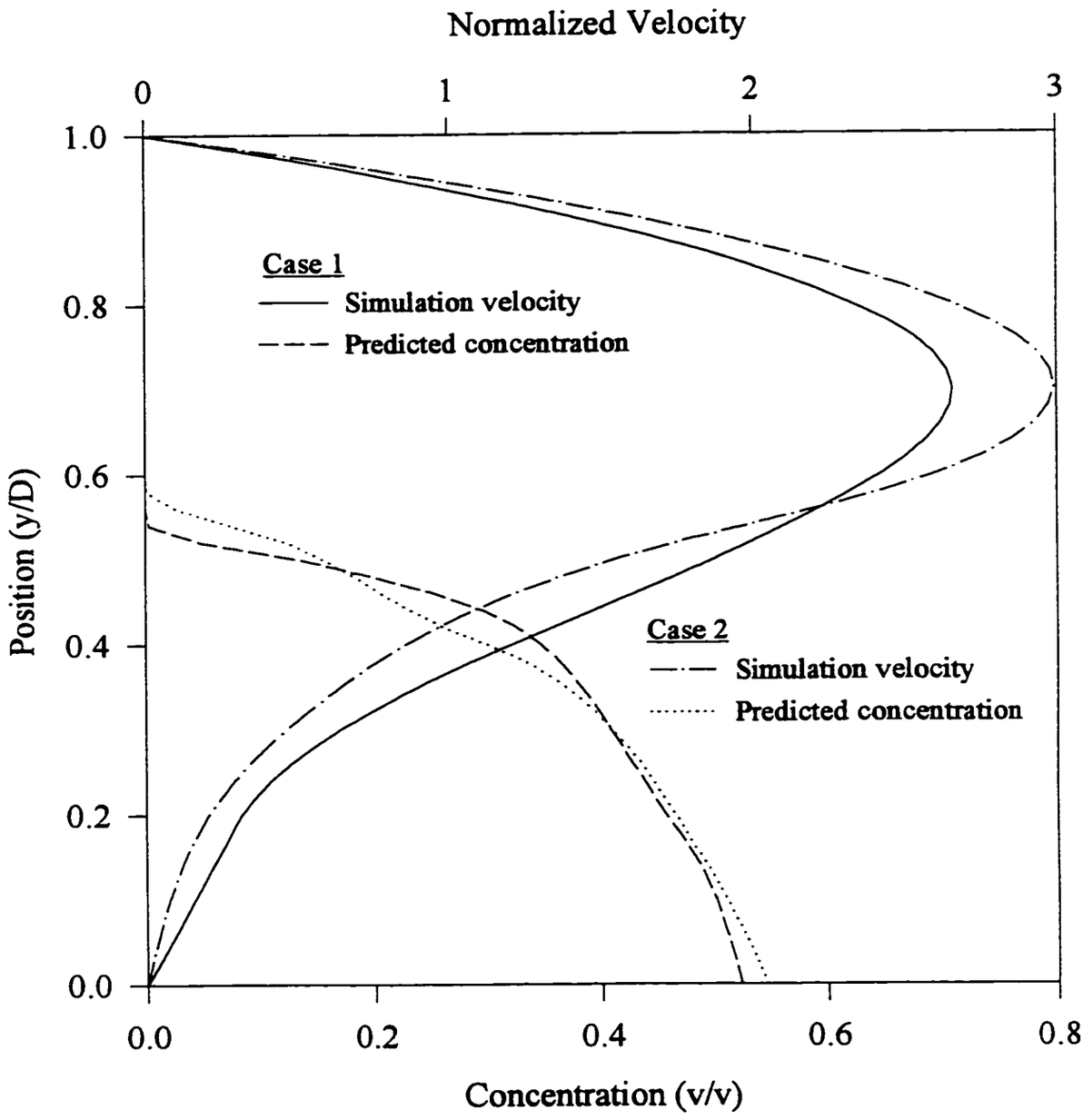

Figure 5.11 : **The sensitivity of Runge-Kutta concentration predictions to the specified velocity distribution with a low viscosity fluid.**

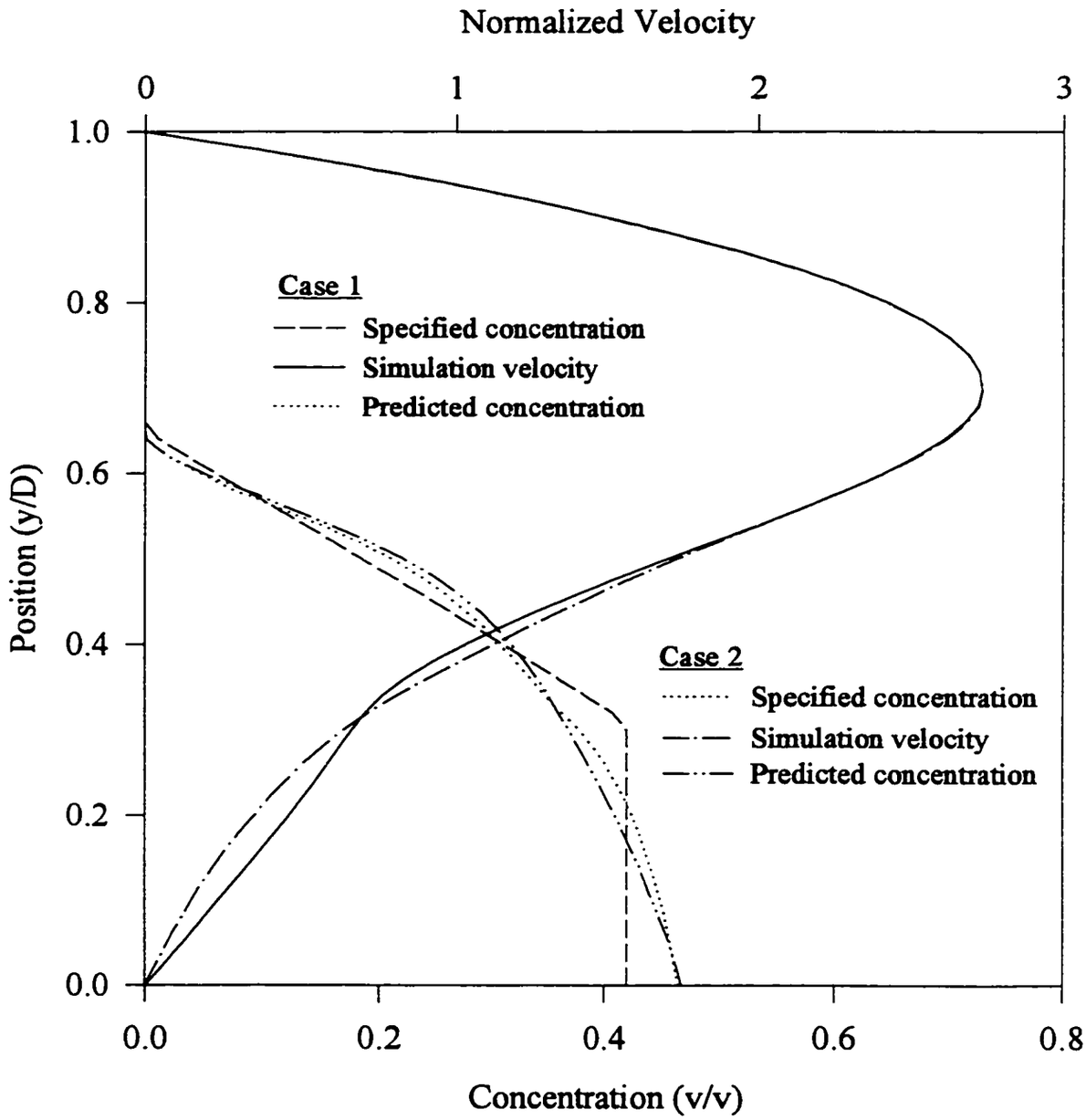

Figure 5.12 : The sensitivity of finite element velocity predictions to the specified concentration distribution with a high viscosity fluid.

where shown earlier in Figure 5.4. The predicted concentration profile shows some deviation from the specified profile in the high solids concentration region of the pipe with a higher value at the bottom predicted.

The predicted concentration profile from the first case was used as the specified concentration profile for the second case. The simulated velocity distribution and predicted concentration profile did not show much variation from the first solutions. The simulated pressure gradients were 5.02 kPa/m for the two cases in comparison to the observed value of 4.74 kPa/m.

5.3 Two-layer model predictions

Use of the two-layer model to predict slurry flow behaviour in both laminar and turbulent flow regimes has also been investigated. Predictions using the computer program listed in Appendix D were made for slurries with Newtonian and Bingham fluid carriers.

The model equations presented in Appendix A were developed for use with Newtonian slurries, mostly aqueous, in turbulent flow. These equations were used as the basis for the model program. The method of Shook (Equations 2.36 and 2.37) for Newtonian carrier fluids was followed for two-layer model predictions in laminar flow.

The existence of a substantial yield stress may have a significant influence on both the friction losses and in the distribution of solids in the pipe. Therefore, modifications to the two-layer model were incorporated into the computer program to account for Bingham carrier fluids. These modifications are discussed in subsequent sections.

5.3.1 The distribution of solids

The distribution of the solids in the pipe affects both the delivered concentration and

the pressure gradient. In turbulent flow, the lower layer concentration and the division between the solids fraction supported by lift forces and those by contact with the wall are determined by correlations. The correlations used here (Equations A.6 and A.7) use the ratio of the bulk velocity to the particle settling velocity. They could be justified by considering the ratio of the turbulent velocity fluctuations to the natural settling velocity of the slurry particles. If these relationships are to be used, the settling rate of particles in a Bingham fluid must be considered.

The investigations of Ansley and Smith (1967) and Dedegil (1986) quantified the reduced settling rates of single particles in stagnant fluids with a yield stress. Although the settling rates of particles in a shearing Bingham fluid have not been quantified, A.D. Thomas (1979) suggested that the settling rates would depend on position in the pipe since the effective viscosity varies with the local shear rate. Thomas also indicated that settling can be slow in these slurry flows.

Dedegil's equations (2.18 to 2.20) were investigated for their use in predicting settling velocities as needed for use with the lower layer concentration correlations (Equation A.6 and A.7). It is noted that Dedegil's equations predict that the settling velocity approaches zero when the yield stress reaches the critical value given by Equation 2.14. Therefore, this equation implies that no particle settling occurs when the yield stress exceeds the critical value so that the particles should remain dispersed in the pipe following mixing in the pump. Simulations using the reduced settling rates of Dedegil in the correlations predicted completely dispersed particles at yield stresses slightly below the critical value. This prediction is in contrast to the concentration profiles reported in section 4.5 where the

flows were stratified even when the yield stress exceeded the critical values.

In turbulent flow it is possible that deflocculation may make the yield stress inconsequential as far as particle settling is concerned. In this case, the settling velocity of the particles may correspond to that given by settling in a Newtonian fluid whose viscosity is equivalent to the Bingham plastic viscosity. With this assumption, the settling velocities given by Equations 2.12 and 2.13 cam be determined which allows the concentration correlations to be used for both Newtonian and Bingham fluids in turbulent flow.

In laminar flow, where suspension by fluid lift forces is not expected to occur, it may be appropriate to assume that all coarse particles are supported by contact with the wall. The concentration in the lower layer is unknown so it must be specified. Concentration distribution measurements can be used to select a value for the lower layer or, without this information, a reasonable assumption of its value must be made.

The effect of the lower layer concentration on predicted pressure gradients is shown in Figure 5.13. The simulation was based on the flow of 4.4 mm spheres in a Kaolin/Bentonite suspension which was reported in Section 4.7.2. The in-situ solids concentration considered here was 0.25 and the contact load fraction was specified as 1.0 in this simulation. Maintaining the contact load constant throughout the velocity range isolated the effect of changing the lower layer concentration. Simulations were made using two values of C_{lim} : 0.50 and 0.40. Measured pressure gradients for the slurry and the carrier are included for reference but it is recalled that with particles of this size, very high pressure gradients were observed when a water carrier fluid was used.

The simulations show that the predicted pressure gradients are fairly insensitive to

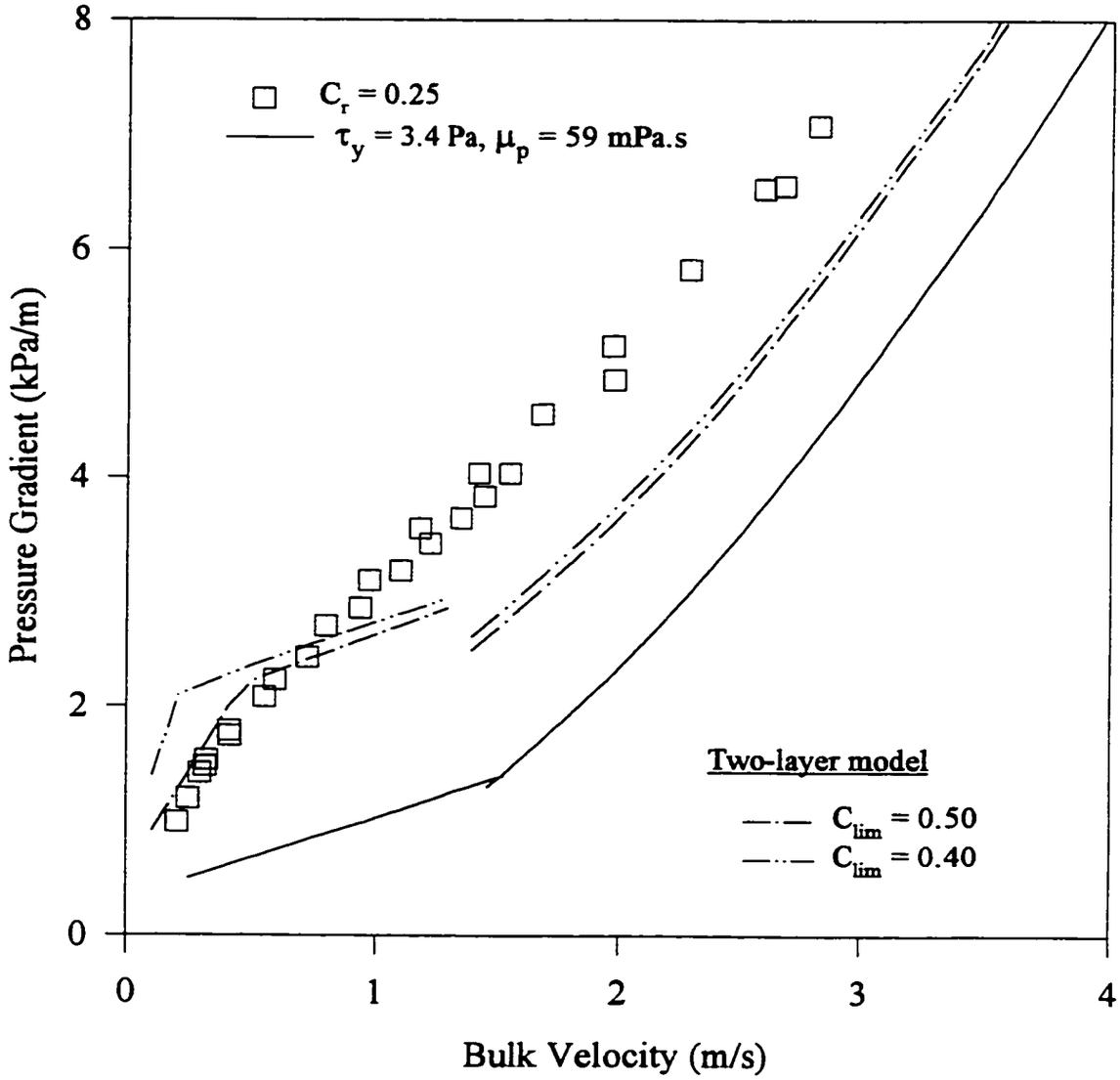

Figure 5.13 : The sensitivity of two-layer model predictions to the lower layer concentration.

the lower layer concentration as long as the velocity is above deposition. The difference in deposition velocity, indicated here by the change in slope in the laminar regime, and the pressure gradients predicted below this velocity are quite significant owing to the difference in pipe cross section available for fluid flow. While a high concentration is expected in a stationary layer, the results here show the need to specify the lower layer concentration if the deposit velocity is to be modelled.

5.3.2 Fluid friction

In turbulent flow, the fluid friction at the pipe wall for the two layers is formulated in terms of the shear stress which is given by Equations A.12 and A.16. The friction factor evaluated for the upper layer is also used as the friction factor for the lower layer. For Newtonian carriers the Fanning friction factor is determined from the correlation of Churchill (1977). For clay suspensions in turbulent flow, deflocculation may reduce the yield stress sufficiently so that the Newtonian friction factor determined using the plastic viscosity may be appropriate. Alternatively, a fluid friction factor may be inferred from the equation of Wilson and Thomas (2.11) for a Bingham fluid.

A comparison between two-layer model predictions made assuming Newtonian fluid friction and Bingham fluid friction is shown in Figure 5.14. The simulation conditions are those of a slurry with 4.4 mm spheres at an in-situ concentration of 0.25 in a Kaolin/Bentonite suspension. A contact load fraction of 0.96 was assumed in the turbulent flow regime based on the experimental measurements presented in Chapter 4 for these particles in a water carrier fluid. It was also assumed that the lower layer concentration was constant at 0.45. Measured pressure gradients are included for reference.

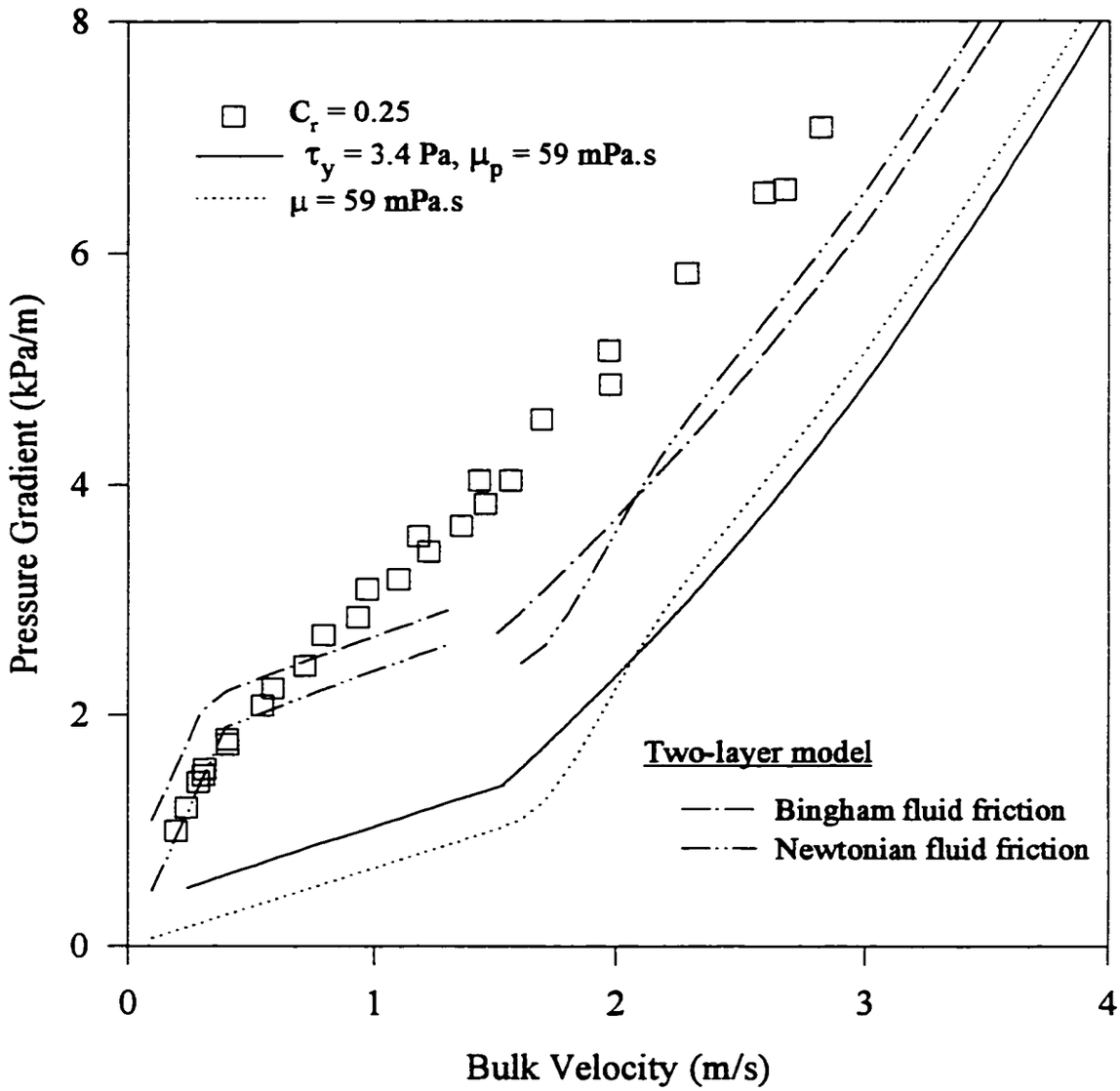

Figure 5.14 : The effect of fluid model selection on pressure gradient predictions of the two-layer model.

For the slurries, the two-layer model predicts a nearly constant increase in the pressure drop because of the Coulombic friction of the coarse particles. In laminar and transitional flow, the prediction made with Newtonian fluid friction is below the Bingham fluid prediction. This difference results from the effect of the yield stress and from the manner in which Churchill's equation (Churchill, 1977) describes fluid friction in the transition region. The pressure drop for the carrier predicted by the Churchill equation is included in Figure 5.14 and shows the same characteristic shape at transition. Above the transition region, the prediction using Newtonian fluid friction is slightly higher than that obtained using Bingham fluid friction.

In laminar pipe flow of a Bingham fluid, the Buckingham equation (2.6) is sometimes used in its simplified form which neglects the fourth order term. This is written as

$$\tau_w = \mu_p\left(\frac{8V}{D}\right) + \frac{4\tau_y}{3} \tag{5.25}$$

where the shear stress at the wall, τ_w, is given by Equation 2.5. This is similar to the Newtonian flow equation but includes the second term to account for the yield stress. When the wall shear stress is high in comparison to the yield stress, this simplification does not introduce much error. The additional term in Equation 5.25 may be appropriate for use with the two-layer model when flow is laminar.

The fluid friction factors in laminar flow were determined using the equations of Shook (2.36 and 2.37) for Newtonian fluids. These friction factors were used to evaluate the shear stresses at the boundaries and at the hypothetical layer interface. In the simulations

with Bingham fluids here, the extra term suggested by the simplified Buckingham equation was added to the fluid shear stress to account for the yield stress. Equations A.12, A.13 and A.16 in laminar flow with Bingham fluids become

$$\tau_1 = \frac{f_1 V_1 |V_1| \rho_1}{2} + \frac{4\tau_y}{3} \tag{5.26}$$

$$\tau_{12} = \frac{f_{12}(V_1 - V_2)|V_1 - V_2| \rho_1}{2} + \frac{4\tau_y}{3} \tag{5.27}$$

$$\tau_{2w} = \frac{f_1 V_2 |V_2| \rho_1}{2} + \frac{4\tau_y}{3} \tag{5.28}$$

The inclusion of the yield stress terms cause the upward shift in the pressure gradient predictions between the Newtonian and Bingham fluid friction cases. This shift gives the proper intercept on the ordinate of pressure gradient graphs for a Bingham fluid.

5.3.3 Interfacial friction factor

The effect of the yield stress on the interfacial friction factor should also be considered since it dictates the difference in velocity of the two layers and therefore, the ratio of delivered concentration to the in-situ concentration. Two methods are available to account for the yield stress at the interface. The first method uses Equation 5.27 to describe the shear stress at the hypothetical interface.

The second method was suggested by Maciejewski et al. (1993) who proposed that the interfacial friction factor is increased in a fashion similar to the increase in particle drag observed in free settling in a Bingham fluid. They suggested that the friction at the hypothetical interface was a function of the Reynolds number which has been modified by the Bingham number as described by Dedegil (1986). Therefore the friction factor is modified to be

$$f'_{12} = f_{12}(1 + Bi_{12}) \qquad where \quad Bi_{12} = \frac{D_{eq} \tau_y}{\mu_p (V_1 - V_2)} \tag{5.29}$$

where f'_{12} is the modified friction factor, f_{12} is the Newtonian friction factor and Bi_{12} is the Bingham number for the interface. In turbulent flow, f_{12} is given by Equation A.14 and in laminar flow, by Equation 2.36b.

Both methods increase the interfacial friction in response to the existence of a yield stress so that the difference in layer velocities is decreased. A measure of the velocities of the layers was provided by the present experiments which used magnetic particles. It was found that with the water and glass sphere slurries, the measured magnetic particle velocities were observed to fall between the layer velocities predicted by the two-layer model (section 4.3).

Figure 5.15 shows a comparison between the measured magnetic particle velocities obtained with slurries composed of 4.4 mm sphere in Kaolin/Bentonite carrier fluids and the layer velocities predicted using Equations 5.27 and 5.29. The magnetic particle velocities were found to be close to the predicted upper layer velocities in laminar flow and above the

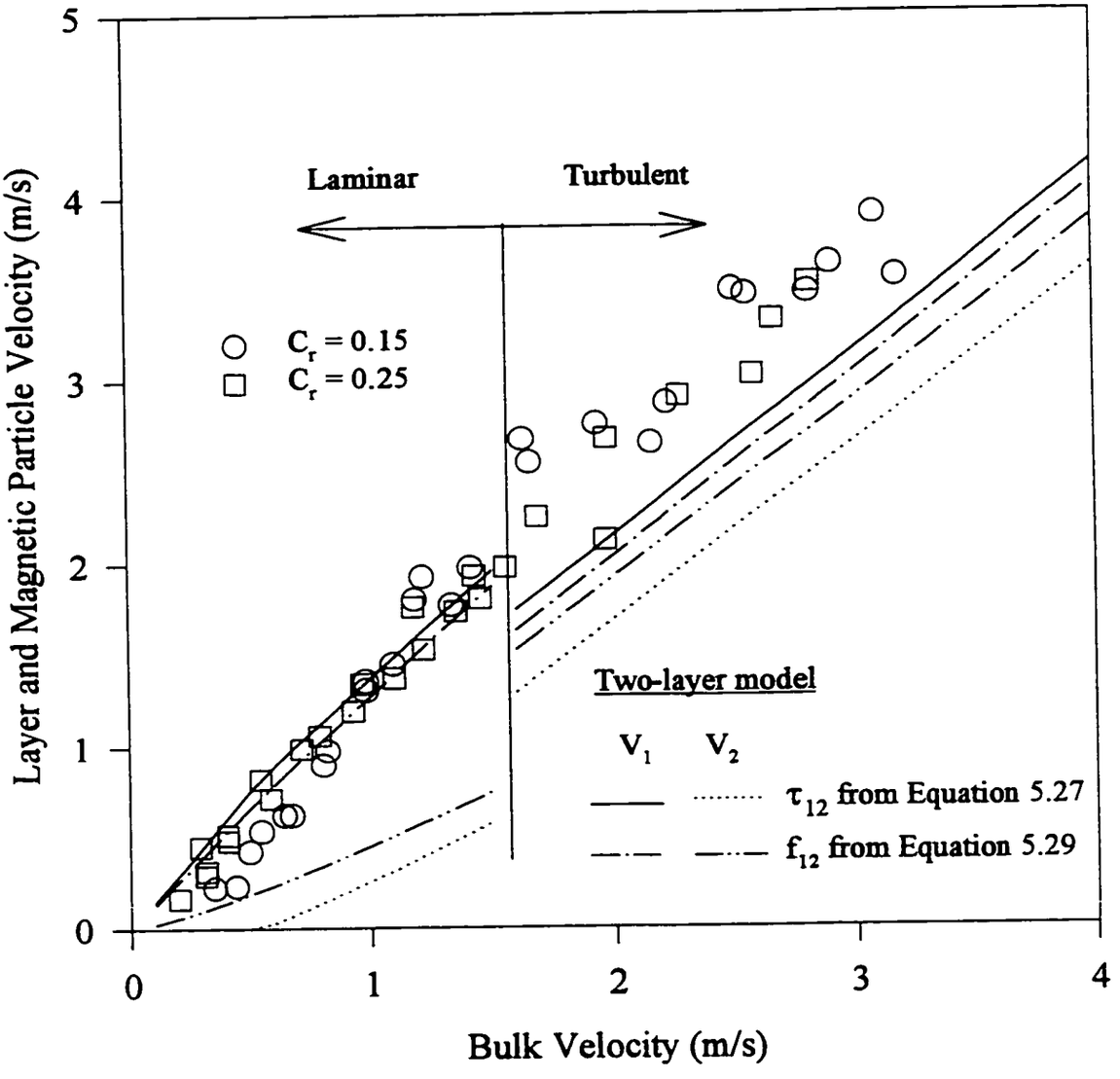

Figure 5.15 : Magnetic particle velocities and layer velocity predictions for different interfacial friction formulations.

predicted upper layer velocities in turbulent flow. This discrepancy could be interpreted as meaning that the interfacial friction factor is overpredicted by these methods. Alternatively, the magnetic particle velocities may not be representative of the velocity at the interface in these carrier fluids.

It is seen that the difference between the layer velocities can be much larger in laminar flow than in turbulent flow. In turbulent flow, where the difference between layer velocities is observed to be small, the use of the upper layer fluid friction factor to determine the lower layer fluid shear stress (Equation A.16) is probably warranted. The same would not be true in the laminar flow regime since the layer velocities are quite different and the fluid friction factor would be sensitive to these differences.

In comparing the layer velocities predicted with the two methods, it is seen that using Equation 5.29 gives less difference between layer velocities as a result of high friction at the interface. This increased friction also leads to the prediction that the lower layer velocity does not go to zero until the bulk velocity is very low.

The friction at the interface which is predicted by the two methods can be compared directly if Equation 5.29 is expressing it in terms of the shear stress at the interface. Using the interfacial friction factor of Shook (Equation 2.36b), evaluated for an interface located at the midpoint of the pipe, the shear stress at that interface (Equation A.13) and Equation 5.29 gives the relation

$$\tau'_{12} = \frac{f_{12}(V_1 - V_2)\,|V_1 - V_2|\,\rho_1}{2} + \frac{\tau_y}{2}\left[16.578 - 34.8165\,\frac{V_2}{V_1} + 18.2385\left(\frac{V_2}{V_1}\right)^2\right] \qquad (5.30)$$

where τ'_{12} is the shear stress evaluated at the interface with Equation 5.29. The velocity dependence of the yield stress term in Equation 5.30 would seem reasonable given the change in effective viscosity with shear rate for a Bingham fluid. When the two layer velocities are similar, the bracketed term of Equation 5.30 approaches zero and no yield stress contribution is predicted. This would seem to be an acceptable limiting condition.

When deposition occurs and the lower layer velocity is zero, the second term of Equation 5.30 becomes $8.289\tau_y$. This is substantially larger than the yield stress contribution predicted by Equation 5.27 ($1.333\tau_y$) which, when combined with the shear stress on the upper pipe wall (Equation 5.26), roughly corresponds to flow through a partially blocked pipe. This suggests that interfacial friction may be overpredicted by Equation 5.29 when flow is near deposition.

5.4 Two-layer model simulations

A number of pressure gradient predictions have been made to examine the effectiveness of the model as it is presented here. Newtonian and non-Newtonian carrier fluid slurry predictions were made in laminar and turbulent flow. The simulations were performed for conditions in which experimental evidence existed for comparison. Experimental conditions which are to be modelled are listed in Table 5.2.

The two-layer model parameters used for modelling are listed in Table 5.3. Values for the contact load component for turbulent flow of slurries containing glass spheres were specified by the values used in section 4.2.1 for water slurries. Other turbulent flow contact load fractions were calculated using Equation A.6. In laminar flow, the contact load fraction was specified to be 1.0 in all cases.

Table 5.2 : Experimental test conditions simulated with two-layer model.

Case Number	Fluid	Fluid Model	Solid	Particle Size (mm)	In-situ Conc.	Pipe Diameter (mm)
1	glycol	Newtonian	sand	0.43	0.20	53
2	oil	Newtonian	sand	0.43	0.20	53
3	Kaolin/ Bentonite	Bingham	glass spheres	1.7	0.15	53
4	Kaolin/ Bentonite	Bingham	glass spheres	1.7	0.25	53
5	Kaolin/ Bentonite	Bingham	glass spheres	4.4	0.15	53
6	Kaolin/ Bentonite	Bingham (large τ_y)	glass spheres	4.4	0.15	53
7	Kaolin/ Bentonite	Bingham	gravel	4.1	0.15	53
8	tailings*	Bingham	gravel	1.9	0.23	263
9	tailings*	Bingham	rock	55	0.09, 0.16	263
* oil sand process tailings						

The lower layer concentrations, C_{lim}, for slurries with glycol, oil and Kaolin/Bentonite carrier fluids were inferred from concentration profile measurements. The lower layer concentration was calculated with Equation A.7 for slurries with the oil sand tailings carrier fluid. In these cases, the maximum concentration was specified to be 0.58

from their maximum packing concentration.

Table 5.3 : Two-layer model parameter specifications.

Case Number	Slurry	Turbulent C_c	C_{lim}	C_{max}	η_s	f_{12} Modifications
1	glycol/ sand	Equation A.6	0.58	-	0.45	none
2	oil/sand	-	0.58	-	0.45	none
3	Kaolin/ glass	0.92	0.45	-	0.45	Equations 5.27, 5.29
4	Kaolin/ glass	0.92	0.45	-	0.45	Equations 5.27, 5.29
5	Kaolin/ glass	0.96	0.45	-	0.45	Equations 5.27, 5.29
6	Kaolin/ glass	0.96	0.45	-	0.45	Equations 5.27, 5.29
7	Kaolin/ gravel	0.96	0.45	-	0.45	Equations 5.27, 5.29
8	tailings*/ gravel	Equation A.6	Equation A.7	0.58	0.45	Equations 5.27, 5.29
9	tailings*/ rock	Equation A.6	Equation A.7	0.58	0.40	Equation 5.27
* oil sand process tailings						

The coefficient of sliding friction, η_s for each solids type was inferred from

measurements obtained with a water carrier fluid.

For each case simulated, the interfacial friction factor was initially calculated for a Newtonian carrier fluid. The interfacial friction factor in the laminar flow regime was calculated by Equation 2.36b. When flow was turbulent, the interfacial friction was calculated using Equation A.14. With the Bingham carrier fluids, the Newtonian friction factors were modified to account for the yield stress in the two ways described in section 5.3.3 for comparison. The first method was to increase the interfacial stress following Equation 5.27. This applies only to the laminar flow regime and in turbulent flow, no correction is made with this method. The second method was to use Equation 5.29 to increase the interfacial friction factor in both the laminar and turbulent flow regimes.

5.4.1 Glycol and sand slurry predictions

The experimental results simulated here were for a sand-glycol slurry which were reported by Gillies et al. (1993). These results were also considered earlier in assessing the finite element model in section 5.2.1. The slurry contained 20% 0.43 mm sand in ethylene glycol at 6 °C and was tested in a 53 mm diameter pipeloop. At this temperature, the glycol viscosity was measured to be 46 mPa.s so that flow was laminar throughout the velocity range. Concentration distribution measurements and visual observations indicated that concentrations in the lower layer were always high.

The measured pressure gradients and results from the two-layer model are shown in Figure 5.16. At the lowest velocities, where a bed was known to exist, flow takes place through a partially obstructed pipe. The model predictions are nearly those which would be calculated for laminar flow through a pipe with the hydraulic equivalent diameter of the

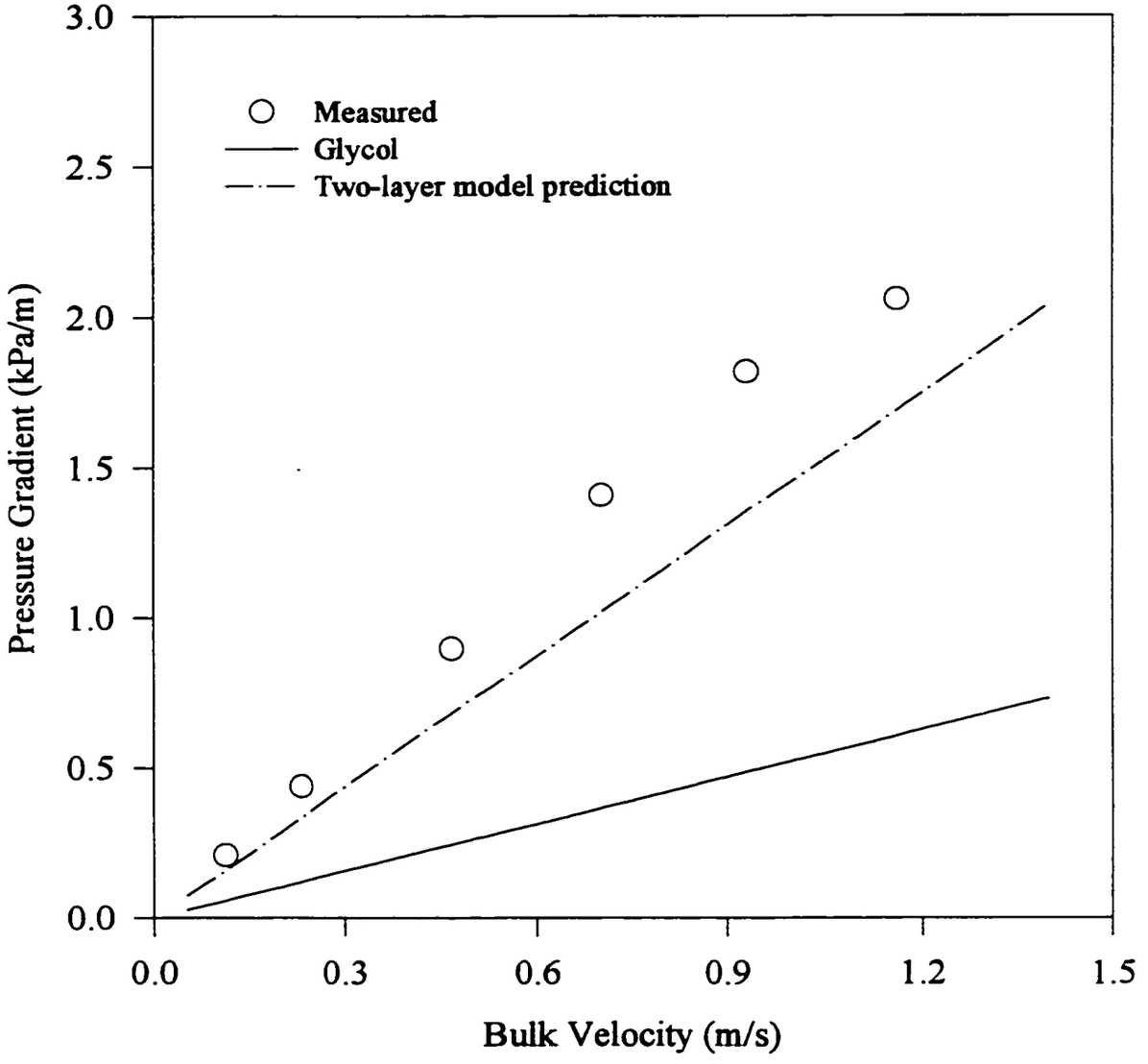

Figure 5.16 : Two-layer model pressure gradient predictions for an ethylene glycol and 20% 0.43 mm sand slurry.

upper layer. The two-layer model underpredicts the pressure gradients throughout the velocity range, possibly because of the use of the hydraulic equivalent diameter.

The pressure gradient predictions for flow through the partially obstructed pipe, and more specifically the impelling force on the lower layer at the interface, are not high enough to overcome the Coulombic friction which opposes motion of the particle bed. In fact, significant particle transport was observed for this slurry at a bulk velocity of 0.7 m/s.

5.4.2 Oil and sand slurry predictions

The model predicted pressure gradients for an oil and sand slurry in a 53 mm diameter pipeloop are compared to the observed behaviour in Figure 5.17. The sand had a median diameter of 0.43 mm and an in-situ concentration of 0.20. The oil was Newtonian and had a viscosity of 1440 mPa.s. The experimental results have been reported previously (Gillies et al., 1994) and were also considered with the finite element simulations.

At velocities below 0.05 m/s, where a stationary bed was known to exist, the model predictions agreed well with the observed pressure gradients. The model predicted that the bed became mobile at a velocity of 0.07 m/s. At higher velocities, where significant particle transport occurred, the pressure gradients predicted by the model were below the observed values.

At a bulk velocity of 0.11 m/s, the model predicts a delivered concentration of 0.045. The measured delivered concentration was 0.146 at this velocity. At a bulk velocity of 0.06 m/s, the model predicted that the particles were stationary in contrast to the measured delivered concentration of 0.086.

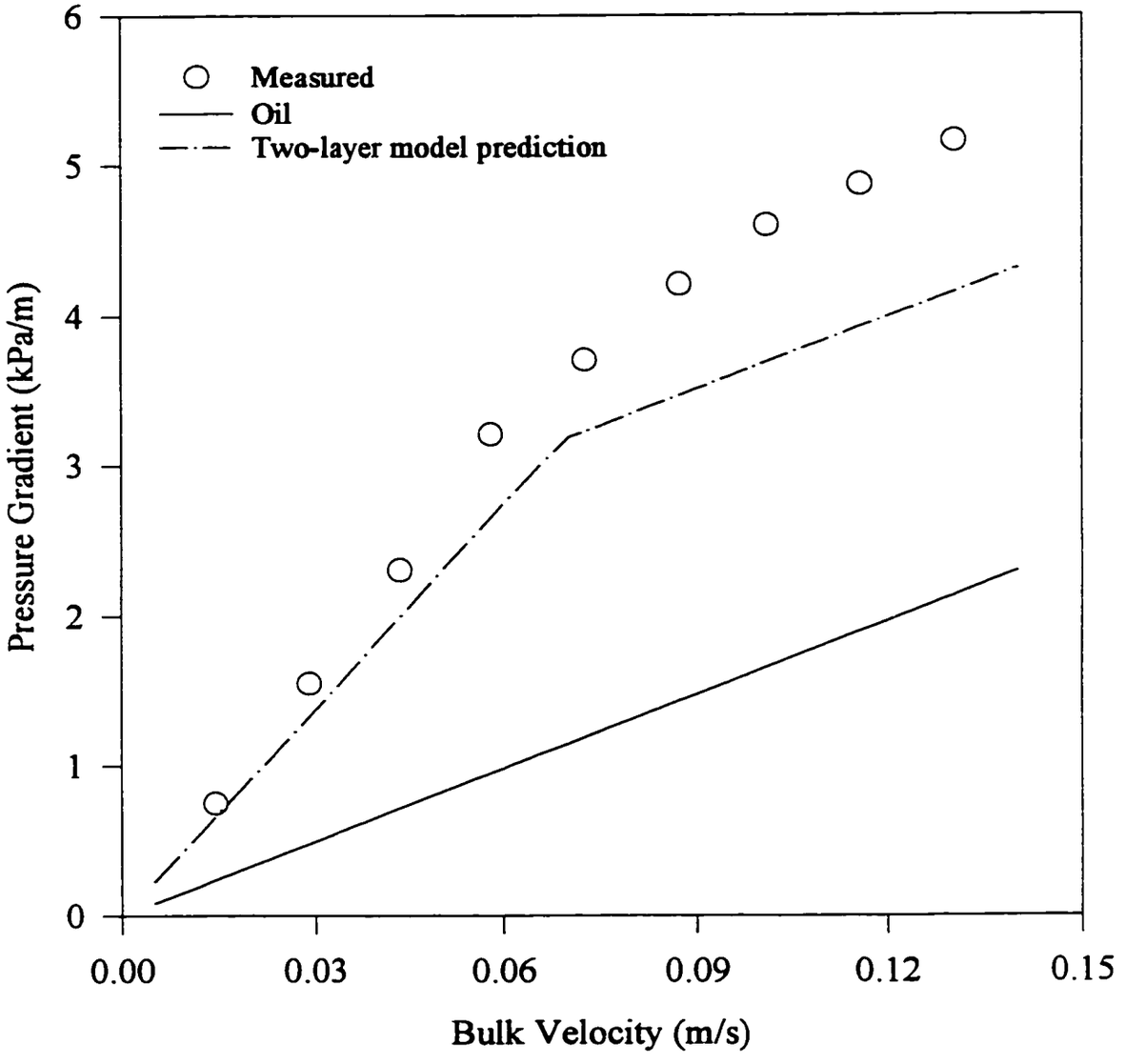

Figure 5.17 : Two-layer model pressure gradient predictions for an oil and 20% 0.43mm sand slurry.

5.4.3 Kaolin/Bentonite slurry predictions

Two-layer model pressure gradient predictions for glass sphere and gravel slurries with Kaolin/Bentonite carrier fluids are compared to experimental results. Figure 5.18 shows the pressure gradients for a slurry containing 1.7 mm glass spheres at an in-situ concentration of 0.15. The two methods for representing friction for a Bingham fluid at the hypothetical interface show negligible difference above deposition. Equation 5.29 predicts that the deposit velocity is below 0.05 m/s while Equation 5.27 predicts a stationary deposit at 0.25 m/s. In the experiment with this slurry, the particles were observed to move with a very slowly sliding bed between bulk velocities of 0.2 and 0.5 m/s.

A discontinuity exists in the predicted pressure gradients at the laminar to turbulent transition. This is due largely to the abrupt change in the calculated fluid friction which occurs at the transition. Figure 5.15 showed the change in the predicted layer velocities at the transition and this also contributes to the discontinuity. In this simulation, there is also a step in the contact load fraction from 1.0 in laminar flow to the specified value of 0.92 in turbulent flow.

These model predictions are in reasonable agreement with observed pressure gradients. At high velocities in laminar flow, the observed pressure gradients are greater than those predicted. When the flow is turbulent, the observed pressure gradients appear to approach the predicted pressure gradients as the bulk velocity increases.

The two-layer model predictions for the 1.7 mm glass spheres at an in-situ concentration of 0.25 are shown in Figure 5.19. With this slurry, the predictions with the two interfacial friction methods nearly coincide at all velocities above deposition. Below

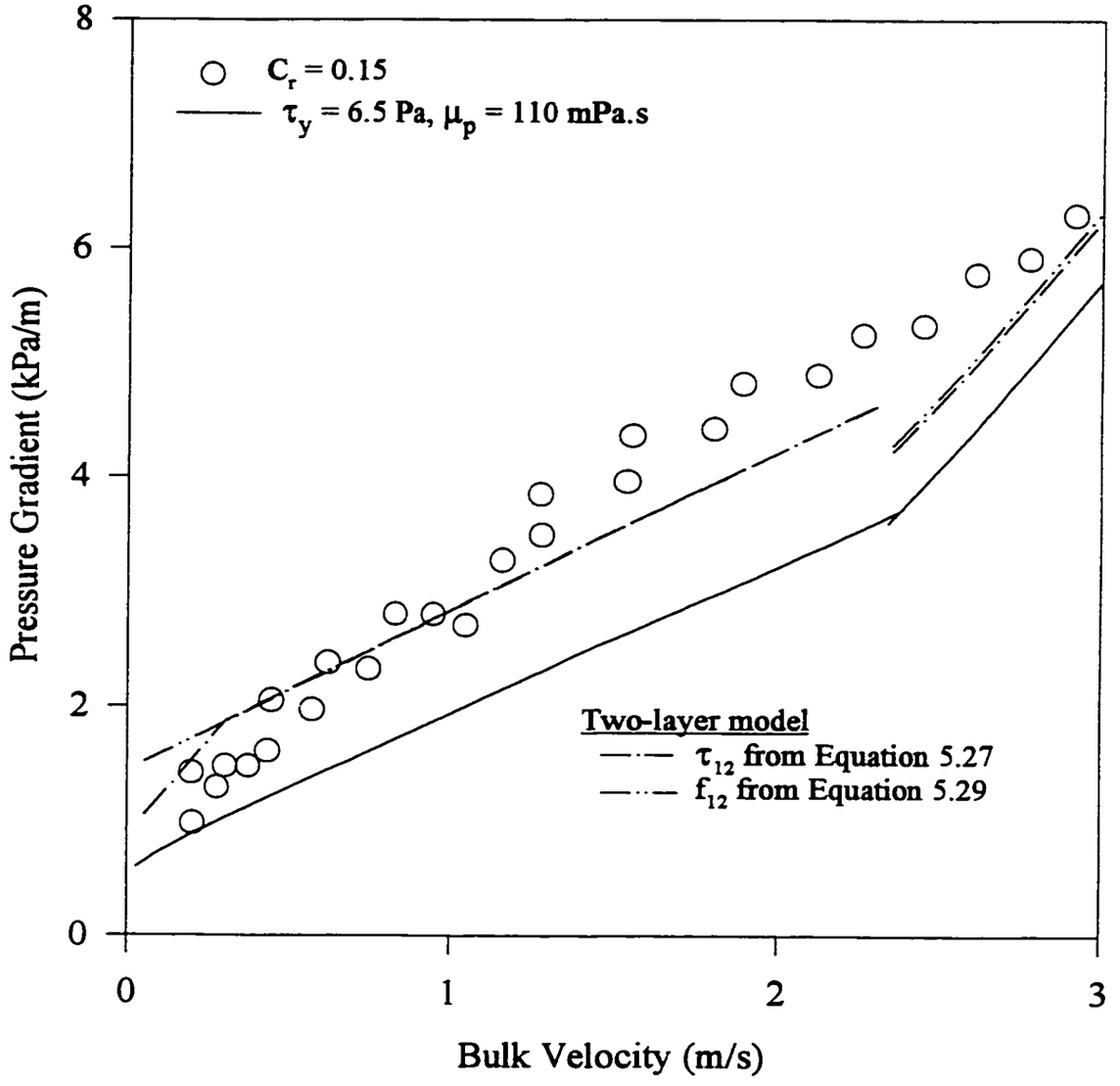

Figure 5.18 : Two-layer model pressure gradient predictions for 15% 1.7 mm spheres in a Kaolin/Bentonite suspension.

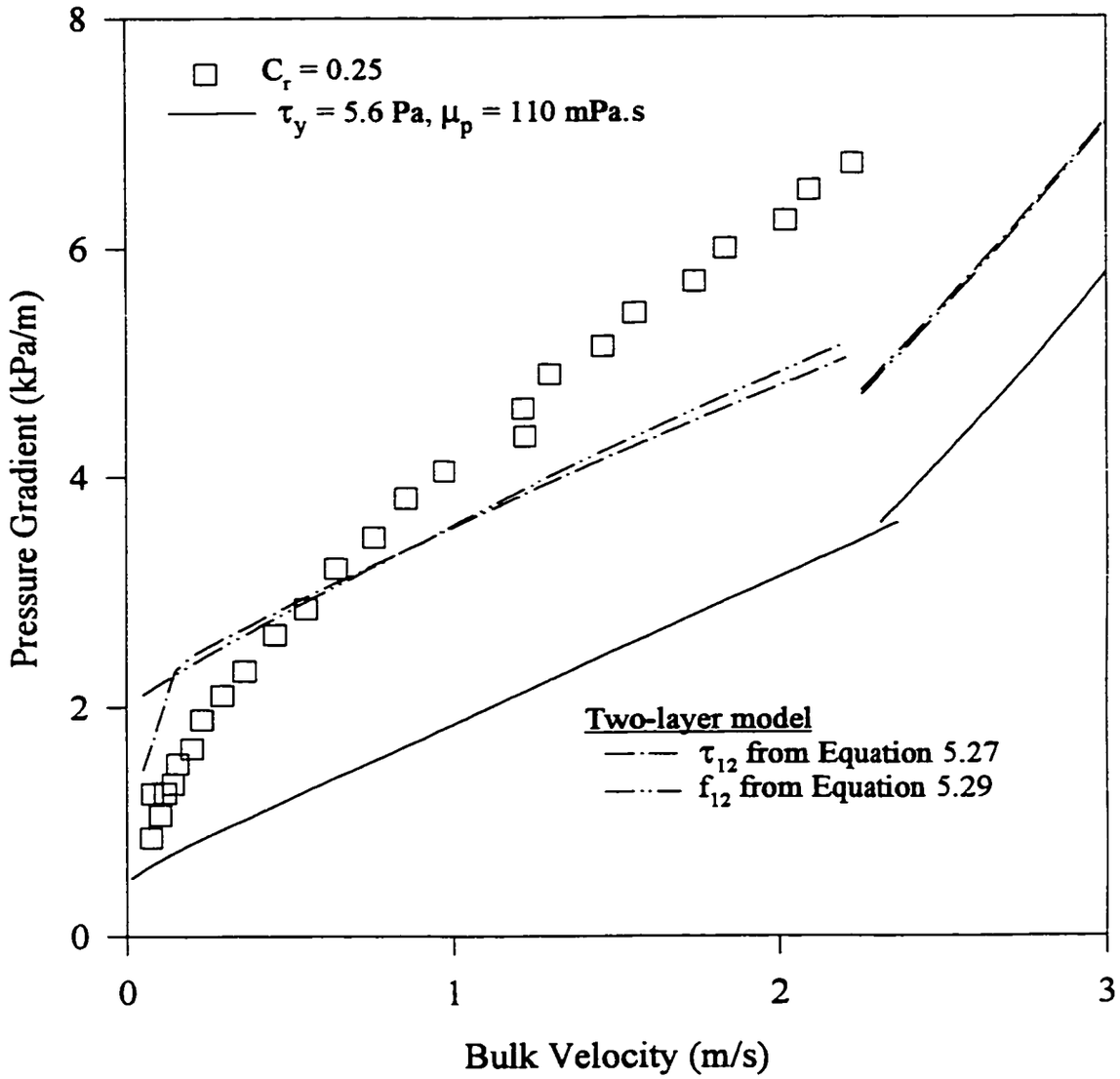

Figure 5.19 : Two-layer model pressure gradient predictions for 25% 1.7 mm spheres in a Kaolin/Bentonite suspension.

deposition, the predicted pressure gradients were higher than the observed values. Above deposition, the models underpredicted the pressure gradient. The observed pressure gradient is seen to increase at a greater rate with bulk velocity than the two-layer model predictions.

Predictions for a Kaolin/Bentonite slurry with 4.4 mm glass spheres at a concentration of 0.15 are shown in Figure 5.20. The observed pressure gradients are always higher than the predicted values at velocities above deposition. The difference between observed and predicted values is substantial at high laminar velocities. At high turbulent velocities, the observed values begin to approach the predicted pressure gradients. It is recalled that pressure gradients were also observed to be high for this particle and pipe size combination with water as a carrier fluid (section 4.2).

With this slurry, a very slowly sliding bed was observed at a bulk velocity of 0.34 m/s. Using Equation 5.27 to determine the interfacial shear stress, a deposition velocity of 0.5 m/s was predicted. The interfacial friction factor evaluated with Equation 5.29 predicted the deposit velocity to be below 0.1 m/s.

The next test condition used a Kaolin/Bentonite suspension with a high yield stress to provide the carrier fluid for 4.4 mm spheres at a concentration of 0.15. The observed and two-layer model predictions for this slurry are shown in Figure 5.21. The predicted pressure gradients are higher than the observed values at low velocities but agree well at higher velocities. There was some uncertainty in the Bingham model parameters with this carrier fluid which may account for some of the difference. The deposition velocity was observed to be 0.36 m/s with this slurry. The predicted deposit velocity was 0.4 m/s when obtained with the interfacial shear stress evaluated from Equation 5.27. Using the interfacial friction

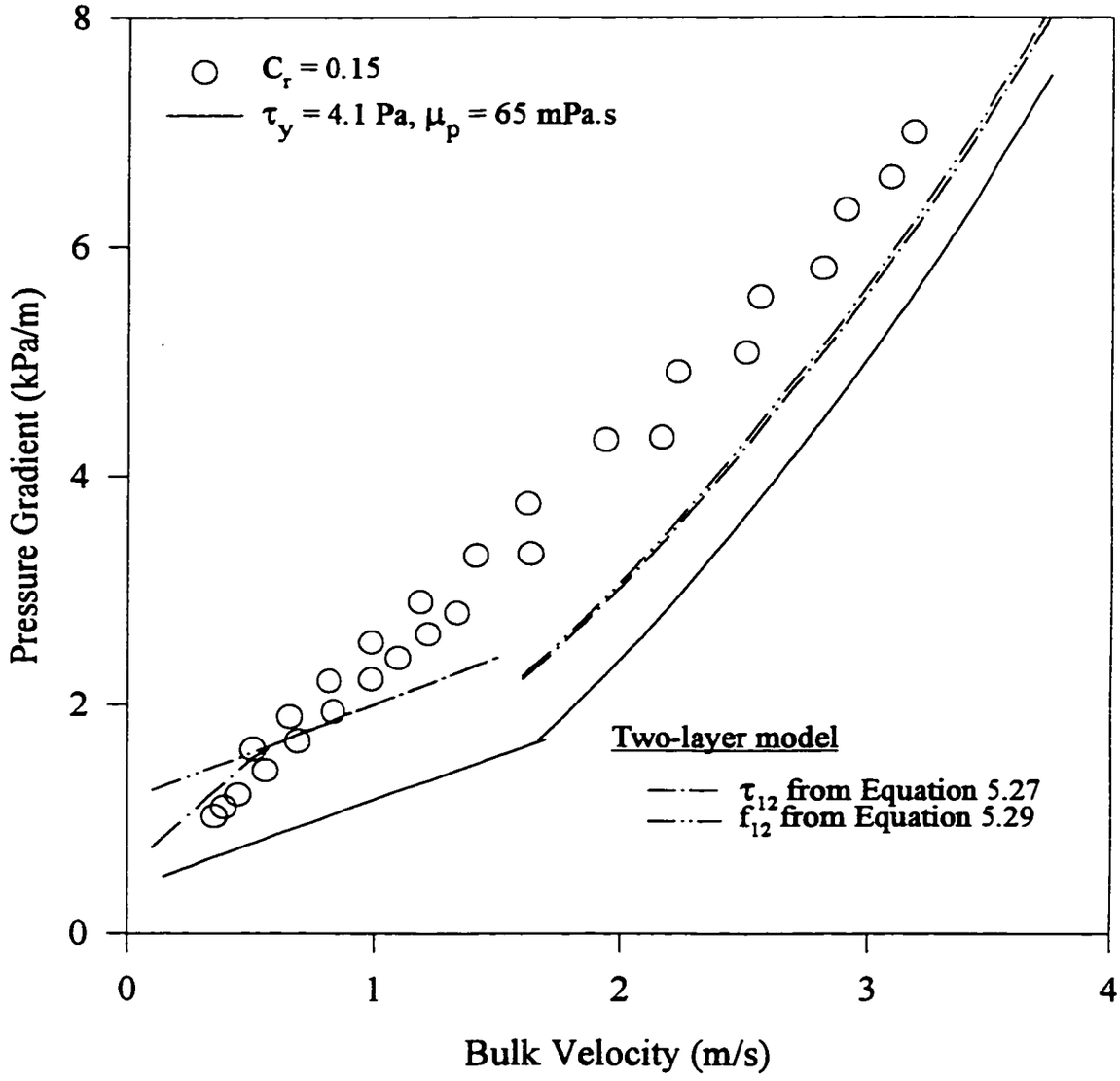

Figure 5.20 : Two-layer model pressure gradient predictions for 15% 4.4 mm spheres in a Kaolin/Bentonite suspension with a low yield stress.

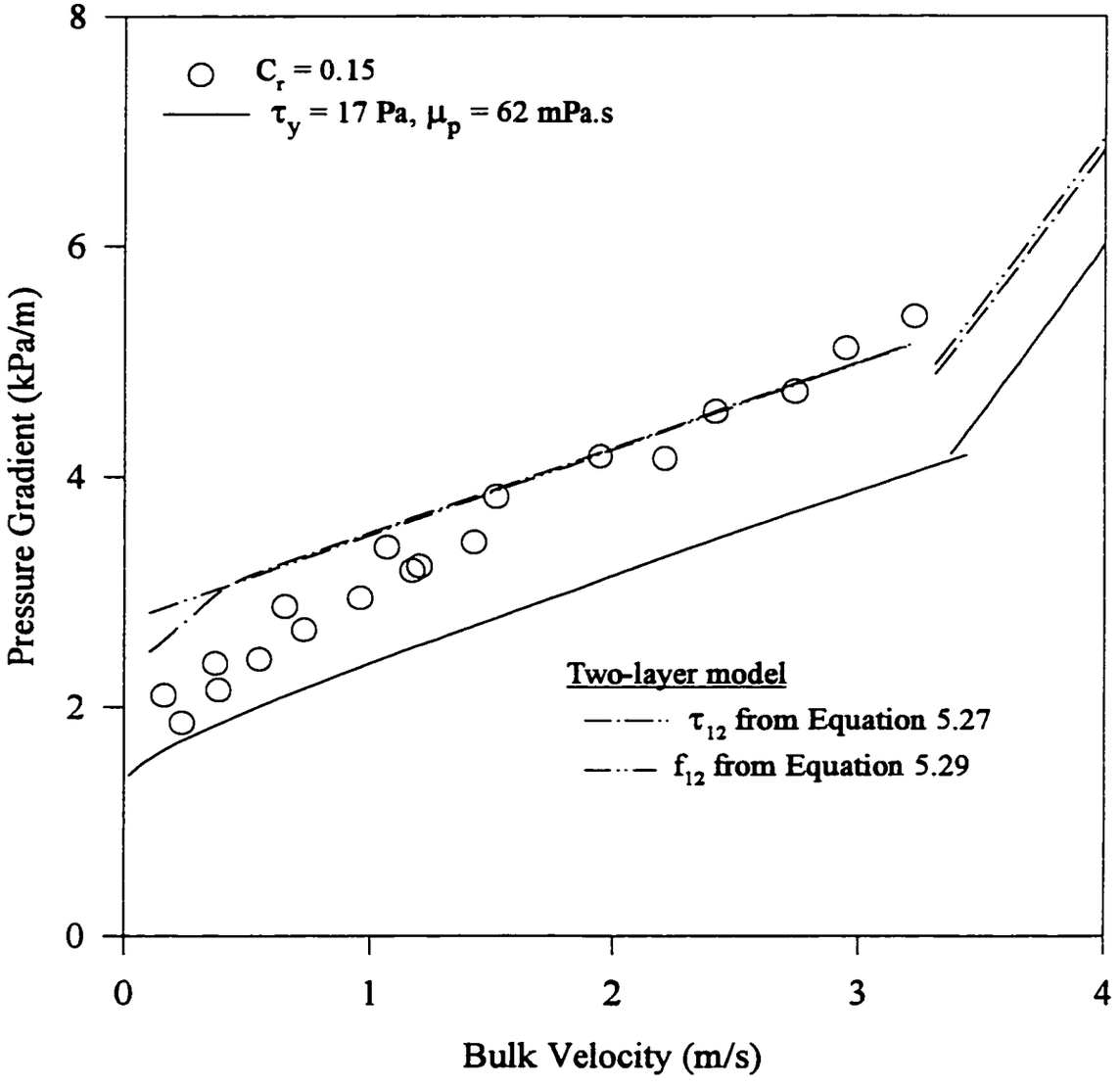

Figure 5.21 : Two-layer model pressure gradient predictions for 15% 4.4 mm spheres in a Kaolin/Bentonite suspension with a high yield stress.

factor from Equation 5.29, the deposit velocity was predicted to be below 0.1 m/s.

Figure 5.22 shows the measured and predicted pressure gradients for a slurry of 4.1 mm gravel in a Kaolin/Bentonite suspension. The coarse particle concentration is 0.15. The observed pressure gradients are higher than the predicted values at all velocities above deposition. As in previous cases, the pressure gradient is observed to increase at a higher rate for an increase in velocity than the two-layer model predictions suggest. At the highest velocities where flow is turbulent, the observed pressure gradient appears to be approaching the predicted values.

With this slurry, a stationary deposit was observed at a bulk velocity of 0.26 m/s. Equation 5.27 predicted a deposit velocity of 0.4 m/s and Equation 5.29 predicted it to be below 0.05 m/s.

5.4.4 Oil sand overburden slurries

Slurries using oil sand overburden as a carrier fluid are considered since this carrier is observed to follow the Bingham fluid model well and experimental data was available for a larger pipe diameter (263 mm). The carrier was an aqueous suspension of fine clays, silicates and dispersed oil droplets. The simulations are based on experimental results taken from two investigations which were reported by Gillies et al. (1992) and Gillies (1993). The first experiments used the fine tailings to transport 1.9 mm gravel and the second to transport 55 mm rock. Two-layer model predictions for these particles transported by water agreed well with the experimental pressure gradients measured in the tests.

The pressure gradients observed and predicted by the two-layer model for 1.9 mm gravel in the fine tailings mixture with a coarse solids concentration of 0.23 are shown in

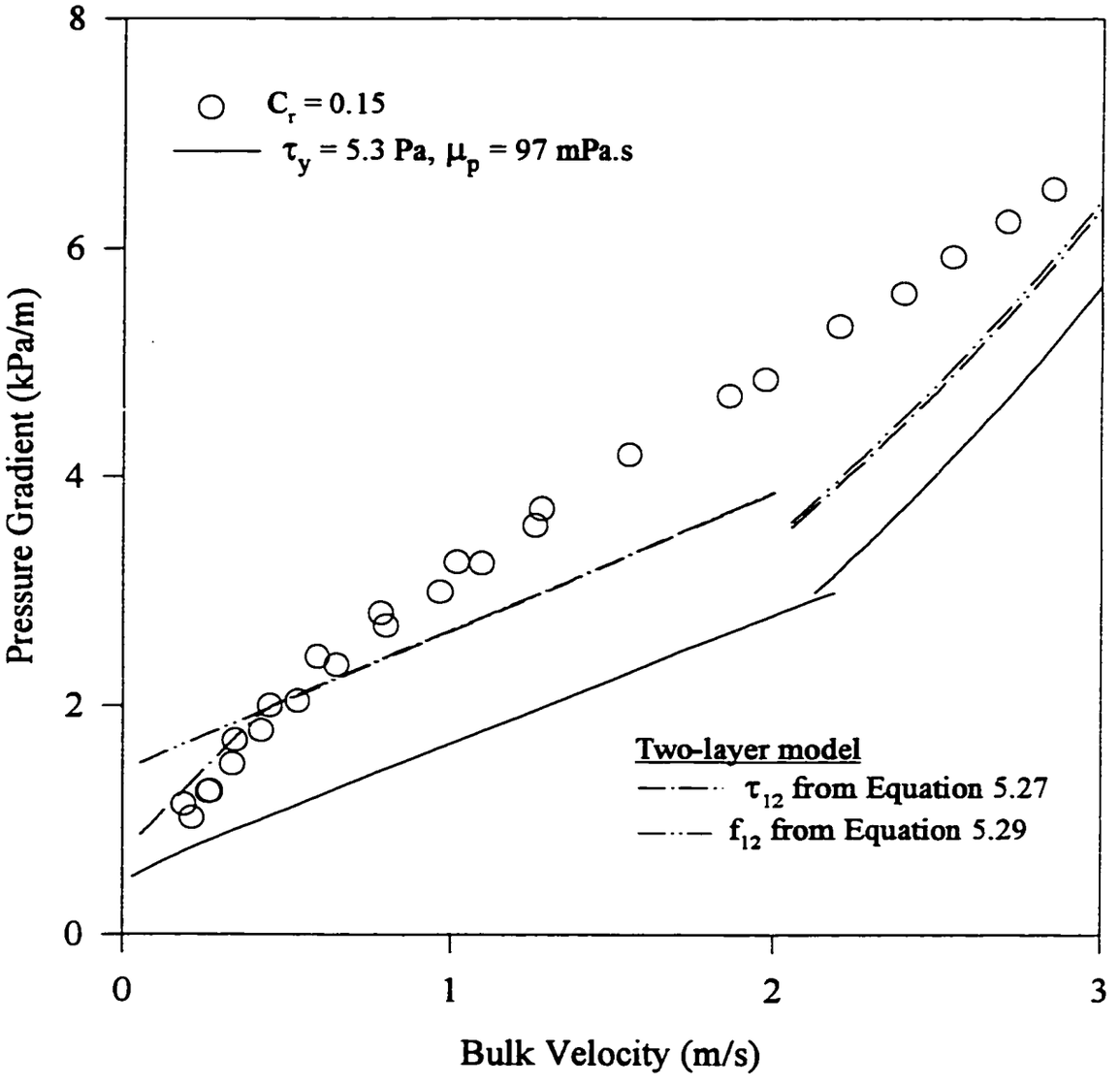

Figure 5.22 : Two-layer model pressure gradient predictions for 15% 4.1 mm gravel in a Kaolin/Bentonite suspension.

Figure 5.23. A stationary bed probably existed throughout the laminar flow regime. The two-layer model predictions using the two interfacial friction methods predict this behaviour. The large difference in the predicted pressure gradients obtained with the two methods in laminar flow is the result of the high fluid yield stress and the difference in the effect this yield stress has on the calculated friction at the stationary interface. The pressure gradient predicted using the modified friction factor (Equation 5.29) is clearly not appropriate with the stationary bed here.

According to the model, solids transport begins when the flow becomes turbulent. Significant particle degradation was known to occur in this slurry which may explain the difference between the observed and predicted pressure gradients in this region. Using 1.5 mm as the median size for the gravel gave good agreement between the predicted and observed pressure gradients in turbulent flow.

The second case considered with the fine tailings had 55 mm rocks making up the coarse solids component of the slurry at concentrations of 0.09 and 0.16. The observed pressure gradients and model predictions are shown in Figure 5.24. Below 2.0 m/s where flows were laminar, the pressure gradients predicted for flows above stationary beds were below those required for incipient motion (Equation A.17). Therefore, stationary beds are predicted for the two concentrations when flow is laminar. The two-layer model pressure gradient predictions were quite low in laminar flow when Equation 5.27 was used to determine the shear stress at the interface as shown in the figure. In turbulent flow, the two-layer model predictions parallel the observed pressure gradients but underpredict the high concentration case slightly. The ratio of the particle diameter to the pipe diameter is large

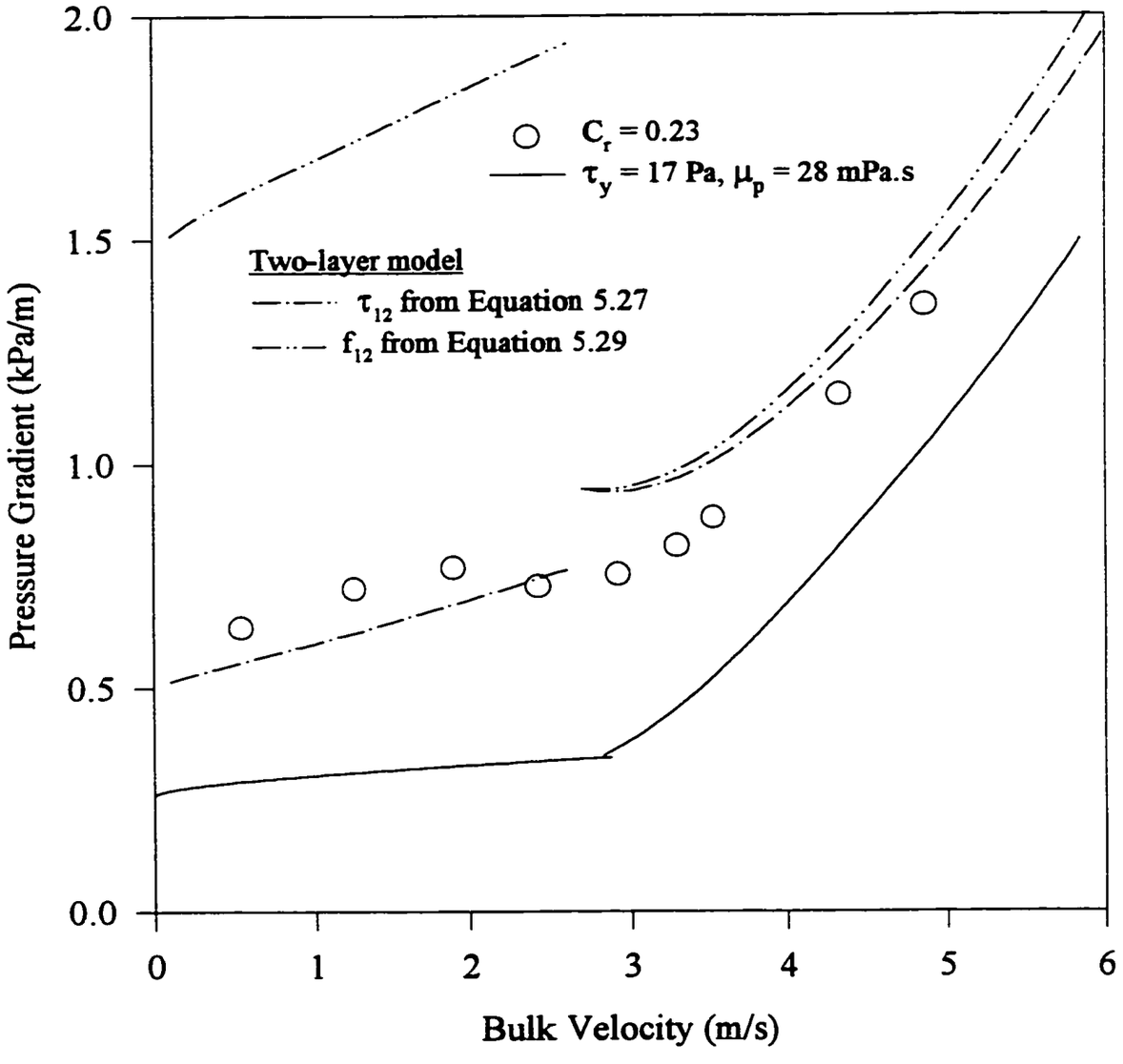

Figure 5.23 : Two-layer model pressure gradient predictions for 1.9 mm gravel and oil sand overburden in a 263 mm diameter pipe.

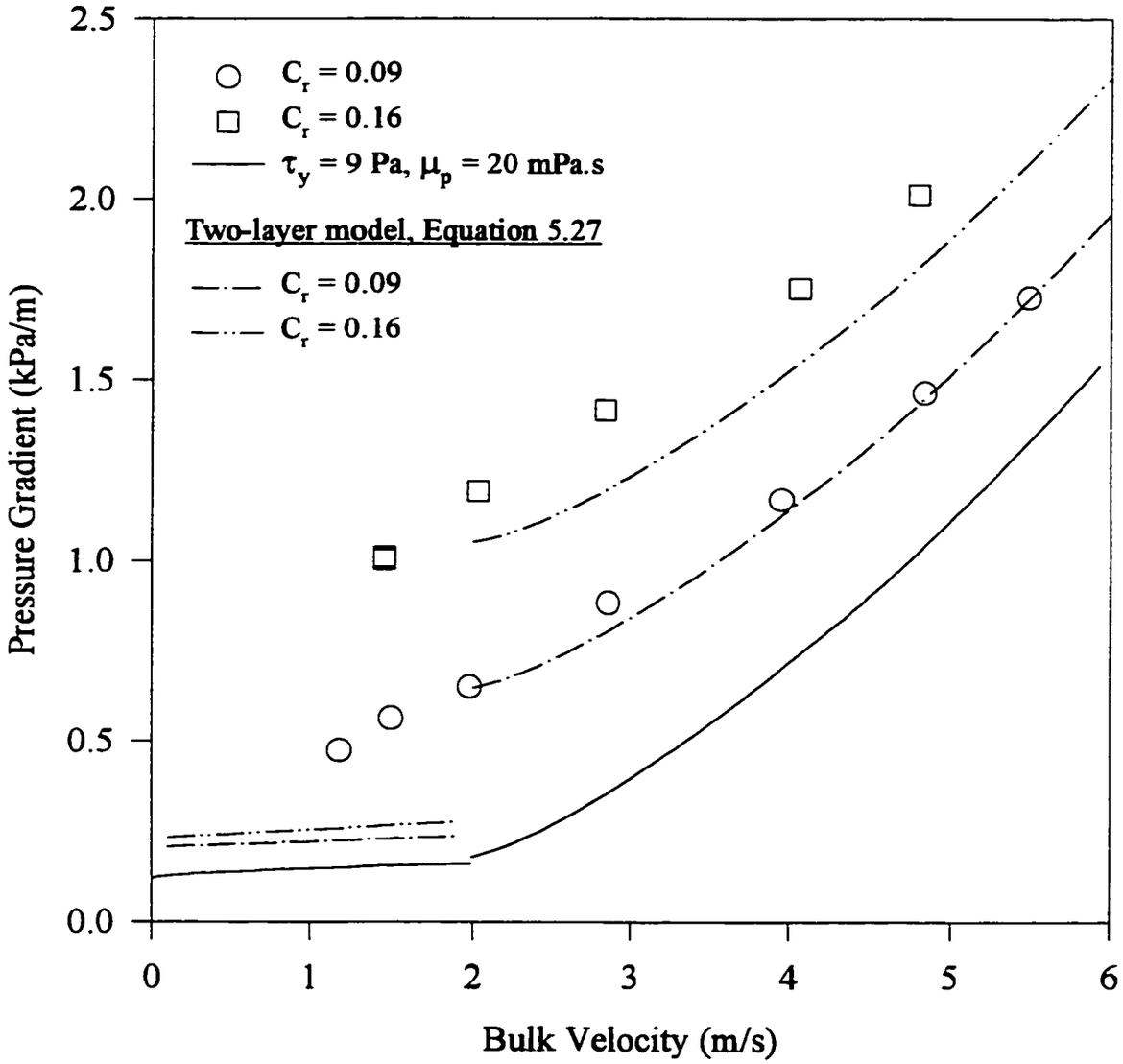

Figure 5.24 : **Two-layer model pressure gradient predictions for 55 mm rock and oil sand overburden in a 263 mm diameter pipe.**

here (d/D = 0.21) as it was with the 4.4 mm spheres in the small diameter pipe (d/D = 0.08) where high pressure gradients were also observed.

5.4.5 Summary

The two-layer model is capable of representing the different flow regimes which occur in slurry flow, from a stationary bed through laminar and turbulent flow. Turbulent flow of slurries can be described quite well with the two-layer model when the carrier fluid is Newtonian. The effect of a Bingham carrier fluid on flow in this regime is not completely understood but it appears that pressure gradient predictions can be calculated with fluid friction factors inferred from a turbulent flow equation for a Bingham fluid such as Equation 2.11.

In laminar flow, the layer velocities, and the corresponding fluid friction factors, can be quite different so that the fluid friction needs to be evaluated for each layer separately. With a Bingham carrier fluid, the yield stress needs to be incorporated in the fluid friction. Equations 5.26 to 5.28 seem to be reasonable in accounting for the yield stress. Pressure gradients with the slurries examined here were observed to increase at a greater rate with bulk velocity than those predicted by the two-layer model. Pressure gradients in excess of the combined fluid friction and solids Coulombic friction were observed.

At the transition from laminar to turbulent flow, discontinuities in the pressure gradient predictions with the present model can occur because of abrupt changes in the fluid friction, layer velocities and solids distribution between layers. Pressure gradients are observed to be higher than predicted in the transition region but approach the two-layer model predictions at higher velocities. This has the appearance of an extended transition

region with the high pressure gradients observed in the laminar flow region continuing into the transition region. The two-layer model does not consider such behaviour.

Settling velocities of particles may be reduced in a fluid with a yield stress, but use of this reduced settling velocity in the contact load and lower layer concentration correlations used here (Equations A.6 and A.7) for turbulent flow does not appear to be appropriate. Use of the plastic viscosity in the correlations seems more reasonable.

Whether a fluid yield stress increases the interfacial friction and therefore reduces the difference in the layer velocities could not be confirmed since delivered concentrations were not available. The pressure gradient predictions are found to be rather insensitive to this interfacial friction in turbulent flow and in laminar flow above the deposition velocity. Differences in the formulation of the interfacial friction factor affect the prediction of the deposition velocity and the delivered concentration.

6 CONCLUSIONS AND RECOMMENDATIONS

6.1 Conclusions

The maximum concentration measured near the bottom of the pipe for stratified slurries of glass spheres in water showed a particle size dependence. The larger particles were slightly less stratified despite their higher settling velocity. The concentration profiles for the two particle sizes did not change significantly with increasing velocity.

Water slurries with 4.4 mm spheres produced unexpectedly high friction losses in a 53 mm pipe which were later confirmed by a second set of tests. The additional loss appears to be velocity dependent. Concentration profiles did not suggest any physical reason for the increase.

In-situ concentration and bulk velocity dominate the concentration profiles for slurries with moderately viscous carrier fluids which follow the Bingham model. Changes in particle and fluid properties are of secondary importance.

Fluid yield stresses at, and slightly above, the theoretical value required to support particles in a stationary fluid do not contribute significantly to particle suspension in horizontal laminar flow. Particles were observed to flow in a stratified layer near the bottom of the pipe.

Friction losses for slurries in laminar flow exceed the sum of the fluid flow losses and the particle sliding friction losses. The increased friction appears to be viscous in nature

since it is velocity dependent.

Particle velocities at the fluid/bed interface for stratified slurry flow appear to increase linearly with bulk velocity at velocities above deposition.

Particle velocities at the bottom of the pipe appear to increase in a quadratic fashion with bulk velocity. This relationship is only slightly sensitive to bulk concentration and is insensitive to fluid properties. Particle size appears to be very important for this phenomenon.

The velocity gradient in a stratified layer of uniform concentration appears to be nearly linear. The velocity gradient increases with decreasing local particle concentration.

A finite element program which treats a slurry as a pseudohomogeneous fluid is capable of predicting the pressure gradient and velocity profile in a pipe for Newtonian and Bingham fluids in laminar flow. The local particle concentration is used to modify the local element viscosity by a relative viscosity function. For non-Newtonian fluids which can be represented by the Bingham model, the relative viscosity function is used to modify the shear component of the Bingham model. The agreement with experimental data is best with viscous carrier fluids.

A dispersive viscosity function based on interparticle contact and the local shear rate can be used to predict the distribution of solids in laminar slurry pipe flow. The results are satisfactory for highly viscous flow but particle dispersion is under predicted with less viscous fluids. An additional mechanism which contributes to an increased particle dispersion and higher friction losses may explain the discrepancies between the velocity and concentration predictions and the observed pipe flow behaviour.

A two-layer model gives satisfactory predictions for slurries with Bingham carrier fluids in turbulent flow. The fluid friction in this model takes the non-Newtonian nature of the fluid into account. The contact load fraction and lower layer concentration are calculated using existing correlations and the ratio of the bulk velocity to the particle settling velocity. For Bingham carrier fluids, settling velocities are calculated using equations which describe settling in Newtonian fluids. The Bingham plastic viscosity is used in place of the Newtonian viscosity in these equations.

The two-layer model appears to work reasonably well in laminar flow. Pressure gradients are underpredicted and indicate additional friction losses beyond simple fluid and Coulombic friction. At present the descriptions of the lower layer concentrations and contact load components in this model are incomplete for laminar flow.

Increased interfacial friction factors which were inferred from reduced particle settling in Bingham fluids seem inappropriate in the two-layer model. They produce only a small effect in turbulent flow and appear to overpredict the friction in laminar flow and near deposition.

6.2 Recommendation

This investigation has shown that slurry transport at high (d/D) values gives pressure gradients which are higher than expected. The mechanism of this increase should be investigated as the occurrence of large particles in industrial slurries becomes more prevalent.

The use of a dispersive viscosity concept to calculate the solids distribution in the pipe in laminar flow seems promising. It would be desirable to obtain more velocity

distribution measurements and to investigate the lateral variation of solids concentration.

Use of the two-layer model with laminar flow requires a systematic investigation into the factors influencing interfacial friction and the lower layer concentration so that they can be described more adequately.

REFERENCES

Ansley, R.W. and Smith, T.N., "Motion of spherical particles in a Bingham plastic", AIChE J., **13**(6): 1193-1196, 1967.

Atapattu, D.D., Chhabra, R.P., and Uhlherr, P.H.T., "Particle drag and equilibrium in viscoplastic fluids", Proc. Intl. Symp. on Transportation of Coal and Other Minerals, Indian Institute of Metals, Bhubaneswar, India, pp. 253-260, 1988.

Bagnold, R.A., "Experiments on a gravity-free dispersion of large solid spheres in a Newtonian fluid under shear", Proc. Roy. Soc., Ser. A **225**: 49-63, 1954.

Beris, A.N., Tsamopoulos, J.A., Armstrong, R.C., and Brown, R.A., "Creeping motion of a sphere through a Bingham plastic", J. Fluid Mech., **158**: 219-244, 1985.

Bird, R.B., Stewart, W.E., and Lightfoot, E.N., *Transport Phenomena*, Wiley, New York, 1960.

Chen, S.S., Fan, L.T., and Hwang, C.L., "Entrance region flow of the Bingham fluid in a circular pipe", AIChE J. **16**(9): 293-299, 1970.

Churchill, S.W., "Friction factor equation spans all fluid flow regimes", Chem. Eng., **84** (24): 91, 1977.

Dedegil, M.Y., "Drag coefficient and settling velocity of particles in non-Newtonian suspensions", Intl. Symp. on Slurry Flows, ASME Vol. FED-38, pp. 9-15, 1986.

Durand, R., and Condolios, E., "Experimental study of the hydraulic transport of coal and solid materials in pipes", Proc. Colloq. on the Hydraulic Transport of Coal, National Coal Board, UK, Paper IV, pp. 39-55, 1952.

Einstein, A., Ann. Phys., Lpz., **19**: 289, 1906.

Fenner, R.T., *Finite Element Methods for Engineers*, Macmillan, London, 1975.

Frankiewicz, T., Pangracs, G., Shook, C.A., Gillies, R.G., and Small, M., "Pipeloop and pipeline flow tests on coal-oil (transCOM) and coal-condensate slurries", Proc. of the 16th Intl. Conf. on Coal and Slurry Technologies, Coal and Slurry Technology Association, pp. 205-216, 1991.

Ghosh, T., Pipeline Flow of Coarse Particles in a Non-Newtonian Carrier Fluid, M.Sc. Thesis, University of Saskatchewan, 1989.

Ghosh, T. and Shook, C.A., "Transport of coarse particles in power law fluids", Proc. Hydrotransport 12 Conf., BHRA, Cranfield, UK, pp. 281-288, 1993.

Gillies, R.G., Pipeline Flow of Coarse Particle Slurries, Ph.D. Thesis, University of Saskatchewan, 1993.

Gillies, R.G., "Overburden pipelining tests in a 263 mm pipe loop for Syncrude Canada Limited", Saskatchewan Research Council, SRC Publication R-1670-2-C-93, 1993a.

Gillies, R.G., McKibben, M., and Shook, C.A., "Physical and numerical modelling of a horizontal well/reservoir system, year 3 final report : Part II Horizontal well physical model", Saskatchewan Research Council, SRC Publication P-110-237-C-93, 1993.

Gillies, R.G., McKibben, M., and Shook, C.A., "Physical and numerical modelling of a horizontal well/reservoir system, year 4 final report : Part II Horizontal well physical model", Saskatchewan Research Council, SRC Publication P-110-267-C-94, 1994.

Gillies, R.G., and Shook, C.A., "Concentration distributions of sand slurries in horizontal pipe flow", Particulate Science and Technology, 1994.

Gillies, R.G., Shook, C.A., and Wilson, K.C., "An improved two layer model for horizontal slurry pipeline flow", Can. J. Chem. Eng. **69**: 173-178, 1991.

Gillies, R.G., Small, M., and McKibben, M., "Rock in sludge tests in 52 and 263 mm pipes : overburden pipelining simulation tests", Saskatchewan Research Council, SRC Publication R-1670-3-C-92, 1992.

Hanks, R.W., "Low Reynolds number turbulent pipeline flow of pseudohomogeneous slurries", Proc. Hydrotransport 5 Conf.,BHRA, Cranfield, UK, paper C2, pp. 23-34, 1978.

Hsu, F-L., Turian, R.M., and Ma, T-W., "Flow of noncolloidal slurries in pipelines", AIChE J., **35**(3): 429-442, 1989.

Leighton, D. and Acrivos, A., "Viscous resuspension", Chem. Engineering Sci., **41**(6): 1377-1384, 1986.

Leighton, D. and Acrivos, A. "The shear-induced migration of particles in concentrated suspensions", J. Fluid Mech., **181**: 415-439, 1987.

Lockyear, C.F., Pullum, L., Duckworth, R.A., Littlejohn, M.H., and Lenard, J.A., "Prediction of pressure gradients for the transport of coarse coal in a fine coal carrier", Transportation Conf., Perth, 1984.

Maciejewski, W., Oxenford, J., and Shook, C.A., "Transport of coarse rock with sand and clay slurries", Proc. Hydrotransport 12 Conf., BHRA, Cranfield, UK, pp. 705-724, 1993.

Newitt, D.M., Richardson, J.F., Abbott, M., and Turtle, R.B., "Hydraulic conveying of solids in horizontal pipes", Trans. Inst. Chem. Engrs., **33** (2): 93-113, 1955.

Perry, R.H. and Green, D.W., *Perry's Chemical Engineers' Handbook, 6th ed.*, McGraw-Hill Book Company, New York, 1984.

Press, W.H., Flannery, B.P., Teukolsky, S.A., and Vetterling, W.T., *Numerical Recipes in Pascal : The Art of Scientific Computing*, Cambridge University Press, Cambridge, 1989.

Roco, M.C. and Shook, C.A., "Modeling of slurry flow: The effect of particle size", Can. J. Chem. Eng., **61**: 494-503, 1983.

Segerlind, L.J., *Applied Finite Element Analysis, 2nd ed.*, John Wiley and Sons, New York, 1984.

Shercliff, J.A., *The Theory of Electromagnetic Flow-Measurement*, Cambridge University Press, Cambridge, 1962.

Shook, C.A., "Suspension mechanism effects for slurries in streamline and turbulent flow", Presented at Symp. on Interaction of Solids and Fluids, Instn. of Chem. Engrs., London, UK, 1980.

Shook, C.A. and Roco, M.C., *Slurry Flow : Principles and Practice*, Butterworth-Heinemann, Boston, 1991.

Shook, C.A., Haas, D.B., Small, M.H., Gillies, R., Husband, W.H.W., "Investigation of the hydraulic transport of tar sand tailings in pipelines up to 20 inches in diameter", Saskatchewan Research Council, SRC Publication E 79-13, 1979.

Shook, C.A., Schriek, W., Smith, L.G., Haas, D.B., and Husband, W.H.W., "Experimental studies on the transport of sands in liquids of varying properties in 2 and 4 inch pipelines", Saskatchewan Research Council, SRC Publication E 73-20, 1973.

Sumner, R.J., Concentration Variations and their Effects in Flowing Slurries and Emulsions, Ph.D. Thesis, University of Saskatchewan, 1992.

Thomas, A.D., "Pipelining of coarse coal as a stabilized slurry - another viewpoint", Proc. Intl. Tech. Conf. on Slurry Transportation, pp. 196-205, 1979.

Thomas, A.D. and Wilson, K.C., "New analysis of non-Newtonian turbulent flow - yield-power-law fluids", Can. J. Chem. Eng., **65**: 335-338, 1987.

Thomas, D.G., "Transport characteristics of suspensions: VII. Relation of hindered-settling floc characteristics to rheological properties", AIChE J., **9**(3): 310-316, 1963.

Thomas, D.G., "Turbulent disruption of flocs in small particle size suspensions", AIChE J., **10**(4): 517-523, 1964.

Thomas, D.G., "Transport characteristics of suspensions: VIII. A note on the viscosity of Newtonian suspensions of uniform spherical particles", J. of Colloid Science, **20**: 267-277, 1965.

Wallis, G.B., *One Dimensional Two Phase Flow*, McGraw-Hill Book Company, New York, 1969.

Wilson, K.C., "A unified physically based analysis of solid-liquid pipeline flows", Proc. Hydrotransport 4 Conf., BHRA, Cranfield, UK, Paper A1, pp. 1-16, 1976.

Wilson, K.C. and Thomas, A.D., "A new analysis of the turbulent flow of non-Newtonian fluids", Can. J. Chem. Eng., **63**: 539-546, 1985.

Xu, J., Gillies, R., Small, M., and Shook, C.A., "Laminar and turbulent flow of Kaolin slurries", Proc. Hydrotransport 12 Conf., BHRA, Cranfield, UK, pp. 595-613, 1993.

APPENDIX A : Two-layer model

The description of the two-layer model presented here follows that which was given by Shook and Roco (1991). Figure 2.3 shows the physical concepts incorporated in the model. Two layers exist which each have a different solid/liquid mixture. The upper layer contains the fraction of solid material which is suspended by fluid lift forces, C_1. The lower layer contains fluid, suspended solids and the solid fraction which is supported by contact with the wall, C_2. In this lower layer, the two solid fractions combine to give a limiting concentration, C_{lim}.

Material balances for the two layers are used to relate layer velocities and concentrations to the bulk quantities.

$$AV = A_1V_1 + A_2V_2 \tag{A.1}$$

$$C_vAV = C_1AV + C_2A_2V_2 \tag{A.2}$$

$$C_r = C_1 + \frac{C_2A_2}{A} \tag{A.3}$$

$$C_{lim} = C_1 + C_2 \tag{A.4}$$

Here A is the cross sectional area, V is the velocity and C is the concentration. The subscripts 1 and 2 indicate the upper and lower layers respectively. No subscript indicates the bulk property for the entire pipe and C_v and C_r are the delivered and in-situ concentrations respectively. C_{lim} is the limiting concentration in the lower layer.

An important aspect of the model is the way in which the total solids fraction is

separated into material which is suspended by fluid forces and that which is supported by contact with the wall. This is described by the contact load fraction, C_c, which is defined by:

$$C_c = \frac{C_2 A_2}{A} \tag{A.5}$$

The contact load fraction is determined from a correlation which relates it to the in-situ concentration. Gillies et al. (1991) proposed

$$\frac{C_c}{C_r} = \exp\left[-0.0184 \frac{V}{V_\infty}\right] \tag{A.6}$$

where the particle settling velocity, V_∞, for spheres is given by Equation 2.12.

The limiting concentration in the lower layer can either be specified or can be calculated using a correlation of the form

$$\frac{C_{max} - C_{lim}}{C_{max} - C_r} = 0.074 \left(\frac{V}{V_\infty}\right)^{0.44} (1 - C_r)^{0.189} \tag{A.7}$$

where C_{max} is the concentration of a loosely packed bed. Another method of determining C_{lim} was proposed by Gillies and Shook (1994) which makes use of a concentration distribution which is predicted by considering turbulent diffusion of the solids. C_{lim} is assigned the concentration predicted at a position of y/D=0.15 relative to the bottom of the pipe.

With the contact load fraction determined from Equation A.6 , and C_{lim} specified or correlated with Equation A.7, the concentrations C_1 and C_2 can be calculated by Equations

A.3, A.4 and A.5.

The momentum equation for each layer and for the entire pipe can be expressed by

Layer 1

$$-\frac{d(P + \rho_1 g h)}{dz} = \frac{\tau_1 S_1 + \tau_{12} S_{12}}{A_1} \qquad (A.8)$$

Layer 2

$$-\frac{d(P + \rho_2 g h)}{dz} = \frac{-\tau_{12} S_{12} + \tau_2 S_2}{A_2} \qquad (A.9)$$

Entire pipe

$$-\frac{d(P + \rho_m g h)}{dz} = \frac{\tau_1 S_1 + \tau_2 S_2}{A} \qquad (A.10)$$

where τ_i is the shear stress on the boundary S_i. The subscript 1 indicates the pipe boundary of the upper layer, 2 the pipe boundary of the lower layer and 12 the interface boundary between the two layers. The momentum equation for the entire pipe uses the average mixture density ρ_m.

$$\rho_m = \rho_s c + \rho_f (1 - c) \qquad (A.11)$$

The shear stress along the upper pipe boundary is fluid like in nature and is assumed to be given by

$$\tau_1 = \frac{f_1 V_1 | V_1| \rho_1}{2} \qquad \text{(A.12)}$$

where the Fanning friction factor f_1 is a function of the pipe Reynolds number for the bulk flow and the pipe wall roughness. Correlations such as that of Churchill's (1977) can be used.

At the interface between the two layers, the shear stress is a function of the difference in layer velocities.

$$\tau_{12} = \frac{f_{12}(V_1 - V_2) | V_1 - V_2 | \rho_1}{2} \qquad \text{(A.13)}$$

where f_{12} is a modified Colebrook friction factor

$$f_{12} = \frac{2(1 + Y)}{\left[4 \log_{10}\left(\frac{D}{d}\right) + 3.36\right]^2} \qquad \text{(A.14)}$$

where

$$Y = 0 \qquad \textit{for } \frac{d}{D} < 0.0015 \qquad \text{(A.14a)}$$

$$Y = 4 + 1.42 \log_{10}\left(\frac{d}{D}\right) \qquad \textit{for } 0.0015 < \frac{d}{D} < 0.15$$

The shear stress along the lower pipe boundary contains both fluid, τ_{2m}, and solids,

τ_{2s} components.

$$\tau_2 S_2 = \tau_{2m} S_2 + \tau_{2s} S_2 \qquad \text{(A.15)}$$

For the fluid component it is assumed that

$$\tau_{2m} = \frac{f_1 V_2 | V_2 | \rho_1}{2} \qquad \text{(A.16)}$$

The solids component is Coulombic in nature so that it is velocity independent and results from the contact load portion of the solid material sliding along the wall.

$$\tau_{2s} S_2 = \frac{D^2 g(\rho_s - \rho_l)(\sin\beta - \beta\cos\beta) C_2 (1 - C_1 - C_2)}{2(1 - C_2)} \qquad \text{(A.17)}$$

β is the angle which defines the location of the layer interface as shown in Figure 2.3.

After the contact load fraction and limiting concentration in the lower layer have been determined from Equations A.6 and A.7, the location of the interface and the boundaries are calculated. Equations A.1, A.8 and A.9 are solved to determine the layer velocities for the specified bulk velocity. Then Equations A.10 and A.2 are solved to determine the pressure gradient and delivered concentration.

APPENDIX B : Pipeline data acquisition program

B.1 Acquisition program FLUID.FOR

```
      PROGRAM FLUID
C
C     Written by Kelly Hill (February 1991)
C     Program to perform data acquisition tasks using RT-11 computer.
C     Programming language is FORTRAN IV (1974)
C     Requires LINK to the assembly language macro ADINP.MAC written by Ed Allen
C     Requires acquisition parameter file of the following format :
C           Header string (10A4)
C           Lower A/D channel number
C           Upper A/D channel number
C           Number of A/D samples per data point
C           First channel name (4A4)
C           First channel slope
C           First channel intercept
C           :
C           Final channel name (4A4)
C           Final channel slope
C           Final channel intercept
C
      Common/PARAM/HEADER(10),LCH,UCH,NSAMP,NAM(4,6)
      Common/PARAM/SLOP(6),INTER(6)
      Common/CONTRL/FILNAM(3)
      Integer I,J,K,CH,SEL,LCH,UCH,NSAMP
      Real HEADER,NAM,SLOP,INTER,FILNAM,RLCH,RUCH,RSAMP
C
      Write(5,*) '1'
      Write(5,*) 'Enter name of acquisition parameter file (A12)'
10    Read(5,10) FILNAM
      Call Assign(2,'DY1:")
      Open(Unit=2,Name=FILNAM,Type='OLD')
      Read(2,20) (HEADER(I),I=1,10)
20    Format(10A4)
      Read(2,*) RLCH
      Read(2,*) RUCH
      Read(2,*) RSAMP
      LCH=Ifix(RLCH)
      UCH=Ifix(RUCH)
      NSAMP=Ifix(RSAMP)
      Write(5,21) (HEADER(I),I=1,10)
21    Format(10A4)
C
      Do 25 I=LCH,UCH
       K=I-LCH+1
       Read(2,26) (NAM(J,K),J=1,4)
26     Format(4A4)
       Read(2,*) SLOP(K)
       Read(2,*) INTER(K)
25    Continue
```

```
      CH=(UCH-LCH)+1
C
97    Call Menu(SEL)
      If (SEL .EQ. 5) Go To 99
       If (SEL .GT. 5 .OR. SEL .LT. 1) Go To 90
       If (SEL .GT. 1) Go To 31
        Call Calib
        Go To 97
31     If (SEL .GT. 2) Go To 32
        Call Zero
        Go To 97
32    If (SEL .GT. 3) Go To 33
        Write(5,*) 'Press "Shift-Prnscr" to toggle printer echo'
        Go To 97
33    Call Acquisition
      Go To 97
90    Write(5,*) '************************'
      Write(5,*) 'Error - Selection out of range'
      Write(5,*) '************************'
      Go To 97
C
99    End
C
C     Subroutines begin here
C
      Subroutine Menu(SEL)
C
      Integer I,SEL
C
      Write(5,*) 'Main Menu'
      Write(5,*) '---------'
      Write(5,*) ' [1] Calibrate Transducer'
      Write(5,*) ' [2] Zero Transducer'
      Write(5,*) ' [3] Send Results to Printer'
      Write(5,*) ' [4] Begin Data Acquisition'
      Write(5,*) ' [5] END'
      Write(5,*) ' '
      Write(5,*) 'Type number of desired operation'
      Read(5,*) SEL
      Return
      End
C
      Subroutine Convert(CHAN,ADVAL)
C
C     Internal voltage conversion of A/D channels - determined from calibration
C
      If (CHAN .EQ. 0) ADVAL=0.00487669*ADVAL-0.267157
      If (CHAN .EQ. 1) ADVAL=0.00487586*ADVAL-0.266636
      If (CHAN .EQ. 2) ADVAL=0.00487614*ADVAL+0.532467
      If (CHAN .EQ. 3) ADVAL=0.00487759*ADVAL-0.299595
      If (CHAN .EQ. 4) ADVAL=0.00487713*ADVAL-0.297293
      If (CHAN .EQ. 5) ADVAL=0.00487798*ADVAL-0.289106
```

```
      Return
      End
C
      Subroutine Calib
C
C     Subroutine to calibrate pressure transducer with a manometer
C     Calibration results are stored in a file for future use using the following format :
C           Header string (10A4)
C           Number of points in regression
C           Point 1voltage recorded, Point 1 pressure calculated
C           :
C           Point n voltage recorded, Point n pressure calculated
C           Linear regression slope, intercept
C           Regression correlation coefficient
C
      Common/PARAM/HEADER(10),LCH,UCH,NSAMP,NAM(4,6)
      Common/PARAM/SLOP(6),INTER(6)
      Common/CONTRL/FILNAM(3)
      Integer LCH,UCH,NSAMP
      Real HEADER,NAM,SLOP,INTER,FILNAM
C
      Dimension ADVOLT(20),DEPEND(20),CALFIL(3),CALHEAD(10)
      Integer CONT,N,I,J,STOR,CHAN,IADVAL,ERR
      Real INDEP,CALFIL,CALHEAD,VAL,RN,ADVOLT,DEPEND
      Real ADSUM,ADSQR,RSAMP,x,y,xy,xs,ys,slope,intercept,r
C
201   Write(5,*) 'Channels now active'
      Do 200 I=LCH,UCH
       Write(5,210) I,(NAM(J,(I-LCH+1)),J=1,4)
210    Format ('  Channel  ',I2,'     ',4A4)
200   Continue
      Write(5,*) 'Enter channel to be calibrated or -1 to quit'
      Read(5,*) CHAN
      If (CHAN .LT. LCH .OR. CHAN .GT. UCH) Go To 399
C
      x=0.
      y=0.
      xy=0.
      xs=0.
      ys=0.
      ERR=0
      N=0
      RSAMP=Float(NSAMP)
270   N=N+1
      Write(5,*) 'Set pressure and enter differential manometer height in cm'
      Read(5,*) VAL
      DEPEND(N)=VAL*9.81*998.8/100.
      ADSUM=0.
      Do 260 J=1,NSAMP
       Call ADINP(CHAN,IADVAL)
       If (IADVAL .GE. 2040) ERR=1
       ADVAL=Float(IADVAL)
```

```
        Call Convert(CHAN,ADVAL)
        ADSUM=ADSUM+ADVAL
260     Continue
        ADVOLT(N)=ADSUM/RSAMP
        x=x+ADVOLT(N)
        y=y+DEPEND(N)
        xy=xy+ADVOLT(N)*DEPEND(N)
        xs=xs+ADVOLT(N)*ADVOLT(N)
        ys=ys+DEPEND(N)+DEPEND(N)
        If (ERR .EQ. 0) Go To 279
        Write(5,*) '*******************************'
        Write(5,*) 'ERROR : Signal has become saturated'
        Write(5,*) '*******************************'
279     Write(5,280) N
280     Format(I4,' points have been taken')
        Write(5,*) 'Enter 1 to include another point or 0 to end'
        Read(5,*) CONT
        If (CONT .EQ. 1) Go To 270
C
        RN=Float(N)
        slope=((RN*xy)-(x*y))/((RN*xs)-(x*x))
        intercept=(y-(slope*x))/RN
        r=((RN*xy)-(x*y))/((((RN*ys)-(y*y))*((RN*xs)-(x*x)))**0.5)
        Write(5,*) 'The linear regression results are :'
        Write(5,320) slope,intercept
320     Format('Slope= ',F12.4,' Intercept= ',F12.4)
        Write(5,330) r,N
330     Format('r= ',F10.7,' Points= ',I4)
C
        Write(5,*) 'Should results be saved : Y=1 N=0'
        Read(5,*)STOR
        If (STOR .NE. 1) Go To 201
        Write(5,*) 'Enter the name of the calibration file'
        Read(5,220) CALFIL
220     Format(3A4)
        Call Assign(2,'DY1:')
        Open(Unit=2,Name=CALFIL,Type='NEW')
        Write(2,310) CHAN
310     Format('Calibration file for channel ',I2)
        Write(2,*) N
        Do 360 J=1,N
          Write(2,*) ADVOLT(J),DEPEND(J)
360     Continue
        Write(2,370) slope,intercept
370     Format('Slope= ',F12.4,' Intercept= ',F12.4)
        Write(2,380) r,N
380     Format('r= ',F10.7,' Points= ',I4)
        Call Close(2)
        Open(Unit=2,Name=FILNAM,Type='OLD')
        Write(2,390) (HEADER(J),J=1,10)
390     Format(10A4)
        Write(2,*) Float(LCH)
```

```
      Write(2,*) Float(UCH)
      Write(2,*) RSAMP
      Do 395 J=1,(UCH-LCH)+1
       Write(2,396) (NAM(I,J),I=1,4)
396    Format(4A4)
       Write(2,*) SLOP(J)
       Write(2,*) INTER(J)
395   Continue
      Call Close(2)
      Go To 201
399   Return
      End
C
      Subroutine Zero
C
C     Subroutine to zero pressure transducers
C
      Common/PARAM/HEADER(10),LCH,UCH,NSAMP,NAM(4,6)
      Common/PARAM/SLOP(6),INTER(6)
      Common/CONTRL/FILNAM(3)
      Integer LCH,UCH,NSAMP
      Real HEADER,NAM,SLOP,INTER,FILNAM
C
      Integer CHAN,I,STOR,IADVAL,ERR
      Real RSAMP,GO,ADSUM,ADSQR,ADZRO,intercept,ADSTDV,ADVAL
C
401   Write(5,*) 'Channels now active'
      Do 400 I=LCH,UCH
       Write(5,410) I,(NAM(J,(I-LCH+1)),J=1,4)
410    Format('  Channel ',I2,'     ',4A4)
400   Continue
      Write(5,*) 'Enter the channel to be zeroed or -1 to quit'
      Read(5,*) CHAN
      If (CHAN .LT. LCH .OR. CHAN .GT. UCH) Go To 499
      Write(5,*) 'Set  "zero" condition and press RETURN'
      Read(5,*) GO
      ERR=0
      ADSUM=0.
      ADSQR=0.
      RSAMP=Float(NSAMP)
      Do 405 J=1,NSAMP
       Call ADINP(CHAN,IADVAL)
       If (IADVAL .GE. 2040) ERR=1
       ADVAL=Float(IADVAL)
       Call Convert(CHAN,ADVAL)
       ADSUM=ADSUM+ADVAL
       ADSQR=ADSQR+ADVAL*ADVAL
405   Continue
      ADZRO=ADSUM/RSAMP
      ADSTDV=((RSAMP*ADSQR)-(ADSUM*ADSUM))
      ADSTDV=(Abs(ADSTDV/(RSAMP*(RSAMP-1.))))**0.5
      intercept=-(SLOP(CHAN-LCH+1)*ADZRO
```

```
      If (ERR .EQ. 0) Go To 419
      Write(5,*) '*******************************'
      Write(5,*) 'ERROR : Signal has become saturated'
      Write(5,*) '*******************************'
419   Write(5,406) CHAN
406   Format('Channel ',I2,' zeroed')
      Write(5,420) (NAM(J,CHAN-LCH+1),J=1,4),ADZRO
420   Format(4A4,' zero= ',F8.5)
      Write(5,430) ADSTDV
430   Format('Sample standard deviation = ',F8.5)
      Write(5,440) intercept
440   Format('New regression intercept = ',F12.4)
      Write(5,450) INTER(CHAN-LCH+1)
450   Format('Stored value was = ',F12.4)
      Write(5,*) 'Use new value for data acquisition Y=1 N=0'
      Read(5,*) STOR
      If (STOR .NE. 1) Go To 401
      INTER(CHAN-LCH+1)=intercept
      Go To 401
499   Return
      End
C
      Subroutine Acquisition
C
      Common/PARAM/HEADER(10),LCH,UCH,NSAMP,NAM(4,6)
      Common/PARAM/SLOP(6),INTER(6)
      Common/CONTRL/FILNAM(3)
      Integer LCH,UCH,NSAMP
      Real HEADER,NAM,SLOP,INTER,FILNAM
C
      Dimension ADSUM(6),ADSQR(6),DEPEND(6),ADVOLT(6)
      Dimension DSTDV(6),ERR(6)
      Integer I,K,L,ERR
      Real ADSUM,ADSQR,DEPEND,ADVOLT,DSTDV,RSAMP,STP
C
      RSAMP=Float(NSAMP)
590   Call Sample(NSAMP,LCH,UCH,ADSUM,ADSQR,ERR)
      K=UCH-LCH+1
      Do 501 I=1,K
       ADVOLT(I)=ADSUM(I)/RSAMP
       DEPEND(I)=INTER(I)+SLOP(I)*ADVOLT(I)
       DSTDV(I)=((RSAMP*ADSQR(I))-(ADSUM(I)*ADSUM(I)))
       DSTDV(I)=(Abs(DSTDV(I)/(RSAMP*(RSAMP-1.))))**0.5
501   Continue
      Do 500 I=1,K
       L=I+LCH-1
       Write(5,503) L
503    Format('Channel ',I2)
       If (ERR(I) .EQ. 0) Go To 509
       Write(5,*) '*******************************'
       Write(5,*) 'ERROR : Signal has become saturated'
       Write(5,*) '*******************************'
```

```
509      Write(5,510) (NAM(J,I),J=1,4),DEPEND(I)
510      Format(4A4,' = ',F12.4)
         Write(5,520) ADVOLT(I),DSTDV(I)
520      Format('Voltage = ',F8.5,' Voltage std.dev. = ',F8.5)
500     Continue
580     Write(5,*) 'Press RETURN to take next reading or enter "S" to stop'
        Read(5,581) STP
581     Format(A2)
        If (STP .EQ. 'S' .OR. STP .EQ. 's') Go To 599
        Go To 590
599     Return
        End
C
        Subroutine Sample(N,LOW,HIGH,ADSUM,ADSQR,ERR)
C
        Dimension ADSUM(6),ADSQR(6),ADVAL(6),IADVAL(6),ERR(6)
        Integer N,I,J,LOW,HIGH,IADVAL,ERR,CHAN
        Real ADSUM,ADSQR,ADVAL
C
        Do 600 I=1,(HIGH-LOW+1)
         ADSUM(I)=0.
         ADSQR(I)=0.
         ERR(I)=0
600     Continue
        Do 610 I=1,N
         Do 620 J=1,(HIGH-LOW+1)
          CHAN=J+LOW-1
          Call ADINP(CHAN,IADVAL(J))
          If (ADINP(J) .GE. 2040) ERR(J)=1
          ADVAL(J)=Float(IADVAL(J))
          Call Convert(CHAN,ADVAL)
          ADSUM(J)=ADSUM(J)+ADVAL(J)
          ADSQR(J)=ADSQR(J)+ADVAL(J)*ADVAL(J)
620      Continue
610     Continue
        Return
        End
```

B.2 Assembly language macro ADINP.MAC

```
        .TITLE ADINP
        .INDENT /V01.00/
; VERSION 01
; E. ALLEN        22-AUG-80
;
; This routine will accept a fast, single analog input.
; Its speed is limited only by the execution time of its statements plus
;A/D conversion time. For good results it must be noninterruptable.
;
; The fortran call is :
;       CALL ADINP(ICHN,IVAL)
;
; where ICHN    is the A/D channel.
;       IVAL    is the returned A/D value.
;
ADSTA=170400            ;A/D status register
ADBFR=170402            ;A/D buffer register
;
ADINP::TST      (R5)+
        MOV     @(R5)+,R0
        BIC     #177700,R0
        SWAB    R0
        MOV     R0,@#ADSTA
        INC     @#ADSTA
LOOP:   TSTB    @#ADSTA
        BPL     LOOP
        MOV     @#ADBFR,@(R5)
        RTS     PC
        .END
```

APPENDIX C : Finite element pipe flow program

FEPIPE.BAS

```
'Finite Element Program for Laminar Pipe Flow written in Quickbasic 4.5
'Constant Strain Triangle Elements
'Based on "Finite Element Methods for Engineers" - Roger T. Fenner (1975)
'
'Effective viscosity based on concentration distribution and
'     fluid parameters for the Herschel-Bulkley model
'Concentration distribution is either specified by two-part linear or cubic
'     profile with no lateral variation
'     Concentration profile can be predicted by ODE described
'     particle shear induced dispertion solved by Runge-Kutta
'     in the y-direction after finite element solution of velocity
'Runge-Kutta solution based on "Numerical Recipes in Pascal" - Press et. al. (1989)
'Mesh specifications for half pipe obtained from running PIPEMESH.BAS
'     for 1-25 concentric rings
'     Twenty ring mesh requires space for -   1950 elements
'                                             1050 nodes
'     Fifteen ring mesh requires space for -  700 elements
'                                             400 nodes

DEFINT I-N
DECLARE SUB ADAPTRK (yrk, crk, dcdyrk, htest, rktol, hnow, hnext)
DECLARE FUNCTION CHORD! (ypos!)
DECLARE SUB CONCPROF ()
DECLARE SUB CONCSOLVE ()
DECLARE SUB DISPVISC (Cdis, ud, dudc)
DECLARE SUB INITRATE ()
DECLARE SUB MESH ()
DECLARE SUB ODE (yrk, crk, dcdyrk)
DECLARE SUB PROFILES ()
DECLARE SUB RUNGE (yrk, crk, dcdyrk, hrk, cnext)
DECLARE SUB TRANSITION (Tflag)
DECLARE SUB VELBC ()
DECLARE SUB VELMATRIX ()
DECLARE SUB VELSOLVE ()
DECLARE SUB VISC ()

DIM SHARED Phi(1950, 3), dPhidx(1950, 3), dPhidy(1950, 3)
DIM SHARED Npti(1950), Nptj(1950), Nptk(1950)
DIM SHARED Nctr(51), Ectr(51), Cctr(51), NptB(100), LRing(25, 2)
DIM SHARED Gstiff(1050, 8), F(1050), Nadj(1050, 8), NNadj(1050)
DIM SHARED Vz(1050), C(1050)
DIM SHARED X(1050), Y(1050)
DIM SHARED Xele(1950), Yele(1950), Vele(1950)
DIM SHARED Effvisc(1950), Aele(1950), Cele(1950)
DIM SHARED dwdx(1950), dwdy(1950)
DIM SHARED Yrkpt(102), Crkpt(102), Ystep(102)

COMMON SHARED Dia, HBTy, HBk, HBn, Pz, rhos, rhof, pi, g
```

```
COMMON SHARED cymid, cylow, yhigh, ymid
COMMON SHARED c0, c1, c2, c3, Cmax, Cshear, Crspec, Cwall, tantheta
COMMON SHARED NRing, Nnode, Nele, NBNw, Ictr, Nrkpt, Nrk
COMMON SHARED itnum, itvsum, itcsum
COMMON SHARED Vtol, Ctol, Verr, Cerr, Orelax
COMMON SHARED NNflag, Cflag, SSflag, RKflag
COMMON SHARED Root$, Dir$, V$
COMMON SHARED Tw, Qbulk, Ub, Cdel, dPcalc, Cmean, Area

pi = 4 * ATN(1)
g = 9.81                'Gravitational constant (m/s2)

'Problem parameter specification
Root$ = "B:\"           'Root directory location
Dir$ = "RESULTS\kao44lop"    'Location of results directory and file name

Pz = 1500               'Pressure gradient (Pa/m)
rhos = 2470             'Solid density (kg/m3)
rhof = 1500             'Fluid density (kg/m3)
Dia = .0525             'Pipe Diameter (m)

NNflag = 1              'Non-Newtonian fluid..flag = 1
HBTy = 4.1              'Herschel-Bulkley Yield Stress (Pa)
HBk = .065              'H-B shear coefficient
HBn = 1!                'H-B shear index

SSflag = 1              'solid shape type..sphere=1, angular=2
Cmax = .58              'maximum solid concentration
Cshear = .58            'maximum concentration capable of shear
Cflag = 1               'C profile type..1=linear,2=cubic
RKflag = 1              'Solve concentration ODE

cylow = .4              'type 1 - two-part linear C profile
cymid = .25
ymid = .4
yhigh = .6

c0 = .411               'type 2 - C=c0+c1*y/D+c2*y/D^2+c3*y/D^3
c1 = 1.15               '       y/D=0 at bottom of pipe
c2 = -5.679
c3 = 4.1

Crspec = .15            'C ODE  - specified concentration
Cwall = cylow           '       initial guess for Runga-Kutta
tantheta = 1!           '       tan(angle of internal friction)

Vtol = .000001          'convergence criteria for velocity
Ctol = .00001           'convergence criteria for concentration
itmax = 1500            'maximum number of iterations

'Begin solution.....
```

```
SCREEN 0: CLS
'Use MESH subroutine to specify local and global element geometry
LOCATE 3, 1: PRINT "Evaluating mesh geometry"
CALL MESH
LOCATE 4, 1: PRINT "Estimating velocity profile and elemental shear rates"
CALL INITRATE
Cerr = 1!
itcsum = 0
Verr = 1!
itvsum = 0
Orelax = 1.5
V$ = INKEY$

VCALC:
loopflag = 1
WHILE loopflag = 1
 LOCATE 6, 1: PRINT "Calculating element effective viscosities"
 CALL VISC
 LOCATE 7, 1: PRINT "Building velocity stiffness and force matrices"
 CALL VELMATRIX
 LOCATE 8, 1: PRINT "Applying velocity boundary conditions"
 CALL VELBC
 LOCATE 9, 1: PRINT "Solving linear velocity equations"
 IF NNflag = 1 THEN
  IF Verr > 1000 * Vtol THEN
   itnum = 25
  ELSEIF Verr > 100 * Vtol THEN
   itnum = 10
  ELSEIF Verr > 10 * Vtol THEN
      itnum = 5
    ELSE
      itnum = 1
  END IF
 ELSE
  itnum = itmax
 END IF
 CALL VELSOLVE
 loopflag = 0
 'So long as tolerences are not met...
 IF Verr > Vtol THEN loopflag = 1
 'So long as the maximum number of iterations are not met
 IF itvsum >= itmax THEN loopflag = 0
 LOCATE 22, 1: PRINT "Press a key to suspend iteration"
 V$ = INKEY$
 IF V$ <> "" THEN GOTO RESULT
WEND

ADVANC:
'Update element shear rates and viscosities
IF NNflag = 1 OR RKflag = 1 THEN
 Ntemp = NNflag
 NNflag = 1
```

```
  CALL VISC
  NNflag = Ntemp
END IF

CCALC:
IF RKflag = 1 THEN
  LOCATE 13, 1: PRINT "Predicting concentration profile by Runge-Kutta"
  CALL CONCSOLVE
  CALL CONCPROF
END IF

RESULT:
'Output the results
'Integrate over the solution domain
Qbulk = 0: Tw = 0: Cmean = 0: Cdel = 0
BCNStrt = (Nnode - NBNw + 1)
FOR M = 1 TO Nele
  I = Npti(M): J = Nptj(M): K = Nptk(M)
  Vele(M) = (Vz(I) + Vz(J) + Vz(K)) / 3
  Cele(M) = (C(I) + C(J) + C(K)) / 3
  Qbulk = Qbulk + Vele(M) * Aele(M)
  Cmean = Cmean + Aele(M) * Cele(M)
  Cdel = Cdel + Vele(M) * Aele(M) * Cele(M)
  'Shear stress values for each element'
  dwdx(M) = Vz(I) * dPhidx(M, 1) + Vz(J) * dPhidx(M, 2)
  dwdx(M) = (dwdx(M) + Vz(K) * dPhidx(M, 3)) / (2 * Aele(M))
  dwdy(M) = Vz(I) * dPhidy(M, 1) + Vz(J) * dPhidy(M, 2)
  dwdy(M) = (dwdy(M) + Vz(K) * dPhidy(M, 3)) / (2 * Aele(M))
  Txz = Effvisc(M) * dwdx(M)
  Tyz = Effvisc(M) * dwdy(M)
  Tz = (Txz ^ 2 + Tyz ^ 2) ^ .5
  IF J >= BCNStrt AND K >= BCNStrt THEN
    'Boundary element'
    S = (dPhidy(M, 1) ^ 2 + dPhidx(M, 1) ^ 2) ^ .5
    Tw = Tw + Tz * S
  END IF
NEXT M
Tw = Tw / (pi * Dia / 2)          'units Pa
Qbulk = 60000 * Qbulk * 2         'units lpm
Ub = Qbulk / (60000 * 2 * Area)   'units m/s
Cmean = Cmean / Area              'In-situ volume fraction
Cdel = (60000 * 2 * Cdel) / Qbulk 'Delivered volume fraction
dPcalc = 4 * Tw / Dia             'units Pa/m

'Determine flow regime for fluid alone..conservative estimate of transition
CALL TRANSITION(Tflag)

MENU:
SCREEN 0
CLS
LOCATE 3, 1
PRINT USING "Velocity Iterations : ####  Tolerence : #.######"; itvsum; Verr
```

```
PRINT USING "Conc. Iterations : ####  Tolerence : #.######"; itcsum; Cerr
PRINT USING "Flowrate =######.## Lpm  Bulk Velocity = ###.###  m/s"; Qbulk; Ub
PRINT USING "Cr = ##.###  Cvd =##.###"; Cmean; Cdel
PRINT USING "Spec. dP = ######.# Pa/m  Calc. dP = ######.# Pa/m"; Pz; dPcalc
PRINT USING "Average Tw = ####.### Pa"; Tw
IF Tflag = 1 THEN
 LOCATE 20, 1
 PRINT "Flow may be approaching turbulent"
END IF
LOCATE 10, 1
PRINT "Select one of the following"
PRINT " "
PRINT "          Centerline Profiles  [1]"
PRINT "            Resume Iterations  [2]"
PRINT "   ODE Concentration Prediction [3]"
PRINT "                 Exit Program  [4]"
INPUT ; SEL
SELECT CASE SEL
 CASE 1
  CALL PROFILES
 CASE 2
  CLS
  IF Verr > Vtol AND itvsum < itmax THEN GOTO VCALC
  IF RKflag = 1 AND Cerr > Ctol THEN GOTO CCALC
 CASE 3
  CLS
  RKflag = 1
  IF Cerr > Ctol THEN GOTO ADVANC
 CASE 4
  STOP
END SELECT
GOTO MENU

END

SUB ADAPTRK (yrk, crk, dcdyrk, hrk, rktol, hnow, hnext)

Stepmax = Dia / (2 * Nrkpt)
Stepmin = Dia / 10000
'Adaptive Runge-Kutta solution
'Find proper step size
errc = 1!
WHILE errc > rktol
 'Two half steps
 CALL RUNGE(yrk, crk, dcdyrk, hrk / 2, chalf)
 CALL ODE(yrk + hrk / 2, chalf, dcdyhalf)
 CALL RUNGE(yrk + hrk / 2, chalf, dcdyhalf, hrk / 2, chole)
 'One whole step
 CALL RUNGE(yrk, crk, dcdyrk, hrk, cwhole)
 yrk = yrk + hrk
 cdif = chole - cwhole
 errc = ABS(chole - cwhole)
```

```
 yDloc = (yrk / Dia) + .5
 LOCATE 15, 1
 PRINT USING "Location #.## y/D, c #.###, dcdy #####.#"; yDloc; crk; dcdyrk
 IF errc < rktol THEN
  hnow = hrk
  IF errc > .0006 * rktol THEN
   hnext = .9 * hrk * EXP(-.2 * LOG(errc / rktol))
  ELSE
   hnext = 4 * hrk
  END IF
  IF hnext > Stepmax THEN hnext = Stepmax
  GOTO DONE
 ELSE
  IF hrk = Stepmin THEN
   LOCATE 18, 1: PRINT "Stepsize reached minimum value"
   GOTO DONE
  ELSE
   hrk = .9 * hrk * EXP(-.25 * LOG(errc / rktol))
   IF hrk < Stepmin THEN hnext = Stepmin
  END IF
 END IF
WEND

DONE:
crk = chole + cdif / 15
IF crk > Cmax THEN crk = Cmax
IF crk < 0 THEN crk = 0
END SUB

FUNCTION CHORD (ypos)

CHORD = SQR((Dia / 2) ^ 2 - ypos ^ 2)
END FUNCTION

SUB CONCPROF

'Map Runge-Kutta profile to Centre axis nodes
FOR N = 1 TO Ictr
 FOR L = 1 TO Nrk - 1
  IF Y(Nctr(N)) = Yrkpt(L) THEN Cctr(N) = Crkpt(L)
  IF Y(Nctr(N)) > Yrkpt(L) AND Y(Nctr(N)) < Yrkpt(L + 1) THEN
   cgrad = (Crkpt(L + 1) - Crkpt(L)) / (Yrkpt(L + 1) - Yrkpt(L))
   Cctr(N) = Crkpt(L) + cgrad * (Y(Nctr(N)) - Yrkpt(L))
  END IF
 NEXT L
 IF Y(Nctr(N)) = Yrkpt(Nrk) THEN Cctr(N) = Crkpt(Nrk)
NEXT N
END SUB

SUB CONCSOLVE

'Solution to solid concentration distribution in y-direction using
```

```
'     adaptive fourth order Runge-Kutta to solve governing ODE

rktol = .0001
WHILE ABS(Cerr) > Ctol
 Cfact = 20        'Scaling factor to limit correction step of BC
 itcsum = itcsum + 1
 hrk = Dia / (4 * Nrkpt)
 crk = Cwall
 'Starting at the bottom of the pipe
 Nrk = 1
 yrk = Ystep(Nrk)
 Yrkpt(Nrk) = yrk
 Crkpt(Nrk) = crk
 WHILE yrk < (Dia / 2)
  CALL ODE(yrk, crk, dcdyrk)
  'Store results needed to generate concentration profile
  IF yrk > Ystep(Nrk + 1) THEN
   Nrk = Nrk + 1
   Yrkpt(Nrk) = yrk
   Crkpt(Nrk) = crk
  END IF
  CALL ADAPTRK(yrk, crk, dcdyrk, hrk, rktol, hnow, hnext)
  hrk = hnext
  IF yrk + hrk > (Dia / 2) THEN hrk = (Dia / 2) - yrk
 WEND
 'Integrate concentration over cross section using Simpson's rule
 ya = Yrkpt(1)
 xa = CHORD(ya)
 yc = (Yrkpt(2) + Yrkpt(1)) / 2
 xc = CHORD(yc)
 yb = (ya + yc) / 2
 xb = CHORD(yb)
 Csum = Crkpt(1) * ((yc - ya) / 2) * (xa / 3 + 4 * xb / 3 + xc / 3)
 Ark = ((yc - ya) / 2) * (xa / 3 + 4 * xb / 3 + xc / 3)
 FOR I = 2 TO Nrk - 1
  ya = (Yrkpt(I - 1) + Yrkpt(I)) / 2
  xa = CHORD(ya)
  yb = Yrkpt(I)
  xb = CHORD(yb)
  yc = (Yrkpt(I + 1) + Yrkpt(I)) / 2
  xc = CHORD(yc)
  Csum = Csum + Crkpt(I) * ((yc - ya) / 2) * (xa / 3 + 4 * xb / 3 + xc / 3)
  Ark = Ark + ((yc - ya) / 2) * (xa / 3 + 4 * xb / 3 + xc / 3)
 NEXT I
 ya = (Yrkpt(Nrk - 1) + Yrkpt(Nrk)) / 2
 xa = CHORD(ya)
 yc = Yrkpt(Nrk)
 xc = CHORD(yc)
 yb = (ya + yc) / 2
 xb = CHORD(yb)
 Csum = Csum + Crkpt(Nrk) * ((yc - ya) / 2) * (xa / 3 + 4 * xb / 3 + xc / 3)
 Ark = Ark + ((yc - ya) / 2) * (xa / 3 + 4 * xb / 3 + xc / 3)
```

```
  Csum = Csum / Ark
  Cerr = Csum - Crspec
  LOCATE 16, 1:
  PRINT USING "Conc. Iter. = ####  Cr Error = #.##### Cwall #.####"; itcsum; Cerr; Cwall
  IF ABS(Cerr) > Ctol THEN
    Cwall = Cwall - Cerr / Cfact
    IF Cwall > Cmax THEN Cwall = Cmax
    IF Cwall < Crspec THEN Cwall = Crspec
  END IF
  LOCATE 22, 1: PRINT "Press a key to suspend iteration"
  V$ = INKEY$
  IF V$ <> "" THEN GOTO TERMIN
WEND
TERMIN:
END SUB

SUB DISPVISC (Cdis, ud, dudc)

'Dispersive viscosity constant of proportionality
Kv = 1!
IF SSflag = 1 THEN
  'Thomas' equation for spherical shaped particles
  ud = Kv * (10.05 * Cdis ^ 2 + .00273 * EXP(16.6 * Cdis))
  dudc = Kv * (20.1 * Cdis + .045 * EXP(16.6 * Cdis))
ELSE
  'Gillies equation for angular particles
  ud = Kv * (10 * Cdis ^ 2 + .0019 * EXP(20 * Cdis))
  dudc = Kv * (20 * Cdis + .038 * EXP(20 * Cdis))
END IF
END SUB

SUB INITRATE

'Subroutine to provide an initial guess for the nodal velocities
'  based on laminar pipe flow of the Herschel-Bulkley fluid alone
'Necessary to evaluate the effective viscosity in the subroutine VISC
'Effvisc initialized to product of HBk value and conc. correction
ry = 2 * HBTy / Pz
TyTw = 4 * HBTy / (Dia * Pz)
FOR N = 1 TO Nnode
  rn = (X(N) ^ 2 + Y(N) ^ 2) ^ .5
  IF rn > ry THEN
    terma = ((rn / (Dia / 2)) - TyTw) ^ ((1 / HBn) + 1)
  ELSE
    terma = 0
  END IF
  termb = (1 - TyTw) ^ ((1 / HBn) + 1) - terma
  Vz(N) = (Dia / 2) * (HBn / (1 + HBn))
  Vz(N) = Vz(N) * ((Dia * Pz / (HBk * 4)) ^ (1 / HBn)) * termb
NEXT N
END SUB
```

```
SUB MESH

'Read meshkey file to define mesh geometry'
LOCATE 4, 1: PRINT "Reading MESHKEY.PRN              "
OPEN Root$ + "MESH\MESHKEY.prn" FOR INPUT AS #1
LINE INPUT #1, junk$
INPUT #1, NRing
LINE INPUT #1, junk$
INPUT #1, Nnode
LINE INPUT #1, junk$
INPUT #1, Nele
LINE INPUT #1, junk$
INPUT #1, NBNw
CLOSE #1
'Coordinates of semi-circular pipe mesh data in true pipe size
'Read normalized X and Y coordinates for Nnode nodal points from disk file
'Rescale X and Y values to actual pipe dimensions
LOCATE 4, 1: PRINT "Reading XYLOC.PRN              "
OPEN Root$ + "MESH\XYLOC.prn" FOR INPUT AS #1
FOR N = 1 TO Nnode
  INPUT #1, X(N), Y(N)
  X(N) = Dia * X(N) / 2
  Y(N) = Dia * Y(N) / 2
NEXT N
CLOSE #1
'Read numbers of the three nodes of each element from disk file
LOCATE 4, 1: PRINT "Reading NODES.PRN              "
OPEN Root$ + "MESH\NODES.prn" FOR INPUT AS #1
FOR N = 1 TO Nele
 INPUT #1, Npti(N), Nptj(N), Nptk(N)
NEXT N
CLOSE #1
'Compute shape factor and element centroid information
LOCATE 4, 1: PRINT "Processing mesh element information"
Cmean = 0
Area = 0
FOR N = 1 TO Nnode
 Ynorm = ((Y(N) / (Dia / 2)) + 1) / 2
 'Concentration is a function of normalized Y/D
 SELECT CASE Cflag
 CASE 1
  IF Ynorm < yhigh THEN
   IF Ynorm < ymid THEN
    C(N) = cylow + (cymid - cylow) * Ynorm / ymid
   ELSE
    C(N) = cymid - cymid * (Ynorm - ymid) / (yhigh - ymid)
   END IF
  ELSE
   C(N) = 0
  END IF
 CASE 2
  C(N) = c0 + c1 * Ynorm + c2 * Ynorm ^ 2 + c3 * Ynorm ^ 3
```

```
  END SELECT
  IF C(N) < 0 THEN C(N) = 0
  IF C(N) > Cmax THEN C(N) = Cmax
NEXT N
FOR M = 1 TO Nele
  I = Npti(M): J = Nptj(M): K = Nptk(M)
  'zeroth term shape coefficient for linear triangular elements
  Phi(M, 1) = X(J) * Y(K) - X(K) * Y(J)
  Phi(M, 2) = X(K) * Y(I) - X(I) * Y(K)
  Phi(M, 3) = X(I) * Y(J) - X(J) * Y(I)
  'x term shape coefficient for linear triangular elements
  dPhidx(M, 1) = Y(J) - Y(K)
  dPhidx(M, 2) = Y(K) - Y(I)
  dPhidx(M, 3) = Y(I) - Y(J)
  'y term shape coefficient for linear triangular elements
  dPhidy(M, 1) = X(K) - X(J)
  dPhidy(M, 2) = X(I) - X(K)
  dPhidy(M, 3) = X(J) - X(I)
  Aele(M) = (dPhidy(M, 3) * dPhidx(M, 2) - dPhidy(M, 2) * dPhidx(M, 3)) / 2
  Xele(M) = (X(I) + X(J) + X(K)) / 3
  Yele(M) = (Y(I) + Y(J) + Y(K)) / 3
  Cele(M) = (C(I) + C(J) + C(K)) / 3
  Cmean = Cmean + Cele(M) * Aele(M)
  Area = Area + Aele(M)
NEXT M
Cmean = Cmean / Area

IF RKflag = 1 THEN
  'Find center nodes
  Ictr = 0
  FOR I = 1 TO Nnode
    IF X(I) = 0 THEN
      Ictr = Ictr + 1
      Nctr(Ictr) = I
    END IF
  NEXT I
  'Swap sort..bottom to top
  FOR I = 1 TO Ictr
    FOR J = I TO Ictr
      IF Y(Nctr(J)) < Y(Nctr(I)) THEN
        temp = Nctr(I)
        Nctr(I) = Nctr(J)
        Nctr(J) = temp
      END IF
    NEXT J
  NEXT I
  'Find elements along center..ordered bottom to top
  FOR L = 1 TO Ictr - 1
    I = Nctr(L): J = Nctr(L + 1)
    FOR M = 1 TO Nele
      nflag = 0
      IF Npti(M) = I OR Npti(M) = J THEN nflag = nflag + 1
```

```
    IF Nptj(M) = I OR Nptj(M) = J THEN nflag = nflag + 1
    IF Nptk(M) = I OR Nptk(M) = J THEN nflag = nflag + 1
    IF nflag = 2 THEN Ectr(L) = M
   NEXT M
  NEXT L
  'Approximate Runge-Kutta point locations to be recorded for profile
  Nrkpt = 101
  savstep = Dia / (Nrkpt - 1)
  FOR I = 1 TO Nrkpt
   Ystep(I) = ((I - 1) * savstep) - (Dia / 2)
  NEXT I
END IF
END SUB

SUB ODE (yrk, crk, dcdyrk)

IF crk > Cmax THEN crk = Cmax
IF crk < 0 THEN crk = 0
'Dispersive viscosity at the Runge-Kutta point
CALL DISPVISC(crk, ud, dudc)

'Determine uf and Gammayz from the elements along centerline
M = 0
FOR L = 1 TO Ictr - 1
  IF yrk >= Y(Nctr(L)) AND yrk <= Y(Nctr(L + 1)) THEN M = L
  IF M > 0 THEN GOTO JUMP
NEXT L
JUMP:
gammayz = dwdy(Ectr(M))
IF NNflag = 1 THEN
  'Check condition of shear for the slurry
  DddD = ABS(SQR(dwdx(Ectr(M)) ^ 2 + dwdy(Ectr(M)) ^ 2))
  TddT = Effvisc(Ectr(M)) ^ 2 * DddD ^ 2
  IF TddT < HBTy ^ 2 THEN
    uf = 1000!
  ELSE
    uf = HBTy / DddD + HBk * (DddD ^ (HBn - 1))
  END IF
ELSE
  uf = HBk
END IF
'Ordinary differential equation for concentration distribution
IF gammayz < .0001 THEN
  dcdyrk = -500
  IF Vz(Nctr(M)) < .001 THEN
    dcdyrk = 0
  END IF
ELSE
  dcdyrk = -(rhos - rhof) * g * tantheta * crk / (uf * gammayz * dudc)
END IF
END SUB
```

```
SUB PROFILES

DIM Vnorm(51), Cprof(51)
'Determine normalized velocity and concentration profile values
FOR I = 1 TO Ictr
  Vnorm(I) = Vz(Nctr(I)) / Ub
  Cprof(I) = C(Nctr(I))
NEXT I
'Graphical profile generation .. border and labels
SCREEN 12: CLS
COLOR 15
IYup = 55: IYdn = 375
IXlf = 107: IXrt = 587
Xscl = 60 / 480: Yscl = 20 / 320
LINE (IXlf, IYup)-(IXrt, IYdn), , B
LOCATE INT(200 * Yscl), INT(40 * Xscl)
PRINT "y/D"
Xloc = 80 * Xscl
FOR I = 1 TO 5
  yloc = (IYup + (I - 1) * (320 / 4)) * Yscl
  LINE (IXlf - 5, INT(yloc / Yscl))-(IXlf, INT(yloc / Yscl))
  LOCATE INT(yloc + 1), INT(Xloc - 1)
  PRINT USING "#.##"; (1 - (I - 1) * .25)
NEXT I
'Velocity profile
COLOR 4
LOCATE INT(20 * Yscl + 1), INT(250 * Xscl)
PRINT "Normalized Velocity"
yloc = 45 * Yscl
FOR I = 1 TO 4
  Xloc = (IXlf + (I - 1) * (480 / 3)) * Xscl
  LINE (INT(Xloc / Xscl), IYup - 5)-(INT(Xloc / Xscl), IYup)
  LOCATE INT(yloc + 1), INT(Xloc)
  PRINT USING "#.#"; I - 1
NEXT I
Vlast = Vnorm(1)
Ylast = 2 * Y(Nctr(1)) / Dia
FOR I = 2 TO Ictr
  Vnew = Vnorm(I)
  Ynew = 2 * Y(Nctr(I)) / Dia
  X1 = 107 + Vlast * 480 / 3
  Y1 = 375 - ((Ylast / 2) + .5) * 320
  X2 = 107 + Vnew * 480 / 3
  Y2 = 375 - ((Ynew / 2) + .5) * 320
  LINE (X1, Y1)-(X2, Y2)
  Vlast = Vnew
  Ylast = Ynew
NEXT I
'Concentration profile
COLOR 2
LOCATE INT(400 * Yscl + 1), INT(250 * Xscl)
PRINT "Solid Concentration"
```

```
yloc = 390 * Yscl
FOR I = 1 TO 4
 Xloc = (IXlf + (I - 1) * (480 / 3)) * Xscl
 LINE (INT(Xloc / Xscl), IYdn + 5)-(INT(Xloc / Xscl), IYdn)
 LOCATE INT(yloc + 1), INT(Xloc)
 PRINT USING "#.##"; (I - 1) / 4
NEXT I
Clast = Cprof(1)
Ylast = 2 * Y(Nctr(1)) / Dia
FOR I = 2 TO Ictr
 Cnew = Cprof(I)
 Ynew = 2 * Y(Nctr(I)) / Dia
 X1 = 107 + (Clast * 480 * (4 / 3))
 Y1 = 375 - ((Ylast / 2) + .5) * 320
 X2 = 107 + (Cnew * 480 * (4 / 3))
 Y2 = 375 - ((Ynew / 2) + .5) * 320
 LINE (X1, Y1)-(X2, Y2)
 Clast = Cnew
 Ylast = Ynew
NEXT I
'ODE predicted Concentration profile
IF RKflag = 1 THEN
 COLOR 3
 LOCATE INT(420 * Yscl + 1), INT(250 * Xscl)
 PRINT "ODE Concentration"
 Clast = Cctr(1)
 Ylast = 2 * Y(Nctr(1)) / Dia
 FOR I = 2 TO Ictr
  Cnew = Cctr(I)
  Ynew = 2 * Y(Nctr(I)) / Dia
  X1 = 107 + (Clast * 480 * (4 / 3))
  Y1 = 375 - ((Ylast / 2) + .5) * 320
  X2 = 107 + (Cnew * 480 * (4 / 3))
  Y2 = 375 - ((Ynew / 2) + .5) * 320
  LINE (X1, Y1)-(X2, Y2)
  Clast = Cnew
  Ylast = Ynew
 NEXT I
END IF
COLOR 15
LOCATE 28, 1
PRINT "Should these profiles be saved to disk [y/n]";
INPUT junk$
junk$ = UCASE$(junk$)
IF junk$ = "Y" THEN
 Outfil$ = Root$ + Dir$ + ".pro"
 OPEN Outfil$ FOR OUTPUT AS #1
 PRINT #1, USING "Vel. Iter. : ####  Tol. : #.#####"; itvsum; Verr
 PRINT #1, USING "Conc. Iter. : ####  Tol. : #.#####"; itcsum; Cerr
 PRINT #1, USING "Flowrate =###.## Lpm  Ub = ###.###  m/s"; Qbulk; Ub
 PRINT #1, USING "Cr = ##.###  Cvd =##.###"; Cmean; Cdel
 PRINT #1, USING "Spec. dP = ######.# Pa/m "; Pz
```

```
  PRINT #1, USING "Calc. dP = ######.# Pa/m"; dPcalc
  PRINT #1, USING "Average Tw = ####.### Pa"; Tw
  PRINT #1, USING "Dia. = #.#### m"; Dia
  IF RKflag = 1 THEN
   PRINT #1, "Normalized  y/D  v/Ub  Cspec  Ccal"
  ELSE
   PRINT #1, "Normalized  y/D  v/Ub  Cspec"
  END IF
  FOR I = 1 TO Ictr
   Ynorm = ((Y(Nctr(I)) * 2 / Dia) + 1) / 2
   IF RKflag = 1 THEN
    PRINT #1, USING "#.###  ##.###  #.###  #.###"; Ynorm; Vnorm(I); Cprof(I); Cctr(I)
   ELSE
    PRINT #1, USING "#.###  ##.###  #.###"; Ynorm; Vnorm(I); Cprof(I)
   END IF
  NEXT I
  CLOSE #1
END IF
END SUB

SUB RUNGE (yrk, crk, dcdyrk, hrk, cnext)

'Fourth order Runge-Kutta
crk2 = crk + hrk * dcdyrk / 2
CALL ODE(yrk + hrk / 2, crk2, dcdyrk2)
crk3 = crk + hrk * dcdyrk2 / 2
CALL ODE(yrk + hrk / 2, crk3, dcdyrk3)
crk4 = crk + hrk * dcdyrk3
CALL ODE(yrk + hrk, crk4, dcdyrk4)
cnext = crk + hrk * (dcdyrk + 2 * dcdyrk2 + 2 * dcdyrk3 + dcdyrk4) / 6
IF cnext < 0 THEN cnext = 0
IF cnext > Cmax THEN cnext = Cmax
END SUB

SUB TRANSITION (Tflag)

'Conservative estimate of turbulent transition based on that of fluid alone
Tflag = 0
'Laminar velocity-pressure gradient for Herschel-Bulkley fluid alone
eta = HBTy / Tw
Ta = 1 + (1 / HBn)
Tb = 2 + (1 / HBn)
Tc = 3 + (1 / HBn)
Vlam = ((eta ^ 2 / Ta) * (1 - eta) ^ Ta) + ((2 * eta / Tb) * (1 - eta) ^ Tb)
Vlam = (Dia / 2) * (Tw / HBn) ^ (1 / HBn) * (Vlam + (1 / Tc) * (1 - eta) ^ Tc)

'Corresponding turbulent pressure gradient from Wilson-Thomas
omega = -2.5 * LOG(1 - eta) - 2.5 * eta * (1 + (eta / 2))
alpha = 2 * (1 + eta * HBn) / (1 + HBn)
Ustar = (Tw / rhof) ^ .5
Vn = Ustar * 2.5 * LOG(rhof * Dia * Ustar / HBk)
Vturb = Vn + Ustar * (11.6 * (alpha - 1) - 2.5 * LOG(alpha) - omega)
```

```
'Lowest velocity corresponds to flow regime of fluid alone for this Pz
IF Vturb < Vlam THEN Tflag = 1
END SUB

SUB VELBC

'Subroutine to identify boundary nodes and to apply conditions
'NBNw : Number of boundary points where velocity specified
FOR I = 1 TO NBNw
 NptB(I) = I + Nnode - NBNw
NEXT I
'Specify velocity zero along pipe boundary points by amplifying diagonal
Amplify = 1E+10
EBC = 0
FOR I = 1 TO NBNw
  IROW = NptB(I)
  Gstiff(IROW, 1) = Gstiff(IROW, 1) * Amplify
  F(IROW) = Gstiff(IROW, 1) * EBC
NEXT I
END SUB

SUB VELMATRIX

DIM Estiff(3, 3), ijk(3)
'Initialize global stiffness and force matrices
FOR I = 1 TO Nnode
 FOR J = 1 TO 8
   Gstiff(I, J) = 0
   Nadj(I, J) = 0
 NEXT J
 Nadj(I, 1) = I
 F(I) = 0
NEXT I
'Build stiffness and force matrices
FOR M = 1 TO Nele
 'Local element node numbers
 ijk(1) = Npti(M): ijk(2) = Nptj(M): ijk(3) = Nptk(M)
 'Local element stiffness matrix
 coeff = Effvisc(M) / (4 * Aele(M))
 FOR IR = 1 TO 3
  FOR IC = 1 TO 3
   Estiff(IR, IC) = dPhidx(M, IR) * dPhidx(M, IC)
   Estiff(IR, IC) = Estiff(IR, IC) + dPhidy(M, IR) * dPhidy(M, IC)
   Estiff(IR, IC) = Estiff(IR, IC) * coeff
   'Add local element stiffness matrix to global matrix
   IROW = ijk(IR)
   ICOL = ijk(IC)
   FOR IA = 1 TO 8
    IF Nadj(IROW, IA) = ICOL THEN GOTO GLOBE
    IF Nadj(IROW, IA) = 0 THEN GOTO ELEME
   NEXT IA
   PRINT "Node "; IROW; " has more than 8 adjacent nodes.": STOP
```

```
ELEME:
    Nadj(IROW, IA) = ICOL
    NNadj(IROW) = IA
GLOBE:
    Gstiff(IROW, IA) = Gstiff(IROW, IA) + Estiff(IR, IC)
   NEXT IC
  NEXT IR
   'Local element force component
  FM = Pz * Aele(M) / 3
  'Add local element force contribution to global force vector
  FOR IR = 1 TO 3
    IROW = ijk(IR)
    F(IROW) = F(IROW) + FM
  NEXT IR
NEXT M
END SUB

SUB VELSOLVE

'Subroutine for solving linear equations by Gauss-Siedel method
iter = 0
WHILE itnum > iter AND Verr > Vtol
  iter = iter + 1
  SumD = 0
  SumDD = 0
  'Obtain new estimate for each unknown
  FOR N = 1 TO Nnode
    DelD = F(N)
    ICMAX = NNadj(N)
    FOR IC = 1 TO ICMAX
      ICOL = Nadj(N, IC)
      DelD = DelD - Gstiff(N, IC) * Vz(ICOL)
    NEXT IC
    DelD = DelD / Gstiff(N, 1)
    SumDD = SumDD + ABS(DelD)
    Vz(N) = Vz(N) + DelD * Orelax
    SumD = SumD + ABS(Vz(N))
  NEXT N
  'Test for convergence
  Verr = SumDD / SumD
  it = itvsum + iter
  LOCATE 11, 1:
  PRINT USING "Velocity Iteration = ####   Tolerance = #.######"; it; Verr
WEND
itvsum = itvsum + iter
END SUB

SUB VISC

'Subroutine to evaluate effective element viscosities
FOR M = 1 TO Nele
 'Adjust effective viscosity for presence of solid particles
```

```
  Cm = Cele(M)
  IF Cm >= Cshear THEN
   Effvisc(M) = 1000!
  ELSE
   IF SSflag = 1 THEN
    'Thomas relative viscosity for spherical particle slurries
    Rnu = 1 + 2.5 * Cm + 10.05 * Cm ^ 2 + .00273 * EXP(16.6 * Cm)
   ELSE
    'SRC relative viscosity for sand particle slurries
    Rnu = 1 + 2.5 * Cm + 10 * Cm ^ 2 + .0019 * EXP(20 * Cm)
   END IF
   IF NNflag = 1 THEN
    I = Npti(M): J = Nptj(M): K = Nptk(M)
    dwdx(M) = Vz(I) * dPhidx(M, 1) + Vz(J) * dPhidx(M, 2)
    dwdx(M) = (dwdx(M) + Vz(K) * dPhidx(M, 3)) / (2 * Aele(M))
    dwdy(M) = Vz(I) * dPhidy(M, 1) + Vz(J) * dPhidy(M, 2)
    dwdy(M) = (dwdy(M) + Vz(K) * dPhidy(M, 3)) / (2 * Aele(M))
    'Check to see if 1/2(T:T) < Ty^2 and a no shear condition exists
    DddD = ABS(SQR(dwdx(M) ^ 2 + dwdy(M) ^ 2))
    TddT = Effvisc(M) ^ 2 * (dwdx(M) ^ 2 + dwdy(M) ^ 2)
    IF TddT < HBTy ^ 2 THEN
     'No shear simulated by significant increase in Effvisc of element
     Effvisc(M) = 1000!
    ELSE
     Effvisc(M) = HBTy / DddD + HBk * Rnu * (DddD ^ (HBn - 1))
    END IF
   ELSE
    Effvisc(M) = HBk * Rnu
   END IF
  END IF
NEXT M
END SUB
```

APPENDIX D : Two layer model program

```
' Two-Layer Model for pipeline slurry flow
' As outlined in "Slurry Flow - Principles and Practice", Shook and Roco
' Changes to contact load fraction from Gillies et al. 1991
' Modifications for non-Newtonian fluid from Maciejewski et al. 1991
' Written 26 July 1995 by Kelly Hill
' Modified 26 February 1996

DEFINT I-N

DECLARE SUB BUCKINGHAM ()
DECLARE SUB CDBING (Cd)
DECLARE SUB CDRAG (Cd)
DECLARE SUB CHURCHILL (Re, eD, f)
DECLARE SUB COLEBROOK (dD, f12)
DECLARE SUB ROOT (A2A, Betai)
DECLARE SUB WILSON ()

DIM SHARED Ub(150), Pz(150), Pzs(150), Cv(150)
DIM SHARED Pflam(150), Pftur(150), Pzf(150)
DIM SHARED V1(150), V2(150), Cc(150), Beta(150)

COMMON SHARED g, pi, Dpipe, dp50, rhos, rhol, Ss
COMMON SHARED Ty, viscp, Vcrit
COMMON SHARED ICctype, IPtype, IFtype
COMMON SHARED NV, tol

' Problem Parameters in SI units
dir$ = "a:\twolayer\"
Dpipe = .053              'Pipe diameter (m)
dp50 = .0044              'Median particle size (m)
rhos = 2470!              'Solid density (kg/m3)
rhol = 1500!              'Liquid density (kg/m3)
Ty = 3.4                  'Yield stress (Pa)
viscp = .059              'Plastic viscosity (Pa.s)
IFtype = 1                'Fluid model type 0=Newtonian
'                             1=Bingham
ICdtype = 0               'Drag coefficient fluid type
FDtype = -1               'f12 increase using (1+Bi)
eps = .000005             'Pipe roughness (m)
etas = .45                'Coefficient of friction at the wall
theta = 0                 'Pipeline angle of elevation (rad)
Clim = .5                 'Limiting solid concentration (v/v)
                          'May be Velocity dependent

Cmax = 0                  'Maximum solid concentration
                          'Specified if Clim is to be calculated

Cr = .25                  'In-situ solid concentration (v/v)

' Contact load selection for turbulent flow
```

```
' ICctype          1     Specified Cc
'                 2     Vinf Cc
'                       IPtype = 1 for spheres
'                             2 for sand
ICctype = 1
IPtype = 1

' Specified Cc value
Ccspec = .96

' General variables
g = 9.80665                'Gravitational constant (m/s2)
pi = 4 * ATN(1!)
tol = .0001                'Convergence criteria
maxit = 2500                'Maximum number of iterations to converge


' Vinf Cc correlation values
b1 = .074
b2 = .44
b3 = .189
b4 = -.0184

' Variable Initialization
Ss = rhos / rhol
eD = eps / Dpipe
dD = dp50 / Dpipe

' Main Program Menu
MENU:
SCREEN 0
COLOR 7, 1: CLS
LOCATE 3, 2: PRINT "Two-Layer Model for Slurry Pipe Flow";
LOCATE 6, 5: PRINT "1)  Pressure Gradient at Single Velocity";
LOCATE 7, 5: PRINT "2)  Pressure Gradient over Velocity Range";
LOCATE 8, 5: PRINT "3)  End Program";
LOCATE 12, 2: INPUT "Select Simulation Operation "; Nsel
SELECT CASE Nsel
 CASE 1
  LOCATE 14, 2: INPUT "Enter Velocity to be Evaluated "; StartV
  EndV = 0
  StepV = 0
  NV = 1
  Ub(1) = StartV
 CASE 2
  LOCATE 14, 2: INPUT "Enter Start Velocity "; StartV
  LOCATE 15, 2: INPUT "Enter End Velocity "; EndV
  LOCATE 16, 2: INPUT "Enter Interval Size "; StepV
  NV = INT((EndV - StartV) / StepV) + 2
  FOR I = 1 TO NV
   Ub(I) = StartV + (I - 1) * StepV
  NEXT I
```

```
  'Determining pressure gradient of fluid alone in pipe
  IF IFtype = 1 THEN            'Non-Newtonian case
   CALL BUCKINGHAM
   CALL WILSON
   Vcrit = Ub(1)
   I = 1
   WHILE I <= NV
    IF Pflam(I) > Pftur(I) THEN
     Vcrit = Ub(I)
     Pzf(I) = Pflam(I) / 1000
    ELSE
     Pzf(I) = Pftur(I) / 1000
    END IF
    I = I + 1
   WEND
  ELSE                          'Newtonian case
   FOR I = 1 TO NV
    Re = Dpipe * Ub(I) * rhol / viscp
    IF Re <= 2100 THEN
     f = 16 / Re
     Pflam(I) = 2 * f * Ub(I) ^ 2 * rhol / Dpipe
     Pzf(I) = Pflam(I) / 1000
    ELSE
     CALL CHURCHILL(Re, eD, f)
     Pftur(I) = 2 * f * Ub(I) ^ 2 * rhol / Dpipe
     Pzf(I) = Pftur(I) / 1000
    END IF
   NEXT I
   Vcrit = 2100 * viscp / (Dpipe * rhol)
  END IF
 CASE 3
  COLOR 0, 7
  END
 CASE ELSE
  GOTO MENU
END SELECT
Iv = 1
CLS

IF IFtype = 1 AND ICdtype = 1 THEN
 CALL CDBING(Cd)
 Vinf2 = 4 * g * dp50 * (Ss - 1) / (3 * Cd) - 2 * pi * Ty / (Cd * rhol)
 IF Vinf2 > 0! THEN
  Vinf = Vinf2 ^ .5
 ELSE
  Vinf = 0!
 END IF
ELSE
 CALL CDRAG(Cd)
 Vinf = (4 * g * dp50 * (Ss - 1) / (3 * Cd)) ^ .5
END IF
```

```
' Velocity range loop
WHILE Iv <= NV

' Begin single velocity solution
SELECT CASE ICctype
 CASE 1
  CcCr = Ccspec
 CASE 2
  IF IFtype = 1 AND ICdtype = 1 THEN
   IF Vinf > 0! THEN
    IF Cmax > 0 THEN
     term = b1 * (Ub(Iv) / Vinf) ^ b2 * (1 - Cr) ^ b3
     Clim = Cmax - (Cmax - Cr) * term
    END IF
    CcCr = EXP(b4 * (Ub(Iv) / Vinf))
   ELSE
    Clim = Cr
    CcCr = .0001
   END IF
  ELSE
   IF Cmax > 0 THEN
    term = b1 * (Ub(Iv) / Vinf) ^ b2 * (1 - Cr) ^ b3
    Clim = Cmax - (Cmax - Cr) * term
   END IF
   CcCr = EXP(b4 * (Ub(Iv) / Vinf))
  END IF
END SELECT
IF Clim <= Cr THEN Clim = Cr
IF Ub(Iv) < Vcrit THEN CcCr = 1
IF CcCr > .0001 THEN              'Normal stratified case
 Cc(Iv) = CcCr * Cr
 C1 = Cr - Cc(Iv)
 C2 = Clim - C1
 Apipe = pi * Dpipe ^ 2 / 4
 A2A = Cc(Iv) / C2
 A1A = 1 - A2A
 CALL ROOT(A2A, Beta(Iv))
 S1 = (pi - Beta(Iv)) * Dpipe
 S2 = Beta(Iv) * Dpipe
 S12 = SIN(Beta(Iv)) * Dpipe
 Deq1 = 4 * A1A * Apipe / (S1 + S12)
 Deq2 = 4 * A2A * Apipe / (S12 + S2)
ELSE                              'Fully dispersed flow
 Cc(Iv) = 0!
 C1 = Cr
 C2 = 0!
 Apipe = pi * Dpipe ^ 2 / 4
 A2A = 0!
 A1A = 1!
 Beta(Iv) = 0!
 S1 = pi * Dpipe
 S2 = 0!
```

```
  S12 = 0!
  Deq1 = Dpipe
  Deq2 = 0!
END IF
rho1 = rhol * (1 + C1 * (Ss - 1))
rho2 = rhol * (1 + Clim * (Ss - 1))
rhom = rhol * (1 + Cr * (Ss - 1))
IF IPtype = 1 THEN
  vr1 = 1 + 2.5 * C1 + 10.05 * C1 ^ 2 + .00273 * EXP(16.6 * C1)
  vr2 = 1 + 2.5 * Clim + 10.05 * Clim ^ 2 + .00273 * EXP(16.6 * Clim)
ELSE
  vr1 = 1 + 2.5 * C1 + 10 * C1 ^ 2 + .0019 * EXP(20 * C1)
  vr2 = 1 + 2.5 * Clim + 10 * Clim ^ 2 + .0019 * EXP(20 * Clim)
END IF
T2sS2 = Dpipe ^ 2 * etas * g * (rhos - rhol)
T2sS2 = T2sS2 * (SIN(Beta(Iv)) - Beta(Iv) * COS(Beta(Iv))) * C2
T2sS2 = T2sS2 * (1 - C1 - C2) / (2 * (1 - C2))

'Velocity Initialization
V1(Iv) = Ub(Iv) / A1A
V2(Iv) = 0
iflag = 0
iter = 1
Locn = Iv
WHILE Locn > 18
  Locn = Locn - 18
WEND

'Layer Velocity Iteration Loop for Specified Bulk Velocity
WHILE iflag = 0
  IF Ub(Iv) < Vcrit THEN      'Laminar case
    V12 = 1.5 * V2(Iv)
    Bdeg = Beta(Iv) * 180 / pi
    Re1 = Deq1 * V1(Iv) * rho1 / (vr1 * viscp)
    f1 = (15.375 - V12 * (1.676 + .007416 * Bdeg) / V1(Iv)) / Re1
    f12 = (17.964 - .0154 * Bdeg - V12 * (9.981 + .0242 * Bdeg) / V1(Iv))
    f12 = f12 / Re1
    IF FDtype >= 1 THEN
      Bi12 = Ty * Deq1 / ((V1(Iv) - V2(Iv)) * viscp)
      f12 = f12 * (1 + Bi12) * FDtype
    END IF
    IF V2(Iv) > .001 AND A2A > .0001 THEN   'Lower layer moving
      Re2 = Deq2 * V2(Iv) * rho2 / (vr2 * viscp)
      f2 = 15.375 - V12 * (1.676 + .007416 * (180 - Bdeg)) / V2(Iv)
      f2 = f2 / (Re2 * vr2)
    ELSE
      f2 = 10000
    END IF
  ELSE                        'Turbulent flow case
    IF IFtype = 1 THEN        'Non-Newtonian..based of fluid friction
      f1 = (Dpipe * Pftur(Iv)) / (2 * Ub(Iv) ^ 2 * rhol)
      f2 = f1
```

```
  ELSE                  'Newtonian
   f1 = (Dpipe * Pftur(Iv)) / (2 * Ub(Iv) ^ 2 * rhol)
   f2 = f1
  END IF
  CALL COLEBROOK(dD, f12)
  IF FDtype >= 1 THEN
   Bi12 = Ty * Deq1 / ((V1(Iv) - V2(Iv)) * viscp)
   f12 = f12 * (1 + Bi12) * FDtype
  END IF
 END IF
 T1 = (f1 * V1(Iv) ^ 2 * rho1) / 2
 T2m = (f2 * V2(Iv) ^ 2 * rho1) / 2
 T12 = (f12 * (V1(Iv) - V2(Iv)) ^ 2 * rho1) / 2
 IF IFtype = 1 AND Ub(Iv) < Vcrit THEN   'laminar, non-Newtonian
  T1 = T1 + 4 * Ty / 3
  T2m = T2m + 4 * Ty / 3
  IF ABS(FDtype) < .01 THEN              'Dedegil correction not being used
   T12 = T12 + 4 * Ty / 3
  END IF
 END IF
 Pz1 = (T1 * S1 + T12 * S12) / (A1A * Apipe) + rho1 * g * SIN(theta)
 IF A2A > .0001 THEN
  Pz2 = (T2m * S2 + T2sS2 - T12 * S12) / (A2A * Apipe)
  Pz2 = Pz2 + rho2 * g * SIN(theta)
 ELSE
  Pz2 = 0!
 END IF
 Pzm = (T1 * S1 + T2m * S2 + T2sS2) / Apipe + rhom * g * SIN(theta)
 IF Pz2 > Pz1 AND V2(Iv) < .001 THEN      'Stationary bed
  Pz(Iv) = Pz1 / 1000
  V1(Iv) = Ub(Iv) / A1A
  V2(Iv) = 0
  Pzs(Iv) = 0
  iflag = 1
  LOCATE Locn, 2
  PRINT USING "Ub = ##.## m/s  Pz = ##.#####   Stationary Bed"; Ub(Iv); Pz(Iv)
  LOCATE Locn + 1, 2
  PRINT "                                    "
 ELSE
  IF A2A < .0001 THEN           'fully dispersed flow
   Pz(Iv) = Pz1 / 1000
   V1(Iv) = Ub(Iv)
   V2(Iv) = Ub(Iv)
   Pzs(Iv) = 0!
   iflag = 1
   LOCATE Locn, 2
   PRINT USING "Ub = ##.## m/s  Pz = ##.#####   Dispersed flow"; Ub(Iv); Pz(Iv)
   LOCATE Locn + 1, 2
   PRINT "                                    "
  ELSE
   Diff = Pz1 - Pz2
   Ptol = ABS((Pz1 - Pz2) / Pz1)
```

```
    IF Ptol < tol THEN              'converged
     Pz(Iv) = Pzm / 1000
     Pzs(Iv) = T2sS2 / (Apipe * 1000)
     iflag = 1
    ELSE                            'adjust velocities
     dPzDV = f12 * rho1 * S12 * (1 + A1A / A2A) ^ 2 / (A1A * Apipe)
     dPzDV = (dPzDV + f1 * rho1 * S1 / (A1A * Apipe)) * V1(Iv)
     dPzDV = dPzDV - f12 * rho1 * S12 * (1 + A1A / A2A) * Ub(Iv) / (A1A * Apipe)
     V1(Iv) = V1(Iv) - Diff / (2 * dPzDV)
     V2(Iv) = (Ub(Iv) - A1A * V1(Iv)) / A2A
    END IF
   END IF
  END IF
  iter = iter + 1
  IF iter > maxit THEN
   PRINT USING " Failed to converge at velocity #.## m/s"; Ub(Iv);
   Pz(Iv) = Pzm / 1000
   iflag = 1
  END IF
WEND

' Final Result Calculations
Cv(Iv) = C1 + C2 * A2A * V2(Iv) / Ub(Iv)
LOCATE Locn, 2
PRINT "                                        "
LOCATE Locn, 2
PRINT USING "Ub = ##.## m/s Pz = ##.#### kPa/m Cv #.####"; Ub(Iv); Pz(Iv); Cv(Iv)
IF V2(Iv) = 0 THEN
 LOCATE Locn, 50: PRINT "Stationary Bed"
END IF
IF A2A < .0001 THEN
 LOCATE Locn, 50: PRINT "Dispersed Flow"
END IF
IF iter > maxit THEN
 LOCATE Locn, 50: PRINT USING "Ptol #.######"; Ptol
END IF
LOCATE Locn + 1, 2
PRINT "                                        "
Iv = Iv + 1
IF Locn = 18 OR Iv > NV THEN
 LOCATE 22, 2: PRINT "Press a key to continue"
 P$ = ""
 WHILE P$ = ""
  P$ = INKEY$
 WEND
 CLS
END IF

WEND                    'Range loop

IF Nsel = 2 THEN
' Graphical output
```

```
SCREEN 12: CLS
COLOR 15
nx = 5: ny = 5
xstp = 1
ΓYup = 55: ΓYdn = 375
ΓXlf = 107: ΓXrt = 587
Xscl = 60 / 480: Yscl = 20 / 320
LINE (ΓXlf, ΓYup)-(ΓXrt, ΓYdn), , B
LOCATE INT(400 * Yscl + 1), INT(250 * Xscl)
PRINT "Bulk Velocity"
Yloc = 390 * Yscl
FOR I = 1 TO nx + 1
  Xloc = (ΓXlf + (I - 1) * (480 / nx)) * Xscl
  LINE (INT(Xloc / Xscl), ΓYdn + 5)-(INT(Xloc / Xscl), ΓYdn)
  LOCATE INT(Yloc + 1), INT(Xloc)
  PRINT USING "#.#"; (I - 1) * xstp
NEXT I
ystp = INT(Pz(NV) / ny) + 1
Xloc = 80 * Xscl
FOR I = 1 TO ny + 1
  Yloc = (ΓYdn - (I - 1) * (320 / ny)) * Yscl
  LINE (ΓXlf - 5, INT(Yloc / Yscl))-(ΓXlf, INT(Yloc / Yscl))
  LOCATE INT(Yloc + 1), INT(Xloc - 1)
  PRINT USING "##.#"; (I - 1) * ystp
NEXT I
COLOR 4
LOCATE INT(200 * Yscl), INT(40 * Xscl)
PRINT "Pzm"
Vlast = Ub(1)
Pzmlast = Pz(1)
FOR I = 2 TO NV
  Vnew = Ub(I)
  Pzmnew = Pz(I)
  x1 = 107 + Vlast * 480 / (nx * xstp)
  y1 = 375 - Pzmlast * 320 / (ny * ystp)
  x2 = 107 + Vnew * 480 / (nx * xstp)
  y2 = 375 - Pzmnew * 320 / (ny * ystp)
  LINE (x1, y1)-(x2, y2)
  Vlast = Vnew
  Pzmlast = Pzmnew
NEXT I
COLOR 2
LOCATE INT(200 * Yscl + 2), INT(40 * Xscl)
PRINT "Pzf"
Vlast = Ub(1)
Pzflast = Pzf(1)
FOR I = 2 TO NV
  Vnew = Ub(I)
  Pzfnew = Pzf(I)
  x1 = 107 + Vlast * 480 / (nx * xstp)
  y1 = 375 - Pzflast * 320 / (ny * ystp)
  x2 = 107 + Vnew * 480 / (nx * xstp)
```

```
 y2 = 375 - Pzfnew * 320 / (ny * ystp)
 LINE (x1, y1)-(x2, y2)
 Vlast = Vnew
 Pzflast = Pzfnew
NEXT I

COLOR 15
' Output of Results to File
LOCATE 28, 2
INPUT "Do you wish results to be stored to a file Y/N"; f$
IF f$ = "y" OR f$ = "Y" THEN
 LOCATE 28, 2
 PRINT "                                                "
 LOCATE 28, 2
 INPUT "Enter file name with extension"; file$
 file$ = dir$ + file$
 OPEN file$ FOR OUTPUT AS #1
 PRINT #1, USING "Dpipe #.####, k #.#######, theta #.###"; Dpipe; eps; theta
 PRINT #1, USING "dp50 #.######, rhos ####, etas #.###"; dp50; rhos; etas
 PRINT #1, USING "rhol ####, Ty ##.#,  viscp #.###, Cr #.###"; rhol; Ty; viscp; Cr
 SELECT CASE ICctype
  CASE 1
   PRINT #1, USING "Cc specified #.### "; Ccspec;
  CASE 2
   IF IPtype = 1 THEN
    PRINT #1, "Cc calc. with Vinf (sphere) ";
   ELSE
    PRINT #1, "Cc calc. with Vinf (sand) ";
   END IF
 END SELECT
 IF Cmax = 0 THEN
  PRINT #1, USING "Clim specified #.### "; Clim
 ELSE
  PRINT #1, USING "Clim calc using Cmax #.### "; Cmax
 END IF
 PRINT #1, " "
 PRINT #1, "  Ub    Pz    Pzs    Cv    V1    V2    Cc    Beta "
 PRINT #1, " (m/s)  (kPa)  (kPa)       (m/s) (m/s)       (rad) "
 PRINT #1, " "
 FOR I = 1 TO NV
 PRINT #1, USING " #.###  ##.###  ##.###  #.###  #.###  #.###  #.###  #.### "; Ub(I); Pz(I); Pzs(I); Cv(I);
V1(I); V2(I); Cc(I); Beta(I)
 NEXT I
 CLOSE #1
END IF
END IF
GOTO MENU

SUB BUCKINGHAM

FOR I = 1 TO NV
 Ttol = 1
```

```
 Tw = viscp * 8 * Ub(I) / Dpipe + 4 * Ty / 3
 WHILE Ttol > tol
  eta = Ty / Tw
  IF eta > 1 THEN
   Tw = Ty / .99
   eta = .99
  END IF
  oldTw = Tw
  Tw = ((viscp * 8 * Ub(I) / Dpipe) + (4 * Ty / 3)) / (1 + (eta ^ 4) / 3)
  Ttol = ABS(Tw - oldTw) / Tw
 WEND
 Pflam(I) = 4 * Tw / Dpipe
NEXT I

END SUB

SUB CDBING (Cd)

ctol = .000001

'Correlation for spheres based on Valentik and Whitmore (1965)
CALL CDRAG(Cd)
Cdold = Cd
eCd = .4
WHILE eCd > ctol
 Vinf2N = 4 * g * dp50 * (Ss - 1) / (3 * Cdold)
 VinfTy = 2 * pi * Ty / (Cdold * rhol)
 IF Vinf2N > VinfTy THEN
  Vinf = (Vinf2N - VinfTy) ^ .5
  IF Vinf > .00000001# THEN
   Rep = (dp50 * Vinf * rhol / viscp) / (1 + (Ty * dp50 / (Vinf * viscp)))
   IF Rep < 8 THEN
    Cd = 24 / Rep
   ELSE
    IF Rep < 150 THEN
     Cd = 22 / Rep + .25
    ELSE
     Cd = .4
    END IF
   END IF
  ELSE
   Cd = 1000
   Cdold = Cd
  END IF
  eCd = ABS(Cd - Cdold)
  Cdold = Cd
 ELSE
  Cd = 1000
  eCd = .1 * ctol
 END IF
WEND
```

```
END SUB

SUB CDRAG (Cd)

ctol = .000001

IF IPtype = 1 THEN
' Cd correlation for spheres based on Clift,Grace and Weber (1978)
 Cdold = .44
 eCd = .44
 WHILE eCd > ctol
  Vinf = (4 * g * dp50 * (Ss - 1) / (3 * Cdold)) ^ .5
  Rep = dp50 * Vinf * rhol / viscp
  IF Rep < .2 THEN
   Cd = 24 / Rep
  ELSE
   IF Rep < 1000 THEN
    Cd = 24 * (1 + .15 * Rep ^ .687) / Rep
   ELSE
    Cd = .44
   END IF
  END IF
  eCd = ABS(Cd - Cdold)
  Cdold = Cd
 WEND
ELSE
' Cd correlations based on observations of sand in water
 Ar = (4 * g * dp50 ^ 3 * (Ss - 1) * rhol ^ 2) / (3 * viscp ^ 2)
 IF Ar < 24 THEN
  Cd = 576 / Ar
 ELSE
  IF Ar < 2760 THEN
   Cd = 80.9 * (Ar ^ -.475)
  ELSE
   IF Ar < 46100 THEN
    Cd = 8.61 * (Ar ^ -.193)
   ELSE
    Cd = 1.09
   END IF
  END IF
 END IF
END IF

END SUB

SUB CHURCHILL (Re, eD, f)

IF Re > 2100 THEN
 A = (-2.457 * LOG((7 / Re) ^ .9 + .27 * eD)) ^ 16
 B = (37530 / Re) ^ 16
 f = 2 * ((8 / Re) ^ 12 + (A + B) ^ (-1.5)) ^ (1 / 12)
ELSE
```

```
 f = 16 / Re
END IF

END SUB

SUB COLEBROOK (dD, f12)
corlg = .4342945
IF dD < .0015 THEN
 Y = 0
ELSE
 Y = 4 + 1.42 * corlg * LOG(dD)
END IF
f12 = (2 * (1 + Y)) / (4 * corlg * LOG(1 / dD) + 3.36) ^ 2

END SUB

SUB ROOT (A2A, Betai)

' Root finder by bisection method
rtol = .000005
Bhigh = pi
A2Ahigh = 1
Blow = 0
A2Alow = 0
Bmid = pi / 2
A2Amid = .5
ADiff = ABS(A2A - A2Amid)
BDiff = ABS(Bhigh - Blow)
WHILE ADiff > rtol AND BDiff > rtol
 IF A2A > A2Amid THEN
  Blow = Bmid
  A2Alow = A2Amid
 ELSE
  Bhigh = Bmid
  A2Ahigh = A2Amid
 END IF
 Bmid = (Bhigh + Blow) / 2
 A2Amid = (Bmid - COS(Bmid) * SIN(Bmid)) / pi
 ADiff = ABS(A2A - A2Amid)
 BDiff = ABS(Bhigh - Blow)
WEND
Betai = Bmid

END SUB

SUB WILSON

FOR I = 1 TO NV
 Vtol = 1
 v = Ub(I)
 Tw = viscp * 8 * v / Dpipe + 4 * Ty / 3
 WHILE Vtol > tol
```

```
  IF Tw < Ty THEN Tw = 1.1 * Ty
  IF Ub(I) < 1 THEN
   Tw = Tw + 1.75 * (Ub(I) ^ 2 - v ^ 2)
  ELSE
   Tw = Tw + .25 * (Ub(I) ^ 2 - v ^ 2)
  END IF
  eta = Ty / Tw
  Ustar = (Tw / rhol) ^ .5
  Restar = Dpipe * Ustar * rhol / viscp
  term = 2.5 * LOG(((1 - eta) ^ 2) / (1 + eta)) + eta * (14.1 + 1.25 * eta)
  v = Ustar * (2.5 * LOG(Restar) + term)
  Vtol = ABS(Ub(I) - v) / Ub(I)
  IF eta >= .99 AND v > Ub(I) THEN Vtol = tol / 10
 WEND
 IF eta < .99 THEN
  Pftur(I) = 4 * Tw / Dpipe
 ELSE
  Pftur(I) = 4 * Ty / Dpipe
 END IF
NEXT I

END SUB
```